UNIVERSITY OF CALGARY

Diffusivity of Light Hydrocarbon Gases in Bitumen

by

William Daniel Loty Richardson

A THESIS

SUBMITTED TO THE FACULTY OF GRADUATE STUDIES

IN PARTIAL FULFILMENT OF THE REQUIREMENTS FOR THE

DEGREE OF DOCTOR OF PHILOSOPHY

GRADUATE PROGRAM IN CHEMICAL AND PETROLEUM ENGINEERING

CALGARY, ALBERTA

FEBRUARY, 2017

ABSTRACT

Most of the world's heavy oil and bitumen reserves are too viscous to be produced without heating or dilution. Thermal recovery methods, which decrease the oil viscosity through heating, are widely applied in Western Canada using steam as a source of heat. Recovery processes using solvent addition to reduce viscosity are of current industrial interest because these processes have the potential to reduce water and energy requirements and could be applied to reservoirs unsuitable for thermal methods. In many solvent based processes, the solvent are gaseous hydrocarbons, and the rate of oil production is partly dependent on diffusive mass transfer of the solvent into the oil. The objective of this thesis is both to collect data and to provide a mathematical model for the diffusion of light hydrocarbons into bitumen.

There is little available diffusivity data at temperatures above room temperature. To supplement the available literature data, diffusivities and solubilities of light hydrocarbon gases in a Western Canadian bitumen were measured from 40 to 90^{o}C and pressures from 300 to 2300 kPa, using a pressure decay method. The gas solubility is a key input into the diffusion model and additional solubility data were collected using constant composition expansion. The solubility data were fit with a modified Henry's Law expression, which was incorporated into the diffusion model.

Existing correlations for solvent diffusivity in heavy oil have a limited range of application and do not account for the compositional dependence of the diffusivity in a physically meaningful manner. In this study, a one dimensional model of the diffusion process based on Fick's Law was developed and fit to the pressure decay data. This model accounted for the swelling of the mixture caused by both mass transfer and the decreasing density of the solvent-oil mixture. The model also accounted for the change in viscosity with mass transfer and could be applied with any diffusivity correlation. A constant and several concentration dependant diffusivity models were assessed. The most suitable concentration dependant model was determined to be a power law relationship between the diffusivity and the viscosity of the mixture. Correlations were developed to predict both the concentration dependant and constant diffusivities with average errors of 23 and 12%, respectively, over the full range of conditions investigated.

ACKNOWLEDGEMENTS

My supervisor, Harvey Yarranton, deserves more thanks than I can possibly give. His support and guidance was invaluable in every stage of this project. Credit also goes to my co-supervisor, Brij Maini, who pushed me in the right direction from the start.

Our team has two incredible lab managers, Florian and Elaine, who are more knowledgeable and skilled in the lab than I could ever dream of being. Without Florian's help and insight I would have spent the better part of my degree, spinning my wheels, trying to commission my equipment. I owe him a huge debt.

The AER/HOPP team has been blessed with wonderful students over the years. My former and current colleagues each deserve individual thanks, as they have all contributed in some way to my success. However, for the sake of space, I'd like to specifically acknowledge Fatemeh, Hamed and Francisco (who fit the density and viscosity models that I was so reliant on) and Catalina Sanchez, whose dedication, intelligence and friendship pushed me to be a better student. I'd also like to wish Franklin the best of luck as he looks to expand our diffusivity methods and models to liquid-liquid systems.

My thanks extend to our group's frequent collaborators Shawn Taylor and Orlando Castellanos who showed their true worth by always asking insightful questions that helped guide my research.

This list wouldn't be complete without including the late Marco Satyro, one of the best teachers that I've ever had and a major influence on my decision to attend graduate school. His constant enthusiasm, humour, love for life, and brilliance has touched everyone he's worked with. His sudden death left a hole in our team that will be difficult to fill.

Thanks to the NSERC Industrial Research Chair in Heavy Oil Properties and Processing, Shell Canada, Schlumberger, Suncor, Petrobras, Nexen, and Virtual Materials Group for funding this project.

Special thanks to Apostolos Kantzas, Franck Diedro and John Bryan for providing the CT data used to test my mathematical model. Thanks also to John Shaw for his help in developing the concentration dependent diffusivity correlation.

Finally, I need to thank my friend and family for putting up with me over the course of my degree. My parents Barbara and Bill and my brother, Mike, have always been supportive and, much like my friends, have been exceedingly patient these past few months while I've avoided any sort of personal interaction for the sake of finishing this thesis.

Also: Kim,

LIST OF TABLES

LIST OF FIGURES

LIST OF SYMBOLS

Upper Case Symbols

A :Proportionality constant in Equation 2.26

:Proportionality constant in Equation 2.27

:Proportionality constant in Equation 4.27

:Proportionality constant in Equation 4.28

:Proportionality constant in Equation 4.29

:Constant of integration in Equation 5.7

A^{∞} :Proportionality constant in Equation 6.2

A_0 :Fitting parameter for dilute gas viscosity equation (equation 4.54) [mPa.s]

:Constant in Equation 6.6

A_c :Cross sectional area [m^2]

A_{AB} :Constant in Margules Equation (2.43)

A_N :Solvent specific parameter in equation 6.29

A_p :Constant in Equation 6.9

A_S :Constant in Equation 6.8

A_T :Constant in Equation 6.7

B^* :Parameter in effective density correlation [kg/m^3MPa]

B_0 :Fitting parameter for dilute gas viscosity equation (equation 4.54) [mPa.s/K]

B_p :Constant in Equation 6.9

B_S :Constant in Equation 6.8

C_0 :Fitting parameter for dilute gas viscosity equation (equation 4.54) [$mPa.s/K^2$]

C_1 :Parameter in vapour pressure correlation (equation 5.5)

C_2 :Parameter in vapour pressure correlation (equation 5.5)

C_3 :Parameter in vapour pressure correlation (equation 5.5)

C_4 :Parameter in vapour pressure correlation (equation 5.5)

C_5 :Parameter in vapour pressure correlation (equation 5.5)

C_s :Concentration of solvent in numerical model [g/cm3]

C_1^* :Parameter in extrapolated vapour pressure equation (equation 5.6)

C_2^* :Parameter in extrapolated vapour pressure equation (equation 5.6)

C_3^* :Parameter in extrapolated vapour pressure equation (equation 5.6)

D :Diffusivity in numerical model [cm^2/s]

D_{AB} :Diffusivity of species *A* in *B* [m^2/s]

$\overline{D}_{AB}$:Maxwell-Stefan diffusivity [m^2/s]

D_{AB}^0 :Infinite dilution diffusivity of species A in B

D_{sb}^{∞} :Infinite dilution diffusivity of solvent in bitumen

D_{sb}^* :Infinite dilution diffusivity of bitumen in solvent

D_A^* :Self-diffusivity of species *A*[m^2/s]

H :Henry's constant

H_b^{Vap} :Heat of vaporization of bitumen [J/mol]

K :Constant in equation 2.12

K_1 :Constant in equation 2.13

K_2 :Constant in equation 2.14

K_3 :Constant in equation 2.14

K_A :K-Value of species *A*

L :Stability limit in numerical model

M_A :Molecular weight of species *A*

N :Avogadro's number

P :Pressure [kPa]

P_c :Critical Pressure [kPa]

$P_{v,A}$:Vapour pressure[kPa]

P_i^* :Hypothetical vapour pressure [Pa]

P_N :Normalized pressure

R :Ideal gas constant [J/kmol.K]

R_A :Radius of diffusing particle[m]

S :Slope

SG :Specific gravity

T :Temperature [K]

T_b :Normal boiling point [K]

T_c :Critical temperature [K]

T_r :Reduced temperature

V :Volume [cm^3]

V_A :Standard liquid molar volume of species *A* [cm^3/mol]

V_{mix} :Volume of the oil-solvent mixture[cm^3]

Z :Compressibility factor

Z_j Compressibility factor of phase j

Lower Case Symbols

a :Number of nearest neighbours

:Fluid specific parameter in Peng-Robinson equation (2.46)

:Parameter in Henry's constant

a_1^* :Fluid specific parameter in effective density correlation [kg/m^3]

a_2^* :Fluid specific parameter in effective density correlation [kg/m^3K]

a_A :Activity of component *A*

b :Number of nearest neighbours in the same layer

:Fluid specific parameter in Peng-Robinson equation (2.46)

:Parameter in Henry's constant

b_1 :Fluid specific parameter in equation 2.52

b_2 :Fluid specific parameter in equation 2.52

b_3 :Fluid specific parameter in equation 2.52

b_4 :Fluid specific parameter in equation 2.52

b_1^* :Fluid specific parameter in effective density correlation [kg/m^3MPa]

b_2^* :Fluid specific parameter in effective density correlation[kg/m^3MPa.K]

c :Parameter in pressure dependant Henry's constant

c_2 :Fluid specific parameter in Expanded Fluid viscosity model

c_3 :Fluid specific parameter in Expanded Fluid viscosity model

c_A :mass concentration of component *A* [kg/m^3]

$c_{A,Pi}$:Solubility of component *A* at initial system pressure [kg/m^3]

$c_A{}^*$:Molar concentration of component *A* [$kmol/m^3$]

c_s :Solvent concentration[kg/m^3]

$c_{s\,eq}$:Concentration of solvent in saturated oil [kg/m^3]

c_{s-int} :Concentration immediately above the interface [kg/m^3]

c_{s0} :Initial solvent concentration [kg/m^3]

f_i^j :Fugacity of species *i* and phase j [kPa]

Δh :Element thickness in numerical model [cm]

h :Height [m]

h_{oil} :Height of oil column [cm]

$\overrightarrow{J_A}$:Mass flux of component *A* [kg/m^{2}s]

$\overrightarrow{J_A{}^*}$:Molar flux of component *A* [kmol/m^{2}s]

k :Boltzmann constant [m^{2}kg/s^{2}K]

:Mass transfer coefficient [m/s]

m :mass diffused [kg]

:Constant in equation 2.36

:Constant in equation 2.37

:Constant in equation 6.20

m_b :mass of bitumen in element [g]

m_{oil} :Mass of oil[g]

$m_s(t)$:Mass of solvent dissolved at a given time [g]

$m_{s,corr}$:Corrected solvent mass diffused [g]

$m_{s,shifted}$: Mass of solvent diffused corrected through the origin [g]

n :Constant specific to the diffusing species

n_0 :Constant in Equation 6.6

n_A :Number of molecules of species A

n_T :Constant in Equation 6.7

n_S :Constant in Equation 6.8

n_p :Constant in Equation 6.9

r_A :Rate of mass of *A* added by reaction per unit volume [kg/m³s]

$r_A{}^*$:Rate of moles of *A* added by reaction per unit volume [kmol/m³s]

r_{leak} :Leak rate from diffusion apparatus [g/min]

t :Time [s]

$\vec{v}$:Mass averaged velocity [m/s]

$\overrightarrow{v^*}$:Molar averaged velocity [m/s]

v_A :Molar volume of species *A*[m^3/mol]

w_A :Mass fraction (weight fraction)

w_{sol} :Solubility in mass fraction

$w_{s,ave}$:Average mass fraction of solvent

x_A :Mole fraction of *A* in liquid phase

y_A :Mole fraction of *A* in vapour phase

y :Dependant variable

z :Position [m]

z_0 :Position of interface [m]

z_f :Constant in equation 2.12

Greek Symbols

α :Thermodynamic correction factor

:fluid specific parameter in Peng-Robinson equation

β_{sb} :Binary interaction parameter between solvent and bitumen in density equation

β_{sb}^{298} :Binary interaction parameter between solvent and bitumen at 298 Kelvin

β :Parameter in Expanded Fluid viscosity model

δ_{ij} :Parameter in mixing rule for dilute gas viscosity

ξ_{AB} :Coefficient of friction between components *A* and *B*

γ_A :Activity coeffiecient of species *A.*

μ :Viscosity [Pa.s]

μ_b :Bitumen viscosity

μ_B :Viscosity of component *B* [Pa.s]

μ_D :Dilute gas viscosity [mPa.s]

μ_{mix} :Viscosity of mixture [mPa.s]

μ_s :Effective viscosity of solvent [mPa.s]

η_A :Chemical potential of species *A* [J/kmol]

η_{A0} :Reference chemical potential of species A [J/kmol]

Φ :Association factor

ϕ_A :Volume fraction of species *A*

φ_A^j :Fugacity coefficient of species *A* in phase *j*

ψ_{AB} :Friction coefficient between components *A* and *B*

θ_{sb} :Binary interaction parameter between solvent and bitumen in EF viscosity model

ρ :Mass density [kg/m^3]

ρ^* :Molar density [kmol/m^3]

ρ_b :Density of bitumen[g/cm^3]

ρ_e :Effective density [kg/m^3]

ρ_{e0} :Parameter in effective density correlation [kg/m^3]

ρ_s :Effective density of solvent [g/cm^3]

ρ_s^0 :Compressed state density [kg/m^3]

ρ_s^* :Parameter in Expanded Fluid viscosity model [kg/m^3]

ρ_{mix} :Density of element in numerical model [g/cm^3]

$\rho_{mix,ave}$:Average density of the solvent oil mixture [g/cm^3]

ω : Acentric factor

Superscripts

j :An arbitrary phase

:Time coordinate index in numerical models

298 :AT 298 Kelvin

* :Infinite dilution of bitumen in solvent

∞ :Infinite dilution of solvent in bitumen

Subscripts

A :An arbitrary component

B :An arbitrary component

b :Bitumen

diff :In the diffusion cell

l :Liquid phase

mix :Of a mixture

n :Position coordinate index in numerical models

s: Solvent

v :Vapour phase

supply :In the supply cylinder

0 :At the initial state

Abbreviations

CSS : Cyclic Steam Stimulation

SADG : Steam Assisted Gravity Drainage

VAPEX: Vapour Extraction

ES-SAGD: Expanded Solvent Steam Assisted Gravity Drainage

LASER: Liquid Addition to Steam for Enhanced Recovery

SAS : Steam Alternating Solvent Process

SAP : Solvent Assisted Process

NMR : Nuclear Magnetic Resonance

PVT : Pressure Volume Temperature

GC : Gas Chromatograph

CT : Computer Tomography

CCE : Constant Composition Expansion

DPDVA: Dynamic Pendant Drop Volume Analysis

CHAPTER ONE: INTRODUCTION

Heavy oils and bitumens are defined as oils with a specific gravity below 20 and 10 °API, respectively (Dusseault, 2001) and they account for up to 70% of the Earth's oil reserves (Alazard and Montadert, 1993). Canadian oil sands and heavy oil deposits are estimated to be over 290 billion cubic meters. Over 95% of these reserves are in Alberta and the remaining, currently recoverable, mineable oil sands and *in situ* heavy oil reserves as of 2014 are estimated to be 26.4 billion cubic meters, placing Alberta third only to Venezuela and Saudi Arabia in established reserves (ERCB, 2015).

Heavy oils and bitumens are substantially more viscous than their conventional counterparts. The viscosity of conventional oils is rarely above 10 mPa.s while the viscosity of bitumen can be over 1 million mPa.s at room temperature. High viscosity heavy oils and bitumens are essentially immobile at reservoir conditions and therefore cannot be produced by conventional methods. Instead, commercial *in situ* recovery processes employ steam injection to reduce the oil viscosity so that it can be produced. Commercially proven thermal methods include cyclic steam stimulation (CSS), steam flooding, and steam assisted gravity drainage (SAGD) (Butler, 1997). Although these processes can achieve high oil recovery, they are energy and water intensive.

As an alternative, solvent injection processes have been proposed where the viscosity is reduced by dilution with the solvent including the vapor extraction process (VAPEX) and the NSolv process. Solvent based methods are of interest because they do not require water and they can decrease the energy consumed to as little as 3% of SAGD for the same production rate (Upreti *et al*., 2007). VAPEX is the solvent vapor analog to the thermal SAGD method and was first proposed by Butler and Morkys (1989). It has not yet been implemented successfully in the field. The N-Solv process is similar to VAPEX but involves injecting a heated solvent vapor that condenses at the solvent/bitumen interface. The oil viscosity is reduced by the combined thermal effect of from the condensing solvents and dilution effect of dissolving solvent in oil (Nenniger, 2012).

Another alternative is to combine solvent and thermal methods to reduce the oil viscosity by both heat and dilution. These processes also can reduce the water and energy requirements to recover the oil. Several solvent-assisted steam based processes have been proposed including Expanded Solvent SAGD (ES-SAGD) (Nasr and Ayodele, 2006), Liquid Addition to Steam for Enhanced Recovery (LASER) (Leute, 2002), the Steam Alternating Solvent Process (SAS) (Zhao, 2004), and the Solvent Aided Process (SAP) (Gupta et al., 2002, 2003).

A key parameter in the design of each of the solvent based and solvent assisted process is the diffusivity of the solvent in the heavy oil or bitumen. The diffusivity of solvent *s* in heavy oil or bitumen *b* is defined via Fick's First Law of Diffusion (Bird *et al.*, 1987) given by:

$$\vec{J_s} = -\rho D_{sb} \frac{dw_s}{dz} \tag{1.1}$$

where D_{sb} is the diffusivity (the proportionality constant between the mass flux of the diffusing solvent, j_s, and the concentration gradient of the diffusing solvent, $\rho dw_s/dz$), ρ is density, w is mass fraction, and z is distance. Equation 1.1 is applied in reservoir simulations to predict the rate at which solvent dissolves into heavy oil or bitumen. The diffusivity is modified for diffusion in porous media to account for dispersion effects (Boustani and Maini, 2001) but the starting point is the diffusivity of the solvent vapor (or liquid) in the oil.

Diffusivity of solvent gases in heavy oil has been studied using many different experimental techniques and modelling approaches. Although the basis for most diffusion experiments is simple, the measurement of diffusivity is often time consuming because of the rates at which diffusion processes occur. As a result, few large datasets that have been collected and fewer attempts have been made to correlate the results.

Several theoretical models have been developed to describe diffusion but these models are only valid under specific conditions and are unsuitable for solvent-heavy oil applications. Most theoretical models show that the diffusivity is inversely proportional to the viscosity of the mixture, although the exact relationship is not known. This relationship is the basis of most

correlations for diffusivity. However, many of the available correlations such as the Wilke and Chang (1955) and Hayduk and Minhas (1982) equations were developed for infinite dilution diffusivity. These correlations are unsuitable for solvent/oil systems where solvent concentrations are relatively high.

An alternative to the viscosity based correlations is the Vignes (1966) equation which is commonly used to model concentration dependent diffusivity. The Vignes equation is a mixing rule of the infinite dilution diffusivities of the two components in each other as liquids. Neither of these infinite dilution diffusivities have been widely measured or correlated for solvent-heavy oil systems.

Despite studying a limited range of conditions, a relationship between diffusivity and viscosity of the solvent-bitumen mixture was developed by Das and Butler (1996) to model the concentration dependent diffusivity of propane in Peace River bitumen. Upreti and Mehrotra (2002) measured the concentration dependence of diffusivity in several solvents (including methane and ethane) in Athabasca bitumen and developed a relationship that modeled the temperature dependence of the average diffusivity.

Much of the available literature studying the diffusivity in solvent-bitumen systems is focused on the development of experimental methods and the mathematical models used to fit the diffusivities. Therefore, there is a need for data sets large enough to develop a predictive correlation.

1.1 Objectives

The overall objectives of this thesis are to measure diffusivities of light *n*-alkanes in a Western Canadian bitumen and to develop a model that describes the diffusion of hydrocarbon gases into heavy oil and bitumen. This model is to include the swelling of the oil, a predictive correlation for diffusivity, the solutions to the continuity equation for systems with simple geometry, and methods of predicting the required physical properties and parameters required for a fully defined model. The specific objectives are as follows:

1. Build a pressure decay based diffusion apparatus and commission the experiment by comparing the diffusivity results for binary mixtures with literature data
2. Measure mass transfer rates of methane, ethane, and propane in bitumen at temperatures from 40 to 180°C.
3. Measure the solubility and saturation pressure of these gases in bitumen over the same temperature range using the diffusion apparatus and validate these results against independently measured saturation pressures from constant composition expansion experiments. Develop solubility correlations that can be used to predict the solubility for use in the diffusion model.
4. Develop a mass transfer model that can be used to predict the swelling of the oil and the solvent concentration profiles in the oil without a direct measurement. The model will be tested against swelling and concentration profiles of solvent oil mixtures measured using computer tomography.
5. Analyze the measured diffusion data with several models for the concentration dependence of the diffusivity. Develop correlations for the parameters of these models for each solvent gas and generalize these parameters for all the gases studied

1.2 Thesis Structure

This thesis is divided into seven chapters including this introduction. The content of the subsequent chapters is outlined below.

Chapter 2 reviews the current theoretical approaches to predict diffusivity in binary liquid mixtures. As none of these approaches are capable of describing liquid diffusion, commonly used correlations are discussed. Methods of modeling solubility are also presented. Published diffusivities and solubilities of hydrocarbon gases in heavy oils are summarized.

Chapter 3 describes in-house diffusivity apparatus and the blind PVT cells used to measure saturation pressure and solubility. The chemicals and materials required and the oil pretreatment procedure are described. The processing of the experimental mass transfer data into a simply modeled form is discussed. The tests used to commission the diffusivity apparatus are presented.

Chapter 4 summarizes the techniques used to model the diffusion experiments and determine the diffusivity of solvent gases in bitumen. Both analytical and numerical approaches are discussed. Calculation methods for density and viscosity required to model oil swelling and the concentration dependence of the diffusivity are also presented.

Chapter 5 presents the results from saturation pressure and solubility experiments. The approaches to modeling saturation pressure are developed and the models are fitted to the experimental data.

Chapter 6 presents the results from the diffusivity experiments. Results for both constant and concentration dependent diffusivities are discussed and correlations for both diffusivity models are developed.

Chapter 7 summarizes the major results and conclusions from this thesis and provides recommendations for future work in this area.

CHAPTER TWO: LITERATURE REVIEW

In this chapter, a brief summary of diffusion theory is provided including the mathematical framework for modeling mass transfer and the estimation of diffusivity through liquids. Common methods for measuring the diffusion of dissolved gases in liquids, particularly gaseous hydrocarbons in oils, are presented. The measurement and modeling of solubility and bubble point pressure are also discussed.

2.1 Mathematical Framework for Diffusion Processes

There is no established theoretical approach to predict the diffusivity of liquids. However, a framework can be created to model diffusion processes based on continuity equations and semi-empirical relationships for diffusivity. This section briefly reviews the basic equations of diffusion, the concept of a chemical potential driving force, and the approaches to solving the diffusion equations.

2.1.1 Continuity Equation

The continuity equation is a mass balance that accounts for mass transferred in and out of a control volume through, flow, diffusion, and reaction. It is given by (Bird *et al.*, 2007):

$$\frac{\partial c_A}{\partial t} = -\nabla(c_A\vec{v}) - \nabla(\overrightarrow{J_A}) + r_A \tag{2.1}$$

where c_A is the concentration in kg/m³ of the diffusing component *A*, *t* is time in s, $\vec{v}$ is the mass averaged velocity in m/s, r_A is the rate of mass addition per unit volume due to reaction in kg/m³s, $\overrightarrow{J_A}$ is the mass flux in kg/m²s, and ∇ is the gradient operartor with respect to position. The mass flux is defined by Fick's first law given previously in Equation 1.1. For a constant density, Equation 1.1 reduces to the following:

$$\overrightarrow{J_A} = -D_{AB}\nabla(c_A) \tag{2.2}$$

where D_{AB} is the mutual diffusion coefficient or diffusivity in m^2/s. Equations 2.1 and 2.2 can be rewritten on a molar basis as follows:

$$\frac{\partial c_A{}^*}{\partial t} = -\nabla\left(c_A{}^*\overrightarrow{v^*}\right) - \nabla\left(\overrightarrow{J_A{}^*}\right) + r_A{}^* \tag{2.3}$$

$$\overrightarrow{J_A{}^*} = -D_{AB}\nabla(c_A{}^*) \tag{2.4}$$

where $c_A{}^*$ is the molar concentration in kmol/m³, $\overrightarrow{v^*}$ is the molar average velocity in m/s, $\overrightarrow{J_A{}^*}$ is the molar flux in kmol/m²s and $r_A{}^*$is the rate of moles of *A* added by reaction per unit volume in kmol/m^{3}s. In systems without reactions or bulk flow and where the mass flow from diffusion is limited to one dimension, Equation 2.1 simplifies to:

$$\frac{\partial}{\partial z}\left(D_{AB}\frac{\partial c_A}{\partial z}\right) = \frac{\partial c_A}{\partial t} \tag{2.5}$$

where *z* is position in m. If the diffusivity is constant, Equation 2.5 simplifies to Fick's second law, given by:

$$D_{AB}\frac{\partial^2 c_A}{\partial z^2} = \frac{\partial c_A}{\partial t} \tag{2.6}$$

2.1.2 Diffusion with a Chemical Potential Gradient

Strictly speaking the driving force for diffusion is not the concentration gradient used in Equation 2.4 but rather the chemical potential gradient which is related to the molar flux as follows (Koojiman and Taylor, 1991; Bird *et al.*, 2007; Ghai *et al.* 1973):

$$\overrightarrow{J_A{}^*} = -\frac{\rho^*\overline{D}_{AB}x_A}{RT}\nabla_{T,P}\eta_A \tag{2.7}$$

where ρ^* is the total molar density in kmol/m^3, *T* is the temperature in K, *R* is the gas constant in J/kmol.K, x_A is the mole fraction of the diffusing species, η_A is the chemical potential of component *A* in J/kmol, and $\overline{D}_{AB}$ is referred to as the Maxwell-Stefan diffusivity (Koojiman and Taylor, 1991) or simply the corrected diffusivity (Ghai *et al.*, 1973 in m^2/s). The chemical potential is often defined in terms of a reference potential as follows:

$$\eta_A = \eta_{A0} + RT \ln(a_A) \tag{2.8}$$

where η_{A0} is the chemical potential at a reference state in J/kmol and a_A is the activity of component A. Equation 2.8 is substituted into Equation 2.7 to obtain the following equation for molar flux:

$$\overrightarrow{J_A{}^*} = -\overline{D}_{AB}\left(\frac{d \ln a_A}{d \ln x_A}\right)\nabla(c_A{}^*) \tag{2.9}$$

Equations 2.9 and 2.4 can be combined to obtain the following relationship relating the mutual diffusivity to the Maxwell Stephen Diffusivity:

$$D_{AB} = \overline{D}_{AB}\left(\frac{d \ln a_A}{d \ln x_A}\right) = \overline{D}_{AB}\alpha \tag{2.10}$$

where α is referred to as the thermodynamic correction factor and is equal to unity for a pure component. This correction factor can become significant in systems with large variations in composition and is often included in models for the diffusivity in systems at high concentration.

2.1.3 Solving the Continuity Equation

Solutions to the continuity equation can vary substantially depending on the type of system, geometry, and initial conditions. Nonetheless, all solutions to the continuity equation require one initial condition and two boundary conditions for each spatial dimension modeled. The initial condition used to model most of the systems of interest in this thesis is zero initial concentration of the diffusing gas; that is:

$$c_A(z, t = 0) = 0 \tag{2.11}$$

For gas-liquid systems, it is common to apply boundary conditions at the gas-liquid interface and at the surfaces of the container, as these are areas where there the most information about the system is known. The three main categories of boundary conditions are the Dirichlet, Neumann,

and Robin (or Cauchy) conditions. The Dirichlet condition directly specifies the value of the variable at the boundary and is expressed as follows:

$$c_A(z = z_0, t) = K \tag{2.12}$$

where z is the spatial variable and t is time. The constants z_0 and K are the values of z and c_A at the boundary. The coordinate system used to model the diffusion process in this thesis is defined such that $z_0 = 0$ at the interface. The Neumann boundary condition specifies the value of the variable's derivative at the boundary and generally has the form:

$$\frac{dc_A}{dz}_{z=z_0} = K_1 \tag{2.13}$$

where K_1 is a constant. The Robin boundary condition is a linear combination of the Neumann and Dirichlet conditions defined as follows:

$$\frac{dc_A}{dz}_{z=z_0} + K_2 c_A(z = z_0, t) = K_3 \tag{2.14}$$

where K_2 and K_3 are constants.

With a fully defined mathematical model, solutions to the continuity equation can be obtained and matched to experimental data. The direct solution of the model is a series of concentration profiles that are a function of position and time. However, few experiments provide a direct measurement of the concentration profile. For example, in this thesis, the mass that diffuses over time through a fixed cross-sectional area is measured. This mass rate is calculated from the concentration profiles using Fick's Law as follows:

$$\frac{dm}{dt} = -A_c D_{AB} \left(\frac{\partial c_A}{\partial z}\right)_{z=0} \tag{2.15}$$

where m is the total mass diffused in kg and A_c is the cross-sectional area of the diffusion cell in m^2. The mass diffused at a given time is determined by integrating this equation to the desired time:

$$m(t) = -A_c D_{AB} \int_0^t \left(\frac{\partial c_A}{\partial z}\right)_{z=0} dt \tag{2.16}$$

This result is equivalent to integrating the concentration profiles with respect to position for each time as follows:

$$m(t) = A_c \int_0^h c_A dz - A_c \int_0^{h_0} c_{A0} dz \tag{2.17}$$

Where h_0 is the initial height of the liquid in m and c_{A0} is the initial concentration profile of *A*. One method may prove superior to the other depending on the nature of the solution of the continuity equation. For simpler equations and boundary conditions, analytical solutions can be obtained. As the equation or boundary conditions become more complicated, it is likely that a numerical solution will be required to match the data. Some analytical and numerical solutions for the systems considered in this thesis are presented in Chapter 4.

2.2 Models for Diffusivity

2.2.1 Theoretical Models

A review of the four major theoretical approaches to liquid diffusion was presented by Ghai *et al*. (1973). These approaches are: the Stokes-Einstein relation, the Darken and Hartley-Crank approach, Erying's theory, the friction coefficient approaches of Lamm, Bearman and Kirkwood, and kinetic theory. These theories can be applied to predict liquid diffusivity for ideal solutions but become invalid as the solution becomes less ideal.

Stokes-Einstein Equation

The Stokes-Einstein relationship is given by the following equation Einstein (1956):

$$D_{AB} = \frac{kT}{4\pi R_A \mu_B}$$

(2.18)

where k is the Boltzmann Constant in m^2kg/s^2K, R_A is the radius of the diffusing particle in m, and μ_B is the viscosity of the continuous phase in Pa.s. This model is only applicable to spherical molecules diffusing through liquids of much smaller molecules.

Darken and Hartley-Crank Equations

The Darken (1948) equation was originally developed for diffusion in molten metals and relates the diffusivity of the mixture to the self-diffusivity of the two components mixed linearly by mole fraction.

$$D_{AB} = (D_A^* x_B + D_B^* x_A)\left(\frac{d \ln a_A}{d \ln x_A}\right) \tag{2.19}$$

where D_i^* is the self-diffusivity of species i. Following a similar approach to Darken, Hartley and Crank (1949) developed the following expression that predicts the mutual diffusion coefficient with a volume weighted average of the self-diffusivity.

$$D_{AB} = (D_A^* \phi_B + D_B^* \phi_A)\left(\frac{d \ln a_A}{d \ln x_A}\right) \tag{2.20}$$

where ϕ_i is the volume fraction of component i. Self-diffusion data are rarely available so Equation 2.19 is commonly written in terms of the infinite dilution diffusivity (Reid *et al.*, 1987) as follows:

$$D_{AB} = (D_{AB}^0 x_B + D_{BA}^0 x_A)\left(\frac{d \ln a_A}{d \ln x_A}\right) \tag{2.21}$$

where D_{ij}^0 is the infinite dilution diffusivity of component i in j.

Carman and Stein (1956) developed an alternative to Equation 2.21 that includes the viscosity of the components and the mixture.

$$D_{AB} = \frac{(D_{AB}^{0} x_B \mu_B + D_{BA}^{0} x_A \mu_A)}{\mu_{mix}} \left(\frac{d \ln a_A}{d \ln x_A}\right) \tag{2.22}$$

Predictions of diffusivity from these models work well for ideal systems but cannot accurately predict the diffusivities of binary systems where the molecules are of substantially different size or shape.

Eyring Theory

Eyring's theory models the diffusion process as an activated rate process. The theory is best applied in dilute or ideal solutions with a uniform concentration. Li and Chang (1955) applied this theory to a fluid with simple cubic packing to achieve the following expression for the infinite dilution diffusivity:

$$D_{AB} = \frac{kT}{\mu_B} \left(\frac{a-b}{2a}\right) \left(\frac{N}{v_A}\right)^{1/3} \tag{2.23}$$

where a is the number of nearest neighbors in total, b is the number of nearest neighbors in the same layer, N is Avogadro's Number and v_A is the molar volume of A. For a simple cubic molecular arrangement (a=6, b=4), this equation is simplified to

$$D_{AB} = \frac{kT}{6\mu_B} \left(\frac{N}{v_A}\right)^{1/3} \tag{2.24}$$

Equation 2.24 can be shown to be $6/2\pi$ of the value from the Einstein-Stokes equation.

Lamm-Dullien Theory

This theory, originally proposed by Lamm (1943, 1944), assumes that diffusion is governed by the friction between molecules (Ghai *et al.*, 1973). The original approach was to relate the chemical potential gradient to the relative velocity of the diffusing component with a friction coefficient as the constant of proportionality. The resulting equation for diffusivity is given by Dullien (1963):

$$D_{AB} = \frac{RT}{\psi_{AB} + \psi_{BA}} \left(\frac{d \ln a_A}{d \ln x_A} \right) \tag{2.25}$$

where ψ_{ij} is the friction coefficients between molecules *i* and *j* per mole of *i*. The friction coefficients in this model are not measurable or related to a measurable quantity and cannot easily be applied to binary systems.

Statistical-Mechanical Approach

Statistical mechanics has been applied to model diffusivities in gases by Chapman and Cowling (1970). Bearman (1960, 1961) substantially advanced this approach and developed the following expression for the diffusivity:

$$D_{AB} = \frac{kTV_m}{\xi_{AB}} \left(\frac{d \ln a_A}{d \ln x_A} \right) \tag{2.26}$$

where $\xi_{AB}$is the coefficient of friction between *A* and *B*. Bearman (1960) showed that this was equivalent to Lamm's Equation (Equation 2.25), and subject to the same limitations. With some simplifying assumptions to the form of the friction coefficients, Bearman (1961) was able to derive the Darken Equation (Equation 2.19).

Kinetic Theory

Arnold (1930) applied the kinetic theory of gases to model liquid diffusion, assuming that the only resistance to diffusion arises from the collision of molecule pairs. The diffusivity predicted with this approach has the following form:

$$D_{AB} = \frac{A}{\mu^{1/2}} \tag{2.26}$$

where *A* is a proportionality constant. Although this model is not commonly applied directly, some empirical correlations have a similar form.

2.2.2 Practical Diffusivity Models

Since no current theory adequately captures the nature of diffusion, empirical and semi-empirical correlations are often used to predicted liquid diffusivity.

Dilute Systems

In many circumstances, particularly in dilute systems, a constant diffusivity is sufficient to model diffusion. In dilute systems, the constant diffusivity is taken as the infinite dilution diffusivity. Correlations for the infinite diffusivity are often based on the work of Hayduk and Cheng (1971) who correlated diffusivity to the viscosity of the continuous phase as follows:

$$D_{AB}^{0} = \frac{A}{\mu^{n}} \tag{2.27}$$

where D_{AB}^{0} is the infinite dilution diffusivity in m^2/s, and μ is the viscosity of the continuous phase in mPa.s, and *A* and *n* are dependent only on the properties of the diffusing component.

Two commonly used correlations for liquids of low viscosity (Reid *et al*., 1987) are the Wilke and Chang (1955) equation, given by:

$$D_{AB}^{0} = \frac{7.4 * 10^{-8}\sqrt{\phi \mathrm{M}_B}T}{\mu_B V_A^{0.6}} \tag{2.28}$$

and the Hayduk and Minhas (1982) equation, given by:

$$D_{AB}^{0} = \frac{13.3 * 10^{-8}T^{1.47}\mu_B^{\left(10.2/V_A - 0.791\right)}}{V_A^{0.71}} \tag{2.29}$$

where M_B is the molar mass of the continuous phase in g/mol, V_A is the standard liquid molar volume of the diffusing species in cm^3/mol, ϕ is a dimensionless association factor equal to unity for non-associating systems and D_{AB}^{0} is the infinite dilution diffusivity in cm^2/s. Values for associating systems are listed in Reid *et al.* (1987).

Non-Dilute Systems

To accurately model diffusion in non-dilute systems, the diffusivity cannot be considered a constant that is invariant with composition (Reid *et al.*, 1987). Many theories and models have been adapted and developed to try and model the compositional dependence of diffusivity. In many cases, the departure from the infinite dilution diffusivity is assumed to be proportional to the thermodynamic correction factor described in Equation 2.10 (Bird *et al.* 1987). For example, the Bearman equation (Bird *et al.*,1987; Bearman 1961) was adapted from a simplified model to predict concentration dependent diffusivities of ideal regular solutions, and is given by:

$$\frac{D_{AB}\mu_{mix}}{(D_{AB}\mu_{mix})_{x_A\to 0}} = \left[1 + x_A\left(\frac{V_A}{V_B} - 1\right)\right]\left(\frac{d\ln a_A}{d\ln x_A}\right) \tag{2.30}$$

Vignes (1966) proposed the following model:

$$D_{AB} = (D^0_{AB})^{x_B}(D^0_{BA})^{x_A}\left(\frac{d\ln a_A}{d\ln x_A}\right) \tag{2.31}$$

The Vignes equation was shown to work very well for ideal systems, but should be used cautiously for non-ideal systems, particularly when there is molecular association (Ghai *et al.*,1973; Dullien, 1971). One limiting factor of the concentration dependent models listed above is that they all require the thermodynamic correction factor as an input. This derivative can be difficult to obtain for systems where there is limited or no available thermodynamic data.

Upreti and Mehrotra (2002) investigated the concentration dependence of the diffusivity of gas into oil. The authors correlated the average measured diffusivity with temperature using the following equation:

$$\ln D_{AB} = d_0 + d_1(T) \tag{2.32}$$

where D_{AB} is the average diffusivity of the diffusing gas in m^2/s, T is temperature in K, and d_o and d_1 are parameters dependent on the diffusing gas and the pressure.

2.3 Methods to Measure Diffusivity

Unlike many other physical properties, there are no standard methods for determining the diffusivity of one substance in another. In general, diffusion measurement methods fall into two major categories: direct methods and indirect methods (Sheikha *et al.*,2005). Direct methods measure the concentration profile of solvent in the oil and this profile is used to determine the diffusivity. In general, direct methods are relatively expensive and are often intrusive (Etminan *et al.*,2010).As a result many indirect methods have been developed to measure the diffusivity. Indirect methods measure another parameter, such as a pressure drop or the volume change of the oil, and do not require a measured concentration profile to determine the diffusivity. Some indirect methods have been adapted or specifically designed to measure the diffusivity of a gas in a liquid. The indirect and non-intrusive direct methods that have been applied to solvent-heavy oil systems are discussed below.

2.3.1 Non-Intrusive Direct Methods

Nuclear Magnetic Resonance

Proton nuclear magnetic resonance (NMR) is a technique that measures the response of hydrogen nuclei to a magnetic field. Because the concentration and orientation of the hydrogen nuclei in the oil and solvent are different, it is expected that these two materials have a different response to the NMR. Hence, the concentration at any location can be calibrated to the concentration of the solvent. To apply this method, an oil sample is placed in a container and a solvent gas is injected above the oil. The NMR response of the liquid phase is measured at a series of depths. The solvent concentration profile is determined from the calibrated NMR response at each depth at a known value of elapsed time after the start of diffusion. Then, the diffusivity is calculated by fitting a diffusion model to the profile. NMR techniques for determining diffusivity have been successfully implemented by several researchers (Wen *et al.*,2005a; Wen *et al*., 2005b; Afashi and Kantzas, 2007)

X-Ray Tomography

The attenuation of x-rays is related to the density of the medium and x-ray tomography is a method to measure density profiles within a medium. To use this technique to obtain diffusivity, an experiment is set up in a similar fashion to the NMR method. X-ray images are taken at a

series of depths over time and the density profiles are determined from a calibration. The density profile is converted into a concentration profile based on the known relationship between the solvent concentration and the oil phase density. X-ray tomography has been successfully applied to measure diffusivity by several authors (Guerrero-Aconcha and Kantzas, 2009; Guerrero-Aconcha *et al.*, 2008; Luo *et al.*, 2007; Luo and Kantzas, 2011, Song *et al*., 2010a; Song *et al*., 2010a; Diedro *et al.* 2015).

Light Absorption

Concentration profiles of solvent in heavy oil can be obtained by measuring the light absorption of the oil column. To implement this method, a thin glass cell is placed between a light source and the light detector. The cell is charged with a heavy oil sample and solvent is injected above the oil. The light absorption of the mixture changes as the solvent diffuses into the oil. After calibration with prepared solutions, the light absorption gradient is converted into a concentration profile. This method has been used for liquid-liquid diffusion (toluene in bitumen) by Oballa and Butler (1989). The method could be adapted for gaseous solvents if the changes in light absorption with increasing solvent concentration are large enough that an absorption gradient can be measured.

2.3.2 Indirect Methods

Pressure Decay Method

Pressure decay methods measure the amount of gaseous solvent that diffuses into the oil based on the pressure drop in the gas phase. The diffusivity is obtained by fitting the data with a suitable diffusion model. The original pressure decay method was developed by Lundberg *et al.* (1963) for methane in polystyrene and was first applied to hydrocarbon systems by Riazi (1996). The method has also been modified to simplify the analysis by maintaining a constant pressure above the oil. Gas is injected into the sample cell to compensate for the solvent which diffuses into the oil (Etminan *et al*., 2010). The mass of the injected gas is measured over time to determine the amount of diffused gas.

Volume Change Method

Volume change methods determine the diffusivity by measuring the oil swelling that occurs when a solvent dissolves into oil. The volume change measurement is usually achieved by tracking the gas-liquid interface in a system constrained to move in one direction. Do and Pinczewski (1991) and Jamialahmadi *et al.* (2006) have implemented this type of experiment.

Saturated Solvent Method

James *et al.* (2012) and James (2009) developed a method for determining the diffusion and solubility of hydrocarbon gases in heavy oil. In their experiment, a diffusion cell is charged with bitumen and connected to a cylinder of liquid hydrocarbons at its saturation pressure. As the hydrocarbon vapour diffuses into the oil, the liquid hydrocarbon reservoir will evaporate to maintain its vapour pressure. The decrease in the height of the hydrocarbon reservoir and the height of the swelling oil phase are both tracked and can be related to the total mass dissolved into the oil similarly to the pressure decay and volume change methods. This experiment is limited to the diffusion of gases near their saturation pressure.

Dynamic Pendant Drop Volume Analysis (DPDVA)

In DPDVA experiments (Yang and Gu, 2006, Yang and Gu, 2007), a droplet of heavy oil is injected into a pressurized vessel containing the gaseous solvent. The dimensions of the oil droplet change as the solvent diffuses into the oil. Sequential photograph are taken of the oil droplet over the course of the experiment and the pressure change is recorded. The diffusivity of the solvent in the oil can be determined by analyzing the changing shape of the droplet and the pressure drop with time.

Balance Methods

Marufuzzaman and Henni (2014) use a microbalance to measure the diffusivity of propane in bitumen. The experiment is set up by filling a small sample vessel with a small amount of bitumen on the microbalance. The system is filled with gas and the pressure is maintained over the course of the experiment. As gas dissolves into the oil, the total mass in of the sample vessel will increase giving a direct measurement of the mass diffused with time. The diffusivity is determined by fitting the mass diffusion data as described for the pressure decay method.

Hele-Shaw Cell

Das and Butler (1996) measured the diffusivity propane in Peace River bitumen using a Hele-Shaw cell. The cell consists of two parallel glass plates open only to one side in an isothermal pressure vessel as described in Das and Butler (1994). The space between the plates is filled with the oil sample and the pressure vessel is filled with gas to the desired pressure. As the gas dissolves into the oil it flows out the open side of the plates and the movement of the gas-bitumen interface is monitored with a camera. These data can be used to calculate the oil production rate. The diffusivity can be calculated from this production rate using a VAPEX model.

2.4 Gas Diffusivity in Bitumen

2.4.1 Available Data

Table 2.1 outlines all the available data to date. The gases considered include carbon dioxide, nitrogen, methane, ethane, and propane. Most of the data were collected at temperatures between 20 and 100°C and pressures below 10 MPa. There are relatively few data points at high pressures and temperatures or for propane and butane.

Table 2.1. Data available from the literature for gas diffusivity in bitumen

Author	Solvent	Oil	T (^{o}C)	P (MPa)	Method	Swelling	Conc. Dependent
Upreti and Mehrotra, 2002	CO_2	Athabasca Bitumen	25-90	4-8	Pressure Decay	Yes	Yes
	CH_4						
	C_2H_6						
	N_2						
Sheikha *et al.*, 2005, 2006	CO_2	Athabasca Bitumen	25-90	8	Pressure Decay	No	No
	CH_4						
	C_2H_6						
	N_2						
Etminan *et al.*, 2010	CO_2	Athabasca Bitumen	50-75	3.2-3.8	Constant Pressure	No	No
Etminan *et al.*, 2014b	C_3H_8	McKay River	24	0.4-0.8	Constant Pressure	Yes	No
Yang and Gu, 2006	CO_2	Lloydminster Heavy Oil	24	2-6	DPDVA	Yes	No
	CH_4		24	6-14			
	C_2H_6		24	1.5-3.5			
Yang and Gu, 2007	C_3H_8	Lloydminster Heavy Oil	24	0.4-0.9	DPDVA	Yes	No
Das and Butler,	C_3H_8	Peace River	21-35	0.82-1.16	Hele-	Yes	Yes

1996	C_4H_{10}	Bitumen	35	0.31	Shaw		
Schmidt *et al.*, 1982	CO_2	Athabasca Bitumen	20-200	5	-	-	-
Schmidt *et al.*, 1986	CO_2	Athabasca Bitumen	20-200	5	-	-	-
	CH_4		50	5	-	-	-
	C_2H_6		20-75	5	-	-	-
Fisher *et al.*, 2000	C_3H_8	Athabasca Bitumen	17	-	NMR	No	No
Jamialahmadi *et al.*. 2006	CH_4	Iranian Crude	25,50	3-25	Volume Change	Yes	No
Zhang *et al.*, 2000	CO_2	Heavy Oil (5 Pa s)	21	3.5	Pressure Decay	No	No
	CH_4						
Tharanivasan *et al.*, 2006	CO_2	Lloydminster Heavy Oil	24	3.5	Pressure Decay	No	No
	CH_4		24	4.9			
	C_3H_8		24	0.5			
Zainal *et al.*, 2011	CH4	Heavy Oil (10.4 Pa s)	60	5.5-7.1	Pressure Decay	No	No
	CH4	Heavy Oil (4730 mPa s)	90	6.6-8.9			
James *et al.*, 2012	C_4H_{10}	Athabasca Bitumen	22-26	0.2-0.25	James	Yes	Yes
Marufuzzaman and Henni, 2014	C_3H_8	Cactus Lake Oil (1816 mPa s) and it's SARA fractions	15-30	0.4-0.6	Balance Method	No	No
Diedro *et al.*, 2015	C_3H_8	Peace River Bitumen	22	0.6	CT	Yes	Yes
		Grosmont Bitumen					

2.4.2 Modeling Diffusion Processes

Dilute Conditions

Modeling at dilute conditions is relatively straight forward because the diffusivity is approximately independent of concentration and there is negligible swelling of the liquid phase. Therefore, analytical solutions to the mass transfer can usually be found. The analytical solutions for pressure decay experiments of dilute systems used in this thesis are provided in Chapter 4.

In the pressure decay method of interest for this thesis, research has mainly focused on dilute conditions and the concentration dependence of diffusivity and the effect of swelling have been neglected; for example, the diffusion of methane, carbon dioxide, and nitrogen into oil (Etminan

et al., 2010; Civan and Rasmussen, 2009; Tharanivasan *et al.,* 2006; Tharanivasan *et al.,* 2004; Sheikha *et al.,* 2005; Sheikha *et al.,* 2006; Zhang *et al.,* 2000; Ghaderi *et al.,* 2011; Yang and Gu, 2006). Neglecting swelling has little impact at dilute conditions but may have significant impact for solvents with high solubility in the liquid such as propane in bitumen. Nontheless, several invertigators have chosen to model systems at non-dilute conditions assuming no swelling (Marufuzzaman and Henni,2014; Sheikha *et al.*, 2005; Sheikha *et al.*, 2006 Tharanivasan *et al.,* 2006). In some cases, this assumption was made to maintain a consistent modeling approact to a series of diffusion experiments using different gases. To limit the complexity of the diffusion model, systems of ethane and propane diffusion into oil are often modeled with a constant diffusivity as well (Marufuzzaman and Henni,2014; Sheikha *et al.,* 2005; Sheikha *et al.,* 2006 Tharanivasan *et al.,* 2006; Yang and Gu, 2007 Fisher *et al.,* 2000).

Non-Dilute Conditions

Modeling non-dilute system has proved more challenging because there is the possibility of substantial swelling in the system and at higher concentrations of dissolved gas, the diffusivity is concentration dependent. In general, a numerical solution to the model of the experiment is required to determine the diffusivity.

Swelling and Density

As hydrocarbon gas dissolves into oil, the volume of the oil increases (swells) from the added mass but also because the density of the liquid phase decreases (Saryazdi *et al.* 2013). The mass transfer in a system with swelling is a moving boundary problem because the domain of the mass transfer (for example a liquid column) is changing with time.

Although the density of oil-solvent mixtures is important in developing an accurate model of the system (Luo *et al.* 2007), gas-oil mixtures are often treated as ideal and any excess volume due to mixing is neglected (James *et al.* 2012; Das and Butler, 1996; Wen and Kantzas, 2005; Salama and Kantzas, 2005; Zhang and Shaw 2007, Yang and Gu, 2005; Yang and Gu, 2005). In this case, the swelling (for example, the movement of the gas-liquid interface) is attributed entirely to the mass of gas entering the liquid. Some researchers have accounted for non-ideal behavior by directly measuring the density at different concentrations and including this data in their models

(Guerrero-Aconcha, 2008; Jamialahmadi *et al.*, 2006; Upreti and Mehrotra, 2002) others have included excess volume term in their liquid density model (Luo *et al*. 2007).

Concentration Dependence

As was shown in Section 2.2, the diffusivity at non-dilute conditions is expected to depend on the composition of the mixture. Treating the diffusivity as a variable can dramatically increase the complexity of the model because it changes the continuity equation from a linear to a non-linear partial differential equation. For a system where the gas solubility in the liquid is low, such as methane in oil, the concentration dependence is often omitted because there is too little composition change to significantly alter the diffusivity.

Das and Butler (1996) measured the diffusivity of propane and butane in Peace River bitumen using a Hele-Shaw cell. They matched their VAPEX model to the produced oil data by adjusting the diffusivity. They assumed diffusivity fit the Hayduk-Cheng Equation (Equation 2.29) and proposed the following correlations.

$$D_{C3B} = 1.309 * 10^{-9}\mu^{-0.46} \tag{2.33}$$

$$D_{C4B} = 4.13 * 10^{-9}\mu^{-0.46} \tag{2.34}$$

where D_{C3B} is the diffusivity of propane in bitumen in m²/s, D_{C4B} is the diffusivity of butane in bitumen in m²/s, and μ is the mixture viscosity in Pa.s. These correlations were created under a narrow range of temperatures (21-35^{o}C) and relatively high solvent concentrations (8-23 wt% propane). Only one experiment was performed using butane, and the exponent was assumed to be equal to that of propane.

Upreti and Mehrotra (2002) used the pressure decay method to determine the concentration dependent diffusivity of nitrogen, carbon dioxide, methane and ethane in Athabasca bitumen. They solved the continuity equation with a pressure dependent boundary condition. They iteratively solved the continuity equation by adjusting the diffusivity value at each solvent concentration to minimize the error in the fitted concentration profiles. The fitted diffusivity

versus concentration for each solvent was not easily fit to any established model for the diffusivity and a simple correlation for the average diffusivity was presented.

Guerrero-Aconcha (2008) used the Vignes Equation (Equation 2.23) to model the diffusivity of liquid *n*-alkanes in heavy oil based on concentration profiles obtained using computer assisted tomography. Since the thermodynamic correction factor was not known, the authors used it as a piecewise fitting parameter.

James *et al.* (2012) measured mass transfer of butane in bitumen using the constant saturation method. They fit three diffusivity models to their experimental data, the Vignes equation (Equation 2.23), a constant diffusivity, and a mass based linear mixing of infinite dilution diffusivities similar to the Darken and Hartley-Crank equations given by:

$$D_{AB} = (D_{AB}^{0} w_B + D_{BA}^{0} w_A) \tag{2.35}$$

Comparing the results of these three models, they concluded that they could not determine the functional form of the concentration dependence with their experimental procedure because all of their models gave very similar matches to the data.

Ghaderi *et al.* (2011) applied the following concentration dependent models for diffusivity in pressure decay experiments.

$$D_{AB} = D_{AB}^{0} e^{m(c_A/c_{A,Pi})} \tag{2.36}$$

$$D_{AB} = D_{AB}^{0} (c_A/c_{A,Pi})^{m} \tag{2.37}$$

where $c_{A,Pi}$ is the solubility of the diffusing component *A* at the initial system pressure in kg/m^3 and *m* is a constant. The model was able to satisfactorily fit synthetic data but the concentration dependent models were not tested on real pressure decay data.

2.5 Solubility and Saturation Pressure of Gas/Bitumen Systems

The solubility of a gas is the limiting amount of gas that can dissolve in a liquid at a given temperature and pressure (saturation pressure) in the two-phase region. The solubility of gases in oil is an important parameter in modeling the diffusion process. It is frequently applied in the boundary conditions used to solve the continuity equation, either directly as an equilibrium condition (Equation 2.12) or as a limiting case of a Robin type equation (Equation 2.14).

2.5.1 Saturation Pressure Measurements

The methods used to measure the saturation pressures of gases in heavy oils include the constant composition expansion, pressure decay, balance, and gas release methods. Each method is outlined below.

Constant Composition Expansion (CCE)

A mixture of gas and bitumen of a known composition is prepared in a PVT cell. The mixture is compressed until it is well above its saturation pressure. Then, the fluid is slowly expanded while both the pressure and volume change are measured. This process can either be performed in small volume steps where the fluid is allowed to equilibrate before the pressure is measured, or as a very slow continuous process. The bubble point is determined from the change in slope of the pressure volume isotherm (Badamchi-Zadeh *et al.*, 2009).

Pressure Decay

The pressure decay apparatus developed by Lundberg *et al.* (1963) can measure both the diffusivity and the solubility of the mixture. As noted previously, this method measures the amount of gas that diffuses into a fluid with time. If an experiment is allowed to run until the gas and liquid phases are in equilibrium, the solubility at the final pressure can be calculated from the total mass diffused.

Balance Method

Marufuzzaman and Henni (2014, 2015) used a microbalance to measure the diffusivity and the solubility of propane in heavy oil. This method directly measures the amount of mass dissolving

into the oil with time at a constant pressure. If an experiment is allowed to run until the gas and liquid phases are in equilibrium, the solubility can be calculated from the initial and final mass.

Gas Release Method

This method is based on the concept that the gas dissolved in oil will come out of solution if the pressure on the system is decreased or the temperature is increased Svrcek and Mehrotra (1982). The oil is saturated with a gas at the measurement pressure, expanded to atmospheric pressure, and the volume of gas is measured. The gas that evolves is captured and weighed. The solubility at the initial conditions is calculated from the initial mass and the mass of evolved gas.

2.5.2 Solubility Data for Gas/Bitumen Systems

Many researchers have investigated the solubility of hydrocarbon gases in heavy oil. Mehrotra and Svrcek (1982a, 1982b, 1984, 1985a, 1985b. 1985c, 1988) measured the solubility and other physical properties of gas-oil mixtures for methane, ethane, carbon dioxide and nitrogen in five different Canadian oils. Other authors have measured the solubility propane and butane in Athabasca bitumen and other heavy oils. There are considerable data at ambient temperatures but very little data available at temperatures above 100°C, Table 2.2.

Table 2.2. Data available from the literature for gas solubility in bitumen

Author	Solvent	Oil	T (^{o}C)	P (MPa)	Method
Badamchi-Zadeh *et al.*, 2009	C_3H_8	Athabasca Bitumen	10-50	0-1.6	CCE
Mehrotra and Svrcek, 1988a, 1988b	CH_4	Cold Lake Bitumen	25-103	2.5-10	Gas Release
	C_2H_6		25-102	1-10	
	CO_2		15-98	2.3-11	
	N_2		30-100	2.5-10.5	
Mehrotra and Svrcek, 1985a	CO	Athabasca Bitumen	25-120	0-10	Gas Release
	C_2H_6				
Mehrotra and Svrcek, 1985b	CH_4	Peace River	22-114	2.5-7.6	Gas Release
	C_2H_6		23-107	1.4-4.3	
	CO_2		22-107	1.6-6.2	
	N_2		23-100	3-9	
Mehrotra and Svrcek, 1985c	CH_4	Wabasca	20-110	0-10	Gas Release
	C_2H_6				
	CO_2				
	CO				

	N_2				
Mehrotra and Svrcek, 1984	CO_2	Marguerite Lake	23-103	0-6.7	Gas Release
Mehrotra and Svrcek, 1982; Svrcek and Mehrotra, 1982	CH_4	Athabasca Bitumen	26-100	1 -10	Gas Release
	CO_2		25-97	1.7-5.5	
	N_2		32-100	2.8-9	
Marufuzzaman and Henni, 2015	C_2H_6	Cactus Lake Oil And it's SARA Fractions	15-30	0.2-2	Balance Method
	CO_2				
Marufuzzaman and Henni, 2014	C_3H_8	Cactus Lake Oil And it's SARA Fractions	15-30	0.05-0.6	Balance Method
Varet *et al.* 2013	CH_4	Athabasca Bitumen	20-80	2.9-16	CCE
	CO_2			3-12	
	CH_4	Venezuelan Heavy Oil		3.1-17	
	CO_2			1.6-11.8	

2.5.3 Gas Solubility Models

Saturation pressures are achieved when the system is at equilibrium and can be modeled using the equality of the chemical potential of each component between the gas and liquid phases. Chemical potential is not a convenient variable to work with, so the equality of fugacity is often used instead (Elliott and Lira, 1999).

$$f_A^v = f_A^l \tag{2.38}$$

where f_A is the fugacity of component A and the superscripts v and l refer to the vapour and liquid phase respectively. The fugacities can be defined as functions of pressure and composition to obtain the following equality (Elliott and Lira, 1999):

$$y_A \varphi_A^v P = x_A \gamma_A P_{v,A} \tag{2.39}$$

where $_{yA}$ and x_A are the mole fractions of component A in the gas and liquid phases, respectively, P is the system pressure in kPa, $P_{v,A}$is the vapour pressure of component in kPa, φ_A^v is the fugacity coefficient of component A in the vapour phase, and γ_A is the activity coefficient of component A in the liquid phase. The fugacity coefficient can be obtained from an equation of state and the activity coefficients from an appropriate activity coefficient model.

For a pure gas phase (as applicable for this thesis), Equation 2.39 simplifies to:

$$P = x_A \gamma_A P_{v,A} \tag{2.40}$$

For an ideal solution, the activity coefficient is unity and Equation 2.40 simplifies to the following:

$$P = x_A P_{v,A} \tag{2.41}$$

Equation 2.41 is usually only applicable at dilute conditions (x_A approaches zero). An alternative for concentrated conditions (x_i approaches unity) is given by (Reid *et al.*, 1987):

$$P = x_A H \tag{2.42}$$

where H is Henry's constant and has the same units as the pressure, P.

For intermediate mole fractions, an activity coefficient model is required. There are many activity coefficient models (Reid *et al.*, 1987). One simple yet flexible example is the Margules (1895) equation for binary mixtures, given by:

$$\ln \gamma_A = [A_{AB} + 2(A_{BA} - A_{AB})x_A]x_B^2 \tag{2.43}$$

where A_{AB} and $A_{BA}$are constant for each binary pair.

Alternatively, an equation of state can be used to determine the fugacities and calculate the saturation pressure. In this case, the equilibrium is defined as follows:

$$y_A \varphi_A^v P = x_A \varphi_A^l P_{v,A} \tag{2.44}$$

where φ_A^l is the fugacity coefficient of component i in the liquid phase. The following expression can be used to calculate the fugacity coefficients (Reid *et al.*, 1987).

$$\mathrm{RT}\ln\varphi_A^j = \int_{v_j}^{\infty}\left[\left(\frac{\partial P}{\partial n_A}\right)_{T,V,n_B} - \frac{RT}{v_A}\right]dv_A - RT\ln Z_j \tag{2.45}$$

where n_A is the moles of component *A*, v_j is the molar volume of phase j and Z_j is the compressibility factor in phase *j*. The pressure, *P* is calculated from an equation of state, such as the Peng-Robinson (Peng and Robinson, 1976) equation of state, which for a pure component is given as:

$$P = \frac{RT}{v_A - b} - \frac{a\alpha}{v_A^2 + 2bv_A - b^2} \tag{2.46}$$

$$a = \frac{0.45724R^2T_c^2}{P_c} \tag{2.47}$$

$$b = \frac{0.07780RT_C}{P_c} \tag{2.48}$$

$$\alpha = \left(1 + (0.37464 + 1.54226\omega - 0.26992\omega^2)(1 - T_r^{0.5})\right)^2 \tag{2.49}$$

$$T_r = \frac{T}{T_c} \tag{2.50}$$

where T_c is the critical temperature, P_c is the critical pressure, and ω is the acentric factor. Mixing rules are used to determine the values of the equation of state parameters, *a* and *b*, (Peng and Robinson, 1976)

A simpler method to model gas-liquid phase behavior is the K-value approach which is based on of the following definition (Reid *et al.*, 1987):

$$K_A = \frac{y_A}{x_A} = \frac{\varphi_A^l}{\varphi_A^v} \tag{2.51}$$

where K_A is the K-value. Values of K_A for various gases and liquids have been tabulated (Whitson *et al.*, 2000) and are very useful for quick calculations or reservoir simulations where the computation cost of phase calculations is kept low to minimize run time. This method has

limited usefulness, as the tabulated K-values are only valid for narrow ranges of conditions Agrawal et al. (2012).

Solubility Models Applied to Gas/Bitumen Systems

Mehrotra and Svrcek (1982) noticed the following empirical trend of solubility with pressure carbon dioxide, methane, and nitrogen in bitumen:

$$w_{sol} = b_1 + b_2 P + b_3 \frac{P}{T} + b_4 \left(\frac{P}{T}\right)^2 \tag{2.52}$$

where w_{sol} is the solubility in wt%, P is the pressure in MPa, T is the temperature in K, and the b coefficients are fitting parameters. This approach was used by Quail et al. (1988) to model methane and carbon dioxide solubility in Saskatchewan heavy oils.

Badamchi-Zadeh *et al.* (2009) modeled the bubble point pressure of mixtures of propane in Athabasca bitumen using Equation 2.40 with a constant activity coefficient of 1.158. Marufuzzaman and Henni (2014, 2015) successfully applied Henry's Law (Equation 2.42) to model the solubility of carbon dioxide, ethane and propane in heavy oils. Varet *et al.* (2013) used the following form of Henry's constant to fit their solubility data for methane and carbon dioxide.

$$H = a - \frac{b}{T} \tag{2.53}$$

where a and b are fitting parameters.

Fu *et al.* (1986) predicted gas solubility data for carbon dioxide and methane in three different bitumens with the Peng-Robison equation of state. When modelling , they used a modified Black and Twu (1983) correlationto predict the pseudo critical properties for the each bitumen as a whole. They matched the experimental data (from Mehrotra and Svrcek (1985b), Robinson and Sim (1980), Fu *et al*. (1984) and Fu and Puntagana (1985) by varying the binary interaction parameters between the solvent and the whole bitumen pseudo component. Mehrotra and Svrcek (1988c) also used the Peng-Robinson equation of state (PR EoS) to model their solubility data

for carbon dioxide, nitrogen, methane, and ethane data (Mehrotra and Svrcek, 1982; Svrcek and Mehrotra, 1982). They divided the oil phase into three pseudo-components: the asphaltenes, the distillable maltenes and the non-distillable maltenes. The interaction parameter between the solvent gas and each pseudo-component was adjusted to fit the data. Kokal and Sayegh (1993) modeled the solubility of carbon dioxide in Lone Rock heavy oil using the PR EoS and a similar three pseudo-component oil characterization. The model was fit to their experimental data by adjusting the binary interaction parameters between the carbon dioxide and the two maltene pseudo-components. Yazdani *et al.* (2010) modeled the solubility of butane in Frog Lake heavy oil also with the PR EoS but dividing the oil into only two pseudo-components.

Agrawal *et al.* (2012) used the Advanced Peng-Robinson equation of state (Virtual Materials Group, 2010) and 16 pseudo-components to model the solubility of carbon dioxide, methane, ethane and propane in bitumen as well as the onset of asphaltene precipitation. The fit was obtained by varying the exponent in a critical temperature based correlation for the interaction parameter between each of the solvent gases (carbon dioxide, methane, ethane and propane) and each bitumen pseudo-component.

Zhang *et al.* (2012) used a cubic plus association equation of state (Kontogeorgis *et al*., 1996) to model data for asphaltene precipitation and the saturation pressure of live oils collected by Fotland (1997), Jamaluddin (2002), and Yonebayashi, 2009. The live oil was split into 8 pseudo-components and 10 known components. The physical properties of the pseudo-components were estimated using the Kesler and Lee (1976) and Riazi *et al*. (1980, 1996) correlations. The binary interaction parameters between all the components were adjusted to match vapour liquid equilibrium and the association terms for the resin-asphaletene and asphaltene-asphaltene interaction were fit to asphaltene precipitation data.

Ma *et al.* (2016) used a simplified Perturbed-Chain Statistical Associating Fluid Theory (PC-SAFT) to model the solubility of methane, ethane and carbon dioxide in Athabasca bitumen. PC-SAFT (von Solms *et al.*, 2003) is a version of the SAFT equation of state developed by Chapman *et al.* (1989). The oil was split into 8 pseudo-components, one for the asphaltenes and 7 for the maltene components. The model was fit to the data by varying the interaction parameters between the gas and the bitumen pseudo-components.

CHAPTER THREE: EXPERIMENTAL METHODS

This chapter outlines the materials and experimental methods used to collect data in this thesis. The procedures to prepare the oil samples are provided. The constant composition expansion method used to measure the saturation pressure of mixtures of gas and bitumen is presented. The pressure decay methods used to measure diffusivity are described in detail.

3.1 Materials

The Western Canadian bitumen sample (WC-B-B3) used in this thesis was provided by Shell Canada. The oil was dewatered by sonication in an ultrasonic bath at 40^{o}C for 4 hours. The mixture was then allowed to settle in a separator heated to no more than 70^{o}C before the water phase was drained from the bottom of the separator. The specific gravity, viscosity, and C5-asphaltene content of the WC-B-B3 bitumen are listed in Table 3.1. A SARA and a spinning band distillation assay for a similar sample from the same field (WC-B-B2, also provided by Shell Canada) are given in Tables 3.1 and 3.2, respectively (Agrawal, 2012). The properties of the WC-B-B2 sample (Motahhari, 2013) are compared with those of the WC-B-B3 sample in Table 3.1.

The following hydrocarbon gases were purchased from Praxair and used for the diffusivity and saturation pressure measurements: methane (99.97 wt% purity), ethane (99.0 wt% purity), propane (99.5 wt% purity), and butane (99.5 wt% purity). *n*-Decane (99.4 wt% purity) and *n*-dodecane (99 wt% purity) purchased from Fisher Scientific and Acros Organics, respectively, were used to commission the diffusivity apparatus. The 98% *n*-Pentane (98 wt% purity) purchased from VWR was used to precipitate asphaltenes from the bitumen.

Table 3.1. Selected properties of WC-B-B2 and WC-B-B3 bitumen (Motahhari, 2013).

Property	WC-B-B2	WC-B-B3	WC-B-B2 Maltenes
Specific Gravity	1.015	1.020	0.984
Viscosity at 20°C and 1 atm, mPa.s	89200	118000	145
Saturates, wt%	17	-	-
Aromatics, wt%	46.9	-	-
Resins, wt%	16.7	-	-
C5-asphaltenes, wt%	19.4	19.2	0

Table 3.2. Spinning band distillation assay of WC-B-B2 bitumen (Agrawal, 2012).

Volume % Distilled	Normal Boiling Point, °C
1.68	218.0
3.36	237.4
5.04	252.4
6.72	267.9
8.40	278.6
10.08	289.4
11.76	301.7
13.44	313.5
15.13	324.0
18.49	339.8
20.17	349.6
21.85	358.0
23.53	367.3
25.21	375.2
26.89	380.0
28.57	382.5
30.25	384.0
31.93	385.0

Maltenes (required for some diffusion experiments) were obtained by deasphalting the bitumen using a method described in Alboudwarej e*t al*. (2003). *n*-Pentane (C5) was added to the bitumen in a 40:1 ratio of *n*-pentane to bitumen by volume. The mixture was sonicated for 45 minutes in an ultrasonic bath at 40^{o}C and left to equilibrate overnight. The precipitated asphaltenes settled to the bottom of the beaker. The pentane-rich supernatant was decanted and filtered using VWR 413 filter paper (particle retention of 5µm) to remove any asphaltenes present. The pentane was evaporated off in a roto-evaporator at 70^{o}C until the mass of the liquid sample remained constant. The maltenes recovered using *n*-pentane are termed maltenes in this thesis. The pentane content in the maltenes is expected to be less than 3.5% (Sanchez-Lemus, 2015). The specific gravity and viscosity of the C5-maltenes from the WC-B-B2 bitumen are listed in Table 3.1. Note, a GC assay of the the WC-B-B2 maltenenes perfoemed by Motahhari (2013) indicate a solvent concentration of 0.41 and 3.83 wt% n-pentane and toluene respectively. No toluene was used in the extraction of the maltenes in this thesis; therefore, the toluene concentration in the maltenes is expected to be negligible.

Several diffusion experiments were also performed with bitumen that was degassed at 176^{o}C. To degas the sample, it was placed in the diffusion cell at atmospheric pressure, heated to 176^{o}C, and vacuumed to 15 kPa for two minutes. The system was then cooled to the temperature of the diffusion experiment. The procedure was found to remove a maximum of 5 wt% of the bitumen based on the pressure increase in the cell while heating and a molecular weight of 550 g/mol for the oil in the gas phase.

3.2 Solubility (Saturation Pressure) Measurement

The solubility (and saturation pressure) of hydrocarbon gases in bitumen was determined with two methods: 1) from the diffusion experiments described later, and; 2) using the constant composition expansion method described below. The volume expansions in this thesis were performed in a PVT apparatus with no sight glass or method to determine phase volume. This PVT apparatus referred to at the blind cell apparatus in this thesis.

The in-house built blind cell apparatus, Figure 3.1, can simultaneously measure the saturation pressure of up to five solvent/bitumen mixtures. This apparatus contains five 100 mL blind cells

(PVT cells with no sight glass) each equipped with a floating piston. The temperature of the PVT cells is maintained by a circulating air bath that can maintain temperature up to 300^{o}C. The volume of the sample in each cell is set by a computer controlled positive displacement pump that can add and remove hydraulic oil from beneath the floating piston with an error of ±0.1mL on the total volume displaced. This apparatus can be operated at temperatures from 21 to 300°C and pressures up to 70 MPa. The temperature measurement is accurate within ±3^{o}C and the pressure sensors on each cell are accurate within ±45kPa.

The cells are assembled with the piston at the bottom and are each weighed. The cells are then filled with 20 to 50 mL of bitumen and weighed again to determine the mass of bitumen added. Even small amounts of volatile gases, like air, will result in an erroneous saturation pressure measurement because these volatile gases come out of solution at higher pressures than the less volatile hydrocarbon solvents of interest. To purge the cell of any impurities, the cell is vacuumed to remove trace air and volatiles from the cell, and then filled with 200 kPa of the hydrocarbon gas to be used in the saturation pressure measurement. This process is repeated two more times to remove all other gases from the system. The cell is then filled to the desired pressure of gas and weighed again to determine the total mass of added gas. The solvent content is determined from the measured masses of bitumen and hydrocarbon gas.

The gas/bitumen mixture is then compressed until it forms a single liquid phase. To ensure a liquid phase, the cell is initially pressurized at least 5000 kPa above the saturation pressures reported in the literature for the gas in question and a comparable heavy oil. Since there is no sight glass in these cells, the initial volume of the liquid phase is unknown.

To expand the gas/bitumen mixture, hydraulic oil is removed from below the piston with the pump and the system is allowed to equilibrate before the pressure measurement is taken. The system is considered equilibrated when the pressure in the blind cell remains constant for an hour at a constant temperature, because the system is not mixed, this can take anywhere from 4 to 24 hours depending on the fluids and the phases present. The mixture is expanded in a series of volume increments and the equilibrated pressure measured at each volume. The pressure is plotted versus volume and the bubble point (saturation pressure), is determined from the change

in slope as shown in Figure 3.2. Note that, since the initial volume of fluid in the cell is not known, its density cannot be determined.

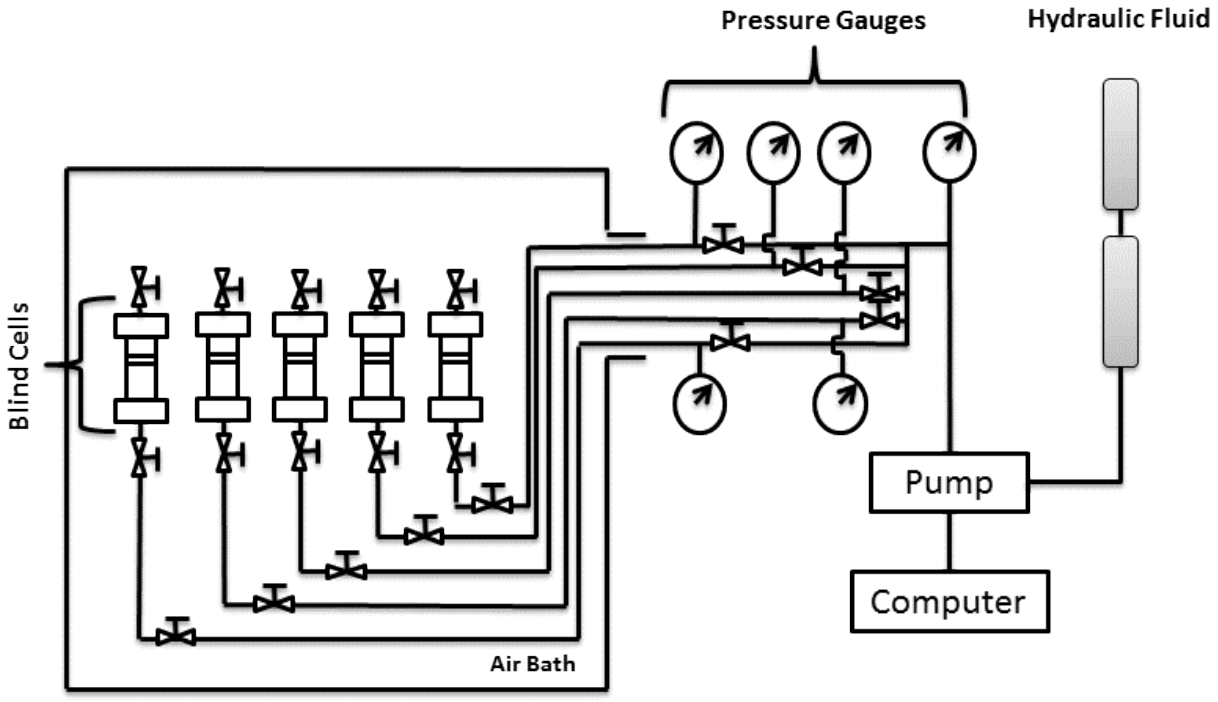

Figure 3.1. Schematic of the blind cell apparatus.

The methodology was validated with *n*-pentane and the measured data are compared with the vapour pressure predicted from the correlations provided in Perry's Chemical Engineers' Handbook (Green and Perry, 2008) in Figure 3.3. The deviations are reported in Table 3.3. The data are within 4% of the correlation above approximately 450 kPa but deviate significantly at lower pressures. The deviation below 450 kPa is larger than the expected error from the pressure measurement indicating that there are other contributing factors to the error.

One source of error is the fluctuation in room temperature. Despite insulating the hydraulic oil lines outside of the oven, the variation in the room temperature over the course of a day can cause a variation of ±50 kPa. However, this variation is compensated for by averaging the pressure data and is smaller than the observed deviation. The main source of error at low pressure is caused by a small amount of air trapped in the lines to the pressure gauge. This air dissolves in the hydraulic oil at higher pressure but evolves when the pressure drops below approximately 500 kPa (depending on the temperature). Hence, the apparatus detects a saturation

pressure in the hydraulic oil at this pressure. Once the hydraulic oil drops below its saturation pressure, the pressure of the system no longer changes and the true saturation pressure of the sample cannot be detected. Figure 3.4 shows that the same deviation occurs in the propane diluted bitumen saturation pressure data collected for this thesis. Therefore, only data above the air/hydraulic oil saturation pressure were considered in this thesis. Note, once the source of the error was identified, a procedure was developed to remove most of the trapped air and, in future, saturation pressure measurements at lower pressure can be made.

As will be presented in Chapter 5, the solubilities from the blind cell experiments were within an average of 8% of the models fit to solubility data collected in this thesis. The solubility model fit to the data from this thesis was shown to predict literature data for different heavy oils with an average deviation of 11%. Hence, the solubilities are considered to be validated with an uncertainty of ±8%

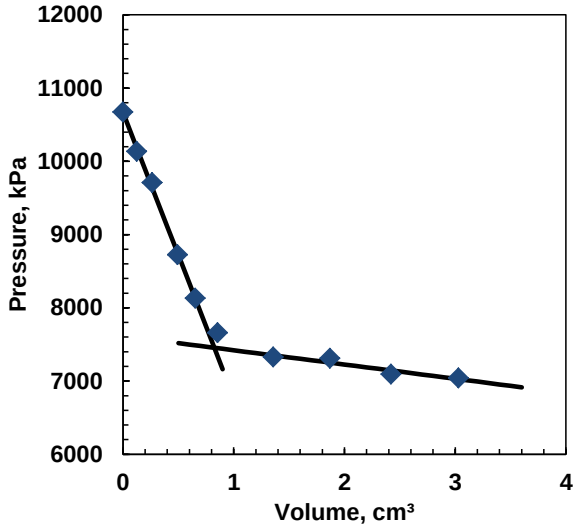

Figure 3.2. Step-wise isothermal expansion of 11.4% propane in bitumen at 180°C.

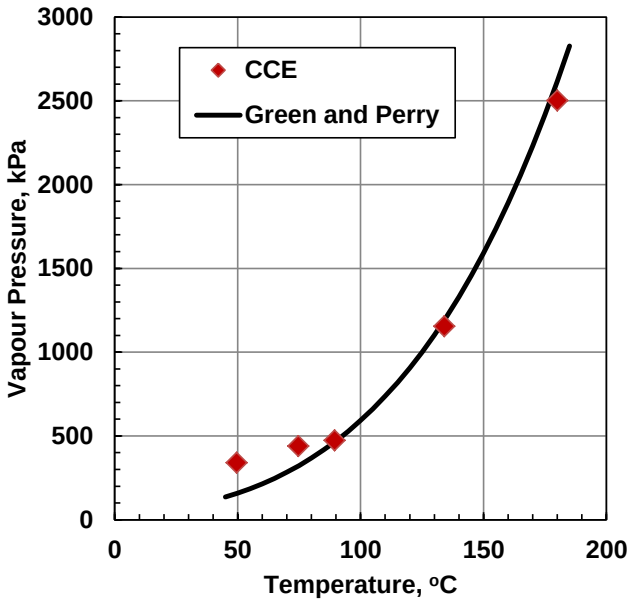

Figure 3.3. Vapour pressure of *n*-Pentane measured using the blind cells compared to the correlation in Green and Perry (2008).

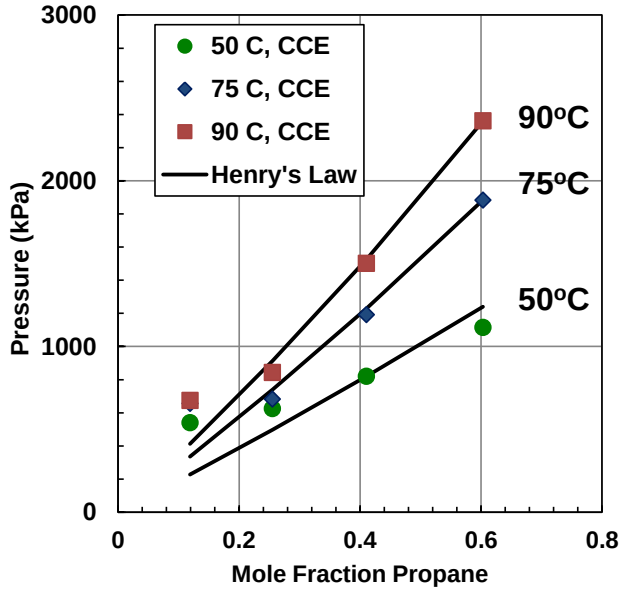

Figure 3.4. Saturation pressure of propane diluted bitumen (this thesis) measured in blind cells.

Table 3.3. Vapour pressure of n-pentane measured in the blind cells and calculated from Green and Perry (2008)

T ^{o}C	Measured Saturation Pressure kPa	Correlation Saturation Pressure kPa	Absolute Error kPa	Relative Error %
47.7	340	158	182	116
74.7	439	321	118	37
89.4	474	464	10	2
134	1154	1193	-39	-3
180	2501	2615	-114	-4

3.3 Diffusivity

3.3.1 Diffusivity Apparatus

The diffusivity of gas in bitumen was measured using both the pressure decay method and constant pressure gas delivery methods, using two apparatus with a common design. The apparatus is based on the design by Etminan *et al.* (2010) which, in turn, is based on the pressure decay apparatus developed originally by Riazi (1996). The apparatus consists of a cylindrical diffusion cell connected to a gas supply cylinder all in a heated oil bath, Figure 3.5. The cells are connected by a block valve, V2, and a pressure regulator, R1. The temperature of the bath is measured with a thermocouple with an accuracy of $\pm 2^{o}$C and the pressures of the gas supply and diffusion cell are measured with pressure transducers with an accuracy of ±21 kPa,

The apparatus was designed for two experimental methods, which each require a different procedure: 1) conventional pressure decay where gas supply and diffusion cell are left open to one another, by opening valve V2 and the whole system pressure decreases as gas diffuses into the oil; 2) constant pressure method where the pressure in the diffusion cell pressure is held constant through the pressure regulator, R1, and pressure decreases only in the gas supply. For both types of experiments, the temperature and both the diffusion cell and gas supply pressures are measured with time and used in the analysis.

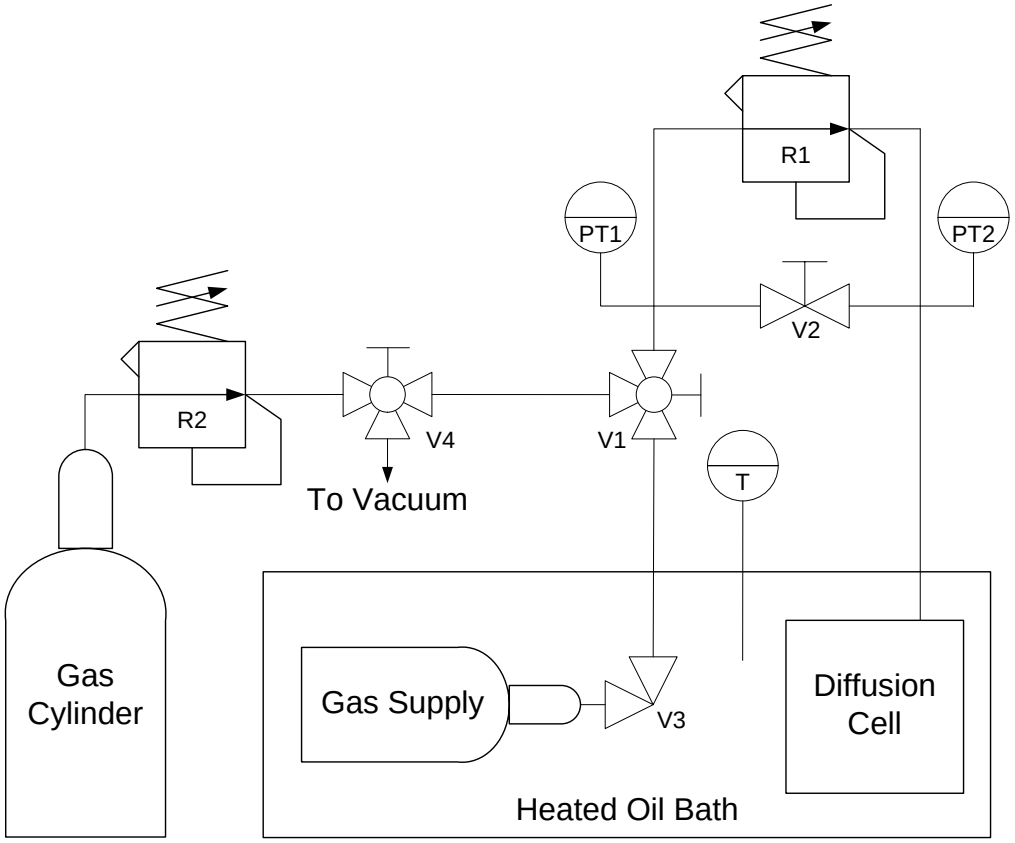

Figure 3.5. Schematic of the diffusivity apparatus

3.3.2 Procedure for Diffusivity Experiments

Start Up:

To start an experiment, 10-50 mL of bitumen is placed in a clean, dry diffusion cell of known mass. The filled diffusion cell is weighed to determine the mass of bitumen added. The diffusion cell is then connected to the gas supply line and placed into the oil bath. The whole system is then vacuumed and purged with the solvent gas three times.

Procedure for Conventional Pressure Decay Mode:

The regulator is bypassed, the diffusion cell is isolated under vacuum by closing valve V2 and the gas supply is filled with gas. The temperature in the bath is then set to the desired temperature and the system is allowed to equilibrate overnight. To run an experiment, Valve V2 is opened slowly to connect the diffusion cell to the gas supply. The gas supply and diffusion cell remain in pressure communication throughout the experiment. As time progresses, gas diffuses

into the oil and the system pressure decreases. The pressure is monitored with both pressure gauges which are used to calculate the change in mass on their respective side of the apparatus. Data collection begins as the system is being heated using a slow sample rate (one measurement every 15 minute). The system is monitored until the temperature and both pressure measurements are constant for at least 2 hours. Once the measurements are stable the time step is decreased to fast sample rate of one measurement every 1-30 seconds while the diffusion cell is filled and the initial data is collected. After two hours, and the initial data has been collected. And the sample rate is decreased to one measurement every 5-15 minutes for the remainder of the experiment.

Procedure for Constant Pressure Mode:

Valve 2 is bypassed, the diffusion cell is isolated under vacuum by closing the regulator, and the gas supply is filled with gas. The temperature in the bath is then set to the desired temperature and the system is allowed to equilibrate overnight. To run an experiment, the regulator, R1, is slowly opened to the desired operating pressure. The regulator maintains a pressure in the diffusion cell constant to ±70, kPa. Hence, the pressure drop occurs only in the gas supply although some variation in the diffusion cell pressure occurs particularly when the regulator is first opened. Both the pressure of the gas supply and of the diffusion cell are monitored as described above.

3.3.3 Processing of Pressure Decay Data

Determination of Mass Transfer

The total mass diffused is calculated from the change in mass in each side of the cell as follows:

$$m_s(t) = \Delta m_{diff} + \Delta m_{supply} \tag{3.1}$$

where $m_s(t)$ is the total mass of solvent diffused with time in g , Δm_{diff} is the mass change in the gas phase of the diffusion cell in g, Δm_{supply} is the change of mass in the sample gas in g. The mass change in each side of the diffusion cell is determined from the real gas law as follows:

$$m_s(t) = \left[\frac{M_s V_0 P_0}{R Z_0 T_0} - \frac{M_s V(t) P(t)}{R Z(t) T(t)}\right]_{diff} + \left[\frac{M_s V_0 P_0}{R Z_0 T_0} - \frac{M_s V P(t)}{R Z(t) T(t)}\right]_{supply} \quad (3.2)$$

where M_s is the molar mass of Solvent in g/mol, R is the ideal gas constant in cm^3 kPa/molK, V is the gas volume in cm^3, P is the pressure in kPa, Z is the compressibility factor of the gas, T is the temperature in K, and t is time in min. The subscript *0* indicate the initial condition in the cell, *diff* refers to the diffusion side of the system, and *supply* refers to the gas supply side of the apparatus.

One issue with solving Equation 3.2 is that the volume of the gas phase in the diffusion cell can change over time when the oil phase swells from the diffusing gas, as was discussed in Chapter 2. This swelling decreases the volume of the gas phase and must be accounted for in the mass balance. The volume of the swollen oil phase is given by:

$$V_{mix} = \frac{m_s(t) + m_{oil}}{\rho_{mix,ave}} \quad (3.3)$$

where V_{mix} is the volume of the solvent-oil mixture in cm³, m_{oil} is the mass of oil in the diffusion cell in g, and $\rho_{mix,ave}$ is the average density of the gas-oil mixture in g/cm^3. The volume of the gas phase in the diffusion cell is then calculated by the difference between the initial gas phase volume and the change in the oil volume due to swelling as follows:

$$V(t)_{diff} = V_0 - \left(V_{mix} - \frac{m_{oil}}{\rho_b}\right) \quad (3.4)$$

The density of the gas-oil mixture is determined using the following empirical non-ideal mixing rules (Saryazdi *et al.*, 2013):

$$\rho_{mix,ave} = \left(\frac{w_{s,ave}}{\rho_s} + \frac{1 - w_{s,ave}}{\rho_b} - w_{save}\left(1 - w_{s,ave}\right)\left(\frac{1}{\rho_s} + \frac{1}{\rho_b}\right)\beta_{sb}\right)^{-1} \quad (3.5)$$

where $w_{s,ave}$ the solvent concentration in the oil phase in wt%, ρ_s is the effective density of the solvent in g/cm^3, ρ_b is the density of the oil in g/cm^3, and β_{sb} is a binary interaction parameter between the solvent and the oil. The component densities and binary interaction parameter determination are described in Chapter 4. The average solvent concentration in the system is calculated from the mass diffused and the total mass of bitumen in the system

$$w_{s,ave} = \frac{m_s(t)}{m_s(t) + m_{oil}} \tag{3.6}$$

If required, the height of the oil is given by:

$$h_{oil} = \frac{V_{mix}}{A_c} \tag{3.7}$$

where h_{oil} is the height of the swollen oil column and A_c is the cross sectional area of the diffusion cell.

Treatment of Leaks

The constant pressure and pressure decay methods described in this chapter are susceptible to leaks in the apparatus. Experiments with large leaks are rejected because mass lost from the leak masks the mass transferred in the diffusion process. For small leaks, the effect of the leak can be corrected for to determine the mass transfer from diffusion. Small leaks from the system manifest themselves as a linear increase in mass diffused over time and become apparent when the oil becomes saturated with gas. Instead of reaching a plateau, a linear increase is mass diffused is observed. The slope of this linear increase is measured and the mass transfer data are corrected by taking the difference between the calculated mass diffused and the amount of gas leaked as follows:

$$m_{s,corr} = m_s(t) - r_{leak} * t \tag{3.8}$$

where $m_{s,corr}$ is the corrected mass diffused in g, r_{leak} is the leak rate in g/min, and t is the time in minutes. Figure 3.6 shows the mass transfer data for a propane bitumen system with a small leak before and after the correction.

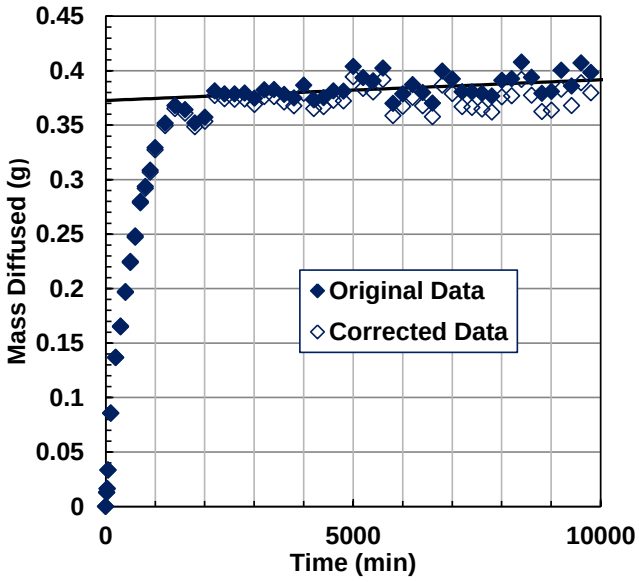

Figure 3.6. Mass of propane diffused onto bitumen at 80.7°C and 720 kPa before and after correction for a small leak.

Treatment of Start Up

Several diffusion experiments with propane in bitumen did not follow the expected mass balance at early times. Recall that the mass transfer at early times is linearly related to the square root of time and must pass through the origin. Figure 3.7 shows that, in some cases, the data follow the expected linear trend but do not pass through the origin. This discrepancy is attributed to errors in the volume measurements, errors in the pressure measurements, and condensation of propane in the apparatus. When the discrepancy was small and a clear linear trend was observed, the data were corrected by shifting the calculated diffusion curve to pass through the origin as follows:

$$m_{s,shifted} = m_s(t) - intercept \tag{3.9}$$

where $m_{s,shifted}$ is the mass of solvent diffused corrected through the origin in g and *intercep*t is the deviation from the origin of the initially calculated mass. In effect, the correction adjusts for an error in the calculated initial mass of gas in the system.

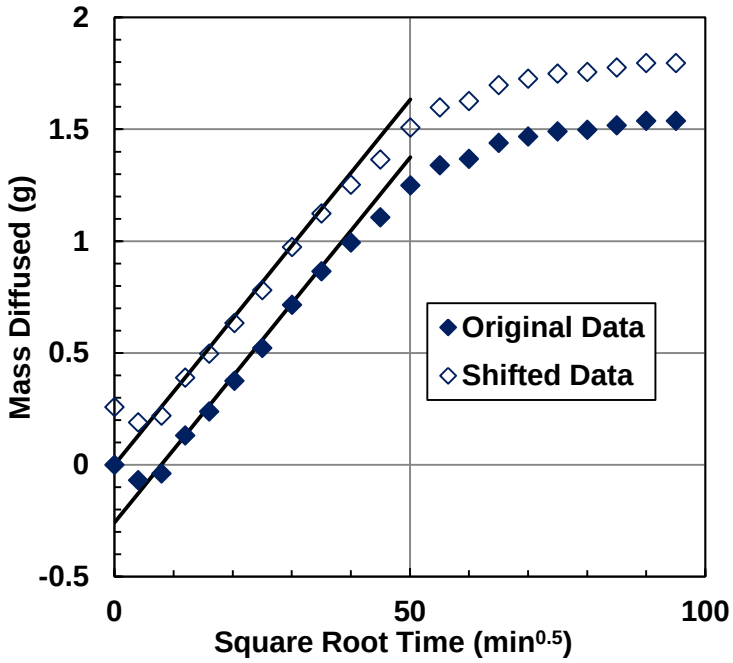

Figure 3.7. Correction for error in initial mass of gas for diffusion of propane into bitumen at 62.3°C and 1080 kPa.

As seen in Figure 3.7, there can be a lag period before the expected linear trend begins. The lag could result from an initial temperature disequilibrium between the two sides of the diffusion system or from a disturbance of the interface when the gas is introduced to the cell. As the gas is introduced to the diffusion cell, it expands and cools causing a temporary drop in temperature. In addition, the initial large volume stream of solvent vapour may disturb the interface of the oil causing a short period of convection. Both effects can account for some instability in the mass diffusion curves at early times.

Use of Processed Data

Figure 3.8 shows the mass of methane diffused into decane over time from a commissioning experiment. In this case, no corrections to the mass diffused were required. The solubility is determined from the plateau and the diffusivity is calculated by modeling the change in mass

over time. Analytical and numerical approaches to modeling the mass transfer are discussed in Chapter 4.

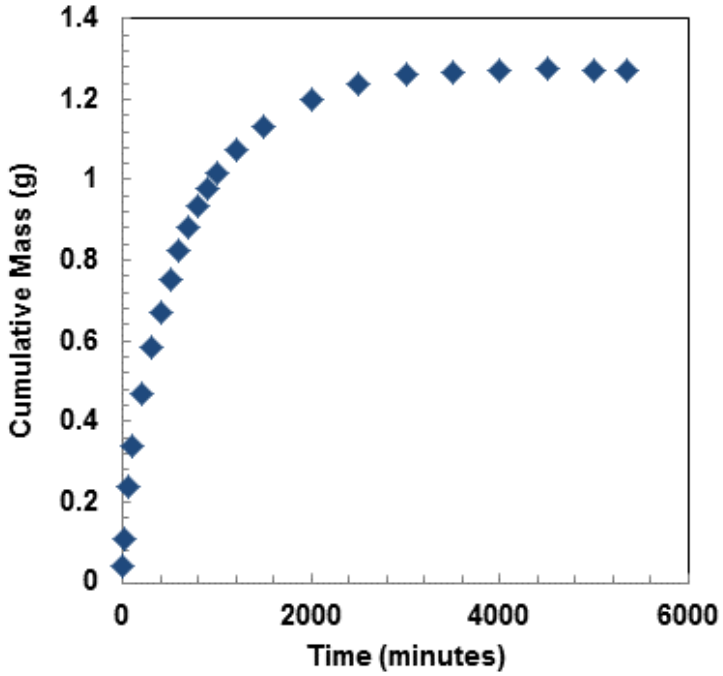

Figure 3.8. Cumulative mass of methane diffused into n-decane at 124^{o}C and 3950 kPa.

3.3.4 Validation of the Pressure Decay Measurements

First, the repeatability of the method was assessed based on four pressure decay experiments performed with methane in bitumen at 100^{o}C and approximately 4200 kPa, shown in Table 6.1. The measured solubilities had a 90% confidence interval of 0.031wt%, coresponsing to a 6.3% deviation from the mean. The measured diffusivites had a 90% confidence interval of 1.6E-10 m^2/s coresponding to a 15% deviation from the mean.

The diffusion apparatus was further tested by measuring the diffusion of methane into *n*-decane and *n*-dodecane and comparing the results with literature data. The solubility was determined from the plateau in mass transferred at the end of the experiment. The diffusivity was determined analytically with both the infinite acting and finite acting solutions presented in Chapter 4. The solutions provided nearly identical diffusivities and the average values of the two methods were used here.

Methane into *n*-Decane

Table 3.4 compares the methane solubilities in *n*-decane measured from the constant pressure diffusion experiments with data collected by Srivastan *et al.*(1992) using constant coposition expansion. The solubility data from this study are comparable with the literature data, with a maximum deviation of 10%. Table 3.5 compares the diffusivities calculated from the pressure decay apparatus data with data collected by Reamer *et al*. (1956) using a constant pressure gas injection method. The diffusivities are up to 25% lower than the literature data.

Table 3.4. Solubility of methane in *n*-decane

T (^{o}C)	**P (kPa)**	**Solubility Srivastan *et al.*, 1992 (mol%)**	**Solubility This Work (mol%)**	**Deviation (%)**
86	3165	0.12	0.115	-5
124	3955	0.14	0.125	-10

Table 3.5. Diffusivity of methane in *n*-decane

T (^{o}C)	**P (kPa)**	**Diffusivity Reamer *et al.*, 1956 (x10^{9} m/s^{2})**	**Diffusivity This Work (x10^{9} m/s^{2})**	**Deviation (%)**
86	3165	11	8.6	-25
124	3955	16	12.5	-20

Methane into *n*-Dodecane

The methane solubilities and diffusivities in *n*-dodecane measured from the constant pressure diffusion experiments are compared with pressure decay (constant pressure boundary condition) data from Etminan *at al.* (2010) and conventional pressure decay data from Jamialahmadi *et al.* (2006). The comparisons for solubility and diffusivity data are provided in Tables 3.6 and 3.7, respectively. The solubility data from this study are comparable with the literature data, with a maximum deviation of 7%. In this case, the diffusivities fall within the range of the literature values (+9 and -48% deviation).

Table 3.6. Solubility in methane in *n*-dodecane

T (^{o}C)	P (kPa)	Solubility Etminan e*t al.* 2010 (wt%)	Solubility Jamialahmadi *et al.* 2006 (wt%)	Solubility This Work (wt%)	Deviation (%)
45	3440	1.6	1.7	1.5	-3, -7

Table 3.7. Diffusivity of methane in *n*-dodecane

T (^{o}C)	P (kPa)	Diffusivity Etminan *at al.* 2010 ($x10^{9}$ m/s^{2})	Diffusivity Jamialahmadi *et al.* 2006 ($x10^{9}$ m/s^{2})	Diffusivity This Work ($x10^{9}$ m/s^{2})	Deviation (%)
45	3440	4.3	9.0	5.0	+9, -48

Overall, the solubilities determined with the new apparatus are consistently lower but still within 10% of the literature values for pure components. As will be presented in Chapter 5, the solubilities from the diffusion experiments were within an average of 11% of the models fit to diffusivity and blind cell experiments. The fit for solubility was shown to predict literature data with an average deviation of 11%. These deviations are larger than the repeatability error of 6.3% and, therefore, the solubilities are considered to be have an uncertainty of 11%.

There is more deviation in the diffusivities which is not surprising considering the notable variation between the results reported in the literature, even for two similar methods. The commissioning data collected in this thesis lies within 50% of the literature values. However, the diffusivity for the methane/n-dodecane system lies between the two results from the literature and is in very good agreement with the diffusion data collected using an analogous constant pressure method by Etminan *et al.* (2010). As will be shown in Chapter 6, the diffusivities of solvents in bitumen measured in this thesis follow the expected trend with viscosity and can be correlated within an average error of 12% with a small pressure correction. This deviation is similar to the repeatability error of 15% and, therefore, the diffusivities are considered to be validated with an uncertainty of ±15%.

CHAPTER FOUR: MODELING PRESSURE DECAY EXPERIMENTS

This chapter presents the mathematical models used to fit the pressure decay data collected in this thesis. The key assumptions and relevant boundary conditions are discussed and simple analytical solutions to Fick's law are provided. A numerical model for mass transfer, accounting for swelling and a concentration dependent diffusivity, is developed. The diffusivity, density, and viscosity models required to implement the mass transfer model are presented.

4.1 Description of Problem

The pressure decay experiments to be modeled were described in Chapter 3 and involve a gas diffusing into a column of oil, Figure 4.1. The gas enters at the gas-oil interface, *z=0*, and reaches a second boundary at the bottom of the oil column, *z = h(t)*. At dilute conditions, the total height is constant. At high dissolved gas concentrations, the oil phase is expected to swell and increase the height of the bitumen column. In this case, the gas-liquid interface will remain set at the origin of the domain and the change in height will be accounted for in the domain length, *h(t)*.

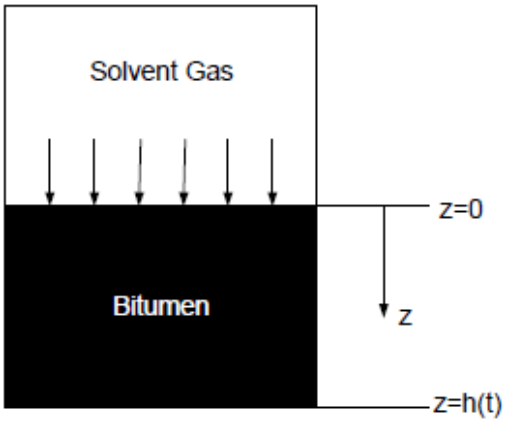

Figure 4.1. Side view of the diffusion cell.

As was discussed in Chapter 2, the mass transfer is determined from the general mass continuity equation given by:

$$\frac{\partial c_A}{\partial t} = -\nabla(c_A * \vec{v}) - \nabla(\overrightarrow{J_A}) + r_A \tag{2.1}$$

$$\overrightarrow{J_A} = -D_{AB}\nabla(c_A) \tag{2.2}$$

where c_A is the mass concentration in kg/m³, $\vec{v}$ is the mass average velocity in m/s, and $\overrightarrow{J_A}$ is the molar flux in kg/m²s, t is the time in s, and D_{AB} is the diffusivity in m^2/s. The first step in solving the continuity equation is to simplify the problem as is appropriate for the geometry and conditions of the experiment. Then, the initial and boundary conditions are set and the simplified continuity equation is solved at these conditions to determine the concentration profiles of the diffusing gas and the total mass of solvent diffused into the oil with time. The mass diffused curve is compared with the experimental data and the value of the diffusivity or the coefficients of the model for the concentration dependent diffusivity are varied until the model fits the experimental data.

4.2 Simplifying Assumptions

The assumptions used to simplify the continuity equation and develop the mass transfer models used in this thesis are listed below.

Isothermal System

Assuming that the system is isothermal gives a significant simplification to model because there is no longer a need to solve the coupled heat and mass transfer equations. The diffusion cell is metal and is placed in a heated oil bath with a relatively large thermal mass. The bath temperature was monitored was stable within 1^oC. The heat of dissolution at any time is expected to be small compared with the rate of heat transfer. As the diffusion cell is filled with gas, there is a small temperature change in the gas phase, which lasts less than two minutes. Therefore, the system was considered to be isothermal.

One Dimensional Diffusion

The assumption of one dimensional diffusion dramatically simplifies the continuity equation. The diffusion cell is a cylinder set up such that the majority of the diffusion is expected to occur perpendicular to the circular cross-section. Any radial diffusion that might occur from wall effects is ignored, as in previous works in pressure decay.

No Chemical Reactions

This assumption also simplifies the continuity equation. The gaseous solvents used in these experiments are constituents of the live oil and therefore the dead oil and solvent are not expected to react. It is possible that at higher temperatures, a thermal cracking reaction could occur which would change the nature of the oil. Cracking reactions are not expected to become significant until a temperature of at least 250^{o}C (Gray, 2015), which is much higher than the pressure decay experiments performed in this thesis. Gray (2015) noted that thermal processing bitumen at as low as 250^{o}C produces hydrogen sulfide, a common indicator of bitumen cracking.

No Second Liquid Phase

Second liquid phases can form from mixtures of solvent and bitumen including light liquid phases and asphaltene-rich phases. Droplets of a light liquid phase or precipitated asphaltene particles would dramatically change the nature of the liquid phase. The dispersed material would cause discontinuities in the fluid and this situation would require a different modeling approach. In addition, the settling of dense asphaltene particles could cause natural convection.

The solvents considered in this study are methane, ethane, and propane. Asphaltene precipitation is not anticipated with methane or ethane (Agrawal *et al.*, 2012) but a light liquid phase can form at ethane contents above 7.2 wt% (Agrawal *et al.*, 2012; Mehrotra and Svrcek, 1985b). Therefore, all diffusion experiments with ethane were conducted at solubilities below this value.

Agrawal *et al.* (2012) performed asphaltene onset experiments with propane in a bitumen from the same field as the sample studied in this thesis. They measured an asphaltene onset concentration using a using a high pressure microscope and found the onset point to be between 13 and 15 wt% propane at 50^{o}C. From experiments performed with *n*-pentane in bitumen in the same paper, it was observed that asphaltene onset solvent content increases with increasing temperature. Therefore, the diffusion experiments were performed at solubilities below the onset condition at 50°C (the lowest anticipated onset condition).

No Natural Convection

The existence of natural convection in the system would dramatically increase the rate of mass transfer. However, mixtures of hydrocarbon solvents in bitumen are less dense than the oil alone. Hence, there would be no density driven convection in the system because an upper layer would always be less dense than a lower layer. Asphaltene precipitation could cause the density gradient required to promote convection. The concentrations of the experiments are kept below this threshold.

Oil is Non Volatile

Having a non-volatile oil ensures that diffusion only occurs in the liquid phase, and no oil diffuses though the gas phase. The bitumen used in this thesis was heated to 70°C to remove water before the diffusion experiments. When the diffusion experiment is begun, the bath was heated and the pressure was monitored in the diffusion cell and gas supply. While heating the system to 90^{o}C, the pressure in the diffusion cell did not increase more than that of the sample cylinder, indicating that little gas was evaporating

Pseudo-Binary System

Although oil is composed of a large number of different molecules, modelling the diffusion process is dramatically simplified by assuming the oil is a single pseudo-component. If the oil is non-volatile, there is no diffusion at all across the upper boundary. However, while the final conditions is a homogeneous mixture, the lighter bitumen components may diffuse from lower bitumen-rich layers to upper solvent-rich layers more rapidly than heavier component. There was no way to test for this effect and it was neglected.

Negligible Density Gradient

The diffusivity experiments modeled in this thesis are generally at low solubility, with only three experiments above 7 wt%. Therefore, at low solubility the density gradients will be small in the oil phase. This assumption allows the combine the density and weight fraction and density into the derivative in Fick's First Law.

Negligible Velocity Contribution

The only velocity in the system is caused by swelling as the solvent dissolves into the bitumen. Then initial velocity was estimated near the interface, where it is expected to be highest. The contribution of convection to the calculated mass diffused was less than 0.1% of the mass diffused from diffusion. The velocity contribution is therefore neglected in the mathematical model.

After applying the above assumptions, the mass balance equation simplifies to the following form, as was discussed in Chapter 2:

$$\frac{\partial}{\partial z}\left(D_{sb}\frac{\partial c_s}{\partial z}\right) = \frac{\partial c_s}{\partial t} \tag{4.1}$$

Where D_{sb} is the diffusivity of solvent in bitumen in m^2/s and c_s is the concentration of solvent in oil in kg/m^3.

4.3 Initial and Boundary Conditions

Diffusion in the cylindrical geometry described in Figure 1 can be modelled using a one dimensional diffusion model that requires one initial and two boundary conditions to solve.

4.3.1 Initial Condition

Two initial conditions are used in modelling the systems of interest in this thesis. For the majority of experiments in this thesis the oil is dead and there is no initial solvent concentration as indicated by the following boundary condition:

$$c_s(z, t = 0) = 0 \tag{4.2}$$

where c_s is the concentration, z is the position in the oil column, and t is the time. A small number of experiments were conducting with the oil phase containing an evenly distributed initial concentration of the solvent gas. To model these systems, the following boundary condition is used.

$$c_s(z, t = 0) = c_{s0} \tag{4.3}$$

where c_{s0} is the initial concentration of solvent gas.

4.3.2 Boundary Conditions

The two boundary conditions required to solve the continuity equation are usually taken at the gas-oil interface and at the bottom of the oil column as was shown in Figure 1. These are the locations in the system where the most information regarding the diffusing gas is available.

At the Gas-Oil Interface

Tharanivasan *et al.*, (2004) compared three different gas-oil boundary conditions used to model pressure decay experiments. For systems of methane diffusing into oil, the following Dirichlet equilibrium boundary conditions was found to best fit the data:

$$c_s(z = 0, t) = c_{s\,eq} \tag{4.4}$$

where c_{seq} is the equilibrium composition of the diffusion cell in kg/m^3. For pressure decay experiments, c_{seq} is defined at the equilibrium pressure at the end of the experiment. For a constant pressure boundary condition experiment, c_{seq} is defined at the operating pressure of the experiment.

Etminan *et al.* (2012) developed a time dependent Robin boundary condition for both methane and carbon dioxide diffusion into bitumen (Etminan *et al.*, 2014a) that accounts for the possibility of mass transfer resistance at the interface, given by:

$$-D_{sb}\left.\frac{dc_s}{dz}\right|_{z=0} = k\left(c_{s-int}(t) - c_s(z = 0, t)\right) \tag{4.5}$$

where D_{sb} is the diffusivity of the solvent (s) through the bitumen (b) in m²/s, k is the mass transfer coefficient in m/s, $c_{A\text{-}int}$ is the concentration immediately above the interface in kg/m³, and $c_A(z=0, t)$ is the concentration immediately below the interface kg/m³. The sensitivity of the

pressure drop to each of these variables was measured. The results were very consistent to those found with a Dirichlet boundary condition Tharanivasan et al, (2004) and; therefore, it was concluded that a Dirichlet condition is sufficient to model pressure decay data of methane in heavy oil. Therefore, in this thesis, Equation 4.4 will be used to model the pressure decay and constant pressure delivery experiments.

At the Bottom of the Oil Column

There are two common boundary conditions taken at the bottom of the oil column. The first is an infinite acting boundary condition where it is assumed that the oil column is infinitely deep and the initial condition of the system is maintained at infinite depth. This boundary condition applies when the diffusing solvent has not yet reached the bottom of the bitumen column. The systems in this thesis where this condition is applied have no initial concentration of dissolved gas and therefore the boundary condition is given by:

$$c_s(z \to \infty, t) = 0 \tag{4.6}$$

The second common boundary condition is the finite acting condition and it is applied before and after the solvent reaches the bottom of the bitumen column. Since the bottom of the oil column is in contact with the metal diffusion cylinder, there will be no gas diffusion though this position. Hence, the concentration gradient is zero at this point and the boundary condition is given by:

$$\left.\frac{dc_s}{dz}\right|_{z=h} = 0 \tag{4.7}$$

where h is the height of the oil column. Equations 4.6 and 4.7 give identical solutions to the continuity equation until the diffusing gas reaches the bottom of the oil column.

In this thesis, the entire range of data collected from pressure decay experiments is analyzed and; therefore, Equation 4.7 is used. Equation 4.6 was used to analyze early time data for some experiments and the results were compared with those obtained with Equation 4.7 in order to validate that the method was implemented correctly.

4.4 Solutions at Dilute Conditions

Analytical solutions to Fick's Law can be obtained when the diffusivity is a constant and there is no swelling; that is, at dilute conditions. The solutions with the infinite and finite acting boundary conditions are provided below.

4.4.1 Infinite Acting Solution

The solution to Fick's Law with the infinite acting boundary condition (Equation 4.6), the equilibrium gas-oil interface equation (Equation 4.3), and no initial solvent content (Equation 4.1) is given by:

$$\frac{c_s}{c_{s\,eq}} = 1 - erf\left(\frac{z}{\sqrt{4D_{sb}t}}\right) \tag{4.8}$$

where *erf* is the error function.

As was discussed in Chapter 2, the mass diffused at a given time is determined from the following integral:

$$m_s(t) = A_c \int_0^h c_s dz \tag{4.9}$$

Equation 4.8 is substituted into Equation 4.9 to obtain the following expression:

$$m_s(t) = 2A_c c_{s\,eq}\sqrt{\frac{D_{sb}t}{\pi}} \tag{4.10}$$

Since the infinite acting boundary condition does not account for the finite nature of the oil column, valid comparisons with experimental data can only be made until the diffusing gas reaches the bottom of the diffusion cell. The experiment is usually run until the oil is saturated with the gas in order to determine $c_{s\,eq}$.

As an example, the infinite acting analysis was applied to the pressure decay data for methane diffusing into *n*-decane. The data are plotted against the square root of time to show the linear infinite acting region, Figure 4.2. The solubility, c_{Aeq}, is determined from the asymptote in the

cumulative mass diffused. The slope of the infinite acting linear region is determined and the diffusivity is calculated by rearranging Equation 4.10 as follows:

$$D_{sb} = \left(\frac{S}{2Ac_{s\,eq}}\right)^2 \pi \tag{4.11}$$

where S is the slope if the linear region.

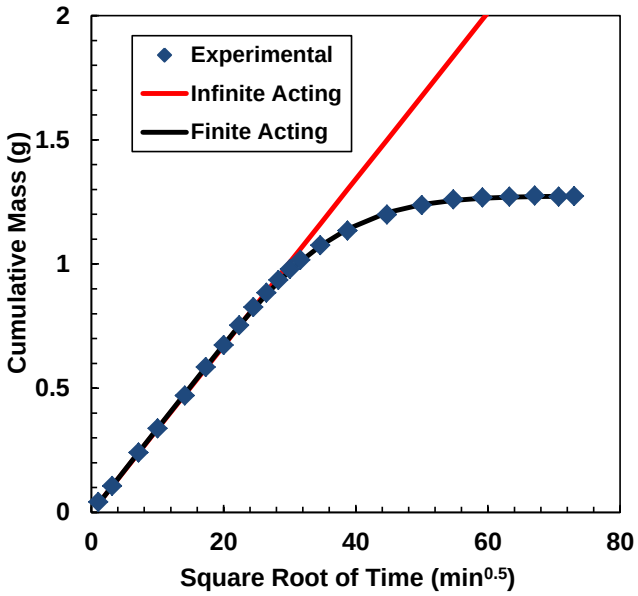

Figure 4.2. Cumulative mass of methane diffused into *n*-decane against square root of time at 123°C and 3950 kPa with infinite and finite acting fits to the data.

4.4.2 Finite Acting Solution

The solution to Fick's Law with the finite acting boundary condition (Equation 4.6), the equilibrium gas-oil interface equation (Equation 4.4), and no initial solvent content (Equation 4.1) is given by:

$$\frac{c_s}{c_{s\,eq}} = 1 - \frac{4}{\pi}\sum_{n=1}^{\infty}\frac{1}{(2n-1)}\sin\left(\left(\frac{2n-1}{2}\right)\frac{\pi}{h}x\right)exp\left(-\left(\left(\frac{2n-1}{2}\right)\frac{\pi}{h}\right)^2 D_{sb}t\right) \tag{4.12}$$

Equation 4.12 is substituted into Equation 4.9 to obtain the following expression relating the total mass diffused to time:

$$m_s(t) = \frac{8A_c c_{s\,eq} h}{\pi^2} \sum_{n=1}^{\infty} \frac{1}{(2n-1)^2} \left(1 - exp\left(-\left(\left(\frac{2n-1}{2}\right)\frac{\pi}{h}\right)^2 D_{sb} t\right)\right) \qquad (4.13)$$

This model is fit to the data by varying both the solubility and the diffusivity to minimize the error. The finite acting solution for the methane diffusion example discussed previously is also presented in Figure 2. Both the finite and infinite acting solutions are identical until the diffusing solvent reaches the bottom on the oil column. Only the finite acting solution can describe the diffusion from this point until the entire fluid column is saturated with methane. The infinite series of equations 4.12 and 4.13 are truncated at *n*=500 where the modeled mass diffused at all times was within 1% of the predicted mass using a truncation of 1000.

4.5 Modelling Diffusion at Non-Dilute Conditions

At non-dilute conditions, the solvent content is high enough to cause significant swelling of the oil column and therefore the upper boundary is no longer in a fixed position. In addition, the diffusivity may be a function of composition and this dependence may become significant at higher solvent contents. Hence, the analytical solutions presented in Section 4.3 are no longer valid. A numerical model was developed to include both swelling and compositionally dependent diffusivities.

4.5.1 Model Description

To set up the model of the pressure decay experiments, the oil phase is divided into layers of equal thickness and the gas phase is assumed to be homogeneous (Figure 4.3). The initial solvent concentration in each oil layer is set to a uniform initial value, usually zero. The solvent concentration at the gas-oil interface is set to the solvent solubility limit and the finite acting boundary condition is applied to the bottom of the column.

At each time step, solvent diffusion from the gas to the oil from each layer to the next is determined from the continuity equation using either a fixed diffusivity or a compositionally

dependent diffusivity. The mass of bitumen in each cell is held constant and only the mass of solvent changes. The density of each cell is updated and the height of the cell recalculated. The mass diffused is the sum of the solvent masses in each cell. The height of the gas-oil interface is the sum of the height of all of the layers. Each step in the calculations is described below.

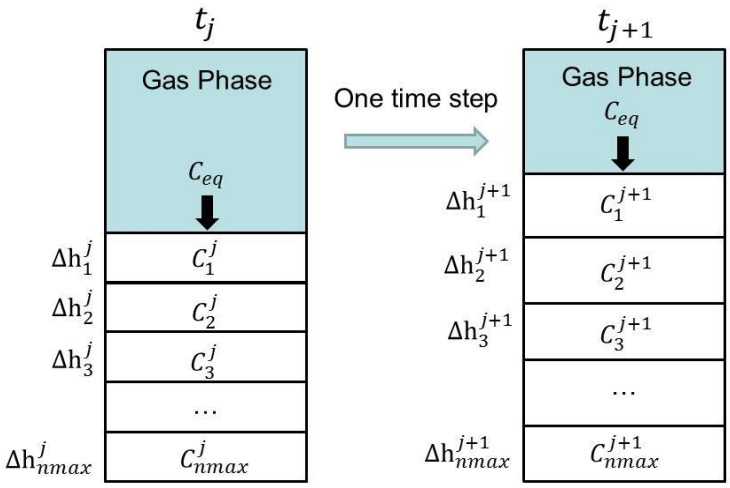

Figure 4.3. Numerical diffusion model for pressure decay experiments.

4.5.2 Discretization of the Continuity Equation

The continuity equation, Equation 4.1, does not include a convective term but does allow the diffusivity to vary with composition. The equation is discretized using a Forward Time Centered Space (FTCS) scheme (Fletcher, 1991). In particular, the two point forward difference method is used to discretize the time derivative and the three point central difference method is used to discretize the spatial derivative as follows:

$$\frac{C_{s_n}^{\,j+1} - C_{s_n}^{\,j}}{t_{j+1} - t_j} = \frac{D_n^j}{\left(\Delta h_n^j\right)^2}\left(C_{s_{n-1}}^{\,j} + C_{s_{n+1}}^{\,j} - 2C_{s_n}^{\,j}\right) + \frac{\left(D_{n+1}^j - D_{n-1}^j\right)}{4\left(\Delta h_n^j\right)^2}\left(C_{s_{n+1}}^{\,j} - C_{s_{n-1}}^{\,j}\right) \tag{4.14}$$

where C_s is the solvent concentration in g/cm³, t is time in minutes, D is diffusivity in cm²/min, Δh_n^j is the height of the layer in cm, n and j are the indexes for vertical position and time. Equation 4.14 is rearranged to solve for the concentration at the subsequent time step as follows:

$$C_{s_n}^{\ j+1} = C_{s_n}^{\ j} + \frac{(t_{j+1} - t_j)}{\left(\Delta h_n^j\right)^2}\Big(D_n^j\left(C_{s_{n-1}}^{\ j} + C_{s_{n+1}}^{\ j} - 2C_{s_n}^{\ j}\right) + \frac{1}{4}(D_{n+1}^j - D_{n-1}^j)(C_{s_{n+1}}^{\ j} - C_{s_{n-1}}^{\ j})\Big) \tag{4.15}$$

Equation 4.15 gives the concentration at each position and time except at the domain boundaries and at the initial time. In the case of a constant diffusivity this equation can be simplified to:

$$C_{s_n}^{\ j+1} = C_{s_n}^{\ j} + \frac{(t_{j+1} - t_j)}{\left(\Delta h_n^j\right)^2} D\left(C_{s_{n-1}}^{\ j} + C_{s_{n+1}}^{\ j} - 2C_{s_n}^{\ j}\right) \tag{4.16}$$

To specify the concentration at these conditions, the boundary conditions and initial conditions must be applied. Using the same method, the finite acting boundary condition, the equilibrium boundary condition at the gas-oil interface, and the initial condition can be discretized to the following:

$$C_{s_{nmax}}^{\ j} = C_{s_{nmax}}^{\ j-1} + \frac{D_{nmax}^{j-1} * (C_{s_{nmax-1}}^{\ j-1} - C_{s_{nmax}}^{\ j-1})\left(t_{j+1} - t_j\right)}{\Delta h_{nmax}^{j-1}} \tag{4.17}$$

$$C_{s_0}^{\ j} = c_{s\,eq} \tag{4.18}$$

$$C_{s_n}^{\ 0} = c_{s0} \tag{4.19}$$

where n_{max} is the bottom layer and c_{s0} is the initial concentration of solvent in the oil. The determination of the diffusivity terms is discussed in Section 4.5.4.

4.5.3 Determination of Layer Thickness and Mass Diffused

The initial thickness of each layer is given by:

$$\Delta h_n^0 = \frac{m_{oil}}{\rho_b * A_c * n_{max}} \tag{4.20}$$

where Δh_n^0 is the initial thickness of each layer in cm, m_{oil} is the initial mass of oil in g, ρ_b is the density of the oil in g/cm³, and A_c is the cross sectional area of the diffusion cylinder in cm^2.

To calculate the layer thickness at each time step, the volume of fluid in each layer must be determined at each time step. The height is then the volume divided by the fixed cross sectional area. The volume is determined from the known mass of bitumen, the mass fraction of solvent in each layer at the given time step, and the density of the mixture. The mass fraction of solvent in each layer is calculated from the concentration of solvent in the layer as follows:

$$w_{s_n}^{\ j} = \frac{A_c * \Delta \mathrm{h}_n^{j-1} * C_{s_n}^{\ j}}{m_{b_n}^{\ j} + A_c * \Delta \mathrm{h}_n^{j-1} * C_{s_n}^{\ j}} \tag{4.21}$$

where $w_{s_n}^{\ j}$ is the mass fraction of solvent in the layer and $m_{b_n}^{\ j}$ is the fixed mass of bitumen in each layer in g. The density of the mixture is obtained from the mixing rules from Saryazdi *et al.* (2013) given by:

$$\rho_{mix_n}^{\ j} = \left(\frac{w_{s_n}^{\ j}}{\rho_s} + \frac{1 - w_{s_n}^{\ j}}{\rho_b} - w_{s_n}^{\ j} * \left(1 - w_{s_n}^{\ j}\right) \left(\frac{1}{\rho_s} + \frac{1}{\rho_b} \right) \beta_{sb} \right)^{-1} \tag{4.22}$$

where $\rho_{mix_n}^{\ j}$ is the density of the mixture in the layer in g/cm³, ρ_s is the effective liquid density of the solvent in g/cm³, ρ_b is the density of the bitumen in g/cm³ and β_{sb} is the binary interaction parameter between the solvent and the oil. The density model is discussed in more detail in Section 4.5.5.

The thickness of each layer is then given by:

$$\Delta \mathrm{h}_n^j = \frac{A_c * \Delta \mathrm{h}_n^{j-1} * C_{s_n}^{\ j} + m_{b_n}^{\ j}}{\rho_{mix_n}^{\ j} * A_c} \tag{4.23}$$

The total height of the oil can be calculated by adding all of the layer thicknesses

$$h = \sum_{n=1}^{nmax} \Delta h_n^j \tag{4.24}$$

The total amount of solvent diffused is determined by summing the total mass of solvent in each of the grid layers.

$$m_s^j = \sum_{n=1}^{nmax} A_c * \Delta h_n^j * C_{s_n}^{\ j} \tag{4.25}$$

where m_s^j is the total mass of solvent diffused into the oil at time step j.

4.5.4 Models for Diffusivity

In this thesis, five models for the diffusivity were studied:

1) constant diffusivity

$$D_{sb} = Constant \tag{4.26}$$

2) the Hayduk and Cheng (1971) equation

$$D_{sb} = \frac{A}{{\mu_{mix}}^n} \tag{4.27}$$

3) the modified Hayduk and Cheng equation

$$D_{sb} = \frac{AT}{{\mu_{mix}}^n} \tag{4.28}$$

4) a modified Bearman (1961) equation

$$D_{sb} = \frac{A}{{\mu_{mix}}^n}\left[1 + x_s\left(\frac{V_s}{V_b} - 1\right)\right]\left(\frac{d \ln a_s}{d \ln x_s}\right) \tag{4.29}$$

5) the Vignes (1966) equation

$$D_{sb} = (D_{sb}^0)^{x_b}(D_{bs}^0)^{x_s}\left(\frac{d\ln a_s}{d\ln x_s}\right) \tag{4.30}$$

where D_{sb} is the diffusivity of solvent in bitumen, μ_{mix} is the mixture viscosity, x is the mole fraction, V is the molar volume, a is the activity, A and n are parameters specific to the fluid mixture, the subscripts s and b refer to the solvent and bitumen respectively, and D_{sb}^0 and D_{bs}^0 are the infinite dilution diffusivities of solvent in bitumen and bitumen is solvent respectively

The models for diffusivity are substituted into the discretized continuity equation (Equation 4.15) and each diffusivity models is adjusted to best fit the data. When using Equation 4.26, the model is fit to experimental data by adjusting the value of D. The models using Equations 4.27 to 4.29 are fit to experimental data by adjusting the parameters A and n. The models using Equation 4.30 are fit to experimental data by adjusting the two infinite dilution diffusivities D_{sb}^0 and D_{ba}^0.

When modelling with a constant diffusivity, no additions need to be made to the modelling methodology described earlier in this chapter. However, when applying the concentration dependent diffusivity models, other inputs may be required including the mixture viscosity, the mole fraction of the components, the molar volumes of the components, and the thermodynamic correction of the solvent in the oil. Each of these parameters are evaluated after the concentration profiles and heights of the layers have been calculated.

Mole Fraction and Molar Volume

The mole fraction of solvent in the layer can be calculated from the weight fraction of solvent (from Equation 4.21) as follows:

$$x_{s_n}^{\ j} = \frac{\frac{w_{s_n}^{\ j}}{M_s}}{\frac{w_{s_n}^{\ j}}{M_s} + \frac{1 - w_{s_n}^{\ j}}{M_b}} \tag{4.31}$$

where ${x_s}_n^j$ is the mole fraction of solvent in the grid layer and M_s and M_b are the molar mass of solvent and bitumen respectively in g/mol. The mole fraction of bitumen in this layer is simply:

$$ {x_b}_n^j = 1 - {x_s}_n^j \tag{4.32} $$

where ${x_B}_n^j$ is the mole fraction of bitumen in the layer.

The molar volume of each component is simply it molecular weight divided by its density. The molecular weights are inputs. The density of the bitumen and solvent are discussed in Section 4.5.5.

Viscosity

The viscosity of each layer is calculated using the Expanded Fluid viscosity correlation (Yarranton and Satyro, 2011) given by:

$$ \mu_n^j - {\mu_D}_n^j = 0.165 * \left(exp\left({c_2}_n^j \beta\right) - 1\right) \tag{4.33} $$

$$ \beta = \frac{1}{exp\left(\left(\frac{{\rho_s^*}_n^j}{\rho_n^j}\right)^{0.65} - 1\right) - 1} \tag{4.34} $$

$$ {\rho_s^*}_n^j = \frac{{\rho_s^0}_n^j}{exp\left(-{c_3}_n^j P\right)} \tag{4.35} $$

where μ_n^j is the viscosity of layer n at time step j in mPa.s, ${\mu_D}_n^j$ is the dilute gas viscosity in mPa.s, ${\rho_s^*}_n^j$ is the pressure dependent compressed state density in kg/m³, P is pressure in MPa, ${\rho_s^0}_n^j$ is the compressed state density in kg/m³, ρ is the density of the mixture in kg/m^3, and c_2 and c_3 are parameters specific to the fluid mixture that that are dimensionless and in MPa^{-1} respectively.

For a binary mixture, the parameters ρ_s^0, c_2, and c_3 are determined as follows:

$$\rho_{s\,n}^{0\,j} = \left[\frac{w_{s_n}^{\ j}}{\rho_{s,s}^{0}} + \frac{1 - w_{s_n}^{\ j}}{\rho_{s,b}^{0}} - w_{s_n}^{\ j} * \left(1 - w_{s_n}^{\ j}\right) * \left(\frac{1}{\rho_{s,s}^{0}} + \frac{1}{\rho_{s,b}^{0}}\right)\theta_{sb}\right]^{-1} \tag{4.36}$$

$$\frac{c_{2,mix}}{\rho_{s\,n}^{0\,j}} = \frac{c_{2,s} w_{s_n}^{\ j}}{\rho_{s,s}^{0}} + \frac{c_{2,b}\left(1 - w_{s_n}^{\ j}\right)}{\rho_{s,b}^{0}} - w_{s_n}^{\ j} * \left(1 - w_{s_n}^{\ j}\right) * \left(\frac{c_{2,s}}{\rho_{s,s}^{0}} + \frac{c_{2,b}}{\rho_{s,b}^{0}}\right)\theta_{sb} \tag{4.37}$$

$$c_{3_n}^{\ j} = \left[\frac{w_{s_n}^{\ j}}{c_{3,s}} + \frac{\left(1 - w_{s_n}^{\ j}\right)}{c_{3,b}}\right]^{-1} \tag{4.38}$$

where θ_{sb} is a binary interaction parameter and subscripts *s* and *b* denote the solvent and the bitumen, respectively. A more detailed description of the Expanded Fluid viscosity model and the determination of its parameters is provided in Section 4.5.6.

Thermodynamic Correction Factor

As described in Chapter 2, the thermodynamic correction factor is defined as follows:

$$\alpha = \frac{d \ln a_s}{d \ln x_s} \tag{4.39}$$

where α is the thermodynamic correction factor. In this thesis the activity was calculated with an activity coefficient such that (Elliot and Lira, 1991):

$$a_s = \gamma_s x_s \tag{4.40}$$

where $\gamma_s$is the activity coefficient. The activity coefficient was determined from the Margules (1895) equation given by:

$$\ln \gamma_s = [A_{sb} + 2(A_{bs} - A_{sb})x_s](1 - x_s)^2 \tag{4.41}$$

where A_{sb} and $A_{bs}$are parameters specific to a given mixture. Equation 4.40 is substituted into Equation 4.39 to obtain the following expression:

$$\alpha = \frac{d\ln(\gamma_s x_s)}{d\ln x_s} = \frac{d\ln\gamma_s}{d\ln x_s} + 1 = x_s\frac{d\ln\gamma_s}{dx_s} + 1 \tag{4.42}$$

Equations 4.41 is then substituted into Equation 4.42 to obtain the thermodynamic correction factor for each layer in terms of the Margules coefficients and the mole fraction of solvent in the layer.

$$\alpha_n^j = 1 + {x_s}_n^j\left[-2\left({x_s}_n^j - 1\right) * \left(A_{sb}\left(3{x_s}_n^j - 2\right) - 3A_{bs} + A_{bs}\right)\right] \tag{4.43}$$

The coefficients of the Margules equation were fitted to the solvent oil saturation pressure data measured for this thesis, as will be discussed in Chapter 5.

4.5.5 Prediction of Mixture Density

The density of mixtures of oil and solvent are required to determine the volume of each layer in the numerical diffusion model. It is also a key input parameter for the viscosity model used to determine compositionally dependent diffusivities. The viscosity model is quite sensitive to the accuracy of the input density. Hence, an accurate density prediction is required.

Saryazdi et al. (2013) demonstrated that a combination of effective solvent densities and non-ideal mixing rules could fit density data for mixtures of oil and solvent to within the accuracy of the measurements. They proposed the following form of mixing rule:

$$\rho_{mix} = \left[\sum_i\sum_j \frac{w_i w_j}{2}\left(\frac{1}{\rho_i} + \frac{1}{\rho_j}\right)\left(1 - \beta_{ij}\right)\right]^{-1} \tag{4.44}$$

where ρ_{mix} is the mixture density in kg/m³, w is the weight fraction of each component, and ρ is the density or effective density of the pure components, and β_{ij} is the binary interaction parameter between components i and j. For binary mixtures or pseudo-binaries such as solvent and bitumen, Equation 4.44 simplifies to the following expression:

$$\rho_{mix} = \left(\frac{w_A}{\rho_A} + \frac{1 - w_A}{\rho_B} - w_A * (1 - w_A) * \left(\frac{1}{\rho_A} + \frac{1}{\rho_B} \right) \beta_{AB} \right)^{-1} \quad (4.45)$$

For gases dissolved in liquids, the solvent liquid density is taken as the effective liquid density; that is, the hypothetical density of that gas when it is part of a liquid mixture. Effective densities were determined for some common gases by Saryazdi *et al.* (2013) and fitted with the following equations.

$$\rho_e = \rho_{e0} + B^* * P \quad (4.46)$$

$$\rho_{e0} = a_1^* + a_2^* T \quad (4.47)$$

$$B^* = b_1^* + b_2^* T \quad (4.48)$$

where ρ_e is the effective density of a gas in liquid in kg/m^3, P is the pressure in MPa, T is temperature in K, and a_1^*, a_2^*, b_1^*, and b_2^* are fluid specific parameters. The parameters for the effective liquid density correlations for the hydrocarbons relevant for this thesis are provided in Table 4.1.

Table 4.1. Parameters for the effective liquid density correlation (Saryazdi *et al.* 2013).

Component	a_1^* **kg/m³**	a_2^* **kg/(m³·K)**	b_1^* **kg/(m³·MPa)**	b_2^* **kg/(m³·MPa·K)**
Methane	532.157	-0.69737	0.42606	0.001143
Ethane	704.900	-0.82749	0.21442	0.002012
Propane	793.847	-0.85489	0.05309	0.002440
Butane	846.443	-0.85024	-0.05448	0.002648

In this thesis the bitumen density was determined by interpolating with pressure and temperature, between experimentally determined bitumen densities measured between 20 and 180^{o}C and between 0.1 and 10 MPA by Saryazdi *et al.* (2013).

If regular solution behavior is assumed (binary interaction parameters set to zero), the use of effective densities in the mixing rules gives density predictions with an average deviation of 0.7% of the measured values for most hydrocarbon/crude oil mixtures. If the binary interaction parameter is fitted to the data, the average deviation is 0.4%. When no data are available, the

following correlation can be used to determine the binary interaction parameter (Saryazdi *et al.* 2013):

$$\beta_{AB} = \beta_{AB}^{298} + 8.74 * 10^{-5}(T - 298) \tag{4.49}$$

$$\beta_{AB}^{298} = -0.092 \left| 0.435 - 2\left(\frac{|v_A^{298} - v_B^{298}|}{(v_A^{298} + v_B^{298})}\right)\right| + 0.022 \tag{4.50}$$

where $\beta_{AB}^{298}$is the binary interaction parameter between components *i* and *j* and 298 K and $v_i^{298}$is the specific volume of component *i* at 298 K in. The mixing rules with the correlated binary interaction parameter fit mixture data for oils and solvents with an average deviation of 0.6%. In this thesis, the correlated binary interaction parameters were used in the numerical modeling.

4.5.6 Prediction of Mixture Viscosity

The viscosity of mixtures of bitumen and solvent are required to account for the compositional dependence of the diffusivity in several the diffusion models. The viscosity of these mixtures are determined with the Expanded Fluid Viscosity Model (Yarranton and Satyro, 2009; Motahhari *et al*., 2013a-c). This model determines the fluid viscosity as a departure from a dilute gas viscosity where the departure is a function of density, as follows:

$$\mu - \mu_D = 0.165 * (exp(c_2\beta) - 1) \tag{4.51}$$

where μ_D is the dilute gas viscosity in mPa.s, c_2 is a fluid specific parameter and the correlating parameter β is given by:

$$\beta = \frac{1}{exp\left(\left(\frac{\rho_s^*}{\rho}\right)^{0.65} - 1\right) - 1} \tag{4.52}$$

where ρ_s^* is the pressure dependent compressed state density in kg/m^3 given by:

$$\rho_s^* = \frac{\rho_s^0}{exp(-c_3 P)} \tag{4.53}$$

where P is pressure in MPa, ρ_s^o is the compressed state density in kg/m³, and c_3 is a fluid specific parameter in MPa^{-1}. The fluid specific parameters c_2, ρ_s^o and c_3 for the pure components relevant for this thesis are listed in Table 4.2. A more extensive set of pure component parameters is available in Motahhari *et al.* (2013b).

The three fluid specific parameters c_2, c_3, and ρ_s^0 for the bitumen were fitted to measured viscosities (Motahhari *et al.* 2013b). Since there is a sizable variation in the magnitude of the viscosity with temperature, fitting the data by minimizing the square error would likely skew the fit towards the point with the highest viscosity. To avoid this problem, the logarithmic error was minimized.

Table 4.2. Expanded Fluid model fluid specific parameters for selected fluids.

Component	**ρ_s^0 kg/m³**	**c_2**	**c_3 x 10^3 MPa^{-1}**
Methane	540	0.1	0.1
Ethane	724	0.156	0.1
Propane	778	0.174	0.1
Butane	813	0.190	0.15
WC-B-B3	1076.6	0.2025	0.31

The dilute gas viscosity at 1 atm is correlated in Yaws' Handbook (1999) as follows:

$$\mu_D = A_0 + B_0 T + C_0 T^2 \qquad (4.54)$$

where A_0, B_0 and C_0 are fitting parameters and T is the temperature in K, Table 4.3. If no parameters are listed the Chung *et al.* (1988) method can be used to estimate the dilute gas viscosity (Motahhari *et al*, 2013b).

Table 4.3. Parameters for calculation of dilute gas viscosity

Component	A_0 x10^4 (mPa.s)	B_0 x10^4 (mPa.s K^{-1})	C_0 x10^8(mPa.s K^{-2})
Methane	3.8435	0.4011	-1.4303
Ethane	0.5142	0.3345	-0.7107
Propane	-5.4615	0.3272	-1.0672
Butane	-4.9462	0.29	-0.6967
WC-B-B3	2.8626	0.0638	0.03729

For mixtures, Equations 4.51 to 4.54 are applied with fluid specific parameters calculated for the mixture. The following mixing rules are used for each fluid specific parameter (Motahari *et al*., 2011):

$$\rho_{s,mix}^{0} = \left[\sum_{i=1}^{nc}\sum_{j=1}^{nc}\frac{w_i w_j}{2}\left(\frac{1}{\rho_{s,i}^{0}}+\frac{1}{\rho_{s,j}^{0}}\right)\left(1-\theta_{ij}\right)\right]^{-1} \tag{4.55}$$

$$\frac{c_{2,mix}}{\rho_{s,mix}^{0}} = \sum_{i=1}^{nc}\sum_{j-1}^{nc}\frac{w_i w_j}{2}\left(\frac{c_{2,i}}{\rho_{s,i}^{0}}+\frac{c_{2,j}}{\rho_{s,j}^{0}}\right)\left(1-\theta_{ij}\right) \tag{4.56}$$

$$c_{3,mix} = \left[\sum_{i=1}^{nc}\frac{w_i}{c_{3,i}}\right]^{-1} \tag{4.57}$$

where *nc* is the number of components in the system and θ_{ij} is a binary interaction parameter that can be used to tune the model to experimental data. If no data are available, θ_{ij} is taken as zero.

The dilute gas viscosity for a mixture can be calculates using the Wilke (1950) method as outlined by Motahari *et al.* (2013).

$$\mu_{D,mix} = \sum_{i}\frac{x_i\mu_{0,i}}{\sum_j x_j\delta_{ij}} \tag{4.58}$$

$$\delta_{ij} = \frac{\left[1+\left(\mu_{0,i}/\mu_{0,j}\right)^{0.5}\left(M_j/M_i\right)^{0.25}\right]^2}{\left[8\left(1+M_i/M_j\right)\right]^{0.5}} \tag{4.59}$$

If θ_{ij} is set to zero, the average errors in the predicted viscosities of mixtures of crude oil and solvent are each generally less than 50% (Motahari *et al.*, 2011; Ramos-Pallares *et al.*, 2016). If

the binary interaction parameter is fitted to the data, the average errors in the fitted viscosities are less than 15%, almost within the experimental error of ±10 %. In this thesis, the binary interaction parameters were determined by fitting experimental data for the relevant solvent/bitumen mixtures (Ramos-Pallares *et al.*, 2016).

4.5.7 Determination of Step Size

When setting up the numerical model, the size of the time step and the initial layer thickness (through the number of layers, n_{max}) must be defined. Generally speaking, the smaller the steps, the more accurate the numerical solution will be. However, if the numerical step size is too small compared to that of the time, the solution will become unstable. The following inequality can be used to determine the appropriate ratio of time step to layer thickness:

$$\frac{(t_{j+1} - t_j)}{\left(\Delta h_n^j\right)^2} < L \tag{4.60}$$

where L is the maximum value of the ratio before the solution becomes unstable and will be different for each experiment. After running the model for several different experiments, the limiting value of L was found to be 2100 min/cm^2.

Sensitivity analyses were also performed on the effect of step size and initial layer size on the predicted mass diffused. Figure 4.4 shows that, within the limits set by Equation 4.60, there was no appreciable sensitivity to the time step at a fixed initial layer thickness. Figure 4.5 shows that there is very little change in the model results at a fixed time step once the initial layer thickness is 0.022 cm or less. To ensure the initial layer thickness is below this threshold in each of the experiments, the oil column was divided into 50 layers (n_{max} = 50). To ensure that the limiting value of L=2100 was not exceeded, a time step of 0.1 minute was used in all cases.

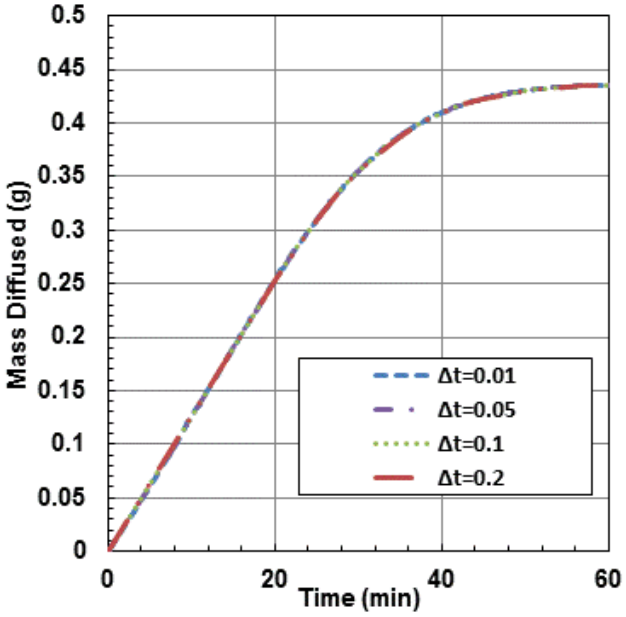

Figure 4.4. Sensitivity of calculated mass transfer to time step size with a constant initial layer thickness of 0.011cm for propane diffusion into bitumen at 80^{o}C and 740 kPa.

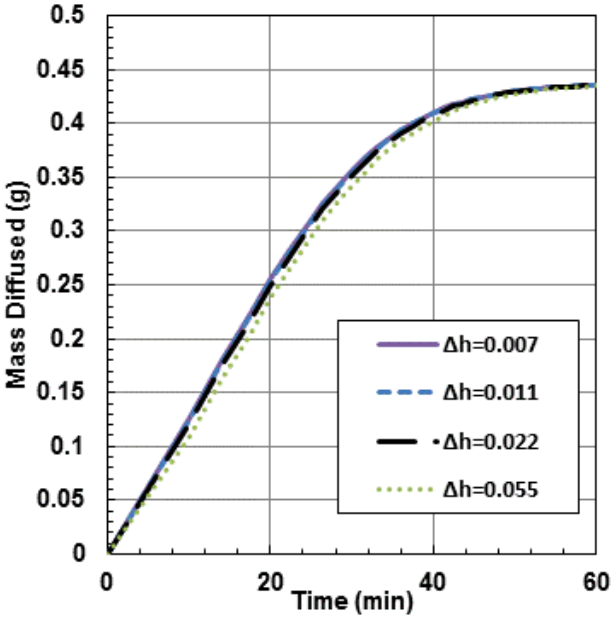

Figure 4.5. Sensitivity of calculated mass transfer to initial layer thickness with a time step of 0.1 minute for propane diffusion into bitumen at 80^{o}C and 740 kPa.

4.5.8 Algorithm for Fitting Experimental Data

The experimental data to be fitted is the mass diffused over time. The algorithm shown in Figure 4.6 is used to fit the data. The model in initialised with the total mass of bitumen, the cross sectional area, the density of the solvent and the oil, the binary interaction parameter for the density mixing rules, the solubility limit of the solvent in the oil, and an initial guess of the diffusivity. At each time step, the concentration of solvent in each layer, the height of each layer, the total mass diffused, and the total height of the oil column are calculated. The calculated mass diffused versus the square root of time is visually compared to the experimental data. If the calculated mass diffused does not match the experimental data, a new diffusivity is guessed and the process is repeated. An example of a fitted model is provided in Figure 4.7.

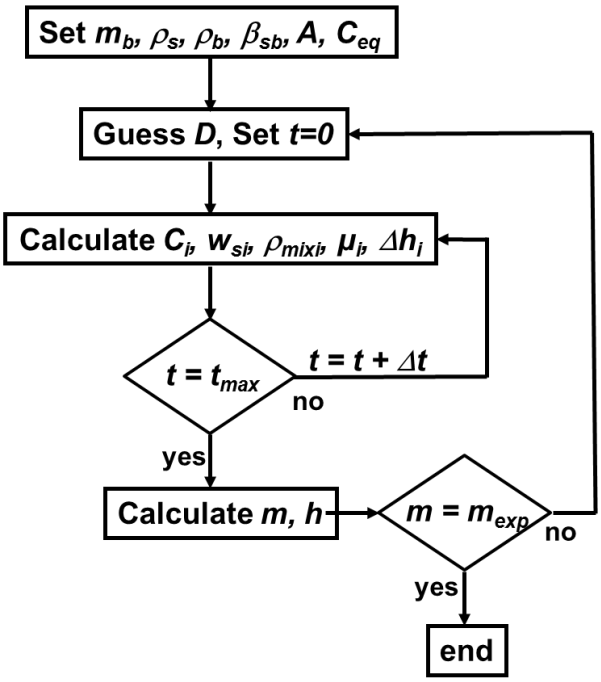

Figure 4.6. Algorithm for the diffusion model.

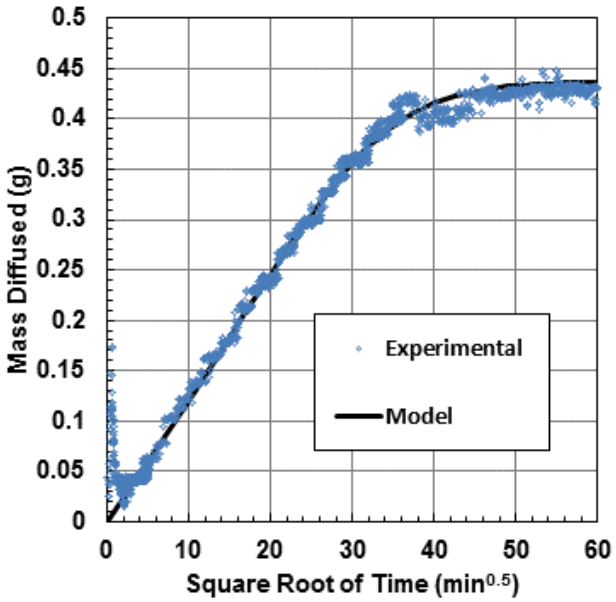

Figure 4.7. Measured and modeled mass of propane diffused into bitumen versus square root of time at 80^{o}C and 740kPa

CHAPTER FIVE: SOLUBILITY RESULTS AND DISCUSSION

This chapter presents the solubility data for methane, ethane, and propane in bitumen collected from both the blind cells and the diffusion experiments. Analytical models for saturation pressure are fit to the experimental data to facilitate error analysis and for use in the numerical diffusion model.

5.1 Data Collected

The solubilities of methane, ethane, and propane in WC-B-B3 bitumen from 50 to 180°C were measured using the diffusivity apparatus. The saturation pressures (and therefore solubilities) of ethane and propane in WC-B-B3 bitumen were measured over the same temperature range in the blind cells. Additional solubility data for methane in Athabasca bitumen was obtained from Svrcek and Mehrotra (1982). The solubility data used in this thesis are provided below for each solvent. Modeling, comparisons, and error analysis are discussed later.

Note that some of the diffusion experiments had large fluctuations in the early time data and could not be interpreted to determine diffusivities. However, a number of these experiments reached a stable plateau which could be used to determine a solubility. Therefore, there are more solubility data points than diffusivity data points.

5.1.1 Methane

Table 5.1 lists solubility data for methane in WC-B-B3 bitumen measured in the diffusivity apparatus. Table 5.2 lists methane solubilities in Athabasca bitumen collected by Mehrotra and Svrcek (1982).

Table 5.1 Solubility of methane in WC-B-B3 bitumen measured in the diffusivity apparatus (*denotes oil that was degassed at 176^{o}C).

Temperature ^{o}C	Pressure kPa	Solubility wt%	Solubility mol%
50	3451	0.42	12
76	4161	0.55	15
100	4226	0.53	15
100	4169	0.48	14
100	4340	0.51	14
101	4119	0.49	14
50*	3513	0.35	10
160*	3332	0.33	10
176*	3615	0.39	11

Table 5.2. Solubility of methane in Athabasca bitumen from Mehrotra and Svrcek (1982).

Temperature ^{o}C	Pressure kPa	Solubility wt%	Solubility mol%
27	9770	1.3	31
27	8250	1.1	27
27	7040	1.0	26
27	5790	0.8	22
27	4460	0.6	18
27	3320	0.5	13
27	2320	0.3	10
27	1590	0.2	7
45	9630	1.1	28
45	8180	1.0	25
45	6390	0.8	21
45	5090	0.6	18
45	4280	0.5	14
45	3180	0.4	12
45	2150	0.2	5
45	1080	0.1	4
68	9650	1.0	26
68	8600	0.9	24
68	7470	0.8	23
68	6290	0.7	20
68	5100	0.6	16
68	3640	0.4	11
68	2450	0.2	7
68	880	0.1	3
100	9440	0.9	25
100	7820	0.8	22
100	5790	0.7	19
100	3820	0.3	10
100	950	0.1	2

5.1.2 Ethane

Tables 5.3 and 5.4 provide the solubility data for ethane in WC-B-B3 bitumen measured in the diffusivity apparatus and the blind PVT cells, respectively.

Table 5.3. Solubility of ethane in WC-B-B3 measured in the diffusivity apparatus (**denotes results from an experiment where the diffusivity was rejected).

Temperature °C	Pressure kPa	Solubility wt%	Solubility mol%
37	2964	6.9	56
42	2168	3.8	40
42**	3316	6.1	53
47	1394	2.1	27
50	1741	3.6	40
58	2962	4.4	44
59	1495	2.4	30
64	1120	1.5	21
64	1751	2.5	31
64	2104	2.9	34
73	774	0.8	13
75	4324	5.3	49
90	4741	4.9	47
100	1916	1.9	25
100	1970	2.6	32

Table 5.4. Solubility of ethane in WC-B-B3 bitumen measured in the blind PVT cells.

Temperature °C	Pressure kPa	Solubility wt%	Solubility mol%
50	5276	10.5	67
50	4103	7.5	58
50	3297	4.3	44
50	2190	2.1	27
75	7813	10.5	67
75	5727	7.5	58
75	4128	4.3	44
75	2448	2.1	27
90	9344	10.5	67
90	6834	7.5	58
90	4802	4.3	44
90	2537	2.1	27
135	11702	10.5	67
135	7046	4.3	44
135	3077	2.1	27

5.1.3 Propane

Tables 5.5 and 5.6 list the solubility data for ethane in WC-B-B3 bitumen measured in the diffusivity apparatus and the blind PVT cells, respectively. Solubility data from two diffusion experiments conducted by Diedro *et al.* (2014) are included in Table 5.5. These two experiments were performed using computer tomography and will be discussed in more detail in Chapter 6. The data were provided courtesy of Dr. Kantzas at the University of Calgary.

Table 5.5. Solubility of propane in WC-B-B3 measured in the diffusivity apparatus (** denotes results from an experiment where the diffusivity was rejected, $ denotes results from CT data provided by Deidro *et al.*, (2016)).

Temperature °C	Pressure kPa	Solubility wt%	Solubility mol%
22$	620	9.5	55
40$	689	5.1	43
43**	633	6.3	44
50	327	2.6	24
50	724	4.6	36
53	982	6.6	45
59	824	3	27
60	602	3.5	30
62	1080	6.8	46
62	1635	12.9	64
64**	1265	8.9	54
64**	1890	8.6	53
70**	824	3.2	28
70	1077	4.5	36
74	523	2.1	21
74	1006	4.5	36
74**	1132	5.9	42
80	607	2.5	23
80	1507	8	51
81	720	2.4	23
81	1367	7.2	48
85	702	2.5	23
86	1374	5.4	40
86	2303	11.4	60

Table 5.6: Solubility of propane in WC-B-B3 from the blind PVT cells.

Temperature °C	Pressure kPa	Solubility wt%	Solubility mol%
50	1114	11.0	60
50	820	5.6	41
50	625	2.8	26
75	1883	11.4	60
75	1191	5.6	41
75	682	2.8	26
89	2360	11.4	60
89	1501	5.6	41
89	843	2.8	26
134	4512	11.4	60
134	2725	5.6	41
134	1551	2.8	26
180	7588	11.4	60
180	4591	5.6	41
180	2877	2.8	26
180	1694	1.1	12

5.2 Modeling Solubility Data

Two analytical approaches for modeling the saturation pressure were considered: Henry's law and an activity coefficient model with the Margules equations. Henry's law, as original formulated is only valid for small concentrations of dissolved gas but is convenient for data fitting with minor modifications. The Margules equation is valid for all compositions in the vapour-liquid region.

5.2.1 Henry's Law

Henry's law is discussed in Chapter 2, but is restated here for convenience (Reid *et al.*, 1987).

$$P = x_s H \tag{5.1}$$

where P is the pressure of the system, x_s is the mole fraction of the dissolved solvent, and H is Henry's constant in the same units as the pressure, P. Henry's constant is expected to be a function of temperature but to be independent of pressure. The following form of Henry's constant was found sufficient to fit the temperature dependence of the data:

$$\ln H = a + \frac{b}{T} \tag{5.2}$$

where a and b are fitting parameters, and T is the temperature in K. Figure 5.1a shows that the temperature dependent constant provides an adequate fit to the solubility data for propane in bitumen but fails to capture the upward curvature of the data at higher solubilities. Equation 5.2 was modified to include a pressure term to better fit the data as follows:

$$\ln H = a + \frac{b}{T} + \frac{c * P}{RT} \tag{5.3}$$

where R is the is the gas constant and c is a fitting parameter. The parameters a, b and c are fit to the data by minimizing the square error between the modeled and experimental solubility. Figure 5.1b shows the improvement to the fit that is possible with such a modification.

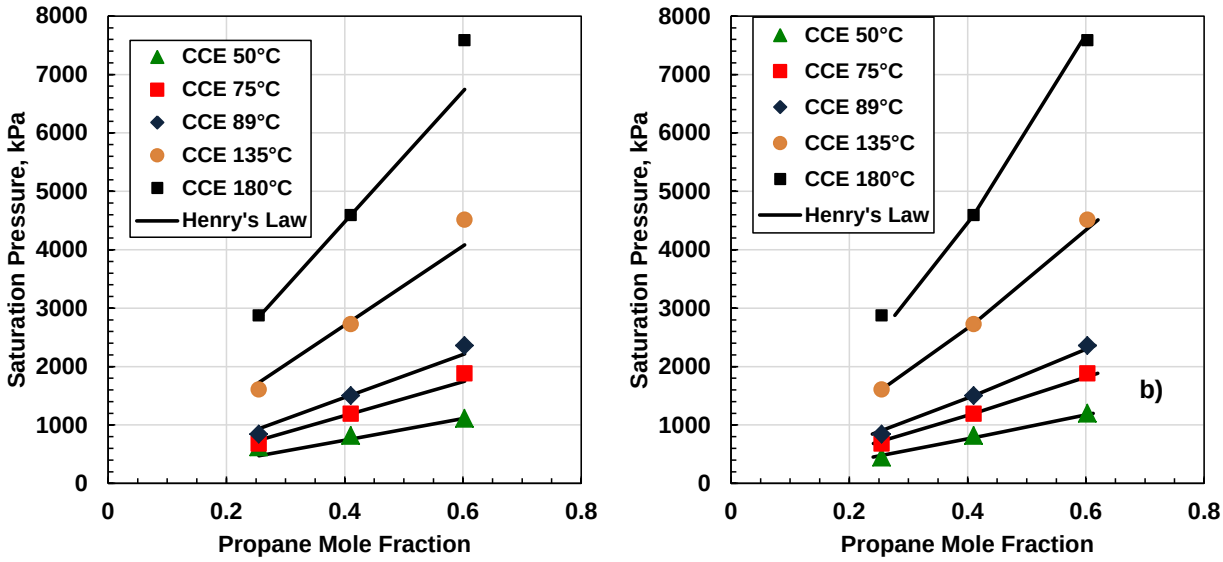

Figure 5.1. Saturation pressure of propane against more fraction of propane in WC-B-B3 bitumen from CCE experiments fit with Henrys Law using: a) temperature dependent constant; b) temperature and pressure dependent constant.

5.2.2 Margules Activity Coefficient Model

The Henry model is a simple empirical fit to the data but strictly speaking only applies to dilute solutions (low solvent contents). As was discussed in Chapter 2, an activity coefficient model is valid for the entire composition range as long as only a liquid and vapour phase are present. For pseudo-binary systems of solvent in oil, the equilibrium pressure can be expressed as follows:

$$P = x_s \gamma_s P_{v\,s} + x_b \gamma_b P_{v\,b} \tag{5.4}$$

where $\gamma_i$is the activity coefficient of species *i* (given by Equation 2.43), $P_{v\,i}$ is the vapour pressure of component *i*, and subscripts *s* and *b* refer to the solvent and bitumen phase. Equation 5.4 also takes into account the vapour pressure of the oil.

The saturation pressure for the solvent can be calculated using correlations listed in Green and Perry (2008).

$$\ln P_{v\,i} = C_1 + \frac{C_2}{T} + C_3 \ln T + C_4 T^{C_5} \tag{5.5}$$

where C_1 to C_5 are fluid specific parameters, T is the temperature in K, and $P_{v\,i}$ is the vapor pressure in Pa. Vapour pressure data only exist up to the critical point and therefore Equation 5.5 is only valid below the critical point. The constants for methane, ethane, and propane are provided in Table 5.7.

Table 5.7. Summary of the parameters for the Green and Perry vapour pressure correlation (Equation 5.5); temperature in K, and pressure in Pa.

Component	C_1	C_2	C_3	C_4	C_5	T_c **(K)**
Methane	39.205	-1324.4	-3.4366	3.1019×10^{-5}	2	190.6
Ethane	51.857	-2598.7	-5.1283	1.4913×10^{-5}	2	305.3
Propane	59.078	-3492.6	-6.0669	1.0919×10^{-5}	2	369.5

To model the saturation pressure of a mixture at a temperature above the solvent's critical point, a hypothetical vapour pressure of the solvent is required. The following correlation was used to estimate the hypothetical vapour pressure of a solvent above its critical temperature:

$$\ln P_i^* = C_1{}^* + \frac{C_2{}^*}{T} + C_3{}^* \ln T \tag{5.6}$$

where P_i* is the hypothetical vapour pressure in Pa and C_1* to C_3* are constants. The constants were determined using three constraints: 1) to match the value of the vapor pressure from Equation 5.5 at the critical temperature; 2) to match the derivative of Equation 5.5 at the critical temperature; 3) to match a hypothetical vapour pressure at the highest recorded temperature in the experiments. This hypothetical vapour pressure is treated as a fitting parameter along with the two Margules coefficients from Equation 5.5 when fitting the experimental vapour pressure. Figure 5.2 compares the predicted vapour pressure of ethane from Equation 5.5 extrapolated beyond the critical point with the hypothetical vapour pressures used in this thesis. The combination of Equations 5.5 and 5.6 was used to fit all of the saturation pressure data for methane, ethane, and propane. Table 5.8 summarized the fitted parameters for the hypothetical vapor pressures above the critical point.

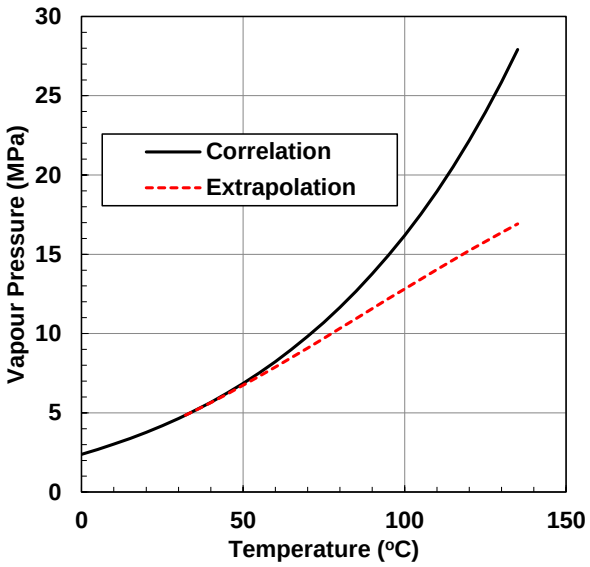

Figure 5.2. Vapour pressure of ethane predicted using the correlation from Green and Perry (2008) and the extrapolation fit along with the Margules (1895) activity coefficient model.

Table 5.8. Summary of the parameters for the hypothetical vapour pressure above the critical point (Equation 5.6). T_{max} is maximum temperature at which saturation pressure was measured in the dataset used in this thesis.

Component	C_1*	C_2*	C_3*	T_{max} (°C)	Fitted Pressure at T_{max} (MPa)
Methane	52.679	-2061.5	-5.0518	100	30.6
Ethane (all)	80.372	-4553.8	-8.7501	135	16.9
Ethane (screened)	80.423	-4556.1	-8.7576	135	16.4
Propane	67.518	-4808.99	-6.6397	180	11.9

The vapour pressure of WC-B-B3 bitumen was measured in the blind cell at 180°C and found to be 500 kPa (Johnston, 2016). Since the bitumen has been dewatered at 60°C and dewatering removes the volatile components, the vapour pressure at 60°C was taken as 101 kPa. The vapour pressures were then fit with the Clausius-Clapeyron equation given by:

$$\ln P_{v\,b} = A - \frac{H_b^{Vap}}{RT} \tag{5.7}$$

where $P_{v\,b}$ is the vapour pressure of the bitumen in kPa, H_b^{Vap} is the heat of vaporization of bitumen in J/mol, R is the gas constant in J/molK, and T is temperature in K, and A is a dimensionless constant of integration. The values of the fitted constants are A=10.685 and H_b^{Vap}/R=2061 K. The vapour pressure of Athabasca bitumen, required for modeling the saturation pressure of methane in oil, was assumed to be the same as that of the WC-B-B3 bitumen.

Note, in most cases, the contribution from the bitumen to the saturation pressure is small. For both methane and ethane, the modeled contribution from the bitumen is never more than 5% of the total saturation pressure. For propane, the average contribution from the bitumen is less than 7%. The contribution is largest at low temperatures and low propane solubility where the combined effects of the low propane vapour pressure and low propane mole fraction lead to a low propane activity.

5.3 Results

5.3.1 Saturation Pressure and Solubility of Methane in Bitumen

Figure 5.3 shows the measured saturation pressure and solubility of methane in bitumen and the fitted modified Henry's law and the Margules activity coefficient models. As expected, the saturation pressure increases with increasing gas content and increasing temperature. The data from this thesis could not be compared directly to the data from Svrcek and Mehrotra (1982) because they were measured at different conditions. Instead, the literature data were fit with the modified Henry's law model (Equation 5.3) and the data from this thesis were compared with the fitted model at the same conditions. The fitted parameters are provided in Table 5.9. The average deviation of the solubility and saturation pressure data from this thesis from the fitted model were 0.95 mol% (8.4%) and 360 kPa (9.5%), respectively. Note, to avoid implicit solutions, the modified Henry's Law model was fitted to the mole fractions with saturation pressure as the input. The deviations in the saturation pressure were determined using the iterative method with the same fitted parameters and mole fraction inputs. The Margules activity coefficient model was fitted to the saturation pressures with mole fractions as the input. The deviations in mole fractions from the Margules equation were calculated using an iterative method and the experimental saturation pressures as inputs.

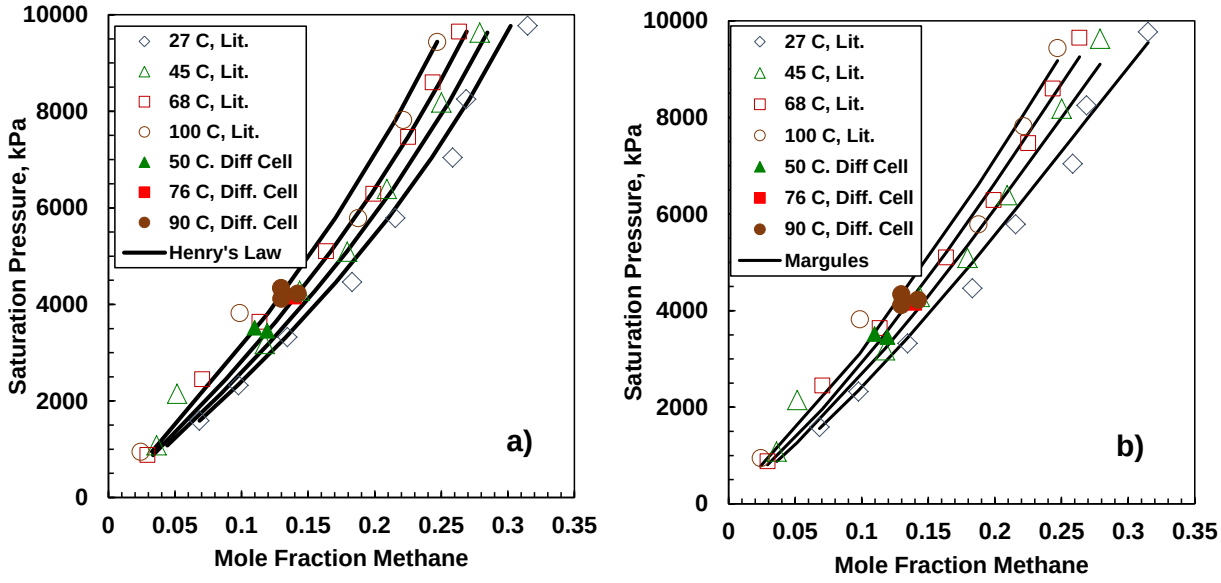

Figure 5.3. Saturation pressure versus mole fraction of mixtures of methane and bitumen fitted with: a) modified Henry's law model; b) Margules activity coefficient model.

To model the methane solubilities, the measurements collected in this thesis and those obtained from Mehrotra and Svrcek were fit simultaneously, as shown in Figure 5.3. The two models provide similar fits to the data although the Margules activity coefficient model is more linear at high concentration compared to the modified Henry's law model. Table 5.9 gives the fitted parameters for the Henry's constant used to fit the solubility data. Table 5.10 gives the fitted parameters for the Margules activity coefficient model. Recall that the hypothetical vapour pressure for methane at the maximum experimental temperature was also fitted and was provided in Table 5.8. Figures 5.4 and 5.5 are cross plots of the fitted versus measured solubilities and saturation pressures, respectively. Both models fit the saturation pressure and solubility data with nearly identical errors (less than 7% average relative deviation) and the cross plots are nearly indistinguishable.

Table 5.9. Summary of Henry constant parameters for methane, ethane, and propane in WC-B-B3 bitumen (R=8.314 LkPa/molK). ARD is the average relative deviation.*Denotes the fit exclusively to methane solubility data from Svrcek and Mehrotra (1982).

Solvent	**A**	**B** **K**	**C** **L/mol**	**ARD Solubility** **%**	**ARD P_{sat}** **%**
Methane*	11.57	-475.2	0.093	6.6	8.3
Methane	11.27	-375.9	0.093	6.6	7.8
Ethane (all)	11.39	-925.1	0.225	9.2	11.6
Ethane (screened)	11.59	-992.2	0.220	7.3	9.5
Propane	12.87	-1713	0.241	7.7	8.8

Table 5.10. Summary of the Margules parameters for methane, ethane, and propane in WC-B-B3 bitumen.

Solvent	**A_{sb}**	**A_{bs}**	**ARD Solubility** **%**	**ARD P_{sat}** **%**
Methane	-0.247	0.939	5.3	6.2
Ethane (all)	-1.832	0.055	9.1	13.4
Ethane (screened)	-1.705	0.085	6.8	9.8
Propane	-0.646	-0.101	8.7	9.4

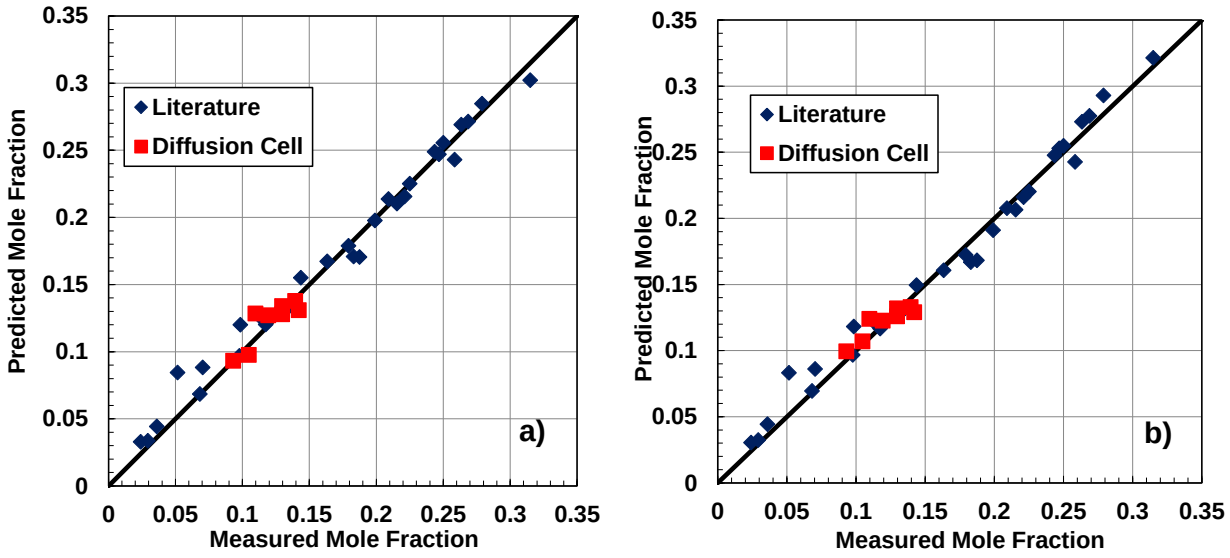

Figure 5.4. Predicted versus measured solubility of methane in Athabasca bitumen (Svrcek and Mehrotra (1982) and WC-B-B3 bitumen (this work): a) modified Henryls law model; b) Margules activity coefficient model.

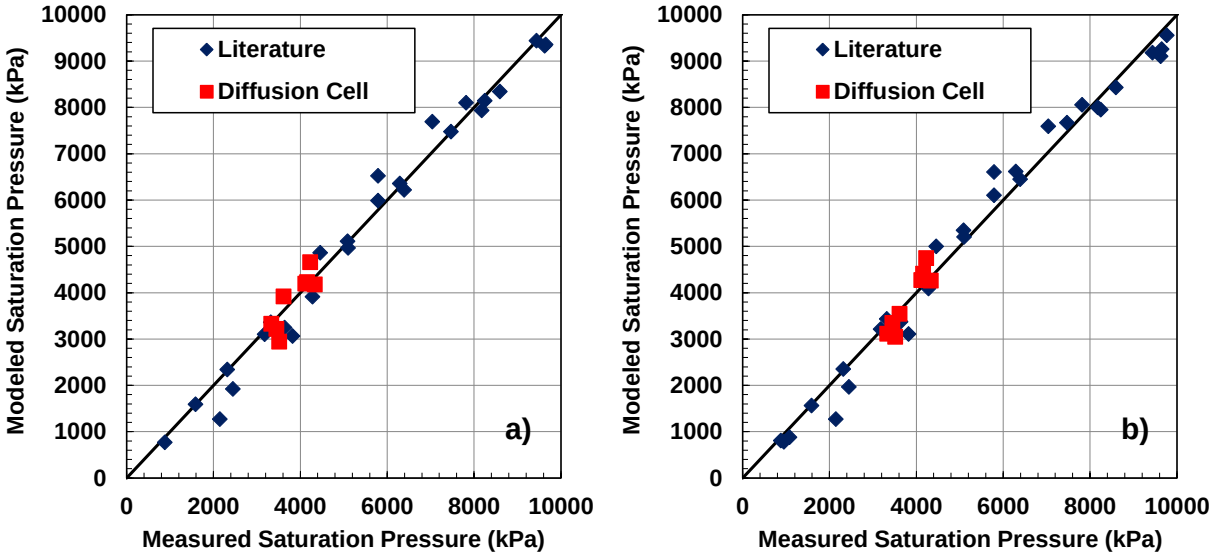

Figure 5.5. Predicted versus measured saturation pressure of methane in Athabasca bitumen Svrcek and Mehrotra (1982) and WC-B-B3 bitumen (this work): a) modified Henryls law model; b) Margules activity coefficient model.

5.3.2 Saturation Pressure of Ethane in Bitumen

The saturation pressure (solubility) data collected for mixtures of ethane and WC-B-B3 bitumen from the diffusion apparatus and the blind cells are shown in Figure 5.6. The combined data set was fit with the modified Henry's law model also shown in Figure 5.6. The model fit the mole fraction data from each experimental method with similar accuracy (AARD of 12% for the diffusion data and 7.5% for the blend cell CCE data) demonstrating that the results from both methods are consistent with each other. The combined AARD was 9.7%. The combined dataset was also fit with the Margules activity coefficient model with an AARD of 14%, Figure 5.7. The dispersion plots are provided in Figure 5.8. Note, as with the methane/bitumen system, the modified Henry's law model was fitted to the mole fractions with saturation pressure as the input. The deviations in the saturation pressure were determined using the iterative method with the same fitted parameters and mole fraction inputs. The Margules activity coefficient model was fitted to the saturation pressures with mole fractions as the input. The deviations in mole fractions from the Margules equation were calculated using an iterative method and the experimental saturation pressures as inputs.

The following outliers were identified based on an averaged deviation from both of the fitted models exceeding 25%:

- diffusion method, 100°C, 31.7 mol% (2.6 wt%), 1929 kPa
- diffusion method, 50°C, 39.6 mol% (3.65 wt%), 1740 kPa
- CCE method, 50°C, 27.3 mol% (2.13 wt%), 2190 kPa

These outliers were removed from the dataset and the models were then refit to the screened data. The modified Henry's Law and Margules activity coefficient model parameters before and after screening were provided in Tables 5.9 and 5.10.

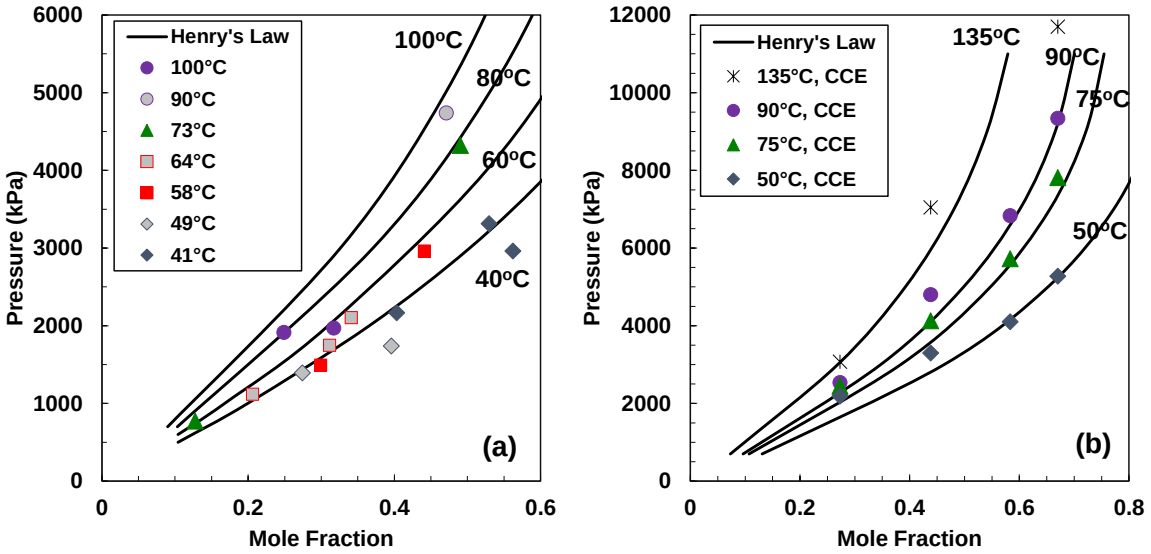

Figure 5.6. Saturation pressure versus mole fraction of ethane bitumen mixtures fitted with modified Henry's law model: a) diffusion cell data; b) blind cell CCE data.

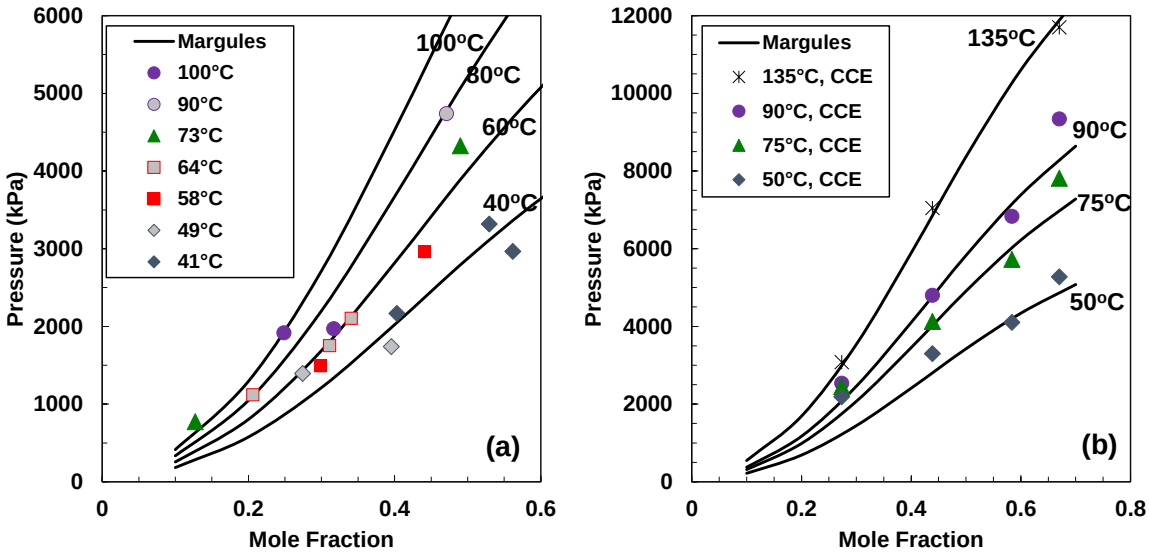

Figure 5.7. Saturation pressure versus mole fraction of ethane bitumen mixtures fitted with modified Margules activity coefficient model: a) diffusion cell data; b) blind cell CCE data.

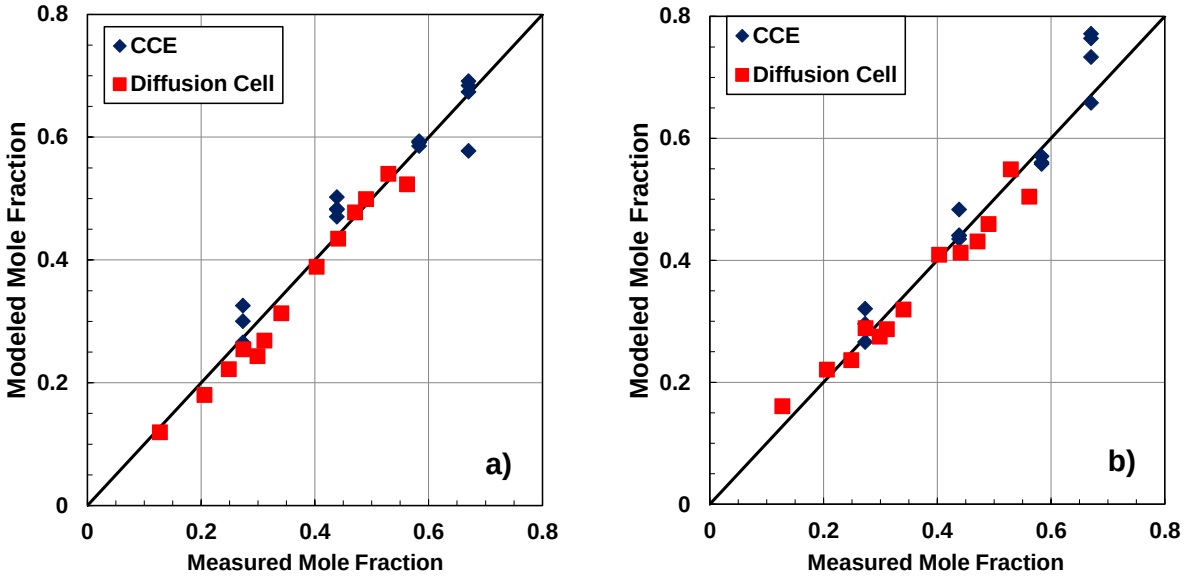

Figure 5.8. Predicted versus measured solubility of ethane in WC-B-B3 bitumen: a) modified Henry's law model; b) Margules activity coefficient model.

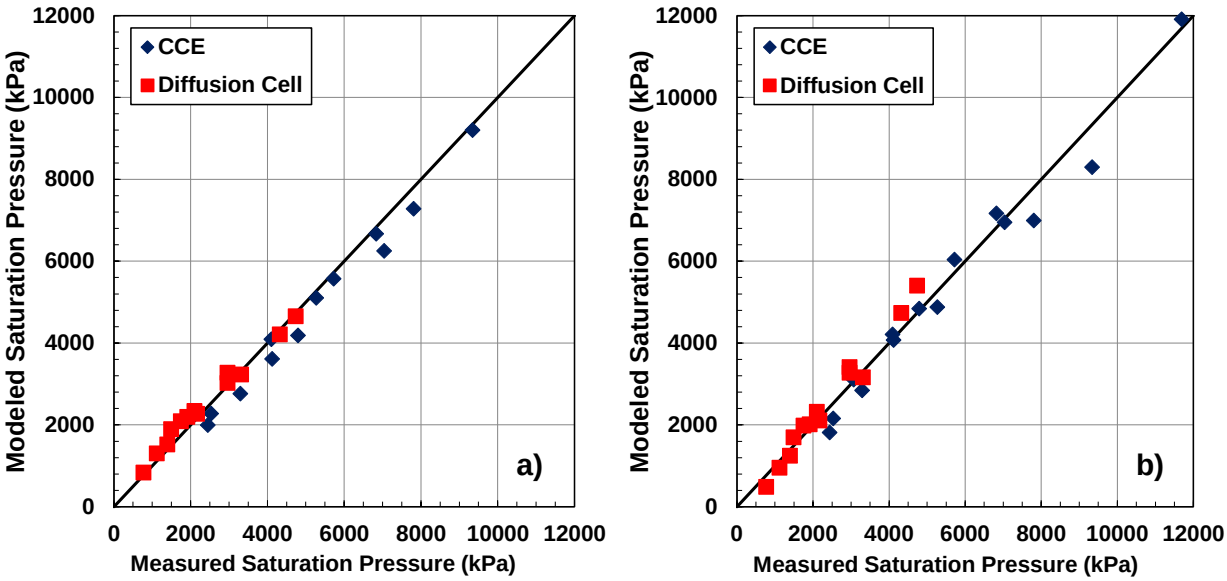

Figure 5.9. Predicted versus measured saturation pressure of ethane in WC-B-B3: a) modified Henry's law model; b) Margules activity coefficient model.

As a further test of the quality of the data, the fitted model was compared with data collected by Mehrotra and Svrcek (1985b) for mixtures of ethane with Cold Lake bitumen Mehrotra and Svrcek, 1988b) and Peace River bitumen Mehrotra and Svrcek, 1985b), Figures 5.10 and 5.11, respectively. Note that a liquid-liquid region was observed at 24°C in both cases, indicated by a circle in the figures. This region forms at temperatures below the critical temperature and pressure of ethane (32°C and 4900 kPa). The measured saturation pressures become nearly constant in the liquid-liquid region and the values above the onset of the second liquid phase were excluded from the comparison with the model. Figure 5.10 shows that the modified Henry's law and Margules activity coefficient models fitted to the data from this study match the data for the Cold Lake bitumen with AARD of 9.7 and 14%, respectively. In other words, the models match the new data with the same accuracy as the original dataset even for a different source bitumen. Figure 5.11 compares the same two models with the data for the Peace River bitumen and the AARD were 6.6 and 12%, respectively. The relatively low errors are misleading because the match above 24°C is excellent while the match at 24°C is poor. It is not obvious if the mismatch at 24°C is an issue with the data or the models. Nonetheless, the agreement between the models and the independent datasets is generally within the scatter of the data even though different bitumen samples were considered.

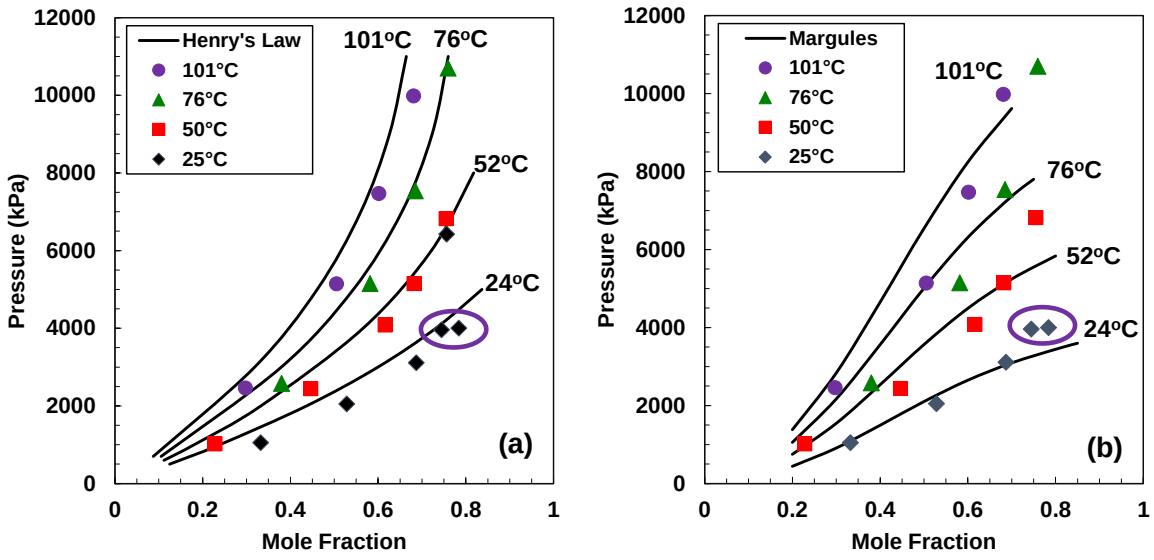

Figure 5.10. Saturation pressure versus mass percent ethane for Cold Lake bitumen (Mehrotra and Svrcek, 1988b) compared with models fitted to WC-B-B3/ethane data: a) modified Henry's law model; b) Margules activity coefficient model. Circle indicates liquid-liquid region.

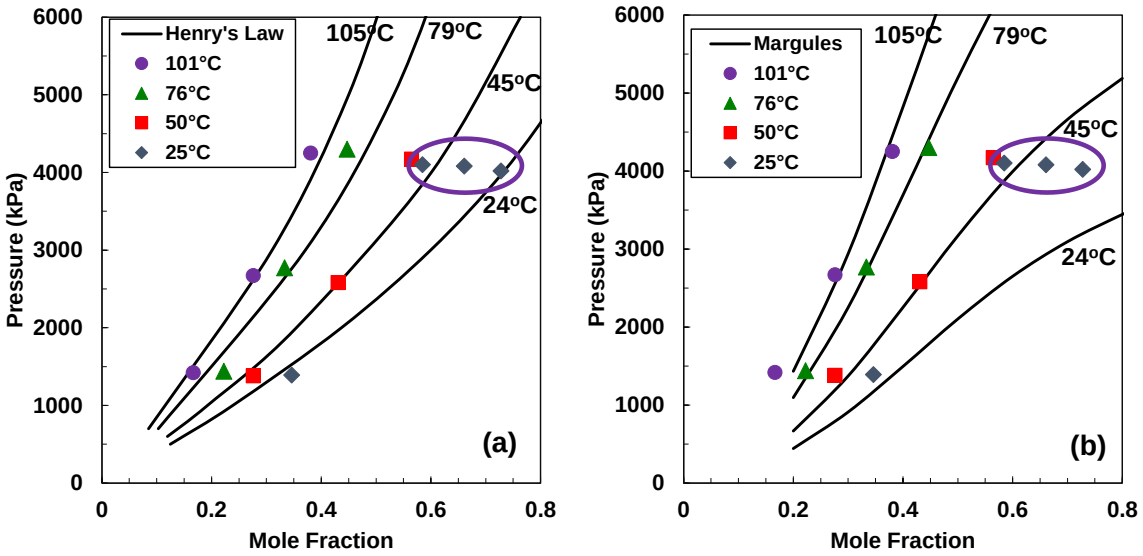

Figure 5.11. Saturation pressure versus mass percent ethane for Peace River bitumen (Mehrotra and Svrcek, 1985b) compared with models fitted to WC-B-B3/ethane data: a) modified Henry's law model; b) Margules activity coefficient model. Circle indicates liquid-liquid region.

Overall, the modified Henry's law model provides a better fit to the data than the Margules activity coefficient model but there are limitations to both models. The Margules activity coefficient model is constrained to match the ethane vapour pressure when the mole fraction of ethane approaches unity. However, a second liquid phase, shown in Figures 5.10 and 5.11, forms not at a pressure near the vapour pressure of ethane but at a mole fraction far below unity. As a result, the model tends to under-predict the saturation pressures, as illustrated in Figure 5.12a. The under-prediction persists at conditions above the critical temperature of ethane (32°C), where the model is constrained to match the extrapolated vapor pressure of ethane when the mixture approaches pure ethane. The same type of deviation is just evident with the fitting of the data from this thesis, which was collected at lower solvent contents, Figure 5.12b. In contrast, the modified Henry's law model fits the entire range of collected data. However, it should not be used for extrapolation because it will predict a non-physical reversal in the saturation pressure curve at high pressures as shown in Figure 5.13. Also note that the data point (CCE method, 135°C, 67.0 mol% = 10.5 wt%, 11700 kPa) cannot be matched with the modified Henry's law model and is likely an outlier.

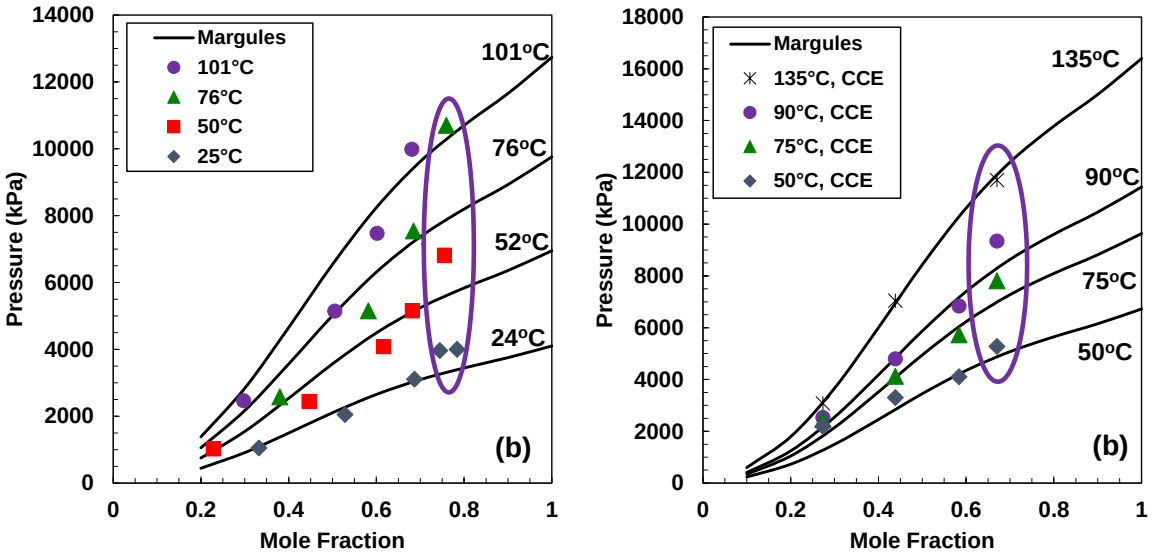

Figure 5.12. Margules activity coefficient model extended to full composition range for: a) Cold Lake bitumen/ethane data from Mehrotra and Svrcek (1988b); b) WC-B-B3 bitumen/ethane data collected for this thesis. The circled region indicates the data is near or above the critical temperature of ethane that is the most severely under-predicted.

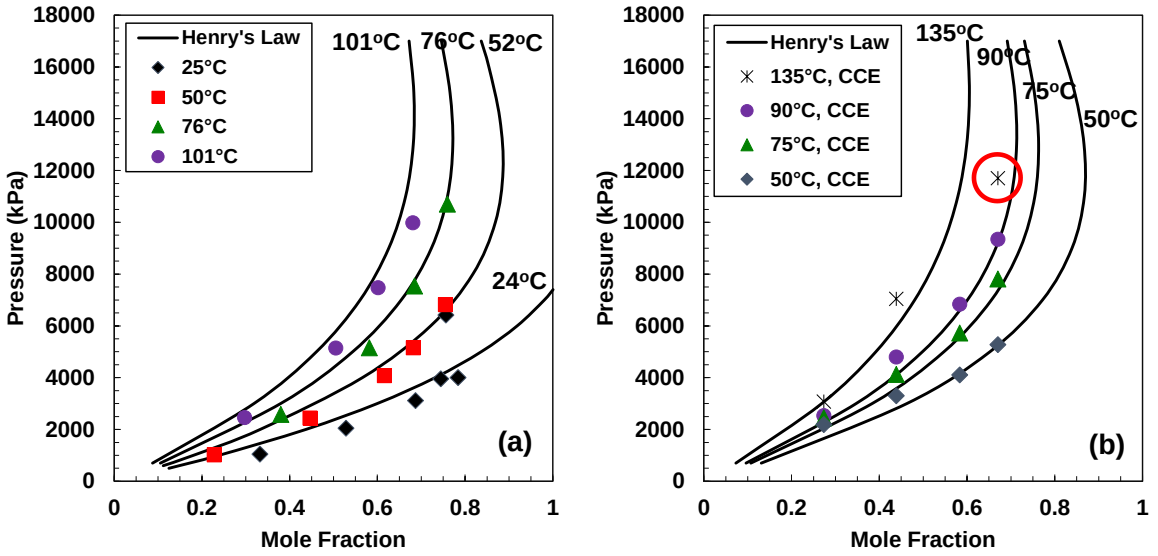

Figure 5.13. Modified Henry's law model extended to full composition range for: a) Cold bitumen/ethane data from Mehrotra and Svrcek (1985b); b) WC-B-B3 bitumen/ethane data collected for this thesis. The circled point cannot be fit with the modified Henry's law model.

5.3.3 Saturation Pressure of Propane in Bitumen

Figures 5.14 and 15 compare the saturation pressure (solubility) data collected from the diffusion apparatus and the blind cells at comparable temperatures. Figure 5.14 shows the full range of data collected while Figure 5.15 expands the scale to focus on the results at the conditions of the diffusion experiments. There are no obvious outliers and the data follows the expected trend. However, there is a large amount of scatter in the data measured using the diffusion cell to the point that some of the measurements at 60°C are intercepting the trends in the CCE data at 90°C. Note, as with the methane/bitumen and ethane/bitumen systems, the modified Henry's law model was fitted to the mole fractions with saturation pressure as the input. The deviations in the saturation pressure were determined using the iterative method with the same fitted parameters and mole fraction inputs. The Margules activity coefficient model was fitted to the saturation pressures with mole fractions as the input. The deviations in mole fractions from the Margules equation were calculated using an iterative method and the experimental saturation pressures as inputs.

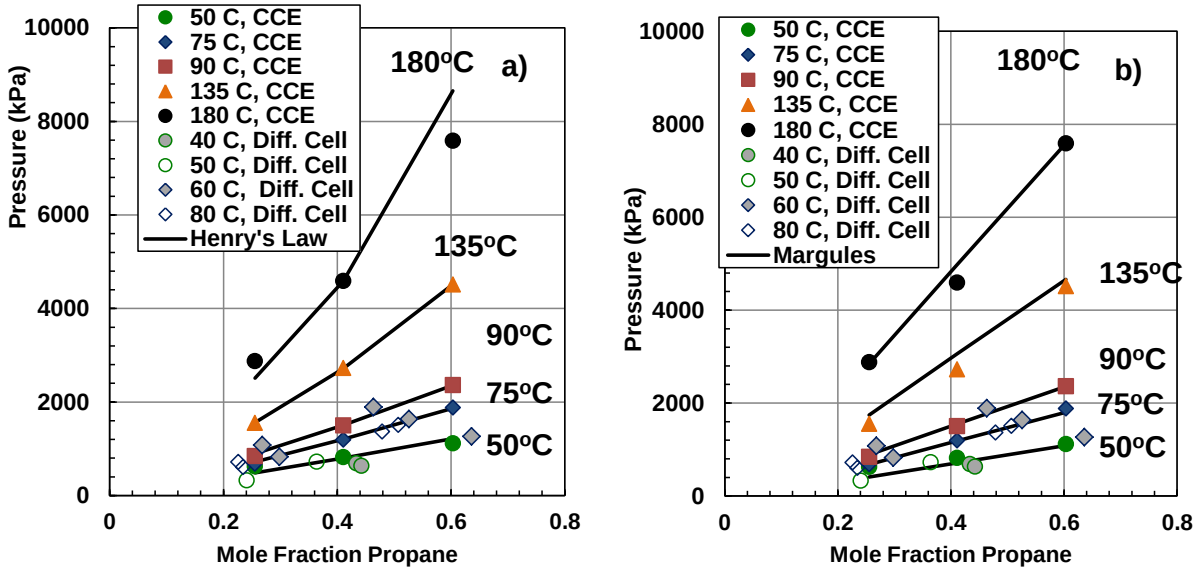

Figure 5.14. Saturation pressure versus mole fraction of mixtures of propane and bitumen fitted with: a) modified Henry's Law model; b) Margules activity coefficient model. Only data in range of diffusion cell experiment are shown.

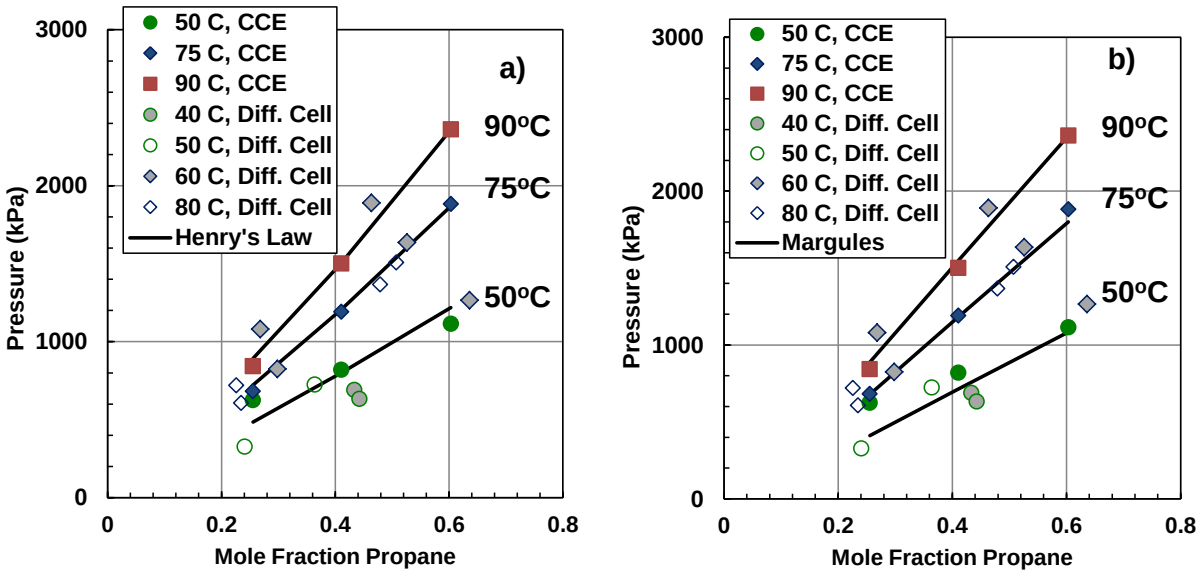

Figure 5.15. Saturation pressure versus mole fraction of mixtures of propane and bitumen fitted with: a) modified Henry's Law model; b) Margules activity coefficient model. Only data in range of diffusion cell experiment are shown.

Figure 5.16 compares the solubility models developed in this thesis to data for mixtures of propane and Athabasca bitumen collected by Badamchi-Zadeh et al. (2009). The Henry's Law predicts both the solubility and saturation pressure with an average error of 11% even though the bitumen was from a different source reservoir. Solubility and Saturation pressure predictions for the Margules Equation have an average error of 13%.

All of the propane solubility and saturation pressure data could be fit using either model. The modeling issues observed with the ethane/bitumen dataset do not arise with the propane/bitumen dataset because a second liquid phase does not form at the range of conditions considered. While all of the data were below the critical temperature and pressure of propane (97°C and 4250 kPa), the saturations were not high enough to form a second phase. Note that extrapolating the models for propane solubility to high pressure and propane concentration result in very similar curves to those of ethane and the same modeling issues would arise.

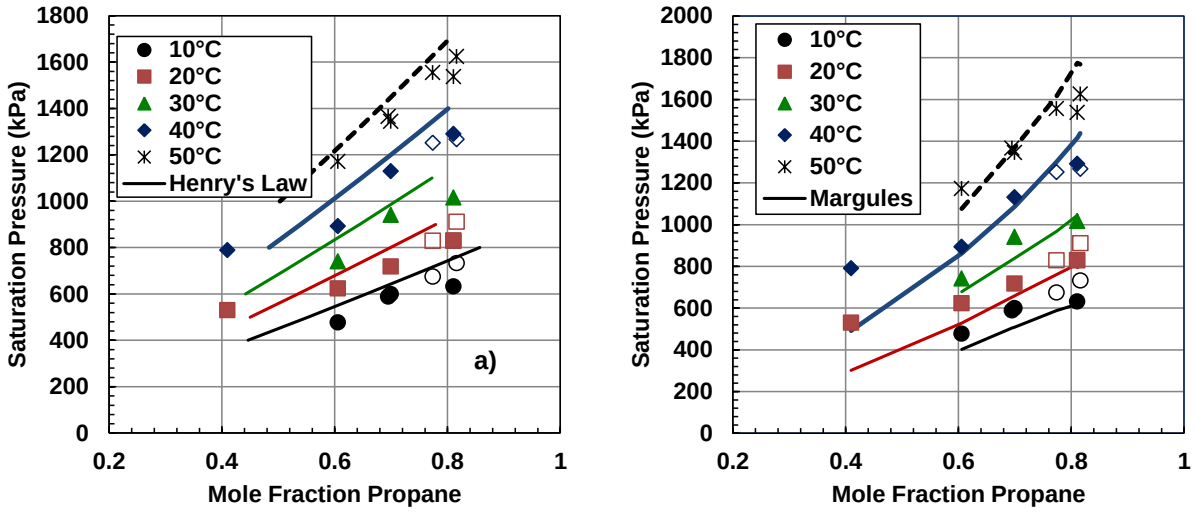

Figure 5.16. Saturation pressure versus mass percent ethane for Athabasca bitumen (Badamchi-Zadeh *et al.*, 2009) compared with models fitted to WC-B-B3 bitumen/propane data: a) modified Henry's law model; b) Margules activity coefficient model. Note, solid symbols were measured using a stepwise CCE method and hollow symbols were measured using a continuous CCE method.

Both the modified Henry's law and Margules activity coefficient models were fit to the combined three sets of data: the diffusion experiments, the CCE experiments, and the two CT diffusion experiments provided by Diedro *et al.* (2014). The fitted models were shown in Figures 5.14 and 5.15. The fitted model parameters are listed in Tables 5.9 and 5.10, respectively. Figures 5.17 and 5.18 are cross plots of the fitted versus measured solubilities and saturation pressures, respectively. Figure 5.19 shows the same data as Figure 5.18 but with the three data points at pressures above 4000 kPa excluded to focus on the low pressure data. Both the modified Henry's law and the Margules activity coefficient models fit the saturation pressure and solubility data with similar errors (less than 9 and 12% average relative deviation, respectively).

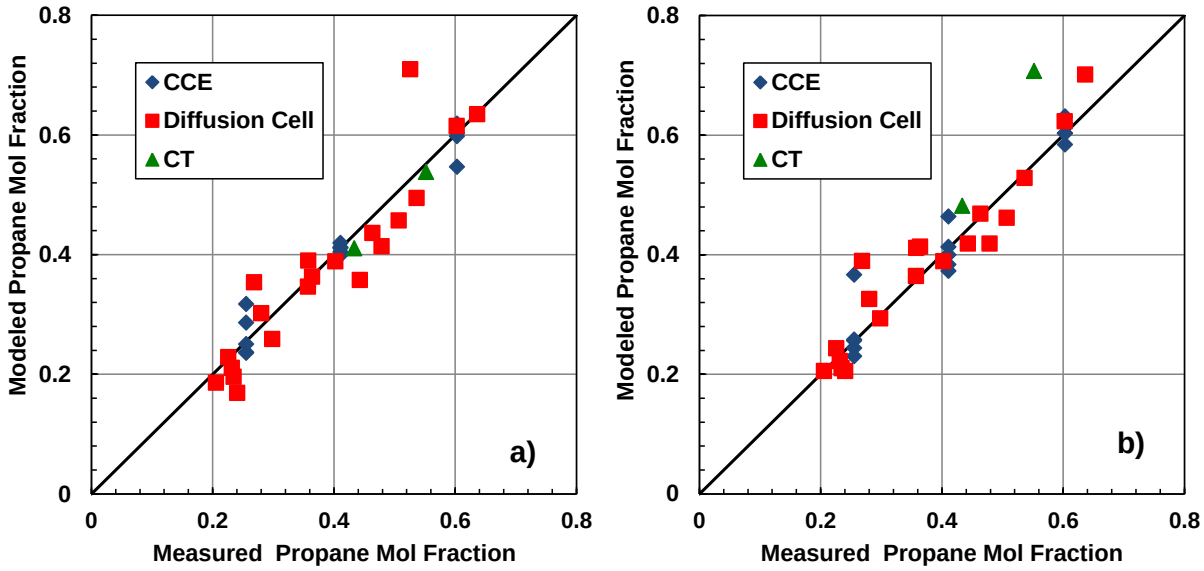

Figure 5.17. Predicted versus measured solubility of propane in WC-B-B3 bitumen: a) modified Henry's law model; b) Margules activity coefficient model.

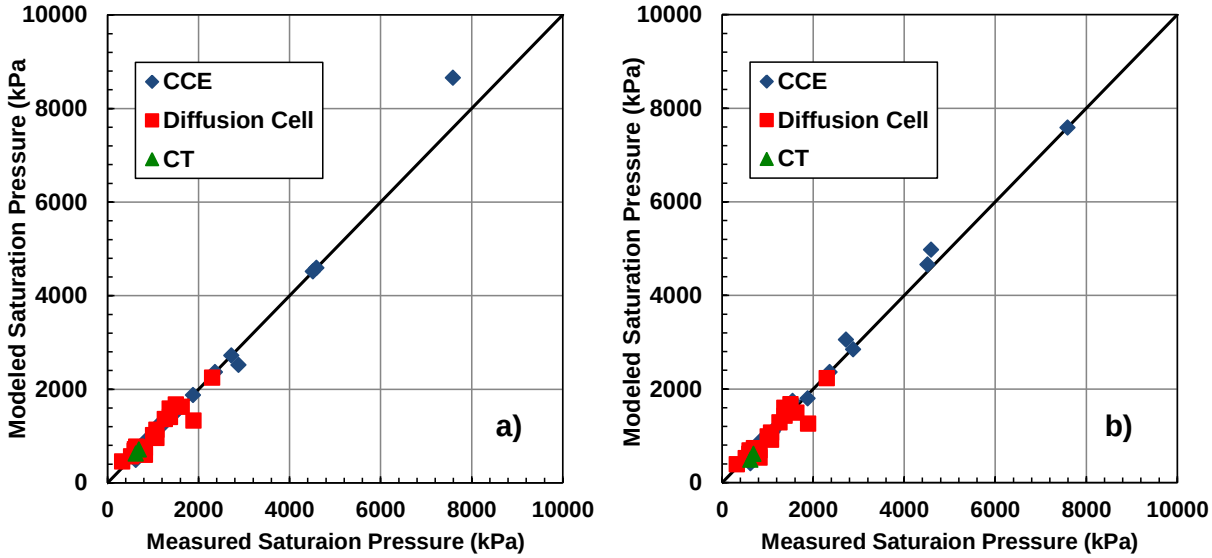

Figure 5.18. Predicted versus measured saturation pressure of propane in WC-B-B3 bitumen: a) modified Henry's law model; b) Margules activity coefficient model.

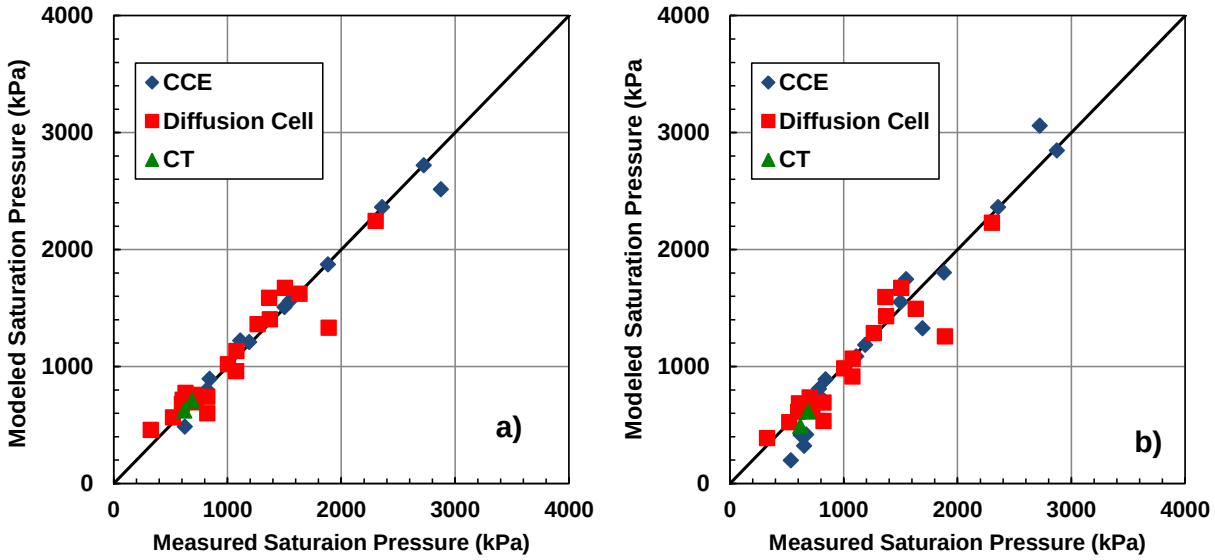

Figure 5.19. Predicted versus measured saturation pressure of propane in Athabasca bitumen and WC-B-B3: a) modified Henry's law model; b) Margules activity coefficient model. Note: the three data points at pressures above 4000 kPa were excluded from these plots to focus on the low pressure data.

5.4 Recommendation

Both the modified Henry's law model and the Margules activity coefficient model fit the experimental data with similar deviations. However, the Margules model tended to under-predict saturation pressures for ethane at higher mole fractions. The modified Henry's law model was able to fit all of the data with the exception of one data point for ethane at 135^{o}C and 67 mol % ethane. This data point is likely an outlier. Therefore, the modified Henry's law model was selected to predict the solubility of methane, ethane and propane in WC-B-B3 if no experimental data was available. Note, the modified Henry's law model should not be extrapolated to pressures above the range of the data used to fit the model because it will predict a non-physical reversal in ethane solubility at high pressures.

CHAPTER SIX: DIFFUSIVITY RESULTS AND DISCUSSION

This chapter presents the diffusivity data collected in this thesis for methane, ethane, propane, and butane in bitumen and bitumen maltenes using the pressure decay method described in Chapter 3. The diffusivity of the solvent in the medium is determined using the numerical model developed in Chapter 4 where the diffusivity is the fitting parameter. The data from each experiment with methane, ethane and propane are fit with a constant diffusivity and with several expressions for a concentration dependent diffusivity. The fitted constant diffusivities are correlated to viscosity with a power law equation based on the Hayduk-Cheng (1971) equation. A correlation for the concentration dependent diffusivity is also developed with endpoints set at the infinite dilution diffusivities of the bitumen in solvent and the solvent in bitumen. The correlations are then tested on: data collected for butane with the same bitumen, data collected for methane with different oil phases (a degassed sample and a maltene cut from the same bitumen, and literature data for other bitumens and solvents).

6.1 Constant Diffusivity Data from Pressure Decay Measurements

Pressure decay data were collected for methane, ethane, propane, and butane in the original oil as well as for methane in a bitumen degassed at 180°C and maltenes separated from the bitumen with pentane. The diffusivities presented in this section are the constant diffusivities fit to these datasets using the numerical model developed in Chapter 4. In reality, the diffusivity changes during the course of the experiment as more solvent diffuses into the medium reducing its viscosity and increasing the diffusivity. The constant diffusivity is an average diffusivity from the initial to the final conditions of the experiment. The constant diffusivities for each solvent in each medium are presented below.

Tables 6.1 to 6.3 provide the constant diffusivities for methane in WC-B-B3 bitumen, WC-B-B3 bitumen degassed at 180^{o}C, and WC-B-B3 maltenes, respectively. Table 6.4 lists constant diffusivities for ethane in WC-B-B3 bitumen. Table 6.5 presents results from ethane diffusivity experiments where the initial solvent concentration in the oil phase is non zero. Table 6.6 lists constant diffusivities for propane in WC-B-B3 bitumen. Table 6.7 presents results from propane diffusivity experiments where the initial solvent concentration in the oil phase is non zero. Table

6.8 lists diffusivities for butane in WC-B-B3. Note that, since only a few preliminary measurements were made for the mixtures with butane, these results are discussed separately later on.

Table 6.1. Diffusivity of methane in WC-B-B3 bitumen.

Temperature ^{o}C	**Pressure kPa**	**Solubility wt%**	**Viscosity mPa.s**	**Diffusivity 10^{-10} m^2/s**
50	3450	0.42	2040	3.0
76	4160	0.55	390	6.0
100	4230	0.53	120	12
100	4170	0.48	120	9.5
100	4340	0.51	120	11
101	4120	0.49	110	10

Table 6.2. Diffusivity of methane in WC-B-B3 bitumen degassed at 176^{o}C**.**

Temperature ^{o}C	**Pressure kPa**	**Solubility wt%**	**Viscosity mPa.s**	**Diffusivity 10^{-10} m^2/s**
50	3510	0.35	1990	4.0
160	3330	0.33	15	34
176	3620	0.39	10	41

Table 6.3. Diffusivity of methane in WC-B-B3 maltenes.

Temperature ^{o}C	**Pressure kPa**	**Solubility wt%**	**Viscosity mPa.s**	**Diffusivity 10^{-10} m^2/s**
56	3500	0.61	115	6.0
68	4020	0.70	63	18
81	4250	0.73	36	25

Table 6.4. Diffusivity of ethane in WC-B-B3 bitumen.

Temperature °C	Pressure kPa	Solubility wt%	Viscosity mPa.s	Diffusivity 10^{-10} m^2/s
37	2960	6.9	7160	3.3
42	2170	3.8	3930	2.3
47	1390	2.1	2410	2.0
50	1740	3.7	1880	2.5
58	2960	4.4	1140	3.5
59	1500	2.4	994	3.5
64	1750	2.6	740	2.9
64	1120	1.5	712	2.7
73	774	0.84	429	3.0
75	4320	5.3	422	6.8
90	4740	4.9	189	9.5
100	1920	1.9	116	7.3
100	1970	2.6	114	5.0

Table 6.5. Diffusivity of ethane in WC-B-B3 bitumen with non-zero initial solvent content.

Temperature °C	Pressure kPa	Initial Solvent wt%	Solubility wt%	Initial Viscosity mPa.s	Diffusivity $10^{-10}m^2/s$
42	3320	3.6	6.1	80	5.5
64	2100	1.5	2.9	110	4.7

Table 6.6. Diffusivity of propane in WC-B-B3 bitumen.

Temperature °C	Pressure kPa	Solubility wt%	Viscosity mPa.s	Diffusivity 10^{-10} m^2/s
50	327	2.6	2120	1.5
50	724	4.6	2090	1.8
59	824	3.0	999	2.8
60	602	3.5	945	2.2
62	1080	6.8	801	3.5
70	1080	4.5	547	4.8
74	523	2.2	452	3.3
74	1010	4.5	445	4.0
80	1510	8.0	290	5.6
81	720	2.4	282	3.8
81	1370	7.2	272	6.0
85	702	2.5	229	3.5
86	1370	5.4	210	5.8

Table 6.7. Diffusivity of propane in WC-B-B3 bitumen with non-zero initial solvent content.

Temperature ^{o}C	Pressure kPa	Initial Solvent wt%	Solubility wt%	Viscosity mPa.s	Diffusivity 10^{-10} m^2/s
64	1890	4.1	8.6	132	8.0
86	2300	5.4	11.4	43	11.5

Table 6.8. Diffusivity of butane in WC-B-B3 bitumen.

Temperature ^{o}C	Pressure kPa	Solubility wt%	Viscosity mPa.s	Diffusivity 10^{10} m^2/s
69	284	3.0	589	4.3
90	738	7.9	182	8.0
90	874	10.1	183	13

6.2 Validation with Data from Computer Assisted Tomography

One disadvantage with the pressure decay approach is that concentration profiles are not measured. Therefore, the concentration profiles predicted by the numerical model could not be validated against these measurements. Instead, concentration profiles for propane in WC-B-B3 bitumen measured using computer tomography (Deidro *et al.*, 2014) were examined. Deidro *et al.* placed bitumen in a horizontal cylinder and propane gas was injected above the bitumen. The density and height of the bitumen along the centerline of a horizontal cylinder (outlined area in Figure 6.1) were measured at time intervals with x-ray scans. Details of the method and calibrations for density are provided elsewhere (Diedro *et al*., 2014).

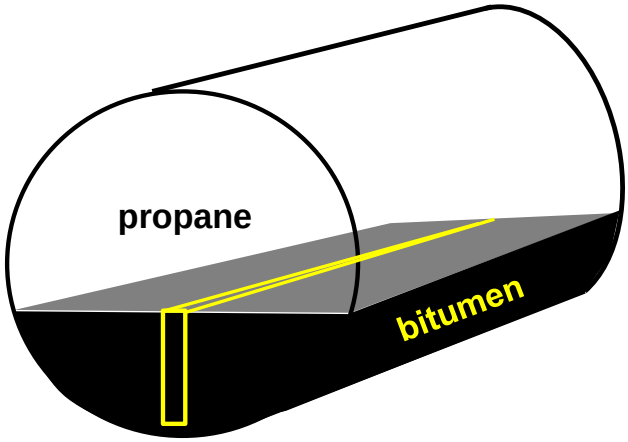

Figure 6.1. Diagram of diffusion cell used by Deidro *et al*. (2014) to measure the diffusivity of propane in bitumen.

Two experiments were performed, one at 22°C and 640 kPa and the other at 40°C and 690 kPa. The total mass diffused over time in these experiments was calculated from the volume of the diluted oil given by:

$$V_{mix} = \frac{m_s + m_b}{\rho_{mix}} \tag{6.1}$$

where V_{mix} is the oil volume at a given time in cm^3, m_s is the total mass of solvent diffused at a given time in g, m_b is the fixed mass of bitumen in the system, and ρ_{mix} is the average density of the mixture. The density of the mixture was determined from a mixing rule (Eq. 4.22; Saryazdi *et al.*, 2013). Eq. 4.22 is substituted into Eq. 6.1 to obtain the following expression:

$$\frac{{m_s}^2}{\rho_s} + m_s\left(\frac{m_b}{\rho_s} + \frac{m_b}{\rho_b} - m_b\left(\frac{1}{\rho_s} + \frac{1}{\rho_b}\right)\beta - V_{mix}\right) + \left(\frac{{m_b}^2}{\rho_b} - m_b V_{mix}\right) = 0 \tag{6.2}$$

where ρ_s and ρ_b are the density of the solvent and bitumen, respectively, and β_{sb} is the binary interaction parameter between the bitumen and solvent. Eq. 6.2 is solved to obtain the mass transferred. Figure 6.2a shows that the mass diffused follows the expected linear trend versus root time.

The concentration profiles were calculated from the mixture density by rearranging Eq. 4.22 into a polynomial in terms of solvent mass fraction as follows:

$${w_s}^2\left(\frac{1}{\rho_s} + \frac{1}{\rho_b}\right)\beta_{sb} + w_s\left(\frac{1}{\rho_s} - \frac{1}{\rho_b}\left(\frac{1}{\rho_s} + \frac{1}{\rho_b}\right)\beta_{sb}\right) + \frac{1}{\rho_b} - \frac{1}{\rho_{mix}} = 0 \tag{6.3}$$

where w_s is the solvent mass fraction at each density, ρ_s is the effective density of the solvent in g/cm³, ρ_b is the density of bitumen in g/cm³, ρ_{mix} is the measured density of the mixture in g/cm³, and β_{sb} is the binary interaction parameter. The mass concentration of the solvent in the mixture, c_s, is given by:

$$c_{s=}w_s\rho_{mix} \tag{6.4}$$

The concentration profiles at 40°C and 690 kPa are shown in Figure 6.2b.

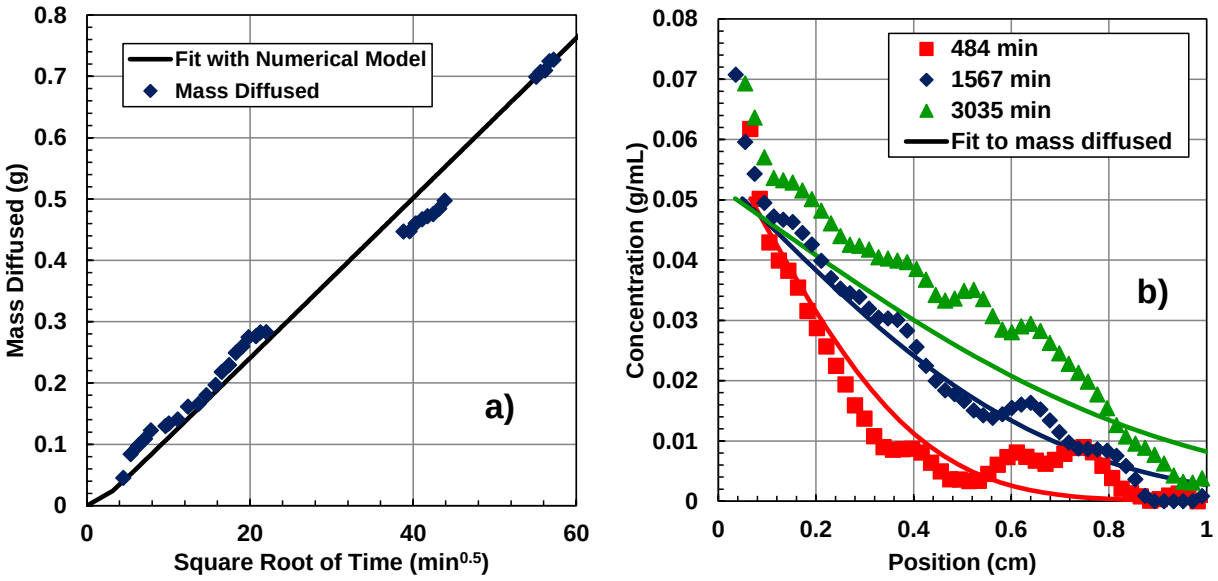

Figure 6.2. Diffusivity data for propane in bitumen measured using the swelling data from computer tomography at 40°C and 690 kPa: a) fit of numerical model to experimental data; b) comparison of the concentration profiles of propane determined from swelling with the independently measured concentration profiles. **Note**: In Figures 2b and 3, the position of zero corresponds to the horizontal centerline of the cylinder and positive values are towards to oil phase. The initial gas-oil interface is below the centerline at approximately 0.08 cm. Swelling shifts the interface towards the centerline (zero).

The solubility used in the model was determined from the concentration profile at the highest experimental time (8624 minutes) shown in Figure 6.3. The solubility was found to be 0.051 g/mL corresponding to the value of the plateau at a position of approximately 0.1 cm. This solubility is very close to that estimated from the Henry's Law model developed in Chapter 5, which had a value of 0.50 g/mL.

Figure 6.3 and Figure 6.2b also show propane concentrations above the solubility limit near the gas-oil interface. These are artifacts related to the resolution of the measurements. The apparent concentrations based on the gas phase density above the exact interface and the liquid density below the interface are averaged. Therefore, the exact position of the interface is challenging to define from the concentration measurements. Here, it is defined as the point where the concentration exceeds the solubility limit; there is often a change in slope at this point.

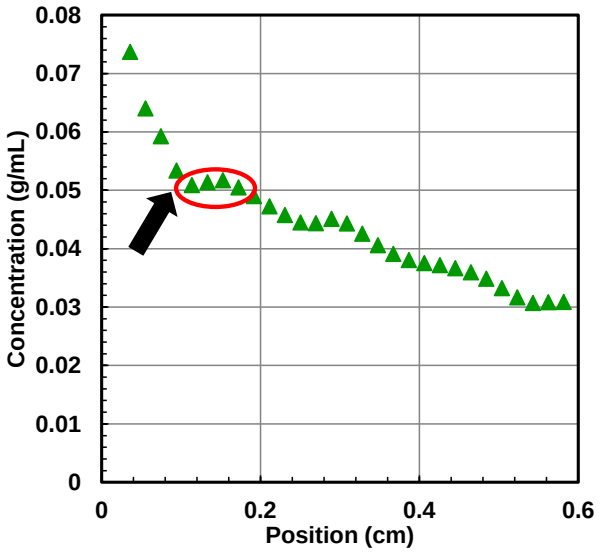

Figure 6.3. Concentration profile of propane in bitumen at 40°C and 690 kPa after 8624 minutes. The plateau indicating the solubility is circled and the interface is indicated by the arrow.

One challenge in interpreting the data is that the mass transfers both vertically and horizontally because the cross-section changes with the height of the fluid. However, the numerical model was developed for one dimensional diffusion. To minimize the mass transfer in the lateral direction, the cylinder was filled to just below the midpoint where the cross sectional area is expected to vary the least with increasing oil height. In addition, only the centerline profile was modeled. The model is expected to represent the early time data accurately but will progressively deviate from the data over time as lateral diffusion becomes more significant.

The model was fit to the mass diffusion data, as shown in Figure 6.2a, by adjusting the constant diffusivity. Table 6.9 lists the constant diffusivities fitted to these data. The diffusivities are the same magnitude as the pressure decay values given in Table 6.6. The predicted concentration profiles are compared with the experimentally determined concentration profiles in Figure 6.2b. As expected, the predicted concentration profiles match the data at early times (484 and 1657 s) within the scatter of the measurement but deviate at later times (3035 s). Hence, the model appears to represent the one dimensional mass transfer process accurately. However, since the model does not include the two-dimensional diffusion, the values from Table 6.9 are used for comparison only and not included in any further analysis.

Table 6.9. Diffusivity of propane in WC-B-B3 bitumen measured with computer tomography by Deidro *et al*. (2014).

Temperature ^{o}C	Pressure kPa	Solubility* wt%	Viscosity mPa.s	Diffusivity $10^{-10}m^2/s$
22	621	7.8	53700	2.2
40	689	5.3	7200	1.3

** Solubilities were predicted with Henry's law (Chapter 5).*

6.3 Comparison with Available Literature Data

This section compares the diffusivity measured in this thesis to the data available in the literature. As noted in Chapter 2, diffusivity is expected to correlate to viscosity and therefore the data are compared on plots of diffusivity versus the initial oil viscosity. The datasets are screened for any obvious inconsistencies and those that pass the screening will be used to test the diffusivity correlations developed later in this chapter. Unless otherwise stated, the reported dataset will be included in the tests.

6.3.1 Methane Data

Upreti and Mehrotra (2002)

Upreti and Mehrotra (2002) determined the diffusivity of methane and ethane in Athabasca bitumen (821000 mPa.s at 25^{o}C) using the pressure decay method. Experiments were performed at 4 and 8 MPa and temperatures from 25 to 90^{o}C. Their one-dimensional diffusion model, which included a pressure dependent saturation boundary condition at the gas-liquid interface, swelling of the oil phase, and a concentration dependent diffusivity, was fit to the pressure decay data by adjusting the diffusivity and the solubility. They also reported their results as a constant diffusivity equal to an average over the range of concentrations measured. The average diffusivities are shown in Figure 6.4. Sheikha *et al.* (2005, 2006) reanalyzed several of these pressure decay experiments with four graphical methods and determined slightly higher diffusivities, Figure 6.4.

Figure 6.4 shows that the results of Upreti and Mehrotra (2002) follow a very similar trend with viscosity as those measured in this thesis. Interestingly, the original results by Upreti and Mehrotra (2002) show a decreasing trend in diffusivity with pressure, contrary to what is

observed in this thesis and in other research in hydrocarbon diffusivity in oils (Jamialahmadi *et al*. (2006), Marrafuzaman and Henni (2014), Yang and Gu (2007)).

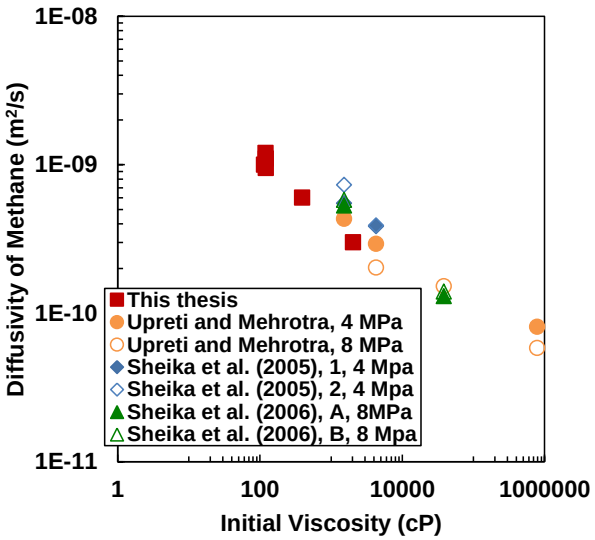

Figure 6.4. Diffusivity of methane in Athabasca bitumen from Upreti and Mehtrotra (2002) and reanalyzed by Sheikha *et al.* (2005, 2006) compared with diffusivities measured in this thesis.

Yang and Gu (2006)

Yang and Gu (2006) and Yang (2005) used Dynamic Pendant Drop Volume Analysis to determine the constant diffusivity of methane in Lloydminster Heavy oil (23000 mPa.s at 24^{o}C) at pressures from 6 to 14 MPa. The experiment was modeled using a radial form of the continuity equation. This model was used to calculate the swelling of an oil droplet suspended in a gas with time using a constant equilibrium boundary condition. The model was fit to experimental; swelling data by adjusting the diffusivity and the oil swelling factor. Their data for methane diffusivity shows a modest increase with increasing pressure. The results are compared with the diffusivity data measured in this thesis in Figure 6.5. The diffusivities reported by Yang (2005) are on a consistent trend with the data measured in this thesis even though their data were collected at much higher pressures.

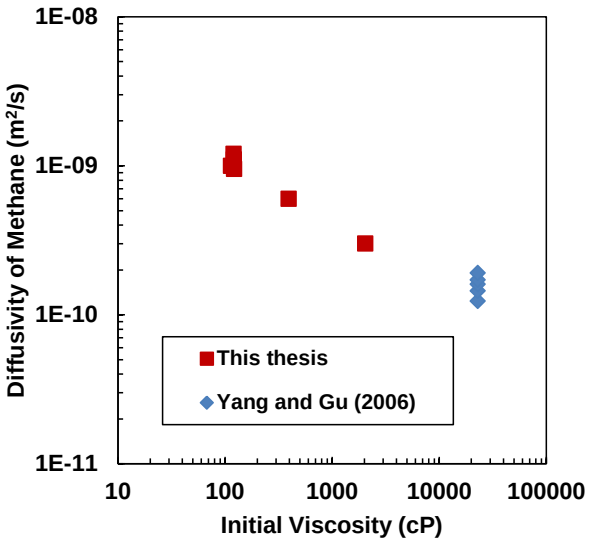

Figure 6.5. Diffusivity of methane in Lloydminster heavy oil from Yang (2005) compared with values measured in this thesis.

Tharanivasan *et al.* (2006)

Tharanivasan *et al.* (2006) measured the diffusivity of methane and propane in heavy oil (20300 mPa.s at 24°C) using the pressure decay method. The pressure decayed from 5030 to 4900 kPa during the experiment They developed three infinite series one-dimensional diffusion models for the concentration profiles based on a constant diffusivity and three different boundary conditions. Similar to this thesis, these profiles were integrated along the oil column to determine the total moles of gas diffused, which was then used to calculate the pressure decay. This pressure decay model was fit to the experimental data by adjusting the diffusivity, the solubility, and in some cases, the interfacial mass transfer coefficient. The result for methane, modeled with a constant boundary condition similar to this thesis, is shown in Figure 6.6 and falls on the same trend versus viscosity as the data collected in this thesis.

Jamialahmadi *et al*. (2006)

Jamialahmadi *et al*. (2006) measured the diffusivity of methane in a light crude oil (extrapolated to 0.35 mPa.s at 25°C and atmospheric pressure) using a moving boundary method. Their one-dimensional diffusion model calculated the average concentration in the liquid with time and used experimentally determined densities of the mixture to calculate the swelling. The model was fit to the experimental swelling data by adjusting a constant or a concentration dependent

diffusivity. They measured the constant diffusivity at 25 and 50°C and pressures ranging from 3 to 28 MPa as shown in Figure 6.6. The diffusivity data appears as a column with respect to the oil viscosity because the pressure dependence of the oil viscosity was not known and the data was plotted against the atmospheric viscosity. Their data are consistent with the trend in the data from the thesis even though the oil viscosity is approximately two orders of magnitude lower.

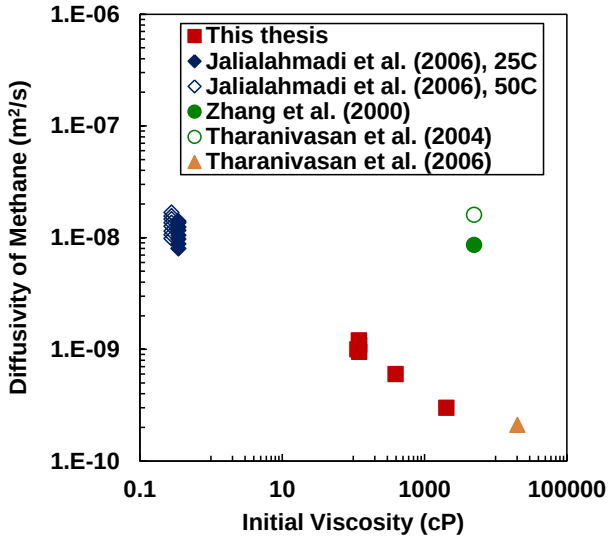

Figure 6.6. Diffusivity of methane in several different oils (Jalialahmadi *et al.* (2006); Zhang *et al.* 2000; Tharanivasan *et al.* 2004, 2006) compared to values measured in this thesis.

Zhang *et al.* (2000)

Zhang *et al.* (2000) used the pressure decay method to determine the diffusivity of 8.6 10^{-9} m^2/s for methane in a heavy oil (5000 mPa.s) at 23.9°C and 3510 kPa. They developed an infinite series diffusion model for the concentration profiles in the oil phase that did not account for swelling and employed a constant diffusivity. A marterial balance on the gaseous solvent was used to calculate the pressure drop of the gas phase by evaluating the rate of mass transfer from the gas to the liquid. This infinite series was truncated to the first term to develop a graphical model easily fit to the experimental data at large times. The pressure decay data from this experiment was reanalyzed by Tharanivasan *et al.* (2004). They developed three infinite series models for the concentration profiles based off of a constant diffusivity and three different boundary conditions. Similar to this thesis, these profiles were integrated along the oil column to determine the total moles of gas diffused, which was used to calculate the modeled pressure

drop. This pressure drop model was fit to the experimental data by adjusting the diffusivity, the solubility and in some cases the interfacial mass transfer coefficient. Their model with a constant equilibrium boundary condition obtain a diffusivity of 1.6 10^{-8} m^2/s. Zhang *et al.* (2000) showed that their model is sensitive to the final equilibrium pressure and the associated solubility, where a lower solubility results in a higher calculated diffusivity. The accuracy of the solubility is important most diffusion models as it has a large influence on the modelled boundary conditions; when matching experimental data an inaccurate solubility could lead to misinterpretation of the data. The pressure decay experiment in this study was not run until the equilibrium pressure was achieved; rather, a non-linear model with the equilibrium pressure as a parameter was fit to the experimental data. The authors noted that their calculated solubility was much lower than the solubility measured by Svrcek and Mehrotra (1985) in a similar oil. This discrepancy could give too high a diffusivity.

Figure 6.6 shows that the diffusivities from Zhang *et al.* are an order of magnitude higher than the data from this thesis and of similar magnitude to the diffusivities in the much less viscous light crude oil from Jamialahmadi *et al*. (2006). In fact, their diffusivity is comparable to that of methane in dodecane (approximately 1 10^{-8} m^2/s, Section 3.3.3). Therefore, the Zhang *et al.* data were not used to test the proposed diffusivity correlations.

6.3.2 Ethane Data

Diffusion coefficients for ethane in Athabasca Bitumen (821000 mPa.s at 25^{o}C) were determined by Upreti and Mehrotra (2002) and reanalyzed by Sheikha *et al.* (2006) as noted in Section 6.3.1. The results for both analyses are plotted in Figure 6.7 against the original oil viscosity. The diffusion coefficients reported by Upreti and Mehrotra (2002) increase with increasing pressure, as expected, and the reported diffusivities for ethane are also slightly lower than those of methane. The data also follows a similar trend to the diffusivity measured in this thesis.

The models of Sheikha *et al.* (2006) substantially decreases the measured value of the diffusivity compared to Upreti and Mehrotra (2002). Sheikha *et al.* (2006) suggest that the deviation occurs because their model not including the swelling in the oil phase. To corroborate this hypothesis, two pressure decay experiments from this thesis were analyzed without accounting for swelling

(propane in WC-B-B3 at 81°C, 1370 kPa and 81°C, 720 kPa). Table 6.10 shows that failing to account for swelling reduced the calculated diffusivity by approximately 20%. As noted by Sheikha *et al.* (2006), this difference is expected to increase with increasing swelling, and would be more substantial at higher pressures and with solvents of higher solubility. Because Swelling was not included in the models from Sheikha *et al.* (2006) only the original results from Upreti and Mehrotra (2002) will be used to test the correlation.

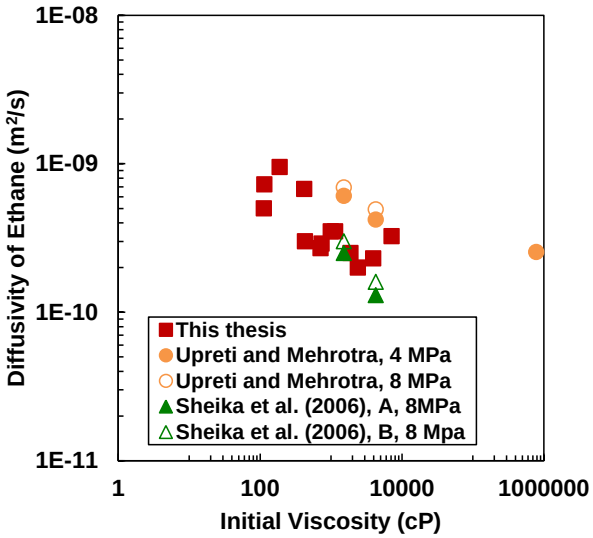

Figure 6.7. Diffusivity of ethane in Athabasca bitumen from Upreti and Mehtrotra (2002) and reanalyzed by Sheikha *et al.* (2005, 2006) compared with diffusivities measured in this thesis.

Table 6.10. Diffusivity of propane in WC-B-B3 at 81°C, modelled with and without accounting for the swelling of the oil phase.

Pressure kPa	**Diffusivity with Swelling 10^{-10} m²/s**	**Diffusivity without Swelling 10^{-10} m²/s**	**Difference %**
720	3.8	2.9	-24
1370	6.0	4.8	-20

Yang and Gu (2006)

Yang and Gu (2006)Yang (2005) used the Dynamic Pendant Drop Volume Analysis method to determine the diffusivity of ethane in Lloydminster heavy oil (23000 mPa.s at 24^{o}C) at pressures from 1.5 to 3.5 MPa using the methods described is Section 6.3.1. Their results are compared to those measured in this thesis in Figure 6.8. The low pressure diffusivities are consistent with the data from this thesis but their diffusivities increase dramatically with increasing pressure. This increase is far above what was observed in this thesis over a larger range of pressures.

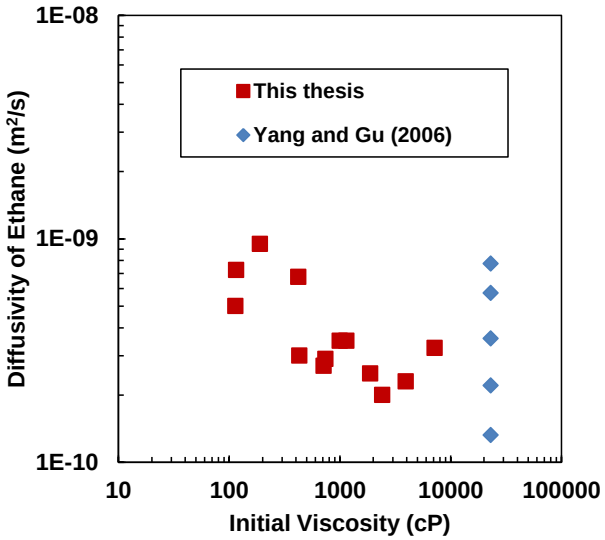

Figure 6.8. Diffusivity of ethane in Lloydminster heavy oil from Yang (2005) compared with values measured in this thesis.

A possible explanation for the relatively high diffusivities is convection. With Yang's method, a pendant bitumen drop is suspended in the ethane gas. As gas diffuses into the oil, the density at the surface will decrease, causing a density gradient between the surface layer and the untouched bitumen at the center of the drop. This density gradient could cause convection, particularly at higher pressures where the gas is more soluble in the bitumen.

The issue of convection was addressed by Yang (2005) based on a critical Rayleigh number value of 1100 at which convection will begin (Tan and Thorpe, 1992,1999). The Rayleigh number increases with increasing interfacial concentration, increasing density difference between the oil and the oil-solvent mixture, and with decreasing viscosity of the mixture. Hence, it will

increase during the course of the experiment and will be more significant at higher solubilities (pressures). Yang (2005) calculated the Rayleigh number for a propane diffusion experiment at 500 kPa as a function of position in the drop and time (up to 150 seconds) and found that the calculated Raleigh number never surpassed a value of 300. The Rayleigh number could surpass the threshold at higher times since the experiment in question lasted 3600 seconds. Note, this analysis was performed for propane which, as a more soluble gas than ethane, would be the most likely to cause the gradients needed to allow convection. However, the oil swelling factor measured for all but one of the ethane diffusion experiments was equal or greater than that used in their stability analysis. Hence, at the high pressures used in the ethane diffusion experiments, there is a substantial decrease in the density of the oil phase which could be enough to cause convection. Although there is a risk that convection affected the measurement, this dataset was included in the correlation tests.

6.3.3 Propane Data

Marrafuzaman and Henni (2014)

Marrafuzaman and Henni (2014) determined the diffusivity of propane in Cactus Lake oil (724 mPa.s at 26^{o}C) using a microbalance. At each temperature investigated, the first experiment was performed by filling the cell to the desired pressure and allowing the system to reach equilibrium. Subsequent experiments were performed by increasing the pressure in the system, without removing any solvent from the oil or depressurizing the system. Therefore the initial solvent content of the oil at a higher pressure should be equal to the saturation concentration at the lower pressure. Viscosity data were given at two of the four temperatures studied.

They modeled the changing average mass fraction of the diffusing propane using an infinite series expression developed by Yokozeki (2002). This model is based on a constant diffusivity and a constant equilibrium boundary condition. It does not account for swelling but can be used to model systems where the liquid contains an initial concentration of the diffusing species. The mass diffused was fit by adjusting diffusivity and the initial concentration (when non-zero).

The viscosity of the mixture at the beginning of each experiment is required to compare their data with others. The initial viscosity of the solvent oil mixture at the beginning of each experiment was estimated using the following double log mixing rule:

$$\ln\ln(\mu_{mix}+1) = w_s \ln\ln(\mu_s+1) + w_b \ln\ln(\mu_b+1) \tag{6.5}$$

where μ_{mix} is the mixture viscosity, μ_s is the solvent viscosity, μ_b is the bitumen viscosity, w_s is the solvent weight fraction, and w_b is the bitumen weight fraction. The effective viscosity of the solvent was calculated with the Hayduk-Minhas (1982) equation as described in Section 6.5.1.

Figure 6.9 shows that, when plotted versus the initial mixture viscosity, the diffusivities determined by Marrafuzaman and Henni (2014) are in the order of magnitude of those measured in this thesis. Their diffusivity data show a greater temperature dependence that the data from this thesis.

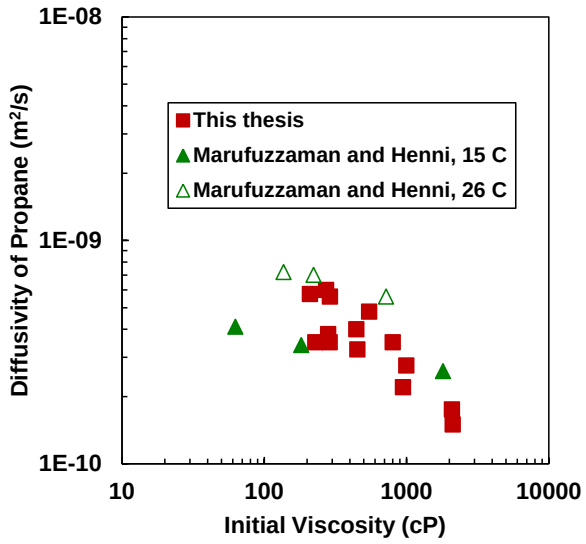

Figure 6.9. Diffusivity of propane in Cactus Lake oil from Marrufuzzaman and Henni (1982) compared with values measured in this thesis.

Das and Butler (1996)

Das and Butler (1996) measured the concentration dependent diffusion coefficients of propane in Peace River Bitumen (67000 mPa.s at 25^{o}C) using a Hele-Shaw cell at temperatures from 21 to 35^{o}C and pressures from 870 to 1230 kPa. They developed a model that predicts the production rate from the Hele-Shaw Cell. This model uses a concentration dependent diffusivity, a constant equilibrium boundary condition, and does not account for swelling. They adjusted the coefficients on the Hayduk and Cheng Equation used to model the diffusivity to match the production rates from ten experiments simultaneously. Figure 6.10 shows that the correlation presented by Das and Butler (1996) is approximately 10 times higher than the diffusivities measured in this thesis.

The high value of the diffusivity reported by Das and Butler (1996) could be explained by the formation of a second asphaltene rich phase, which would decrease the viscosity of the oil rich phase and could possibly cause convection. In 6 of the 10 experiments the predicted solubility was over 15 wt%, the threshold concentration for the onset of asphaltene precipitation (Agrawal *et al.*, 2012) and four were over the 18% limit shown by Mancilla-Polanco (2017). Note, the solubilities of propane in the bitumen were predicted by Das and Butler (1996) using HYSIM and critical properties by Mehrotra *et al.* (1985b) and are within 7% of the Henry's law correlation developed for propane in Chapter 5. Given the high probability of asphaltene precipitation, these data were not used to test the diffusivity correlations.

Yang and Gu (2007)

Yang and Gu (2007) measured the diffusivity of propane in Lloydminster heavy oil (23000 mPa.s at 24^{o}C) at pressures from 400 to 900 kPa using the Dynamic Pendant Drop Volume method discussed in Section 6.3.2. Figure 6.11 shows that as with their ethane data, the diffusivity increases with pressure much more than the data collected in this thesis. The propane solubilities in these experiments are below the expected onset of asphaltene precipitation and therefore the data are not affected by asphaltene settling. Although there is a risk that convection affected the measurements, this dataset was included in the correlation tests.

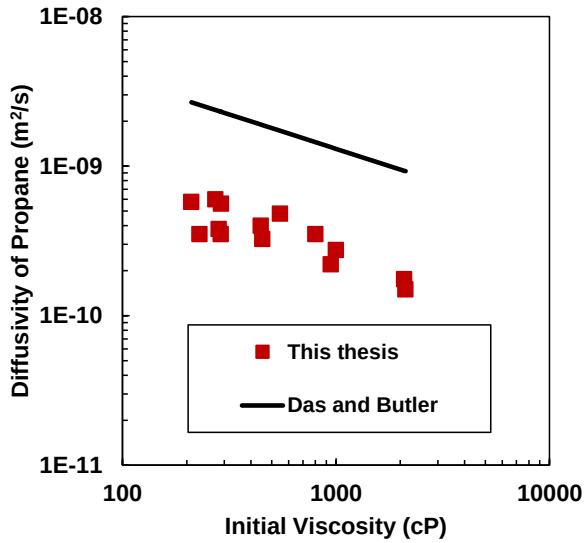

Figure 6.10. Correlations for propane diffusivity in Peace River bitumen from Das and Butler (1996) compared with propane diffusivity from thesis.

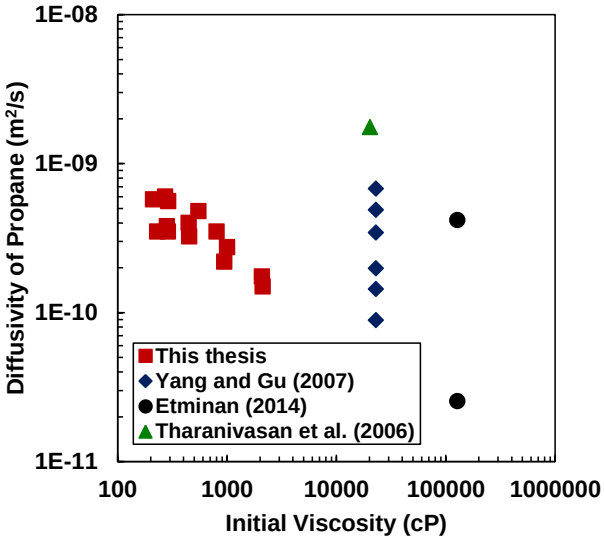

Figure 6.11. Diffusivity of propane in Lloydminster heavy oil from Yang and Gu (2007) and in McKay River bitumen from Etminan *et al.* (2014b) compared with diffusivities from this thesis.

Tharanivasan *et al.* (2006)

As discussed previously, Tharanivasan *et al.* (2006) measured the diffusivity of methane and propane in heavy oil (20300 mPa.s at 24^{o}C) using the pressure decay method. The pressure decayed from 765 to 380 kPa during the experiment. Note, the diffusion coefficients measured

by Tharanivasan *et al.* (2006) were 2.1 10^{-10} m^2/s for methane and 17.6 10^{-10} m^2/s for propane in heavy oil. The increase in diffusivity from methane to propane is contrary to the expectation that diffusivity decreases with increasing molecular weight of the gaseous solvent. This result is 3-20 times larger than that reported by Yang and Gu (2007) at comparable pressures, shown in Figure 6.11. Tharanivasan *et al.* (2006) also suspect that at the initial pressure there is a possibility of asphaltene precipitation, which could account for the high measured diffusivity. Because of these uncertainties and the high value of the reported diffusivity, this experiment will not be used to test the correlation.

Etminan *et al.* (2014b)

Etminan *et al.* (2014b) measured the diffusivity of propane in bitumen from the McKay River reservoir (128000 mPa.s, 1002.7 kg/m³ at 24°C) at 413 and 827 kPa using the pressure decay method. Their one-dimensional diffusion model included the swelling of the oil phase with time, a constant equilibrium boundary condition, and a constant diffusivity. The diffusivity was adjusted to match the total mass diffused in the pressure decay experiments. Figure 6.11 shows that their diffusivity at 413 kPa is consistent with the data from this thesis but the diffusivity at 827 kPa is considerably higher. The solubility reported for the 827 kPa experiment is 0.159 g/cm³. Based on a calculated effective density of propane of 540 kg/m^3 at these conditions, the propane solubility is approximately 18 wt%. It is possible that an asphaltene-rich phase formed during this experiment.

Diedro et al. (2015)

Diedro et al. (2015) measured the diffusivity of propane in Peace River bitumen (the same bitumen used in this thesis) and a Grosmont bitumen (1.2 10^7 mPa.s at 22 °C) using a Computer Tomography method (CT). The CT determined concentration profiles were calculated from the experimental densities assuming ideal mixing between the solvent and the bitumen. They calculated the diffusion coefficient and a function of solvent content using the slopes and intercepts method (Sarafianos, 1986; Guerrero-Aconcha *et al.* 2008) and determined that the gaseous solvent diffusivities were approximately constant on a log scale over the concentration ranges observed. After averaging the diffusivity, they calculated concentration profiles using a simple solution to Ficks Second Law with a constant equilibrium boundary condition and no

swelling. The predicted concentration profiles were then manually adjusted to match the moving boundary of the oil phase. This simple model could accurately represent the solvent penetration into the oil. The same Peace River bitumen experiment was analyzed in Section 6.2 to obtain a diffusivity of 2.2 10^{-10} m^2/s which is twice the value reported using CT ($1.1*10^{-10}$ m^2/s). Figure 6.12 shows that both values are above the trend versus viscosity of the data from this thesis. Note that the viscosity of the Grosmont bitumen may be too high to measure accurately; that is, without viscous heating or non-Newtonian effects. The uncertainties in the CT method analysis are significant as discussed in Section 6.2 and therefore these data were not included in the correlation testing.

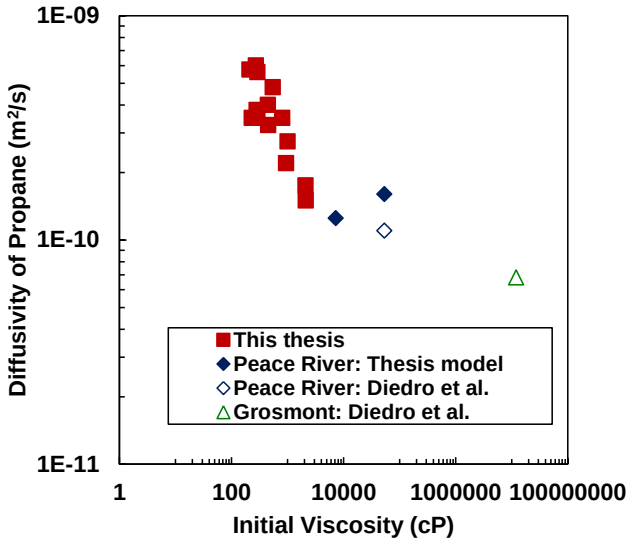

Figure 6.12. Diffusivity of propane in Peace River and Grosmont bitumens from Diedro *et al.* (2015) compared with diffusivities from this thesis.

6.3.4 Butane Data

James *et al.* (2012) and James (2009) determined diffusivities of butane in Athabasca Bitumen twice (238441 mPa.s at 26°C) and 242 kPa by measuring the swelling of the oil phase with time. They a developed a one-dimensional diffusion model used to describe the swelling of the oil phase with a constant equilibrium boundary condition, the convective term in the continuity equation, and several concentration dependent diffusivity models. James *et al.* (2012) fit their model to experimental swelling data by adjusting the parameters in the diffusivity model. The diffusivity was recalculated here using the constant diffusivity model from Chapter 4 fit to the

mass of diffused butane determined from the changing height of the experimental butane column. The diffusivity reported by James *et al.* (2012) was 4.35 10^{-10} m^2/s and the recalculated value was 4.5 10^{-10} m^2/s, showing a very good agreement between the two mathematical models.

Figure 6.13 shows that the diffusivities from James (2009) are very high compared to those of propane and butane measured in this thesis. This high value is likely due to the formation of a second liquid phase in this experiment. The butane solubility predicted by James *et al.* (2012) was between 40 and 60 wt%. According to Agrawal *et al.* (2012), a second phase asphaltene rich phase would form at approximately 15 wt% for propane and 45 wt% for pentane in a similar bitumen at the same pressure and temperature. Therefore, at 40 wt% butane content, there would almost certainly be a second asphaltene phase. Therefore, these data were not used to test the diffusivity correlations.

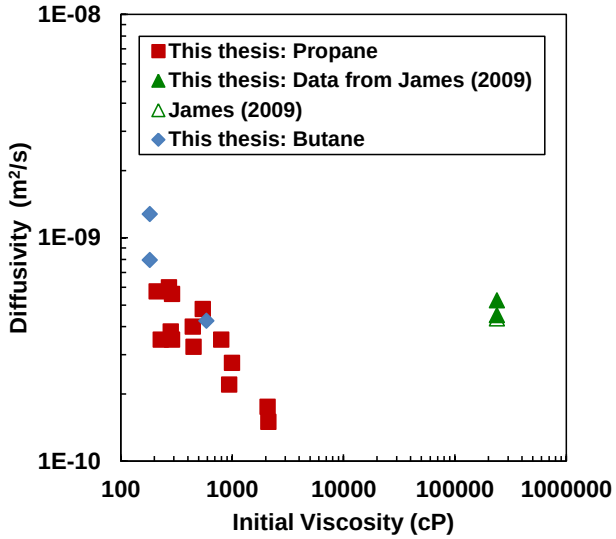

Figure 6.13. Diffusivity of butane in Athabasca bitumen from James (2009) and recalculated in this thesis compared with diffusivities from this thesis.

6.4 Correlations for Constant Diffusivity

As noted in Chapter 2, diffusivity is expected to correlate to viscosity. However, the constant diffusivity is an average over the concentration (and viscosity) range of the experiment rather than at a fixed concentration (or viscosity). Ideally, this average diffusivity should be correlated to an average viscosity but there is no simple way of determining such a value. Therefore, the

correlations presented in this section will be developed using the initial viscosity of the oil phase. Concentration dependent diffusivity will be considered later. Note, only data from this thesis was used to develop the correlations.

Figure 6.14a shows the constant diffusivities listed in Section 6.1 versus the initial oil viscosity. Since many correlations use diffusivity/temperature (*D/T*), the *D/T* values are shown in Figure 6.14b. Not surprisingly, there is considerable scatter in the data when the viscosity changes in the medium are ignored. Nonetheless, both diffusivity and *D/T* tend to increase as the original oil viscosity decreases. Also as expected, the smallest molecule, methane, tends to have the highest diffusivity. There appears to be two outliers at low temperature (high viscosity) one for ethane and one from the CT experiments. However, as will be shown later, the outliers are a result of assuming a constant diffusivity. The ethane outlier disappeared when modeled with a concentration dependent diffusivity; the CT experiment outlier was not analyzed further as discussed previously. Note, only a few data points were collected for butane. These data were not used to develop diffusivity correlations but will be used as a test case later.

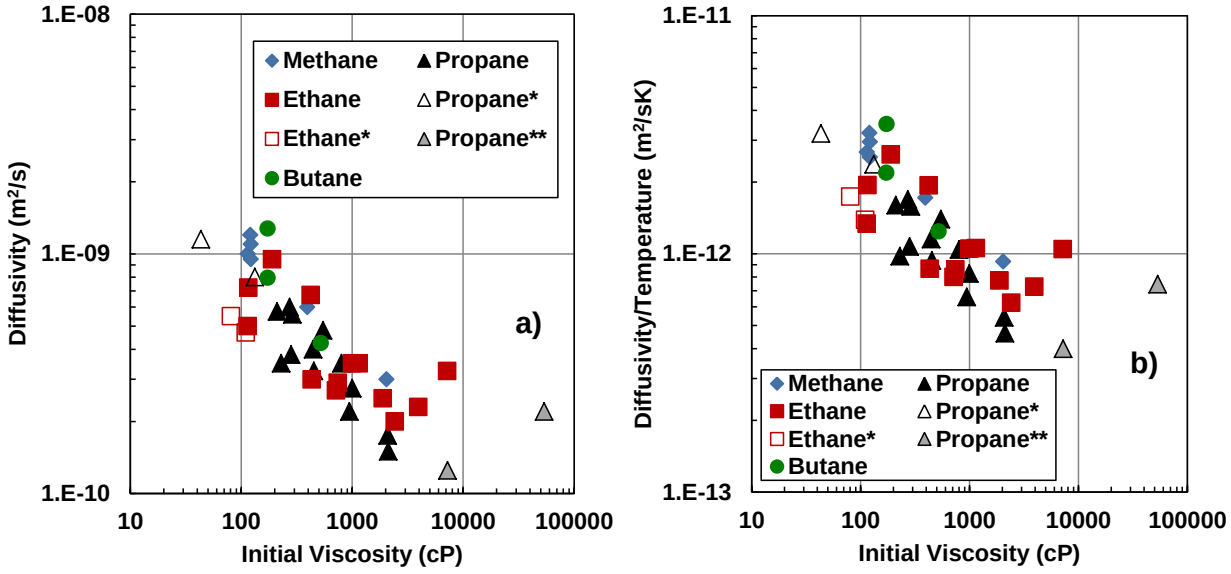

Figure 6.14. Relationship between constant diffusivity and initial oil viscosity: a) diffusivity versus initial oil viscosity; b) diffusivity/temperature versus initial oil viscosity. * Denotes experiments performed with an initial solvent concentration in the oil and ** denotes the results of the CT experiments.

6.4.1 Correlation with Hayduk-Cheng Equation

The data were first modelled using the Hayduk and Cheng (1971) equation given by:

$$D_{sb} = \frac{A_o}{\mu_o^{n_o}} \tag{6.6}$$

where D_{sb} is the diffusivity of solvent in bitumen in m^2/s, μ_o is the initial viscosity of the oil phase in mPa.s, and A_o and n_o are fitting parameters. This equation was initially developed for dilute conditions, but the viscous dependency is similar to other diffusivity models for concentrated conditions.

The constant diffusivity data for each solvent were fitted independently and the fitted parameters are provided in Table 6.11. Then, for ease of correlation, the data were refitted with a common exponent to obtain the parameters listed in Table 6.12. The errors from either method are comparable as shown in the dispersion plots, Figure 6.15. In each case, the average error is within 32% but the maximum error for the ethane is over 100%. Interestingly, the points with the highest errors are different for each model although similar in magnitude. After the exponent was fixed using the combined data, the parameter *A* trends monotonically from methane to propane indicting that a more general correlation can be constructed. However, this form of the correlation is not recommended because the errors are too high even with the direct fit to the data.

Table 6.11. Parameters of the Hayduk and Cheng (1971) equation fit to pressure decay results independently for each solvent. Units are m²/s for diffusivity and mPa.s for viscosity.

Solvent	A_o **(x** 10^8**)**	n_o	**AARD %**	**MARD %**
Methane	0.760	0.425	6.4	21
Ethane	0.121	0.180	27	101
Propane	1.043	0.534	16	39

Table 6.12. Parameters of the Hayduk and Cheng (1971) equation fit to pressure decay results with the same exponent for all solvents. Units are m²/s for diffusivity and mPa.s for viscosity.

Solvent	A_o (x 10^8)	n_o	AARD %	MARD %
Methane	0.806	0.433	6.4	18
Ethane	0.736	0.433	32	105
Propane	0.581	0.433	17	37

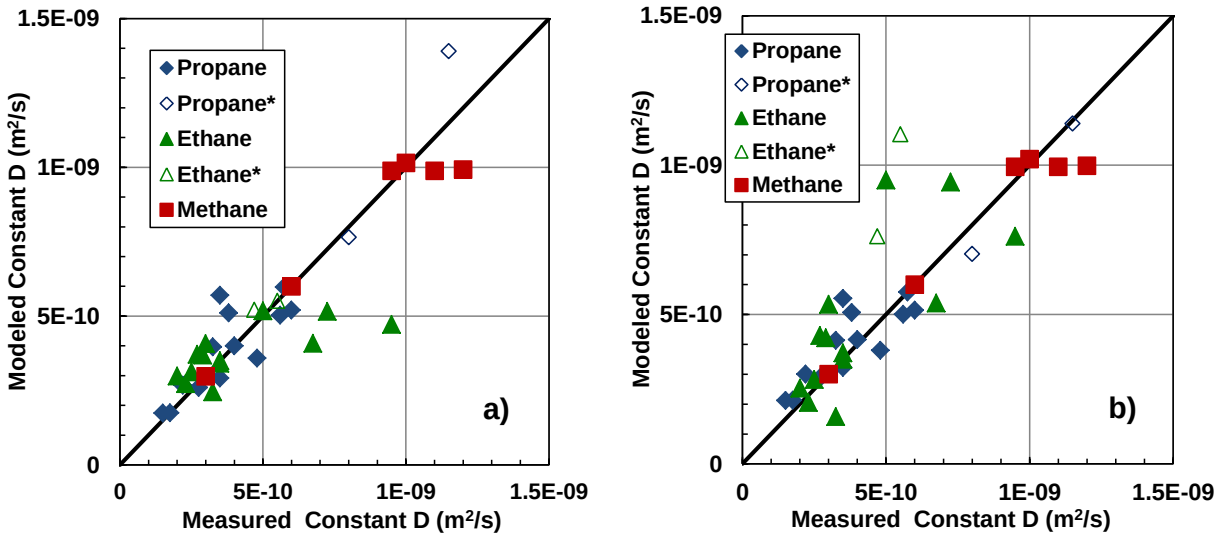

Figure 6.15. Dispersion of modeled (Hayduk-Cheng correlation) versus measured constant diffusivity: a) fit independently for each component; b) fit with a constant exponent. * denotes experiments with solvent initially dissolved in the oil.

6.4.2 Correlation with Modified Hayduk-Cheng Equation

As noted in Chapter 2, several correlations of diffusivity to viscosity, such as the Stokes-Einstein equation and the Wilke and Chang (1955), correlation include a proportionality to temperature. Therefore, the Hayduk and Cheng (1971) equation was modified to include a temperature proportionality as follows:

$$D_{sb} = \frac{A_T T}{\mu_o^{n_T}} \tag{6.7}$$

where T is the temperature in K, μ_o is the initial viscosity of the oil phase in mPa.s, and A_T and n_T are fitting parameters in consistent units.

The fitted parameters for constant diffusivity data fitted independently for each solvent were are provided in Table 6.13. The parameters refitted with a common exponent are listed in Table 6.14. The error from either method are comparable, Figure 6.16, except that the maximum error for ethane is higher when the common exponent is used. In each case, the average error is within 31% but the maximum error for the ethane still exceeds 100%. After the exponent was fixed, the parameter *A* still trends monotonically from methane to propane. This form of the correlation is still not recommended because the errors are too high.

Table 6.13. Parameters of the modified Hayduk and Cheng equation. Units are m²/s for diffusivity and mPa.s for viscosity.

Solvent	A_T***10^{11}**	n_T	**Average error %**	**Maximum error %**
Methane	1.603	0.374	6.2	20
Ethane	0.418	0.199	25	78
Propane	1.666	0.438	16	37

Table 6.14. Parameters of the modified Hayduk and Cheng equation fit with a single exponent. Units are m²/s for diffusivity and mPa.s for viscosity.

Solvent	A_T ***10^{11}**	n_T	**Average error %**	**Maximum error %**
Methane	1.598	0.373	6.4	19
Ethane	1.379	0.373	31	108
Propane	1.174	0.373	19	37

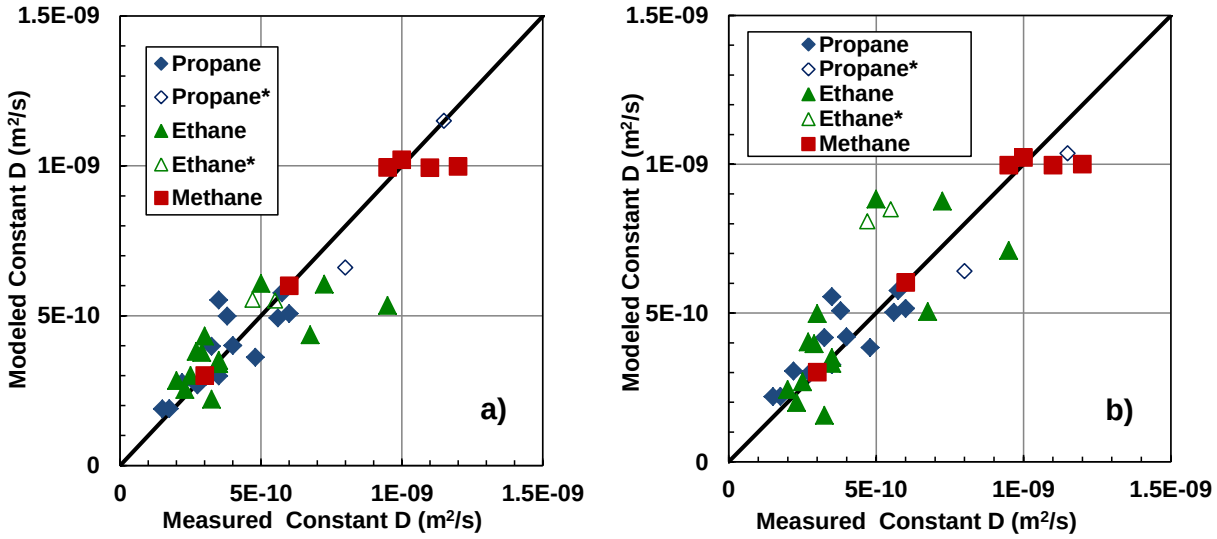

Figure 6.16. Dispersion of modeled (modified Hayduk-Cheng correlation) versus measured constant diffusivity: a) fit independently for each component; b) fit with a constant exponent. * denotes experiments with solvent initially dissolved in the oil.

6.4.3 Correlation with Solubility Corrected Hayduk-Cheng Equation

The main deficiency of the proposed approach is that the "average" viscosity appropriate for the correlation differs from the original viscosity and depends on how much solvent diffuses into the oil; that is, on the solubility of the solvent. The solubility depends directly on pressure and therefore either a solubility or pressure based adjustment could improve the quality of the correlation.

The following empirical linear solubility correction was added to the temperature modified Hayduk and Cheng equation:

$$D_{sb} = \frac{(A_S + B_S * w_S)T}{\mu_o^{n_s}} \tag{6.8}$$

where w_S is the solubility of solvent in oil in mass fraction, T is the temperature in K, μ_o is the initial viscosity of the oil phase in mPa.s and A_S, B_S and n_S are fitting parameters in consistent units. Tables 6.15 and 6.16 list the fitted parameters for model fit to the data for each solvent individually and with a constant exponent, respectively. Figure 6.17 shows the dispersion of

error for the two methods. The addition of the solubility correction substantially improves the quality of the fit to the data. The maximum deviation is less than 60% even when a single common exponent is used. However, neither A_S nor B_S follow a consistent trend from methane to propane when a single exponent is used for all solvents. As an alternative, the parameter B_S was also fixed, but even then, there was no consistent trend in the A_S parameter with the different solvents, as shown in Table 6.17.

Table 6.15. Parameters for the solubility corrected modified Hayduk and Cheng equation. Units are m²/s for diffusivity and mPa.s for viscosity.

Solvent	A_S **(x 10^{12})**	B_S **(x 10^{10})**	n_S	**AARD %**	**MARD %**
Methane	13.84	2.605	0.366	6.3	22
Ethane	5.295	1.950	0.345	16	54
Propane	7.282	1.015	0.391	10	39

Table 6.16. Parameters for the solubility corrected modified Hayduk and Cheng equation fit with a single exponent. Units are m²/s for diffusivity and mPa.s for viscosity.

Solvent	A_S **(x 10^{12})**	B_S **(x 10^{10})**	n_S	**AARD %**	**MARD %**
Methane	15.18	1.067	0.370	6.2	20
Ethane	6.277	2.289	0.370	16	56
Propane	6.472	0.916	0.370	10	36

Table 6.17. Parameters for the solubility corrected modified Hayduk and Cheng equation fit with a single exponent and single B_s. Units are m²/s for diffusivity and mPa.s for viscosity.

Solvent	A_S **(x 10^{12})**	B_S **(x 10^{12})**	n_S	**AARD %**	**MARD %**
Methane	11.45	6.081	0.308	20	48
Ethane	8.655	6.081	0.308	26	77
Propane	9.458	6.081	0.308	25	49

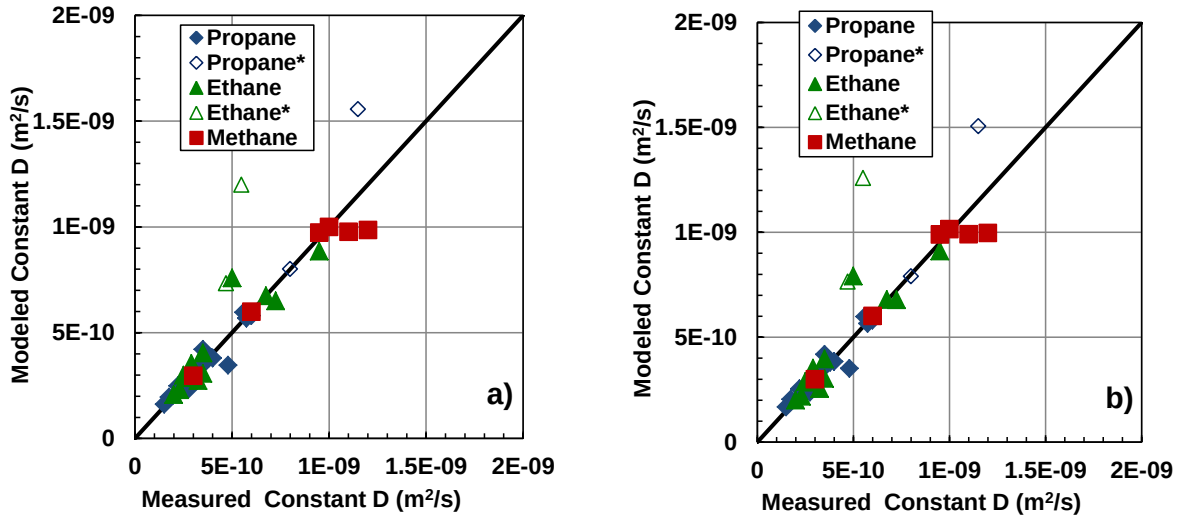

Figure 6.17. Cross plots of modelled versus measures constant diffusivity using the solubility corrected modified Hayduk-Cheng correlation a) fit independently for each component b) fit with a constant power. *denotes experiments with solvent initially dissolved in the oil.

Since pressure is more readily available, the following alternative pressure correction to the temperature modified Hayduk and Cheng equation was also tested:

$$D_{sb} = \frac{(A_P + B_P * P)T}{\mu_o^{n_P}} \tag{6.9}$$

where P is the pressure in kPa, T is the temperature in K, μ_o is the initial viscosity of the oil phase in mPa.s and A_P, B_P, and n_P are fitting parameters in consistent units. Tables 6.18 to 6.20 list the fitted parameters for model fit to the data for each solvent individually, with a constant exponent, and with both a constant exponent and a constant parameter B_P, respectively. Figure 6.18 shows the dispersion of error for the three methods. The addition of the pressure correction provides a better fit to the data than the solubility correction with a maximum deviation less than 42% even when a single common exponent and a single parameter B_P are used. The A_P parameter increases monotonically from methane to propane but, unless it is fixed, the B_P constant still does not follow a consistent trend. When fitting with a constant exponent and constant B_P, the parameter A_P had a linear relationship with the molecular weight of the solvent, as shown in Figure 6.19.

Table 6.18. Parameters for the pressure corrected modified Hayduk and Cheng equation. Units are m²/s for diffusivity and mPa.s for viscosity.

Solvent	A_P **(x 10^{12})**	B_P **(x 10^{15})**	n_P	**AARD %**	**MARD %**
Methane	9.978	0.985	0.350	6.1	22
Ethane	2.312	1.366	0.239	13	38
Propane	2.367	3.250	0.261	6.8	24

Table 6.19. Parameters for the pressure corrected modified Hayduk and Cheng equation fit with a single exponent. Units are m²/s for diffusivity and mPa.s for viscosity.

Solvent	A_P **(x 10^{12})**	B_P **(x 10^{15})**	n_P	**AARD %**	**MARD %**
Methane	0.092	2.037	0.244	10	19
Ethane	2.424	1.398	0.244	13	39
Propane	2.005	3.075	0.244	6.9	22

Table 6.20. Parameters for the pressure corrected modified Hayduk and Cheng equation fit with a single exponent. Units are m²/s for diffusivity and mPa.s for viscosity.

Solvent	A_P **(x 10^{12})**	B_P **(x 10^{15})**	n_P	**AARD %**	**MARD %**
Methane	0.633	2.393	0.289	7.5	19
Ethane	2.655	2.393	0.289	16	42
Propane	4.201	2.393	0.289	9.7	28

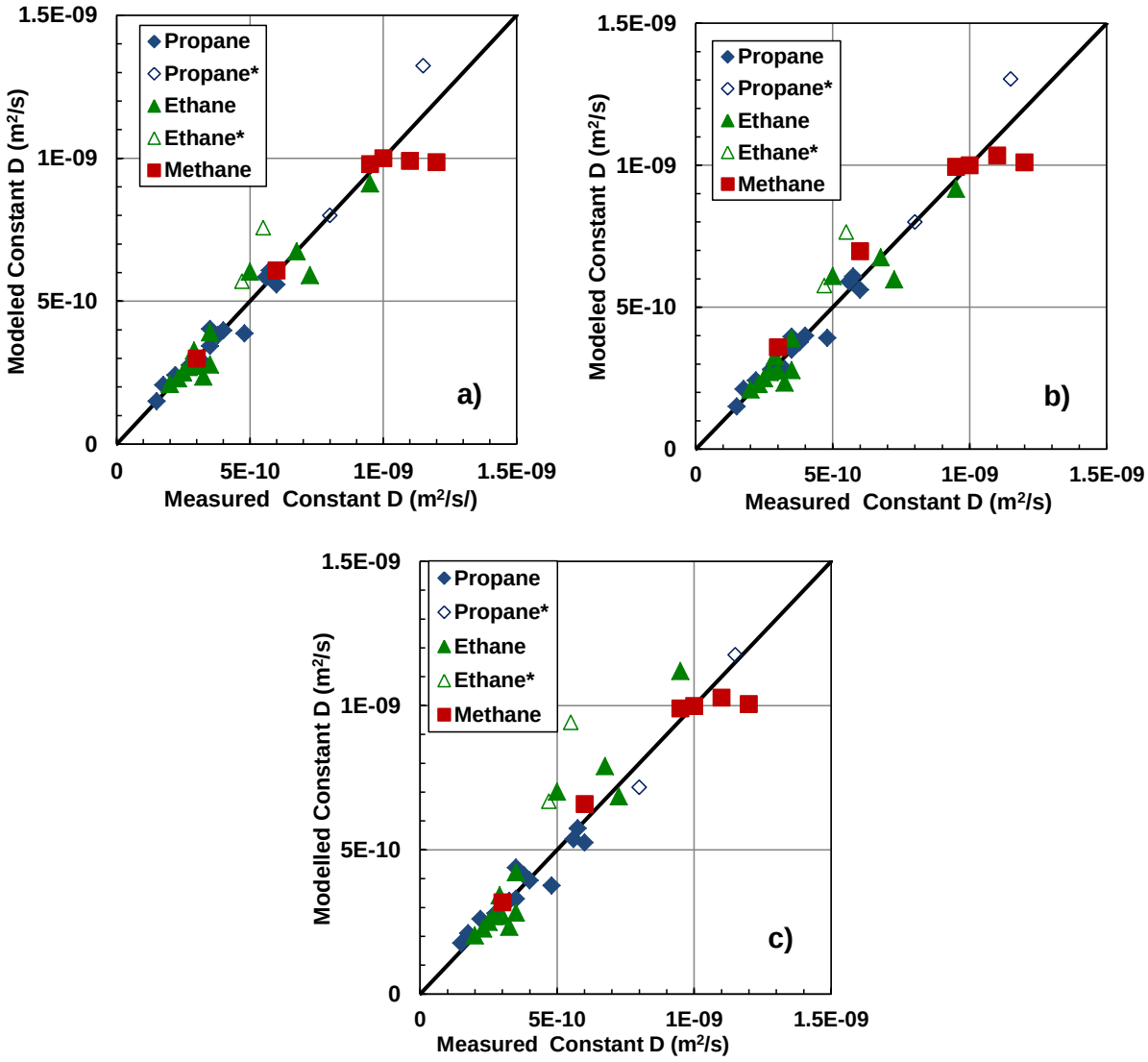

Figure 6.18. Dispersion of modeled (pressure corrected modified Hayduk-Cheng correlation) versus measured constant diffusivity: a) fit independently for each component; b) fit with a constant exponent. c) fit with a constant exponent and parameter B_P. * denotes experiments with solvent initially dissolved in the oil.

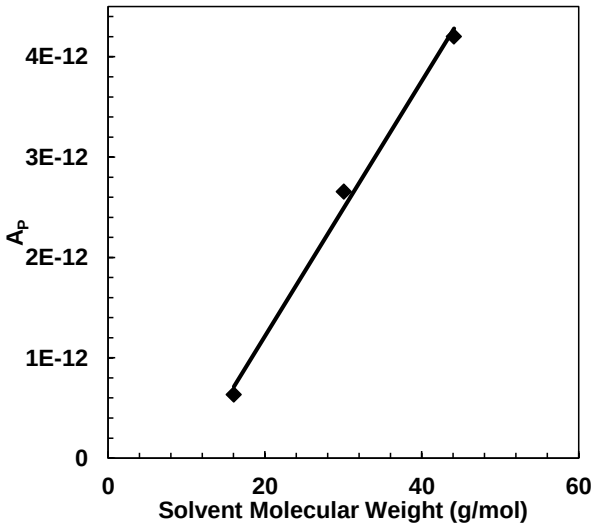

Figure 6.19. Parameter A_P for each solvent fit with a constant power and B_P parameter plotted against the molecular weight of the solvent.

The A_p parameter was correlated to the solvent molecular weight and the constant diffusivity data were fit a final time with a constant power, constant B_P and the parameter A_P to obtain the following correlation:

$$D_{sb} = \frac{(1.104 * 10^{-13} M_S - 7.869 * 10^{-13} + 2.224 * 10^{-15} P)T}{\mu_o^{0.280}} \quad (6.10)$$

where M_S is the molecular weight of the solvent. P is the pressure in kPa, T is the temperature in K, μ_o is the initial viscosity of the oil phase in mPa.s and D_{sb} is the constant diffusivity of solvent in bitumen in m^2/s. The deviation from the measured diffusivities is no more than 40%, Table 6.21. Figure 6.20 shows the dispersion of error.

Table 6.21. Relative deviation of the correlated diffusivities from the experimental data for each solvent.

Solvent	**AARD %**	**MARD %**
Methane	8.3	19
Ethane	16	40
Propane	10	27

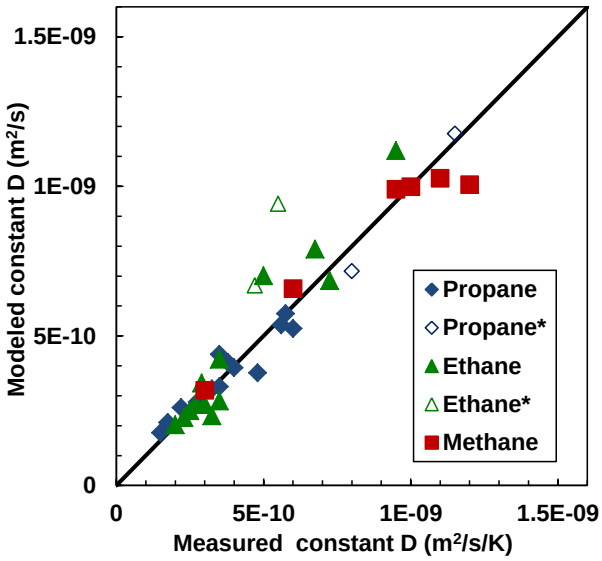

Figure 6.20. Dispersion of diffusivities correlated with the pressure corrected Hayduk-Cheng correlation. * denotes experiments with solvent initially dissolved in the oil

6.5 Concentration Dependent Diffusivity

As previously discussed, diffusivity is known to depend on viscosity. Since viscosity depends on the concentration of the solvent in the medium, then diffusivity must also depend on concentration. To test this hypothesis, four two-stage pressure decay experiments were performed with zero initial solvent concentration and then with a non-zero initial solvent concentration in the oil. The first stage was performed at a lower pressure. At the end of the first stage the oil was saturated with the solvent at the relatively low solubility corresponding to the relatively low pressure. In the second stage, the pressure was increased to achieve a new higher solubility end point and a second pressure decay was performed. Table 6.22 shows that in all cases, the diffusivity was higher in the second stage than in the first. In other words, the higher solvent content led to a higher diffusivity, confirming the concentration dependence of diffusivity.

Table 6.22. Constant diffusivity of ethane and propane in WC-B-B3 bitumen with and without solvent initially dissolved in oil.

Solvent	T °C	P kPa	Initial Solvent wt%	Solubility wt%	Viscosity mPa.s	Diffusivity 10^{-10} m^2/s
Ethane	42	2168	0	3.8	3900	2.3
Ethane	42	3316	3.6	6.1	80	5.5
Ethane	64	1120	0	1.5	710	2.7
Ethane	64	2104	1.5	2.9	110	4.7
Propane	64	1290	0	4.1	750	-
Propane	64	1890	4.1	8.6	130	8.0
Propane	86	1374	0	5.4	210	5.8
Propane	86	2303	5.4	11.4	43	11.5

The implication of this concentration dependence is that diffusivity will change throughout the mass transfer process as the solvent concentration changes. Therefore, the mass transfer is best modeled with a diffusivity that is calculated at each point in space and time as a function of concentration (or viscosity). In this case, viscosity was selected over concentration because the relationship between diffusivity and viscosity is well established. The diffusivity of solvent in bitumen was assessed using each of the following three equations:

1) a modified Hayduk and Cheng (1971) equation

$$D_{sb} = \frac{AT}{{\mu_{mix}}^n} \tag{6.11}$$

2) a modified Bearman (1961) equation

$$D_{sb} = \frac{AT}{{\mu_{mix}}^n}\left[1 + x_s\left(\frac{V_s}{V_b} - 1\right)\right]\left(\frac{d\ln a_s}{d\ln x_s}\right) \tag{6.12}$$

3) the Vignes (1966) equation

$$D_{sb} = (D_{sb}^0)^{x_B}(D_{bs}^0)^{x_A}\left(\frac{d\ln a_s}{d\ln x_s}\right) \tag{6.13}$$

Where applicable, the mixture viscosity was used instead of the initial bitumen viscosity. Note that temperature dependence was added to the original Hayduk and Cheng (1971) equation. An exponent was added to the mixture viscosity term in the original Bearman equation because the original formulation over-emphasized the viscous effect for the systems modeled in this thesis. The temperature dependence was added for consistency with the modified Hayduk and Cheng equation. The Vignes equation was not modified. The viscosity dependent diffusivities were implemented in the numerical model as described in Chapter 4.

A major challenge in implementing the concentration dependent viscosity is that the concentration dependent diffusivity correlations each have two fitting parameters and equally good fits to the experimental data can be obtained from multiple sets of parameters. Figure 6.21 shows that three unique sets of parameters for the modified Hayduk and Cheng equation and the Vignes equation give nearly indistinguishable fits to the mass transfer data. This observation is consistent with James *et al.* (2012), who concluded that various models for concentration dependent diffusivity of butane in bitumen give equally good fits to total mass diffused data.

The concentration profiles predicted from each of these fits are also very similar, as shown in Figure 6.22. The profiles predicted from the three sets of parameters from the Hayduk and Cheng equation are indistinguishable; note that one set was removed to avoid clutter. There are slight differences between the profiles predicted form the Hayduk and Cheng equation and the Vignes model. As they predict the same total mass diffused, the area under the each profile is the same at a given time. The Vignes model and Hayduk-Cheng determined profiles cross over one another at lower times but are nearly identical at 2500 minutes. Despite the slight differences between models, the concentration profiles have similar shapes. Even with concentration profile data, it would be difficult to determine the appropriate model given the scatter in experimentally determined concentration profiles shown in shown in Figure 6.2 (Section 6.2).

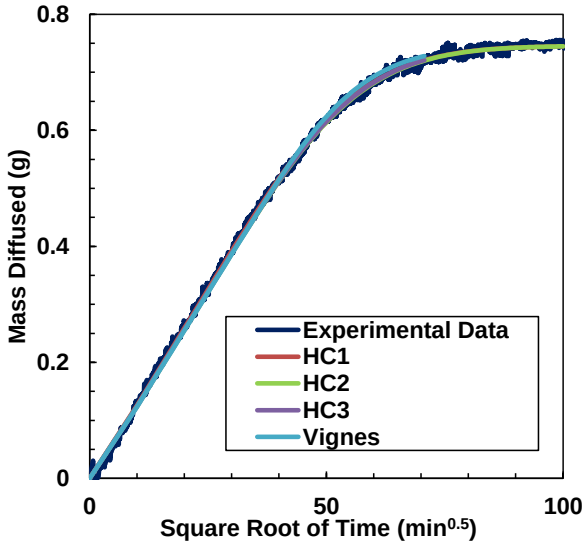

Figure 6.21. Modeling propane diffusion into bitumen at 60°C and 600 kPa using the three different sets of parameters for the modified Hayduk and Cheng (HC) and the Vignes equations. The three different sets of parameters fitted for the Hayduk and Cheng equation are: n=0.3, $A=3.40*10^{-12}$ (HC1); n=0.6, $A=4.68*10^{-12}$ (HC2); n=0.4, $A=5.91*10^{-12}$ (HC3).

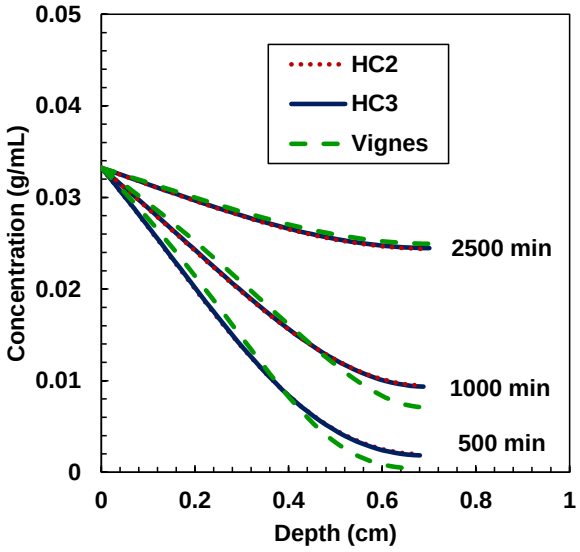

Figure 6.22. Concentration profiles predicted from modeling propane diffusion into bitumen at 60°C and 600 kPa using the two different sets of parameters for the modified Hayduk and Cheng and the Vignes equations. The sets of parameters fitted for the Hayduk and Cheng equation are: n=0.6, $A=4.68*10^{-12}$ (HC2); n=0.4, $A=5.91*10^{-12}$ (HC3).

To determine a unique fit to the experimental data, either one parameter must be calculated or a relationship between the two parameters must be obtained. For the modified Hayduk and Cheng

equation, the end point diffusivities provide a means to constrain the solution. At infinite dilution (of solvent), the diffusivity is given by:

$$D_{sb}^{\infty} = \frac{AT}{{\mu_b}^n} \tag{6.14}$$

where D_{sb}^{∞} is the infinite dilution diffusivity of solvent in bitumen and μ_b is the viscosity of the bitumen. At infinite dilution of bitumen (almost pure solvent), the diffusivity is given by:

$$D_{bs}^{*} = \frac{AT}{{\mu_s}^n} \tag{6.15}$$

where $D_{sb}^{*}$the diffusivity of the solvent in a solvent medium infinitely dilute in bitumen and μ_s is the viscosity of the liquid solvent. Once the endpoints are determined, the parameters *A* and *n* can be determined as follows:

$$n = \frac{\log \frac{{D_{bs}}^{*}}{{D_{sb}}^{\infty}}}{\log \frac{\mu_s}{\mu_b}} \tag{6.16}$$

$$A = \frac{{D_{sb}}^{\infty}}{T} {\mu_b}^n \tag{6.17}$$

Hence, if either the infinite dilution or maximum concentration diffusivities can be determined independently, the other endpoint can be determined by fitting the diffusivity data. The same approach was applied to the Bearman and the Vignes equations except that, in the latter case, the two end point diffusivities are input directly in the equation.

6.5.1 Diffusivity at Infinite Dilution of Bitumen in Solvent (Independently Determined)

The diffusivity at infinite dilution of bitumen was selected as the endpoint to be determined independently because it is a more suitably described by the existing infinite dilution correlations (designed for large species diffusing though a low molecular weight liquid). If diffusion at this condition is simply controlled by solvent molecules moving through solvent, then the appropriate end point is the self-diffusion coefficient of the solvent. However, the mass transfer process involves both solvent moving through bitumen and bitumen moving through solvent (swelling must involve the movement of bitumen). Hence, the diffusivity represents mutual diffusion. In

this case, the appropriate endpoint is the infinite dilution diffusivity of bitumen in solvent. Both types of endpoint are evaluated below.

Self-Diffusion Coefficient End Point

Self-diffusion coefficients for saturated liquid propane were measured by Greiner-Schmid *et al.* (1991). Their data was fit with the modified Hayduk-Chang equation as follows:

$$D_s^* = 5.1 * 10^{-12} \frac{T}{\mu_s^{0.951}} \tag{6.18}$$

where D_s^* is the propane self-diffusivity in m^2/s and μ_s is the viscosity of liquid propane in mPa.s. The liquid propane viscosity was calculated using the Expanded Fluid model with the effective density of propane as the input. This approach could only be applied to propane self-diffusion as there was little self-diffusion data available for methane and ethane in the appropriate range of temperatures and pressures. The calculated self-diffusion coefficients are shown in Figure 6.23.

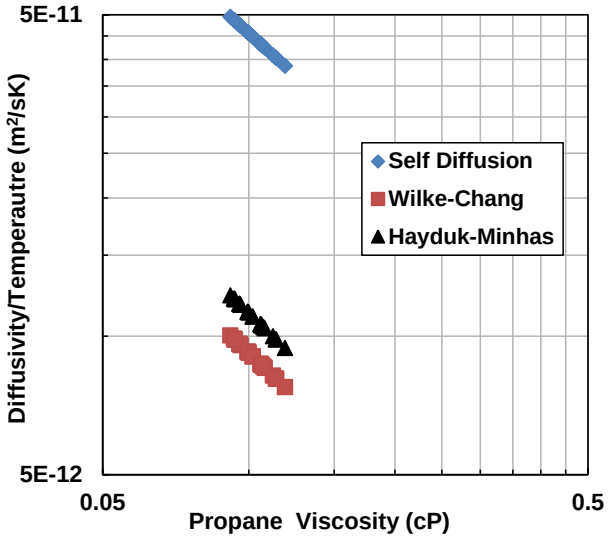

Figure 6.23. Self-diffusivity/temperature of propane and infinite dilution diffusivity/temperature of bitumen in liquid propane calculated at the experimental conditions.

Infinite Dilution of Bitumen End Point

This infinite dilution diffusivity was calculated using the Wilke-Chang Equation (1955) and the Hayduk-Minhas (1982) equation. Both equations are described in Section 2.2.2 and require the molecular weight and viscosity of the medium and the molar volume of the diffusing species at its normal boiling point. In this case, the solvent in the medium and bitumen is the diffusing species. The liquid solvent viscosity was calculated using the Expanded Fluid model with the effective density of the solvent as the input. A hypothetical average normal boiling point of the bitumen was estimated using the Soreide Correlation (Riazi 2005)

$$T_b = 1071.28 - 9.417 * 10^4 * \exp[-4.922 * 10^{-3} M_b - 4.7685 * SG + 3.462 * 10^{-3} * M_b * SG] * {M_b}^{-0.03522} * SG^{3.266} \quad (6.19)$$

where T_b is the normal boiling point in K, M_b is the molecular weight (520 g/mol), and SG is the specific gravity (1.017). The calculated normal boiling point and molar volume of the WC-B-B3 bitumen were 496^{o}C and 770cm^3/mol, respectively. The infinite dilution of bitumen endpoints for propane are compared in Figure 6.23. They are both approximately an order of magnitude lower than the self-diffusion coefficients. The infinite dilution diffusivity predicted from the Hayduk-Minhas and Wilke-Chang equations are very similar and were found to give nearly identical parameters when fitting the propane mass transfer data. The infinite dilution diffusivities of bitumen from the Haydak-Minhus equation were used in this thesis because it was developed from a larger dataset. Tabulated values are provided in Appendix A.

6.5.2 Diffusivity at Infinite Dilution of Solvent in Bitumen (Fitted to Mass Transfer Data)

Once the infinite dilution of bitumen end point was determined, the diffusivity at infinite dilution of solvent endpoint was calculated by fitting the mass transfer data. Each of three infinite dilution of solvent end points are evaluated below. Self-diffusion data at the conditions of interest in this thesis were only found for propane and therefore the self-diffusivity constraint was only used in the analysis of propane data. As will be discussed later, the modified Bearman equation resulted in large scatter in the infinite dilution diffusivity for propane in bitumen and therefore was not tested on the other solvents.

Tables 6.23 and 6.24 list the infinite dilution diffusivity of methane and ethane, respectively, in bitumen determined from the Modified Hayduk-Cheng equation and the Vignes model. Table 6.25 lists the infinite dilution diffusivity of ethane in bitumen calculated from experiments with a non-zero initial solvent content in the bitumen. Table 6.26 lists the infinite dilution diffusivity of propane in bitumen determined from the Modified Hayduk-Cheng equation, where the parameters were constrained using the self-diffusivity of propane. Table 6.27 list the infinite dilution diffusivity of propane in bitumen calculated form experiments with an initial solvent content in bitumen using the same constraint. Table 6.28 lists the infinite dilution diffusivity of propane in bitumen determined from the Modified Hayduk-Cheng, Bearman, and Vignes equations, where the parameters were constrained using the infinite dilution diffusivity of bitumen in propane. Table 6.29 lists the infinite dilution diffusivity of propane in bitumen calculated form experiments with an initial solvent content in the bitumen using the same constraints. Table 6.30 lists the infinite dilution diffusivity of propane in bitumen determined from the Modified Hayduk-Cheng equation where the parameters were constrained using the infinite dilution diffusivity of bitumen in butane.

Table 6.23. Infinite dilution diffusivity of methane in bitumen fit to the experimental data with the modified Hayduk-Cheng and Vignes equations using the infinite dilution diffusivity as the constraint.

T °C	P kPa	w_s* wt%	μ mPa.s	D_{sb}^{∞} Hayduk-Cheng 10^{-10} m^2/s	D_{sb}^{∞} Vignes 10^{-10} m^2/s
50	3450	0.42	2040	2.74	2.00
76	4160	0.55	393	5.50	4.00
100	4230	0.53	120	10.72	8.00
100	4170	0.48	122	8.65	6.50
100	4340	0.51	121	9.94	7.50
101	4120	0.49	114	9.72	7.25

Table 6.24. Infinite dilution diffusivity of ethane in bitumen, fit to the experimental data with the modified Hayduk-Cheng and Vignes equations using the infinite dilution diffusivity as the constraint.

T °C	P kPa	w_s* wt%	μ mPa.s	D_{sb}^{∞} Hayduk-Cheng 10^{-10} m^2/s	D_{sb}^{∞} Vignes 10^{-10} m^2/s
37	2964	6.9	7163	0.83	0.19
42	2168	3.8	3933	1.22	0.39
47	1394	2.1	2408	1.30	0.60
50	1741	3.7	1880	1.18	0.38
58	2962	4.4	1144	1.72	0.50
59	1495	2.4	994	2.45	1.05
64	1751	2.6	740	2.00	0.85
64	1120	1.5	712	2.05	1.05
73	774	0.84	429	2.50	1.70
75	4324	5.3	422	3.21	0.95
90	4741	4.9	189	5.84	1.90
100	1916	1.9	116	5.69	2.80
100	1970	2.6	114	3.42	1.35

Table 6.25. Infinite dilution diffusivity of ethane in bitumen fit to the experimental data with the modified Hayduk-Cheng and Vignes equations using the infinite dilution diffusivity as the constraint. Data from experiments with non-zero initial ethane concentration in bitumen (w_s^o).

T °C	P kPa	w_s^o wt%	w_s* wt%	μ mPa.s	D_{sb}^{∞} Hayduk-Cheng 10^{-10} m^2/s	D_{sb}^{∞} Vignes 10^{-10} m^2/s
42	3316	3.6	6.1	4122	2.06	0.45
64	2104	1.5	2.9	638	2.92	0.98

Table 6.26. Infinite dilution diffusivity of propane in bitumen fit to the experimental data with the modified Hayduk-Cheng Equation and the self-diffusivity of propane as the constraint.

T °C	P kPa	w_s* wt%	μ mPa.s	D_{sb}^{∞} 10^{-10} m^2/s
50	327	2.6	2116	0.83
50	724	4.6	2087	1.28
59	824	3.0	999	2.02
60	602	3.5	945	1.05
62	1080	6.8	801	1.11
70	1077	4.5	547	2.60
74	523	2.2	452	2.79
74	1006	4.5	445	2.09
80	1507	8.0	290	1.88
81	720	2.4	282	2.54
81	1367	7.23	272	2.21
85	702	2.5	229	2.38
86	1374	5.4	210	3.29

Table 6.27. Infinite dilution diffusivity of propane in bitumen fit to the experimental data with the modified Hayduk-Cheng equation and the self-diffusivity of propane as the constraint. Data from experiments with non-zero initial propane concentration in bitumen (w_s^o).

T °C	P kPa	w_s^o wt%	w_s* wt%	μ mPa.s	D_{sb}^{∞} 10^{-10} m^2/s
64	1890	4.1	8.6	753	2.06
86	2303	5.4	11.4	210	2.81

Table 6.28. Infinite dilution diffusivity of propane in bitumen fit to the experimental data with the modified Hayduk-Cheng, Bearman, and Vignes equations using the infinite dilution diffusivity as the constraint.

T °C	P kPa	w_s* wt%	μ mPa.s	D_{sb}^{∞} Hayduk-Cheng 10^{-10} m^2/s	D_{sb}^{∞} Bearman 10^{-10} m^2/s	D_{sb}^{∞} Vignes 10^{-10} m^2/s
50	327	2.6	2116	1.51	1.37	0.88
50	724	4.6	2087	1.13	1.13	0.45
59	824	3.0	999	2.45	2.34	1.30
60	602	3.5	945	1.33	1.33	0.63
62	1080	6.8	801	1.63	1.95	0.53
70	1077	4.5	547	3.42	3.56	1.50
74	523	2.2	452	3.13	2.88	1.98
74	1006	4.5	445	2.66	2.66	1.15
80	1507	8.0	290	2.94	3.74	0.95
81	720	2.4	282	2.98	2.75	1.65
81	1367	7.2	272	3.40	4.50	1.20
85	702	2.5	229	2.81	2.60	1.30
86	1374	5.4	210	4.29	4.29	1.70

Table 6.29. Infinite dilution diffusivity of propane in bitumen fit to the experimental data with the modified Hayduk-Cheng, Bearman, and Vignes equations using the infinite dilution diffusivity as the constraint. Data from experiments with non-zero initial propane concentration in bitumen (w_s^o).

T °C	P kPa	w_s* wt%	μ mPa.s	D_{sb}^{∞} Hayduk-Cheng 10^{-10} m^2/s	D_{sb}^{∞} Bearman 10^{-10} m^2/s	D_{sb}^{∞} Vignes 10^{-10} m^2/s
64	1890	8.6	753	3.56	5.55	1.23
86	2303	11.4	210	5.82	11.7	1.70

Table 6.30. Infinite dilution diffusivity of butane in bitumen fit to the experimental data with the modified Hayduk-Cheng Equation using the infinite dilution diffusivity as the constraint.

T °C	P kPa	w_s* wt%	μ mPa.s	D_{sb}^{∞} 10^{-10} m^2/s
69	284.3	3.0	589	2.74
90	738.2	7.9	182	9.94
90	874.3	10.1	183	9.72

6.5.3 Correlating the Infinite Dilution Diffusivity of Solvent in Bitumen

In the previous section, the infinite dilution of solvent diffusivity endpoint was determined from three different forms of the concentration dependent diffusivity (Hayduk-Cheng, Bearman, and Vignes) with two different endpoint constraints (self-diffusion and infinite dilution of bitumen from Hayduk-Minhas). As shown in Figure 6.24, the endpoint diffusivity/temperature (*D/T*) appears to correlate to the original oil viscosity. Therefore, the following correlation was fit to the infinite dilution diffusivity data for each solvent with each diffusivity model and endpoint constraint:

$$D_{sb}^{\infty} = \frac{A^{\infty} T}{{\mu_b}^m} \tag{6.20}$$

where A^{∞} and m are fitting parameters. Note: these constant are not the same as those used to fit the pressure decay data but are are specific to fitting the infinite dilution diffusivity. The combinations of diffusivity model and endpoint constraint are examined below to determine the best correlation to the original oil viscosity.

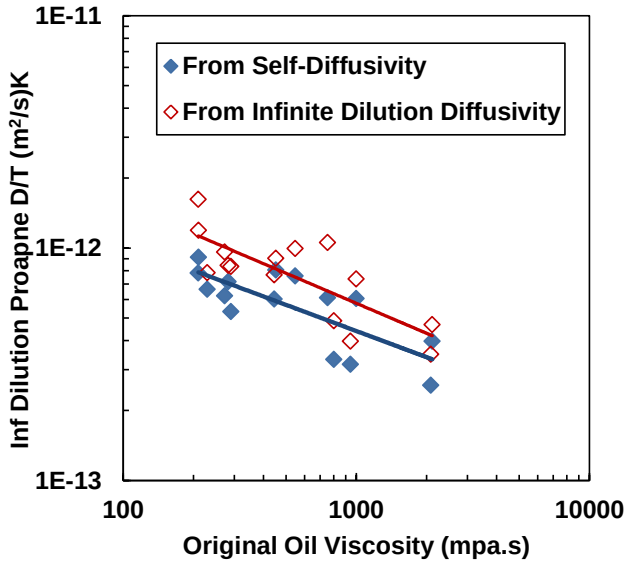

Figure 6.24. Infinite dilution diffusivity of propane in bitumen determined from the modified Hayduk-Cheng equation constraining the equation with propane self-diffusivity endpoint constraint.

Comparison of Endpoint Constraints

Figure 6.24 compares the infinite dilution diffusivity of propane in bitumen calculated from the self-diffusivity of propane and the infinite dilution diffusivity of propane in bitumen as the value of the propane self-diffusivity is higher that the infinite dilution diffusivity of bitumen in propane, it is reasonable that the resulting infinite dilution diffusivity from the self-diffusion constraint is slightly lower than the infinite dilution constraint. Both of the relationships for the infinite dilution diffusivity of propane in bitumen have similar exponents and the average errors are very similar with the self-diffusivity constraint having slightly less maximum error, Table 6.31.

Since using the solvent self-diffusivity gives less error and it is based on the extrapolation of experimental data, it would normally be the best choice to constrain the concentration dependent diffusivity model. However, due to the limited availability of self-diffusivity data for the gases of interest in this thesis, the Hayduk-Minhas equation was used to constrain the diffusivity equation and develop the correlations later in this chapter.

Table 6.31. Parameters of the infinite propane dilution diffusivity correlation fit to values determined by fitting propane diffusion data with the modified Hayduk-Cheng equation with the self-diffusion and infinite dilution of bitumen endpoints. Units are m²/s for diffusivity and mPa.s for viscosity.

Endpoint	A^{∞} **(x 10^{12})**	***m***	**AARD %**	**MARD %**
Self-diffusion	5.32	0.362	21	39
Infinite dilution of bitumen	8.60	0.380	22	53

Comparison of Concentration Dependent Diffusion Equations

Modified Hayduk and Cheng Equation: The infinite dilution *D/T* of solvent in bitumen from the modified Hayduk-Chang equation (constraining the equation with the infinite dilution diffusivity of bitumen in the solvents) is shown versus the initial oil viscosity in Figure 6.25. The fitted parameters for the infinite dilution of solvent diffusivity are provided in Table 6.32. As expected, the infinite dilution diffusivity for each solvent increases with decreasing viscosity and the smaller solvents generally have higher diffusivity. The infinite dilution diffusivity of methane

is larger than that of the other two solvents. The difference between ethane, propane, and butane diffusivities is within the scatter of the data.

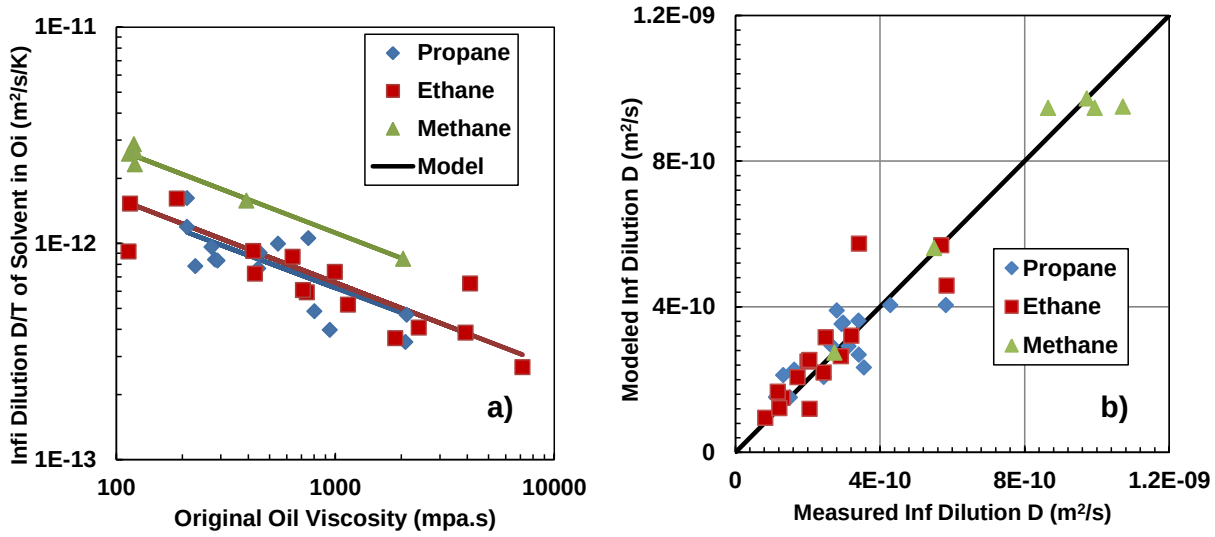

Figure 6.25. Infinite dilution of solvent diffusivity determined by fitting mass transfer data with the modified Hayduk-Cheng equation (symbols) and correlation to initial oil viscosity (lines): a) ratio of diffusivity to temperature versus viscosity; b) dispersion of error of predicted versus measured diffusivity.

Table 6.32. Parameters of the infinite solvent dilution diffusivity correlation fit to values determined by fitting solvent diffusion data with the modified Hayduk-Cheng equation. Units are m²/s for diffusivity and mPa.s for viscosity.

Solvent	A^{∞} **(x 10^{12})**	***m***	**AARD %**	**MARD %**
Methane	16.33	0.388	4.8	13
Ethane	9.72	0.390	20	72
Propane	8.60	0.380	22	53

The exponents, *m*, of the infinite dilution models for the three solvents are all similar. Therefore, the infinite dilution diffusivity data were refit with a fixed exponent of 0.403. The refitted *D/T* are shown in Figure 6.26 and the refitted parameters are listed in Table 6.33. There was negligible change in the deviations with this simplified correlation and; therefore, it is the recommended option.

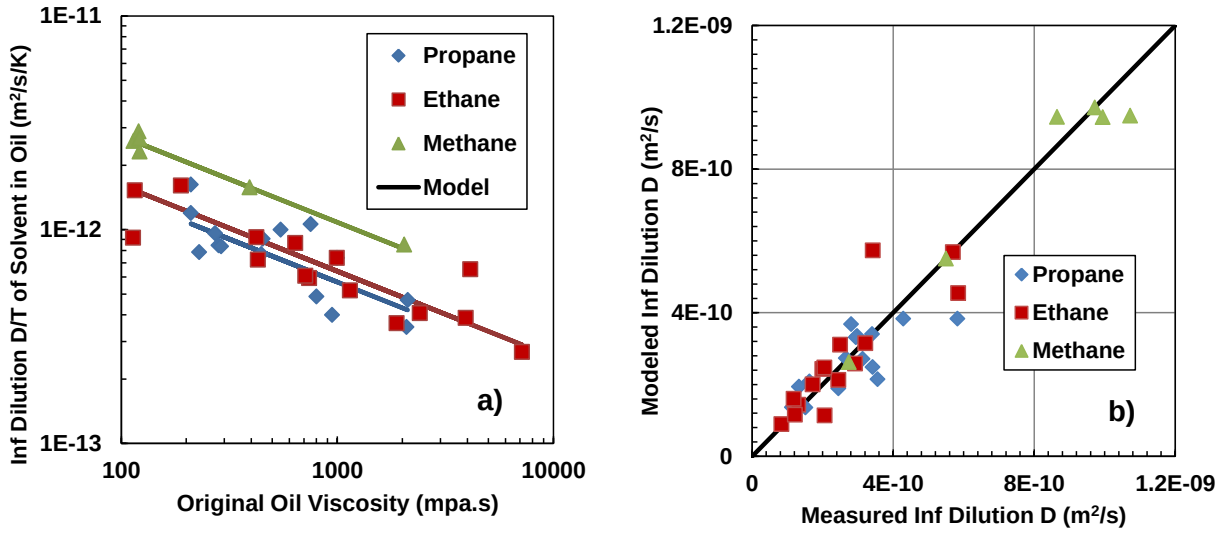

Figure 6.26. Infinite dilution of solvent diffusivity determined by fitting mass transfer data with the modified Hayduk-Cheng equation (symbols) and correlation to initial oil viscosity (lines): a) ratio of diffusivity to temperature versus viscosity; b) dispersion of error of predicted versus measured diffusivity. Data for all solvents fit with the same exponent in the power law model.

Table 6.33. Parameters of the infinite solvent dilution diffusivity correlation fit to values determined by fitting solvent diffusion data with the modified Hayduk-Cheng equation. The correlation exponent was fixed at m = 0.403. Units are m²/s for diffusivity and mPa.s for viscosity.

Solvent	A^{∞} (x 10^{12})	AARD %	MARD %
Methane	17.53	5.0	11
Ethane	10.34	20	68
Propane	9.20	23	66

Modified Bearman Equation: The infinite dilution *D/T* of solvent in bitumen from the modified Bearman equation (constraining the equation with the infinite dilution diffusivity of bitumen in the solvents) is shown versus the initial oil viscosity in Figure 6.27. The fitted parameters for the infinite dilution of solvent diffusivity are provided in Table 6.34. The predicted diffusivity from this model does not correlate well with viscosity; the scatter in the data is large, with a maximum relative error of 158%. There are two obvious outliers from the trend, but data from these two experiments are much closer to trend for the other models investigated in this thesis. Hence, the Bearman model was not investigated further.

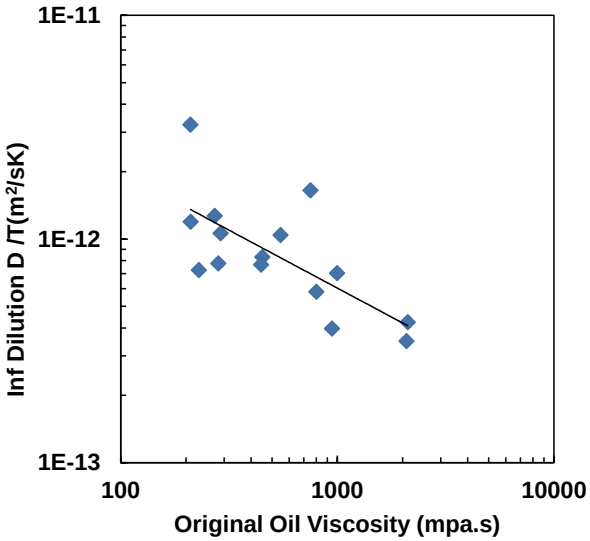

Figure 6.27. Infinite dilution diffusivity of propane in bitumen determined from the modified Bearman equation equation (symbols). Line is power law fit to the data.

Table 6.34. Parameters of the infinite solvent dilution diffusivity correlation fit to values determined by fitting solvent diffusion data with the modified Bearman equation. Units are m²/s for diffusivity and mPa.s for viscosity.

Solvent	A^{∞} **(x** 10^{12}**)**	***m***	**AARD %**	**MARD %**
Propane	16.12	0.477	35	158

Vignes Equation: The infinite dilution *D/T* of solvent in bitumen from the Vignes equation (constraining the equation with the infinite dilution diffusivity of bitumen in the solvents) is shown versus the initial oil viscosity in Figure 6.28. The fitted parameters for the infinite dilution of solvent diffusivity are provided in Table 6.35. The infinite dilution dilutions diffisivities fit to the pressure decay data using the Vignes equation follow the expected trends with viscosity as observed with the Hayduk-Cheng equation.

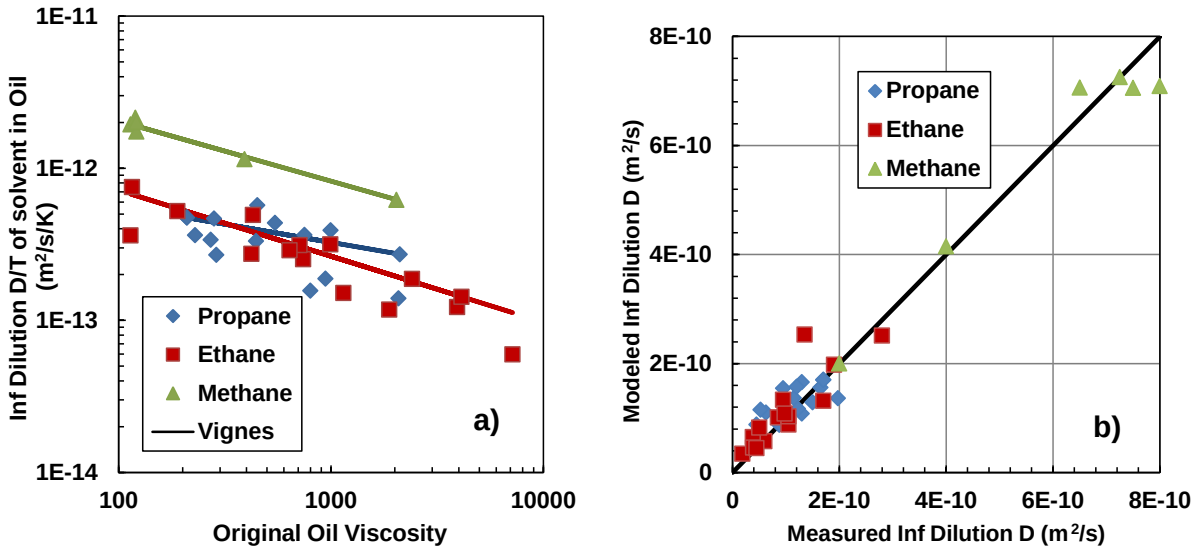

Figure 6.28. Infinite dilution of solvent diffusivity determined by fitting mass transfer data with the Vignes equation (symbols) and correlation to initial oil viscosity (lines): a) ratio of diffusivity to temperature versus viscosity; b) dispersion of error of predicted versus measured diffusivity.

Table 6.35. Parameters of the infinite solvent dilution diffusivity correlation fit to values determined by fitting solvent diffusion data with the Vignes equation. Units are m²/s for diffusivity and mPa.s for viscosity.

Solvent	A^{∞} **(x** 10^{12}**)**	***m***	**AARD %**	**MARD %**
Methane	12.7	0.396	5.1	13
Ethane	5.30	0.434	22	47
Propane	1.71	0.240	23	54

The exponents of this model are dissimilar and do not follow a clear trend. Nonetheless, the infinite dilution diffusivity data were refit with a fixed average exponent of 0.418. The refitted *D/T* are shown in Figure 6.29 and the refitted parameters are listed in Table 6.36. The deviations from the data increases with this simplified correlation particularly for methane. The predicted diffusivity of propane is also slightly higher than that predicted for ethane, which seems unlikely for a larger, chemically similar molecule. This counter-intuitive trends may arise from the thermodynamic correction factor used in the Vignes model used to match the data. The compositional derivative of the activity coefficient was obtained from the Margules Equation fit only to the saturation pressure of the solvent-oil mixture. For methane, the saturation pressure

data was supplemented from literature and differences between the oil samples could contribute to the error.

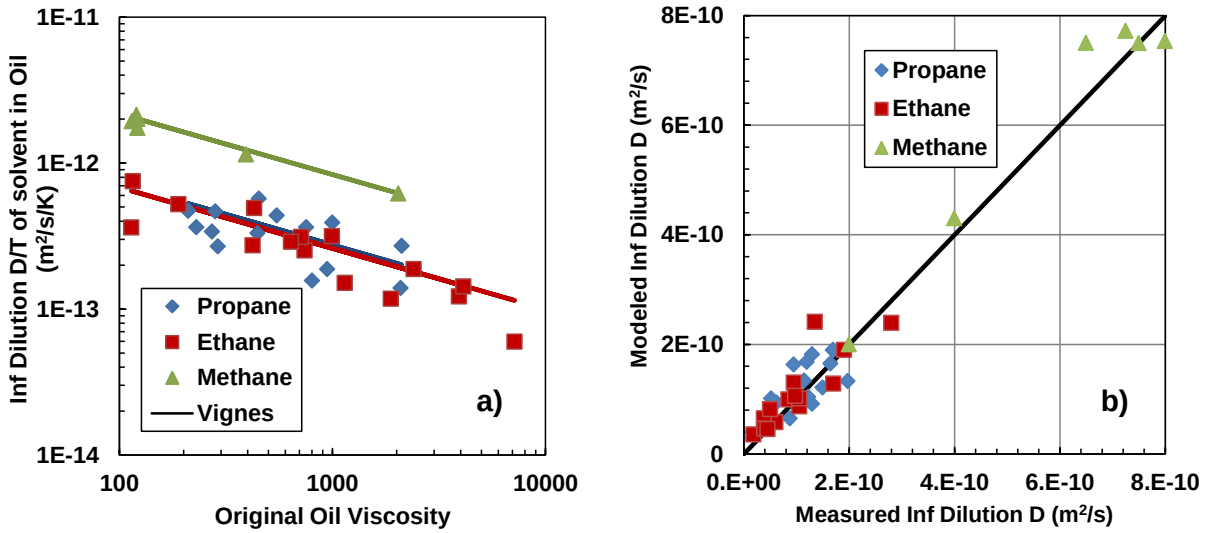

Figure 6.29. Infinite dilution of solvent diffusivity determined by fitting mass transfer data with the Vignes equation (symbols) and correlation to initial oil viscosity (lines): a) ratio of diffusivity to temperature versus viscosity; b) dispersion of error of predicted versus measured diffusivity. Data for all solvents fit with the same exponent in the power law model.

Table 6.36. Parameters of the infinite solvent dilution diffusivity correlation fit to values determined by fitting solvent diffusion data with the Vignes equation. The correlation exponent was fixed at $m = 0.418$. Units are m²/s for diffusivity and mPa.s for viscosity.

Solvent	**A^{∞} (x 10^{12})**	**AARD %**	**MARD %**
Methane	14.92	37	56
Ethane	4.67	21	44
Propane	4.92	28	49

Conclusion: Both the modified Hayduk-Cheng and the Vignes approach lead to similar quality correlations for the infinite dilution diffusivity of solvent. However, the Vignes approach requires the determination of the activity coefficient derivative and lack of data limits the applicability of this approach. The Hayduk-Cheng approach is simpler and provides a good basis for a correlation of the infinite dilution diffusivity of solvent to the initial oil viscosity.

6.5.4 Generalizing the Infinite Dilution Diffusivities of Solvents in Bitumen

In the previous section, it was established that the approach that provided the best correlation for the infinite dilution of solvent diffusivity to the initial oil viscosity is the modified Hayduk-Cheng equation with the Hayduk-Minhas infinite dilution of bitumen diffusivity endpoint. However, up to now, the data for each solvent were fitted separately. To generalize the correlation, the values of A^{∞} and m determined with this approach must be related to the solvent type. The exponent was fixed at a constant value of m = 0.403 and therefore only a correlation for the A^{∞} parameter is required.

Recall that the Wilke and Chang (1955) and Hayduk and Minhas (1982) equations for infinite dilution diffusivity are a function of the molar volume of the diffusing species (in this case the solvent) at its normal boiling point. Therefore, the A^{∞} parameter was correlated to the solvent molar volume. Table 6.37 lists the molar volume of the solvents used in the thesis at their normal boiling points (NIST, 2016). The A^{∞} parameters were correlated to the molar volumes with the following relationship:

$$A^{\infty} = \frac{5.18 * 10^{-10}}{V_s^{0.946}} \tag{6.21}$$

where V_s is the liquid molar volume of the solvent at its normal boiling point in cm^3/mol. The correlation fit the values with an average absolute relative deviation of 7.7%, Figure 6.30.

Figure 6.31 shows the correlated infinite dilution diffusivities versus the initial oil viscosity. Table 6.38 lists the correlated parameters for this model and the average and maximum errors of the infinite dilution diffusivity prediction. The correlation of A^{∞} does not dramatically affect the quality of the fit to the infinite dilution data.

Table 6.37. Normal boiling point of methane, ethane, propane, and their liquid density and molar volume at the boiling point.

Solvent	Normal Boiling Point ^{o}C	Liquid Molar Density mol/m^3	Liquid Molar Volume cm^3/mol
Methane	-161.5	26327	37.98
Ethane	-88.6	18090	55.28
Propane	-42.1	13174	75.91

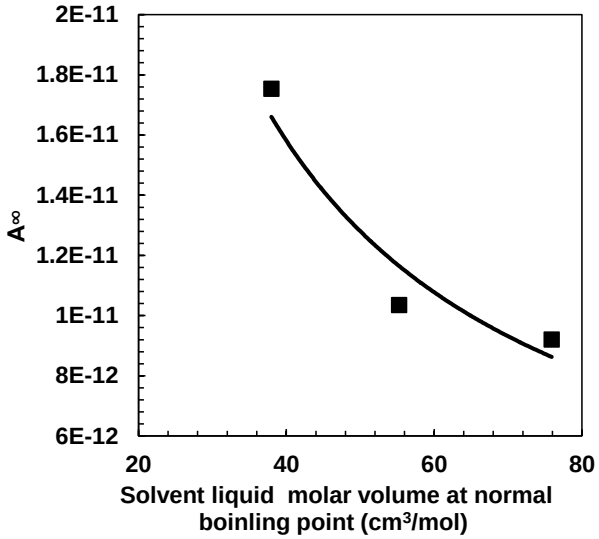

Figure 6.30. Experimentally determined and fitted A^{∞} parameter for each solvent versus the solvent molar volume at its normal boiling point.

Table 6.38. Correlated parameters to the infinite dilution diffusivity model of solvents in heavy oil. Units are m^2/s for diffusivity and mPa.s for viscosity.

Solvent	Correlated $A^{\infty}(x\ 10^{12})$	*m*	AARD %	MARD %
Methane	16.61	0.403	8.2	16
Ethane	11.64	0.403	28	89
Propane	8.63	0.403	25	92

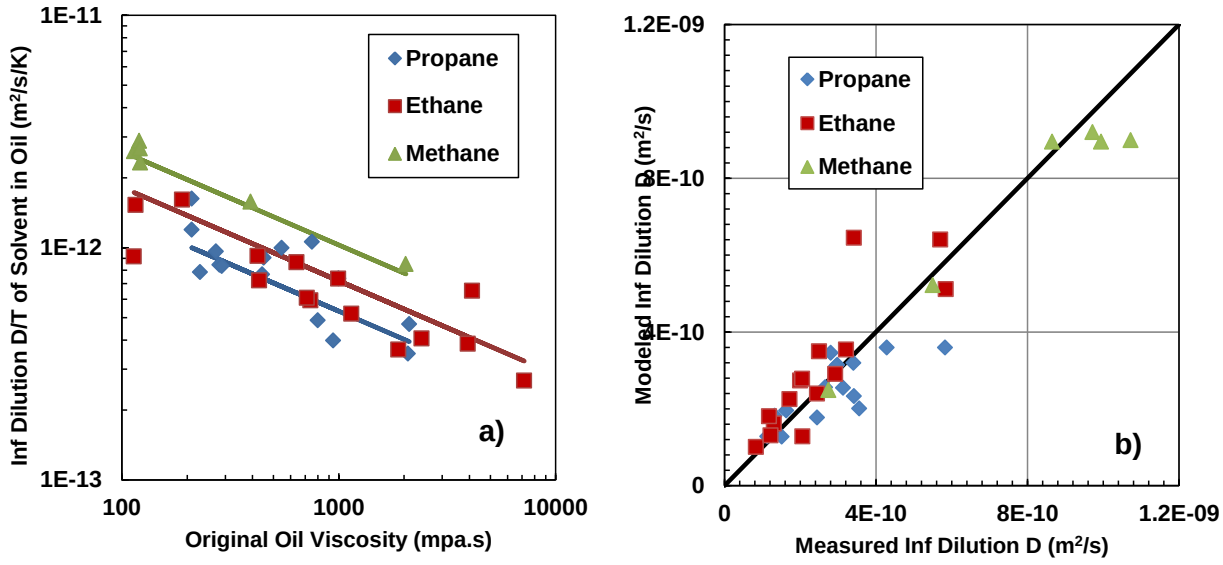

Figure 6.31. Infinite dilution of solvent diffusivity fit with the correlated infinite dilution diffusivity model: a) ratio of diffusivity to temperature versus viscosity; b) dispersion of error of predicted versus measured diffusivity.

6.5.5 Generalized Correlation for Concentration Dependent Diffusivity

For convenience, the concentration dependent diffusion model developed over the previous sections is summarized here. The concentration dependent diffusivity of gaseous solvent in bitumen is given by the following equation:

$$D_{sb} = \frac{AT}{{\mu_{mix}}^{n}} \tag{6.22}$$

where D_{sb} is the diffusivity of solvent in bitumen in m^2/s, T is the temperature in K, μ_{mix} is the viscosity of the solvent and bitumen mixture in mPa.s, and the parameters A and n are given by:

$$n = \frac{\log \frac{{D_{bs}}^{\infty}}{{D_{sb}}^{\infty}}}{\log \frac{\mu_s}{\mu_b}} \tag{6.23}$$

$$A = \frac{{D_{sb}}^{\infty}}{T} {\mu_{bit}}^{n} \tag{6.24}$$

where μ_s is the predicted viscosity of the liquid solvent in mPa.s, μ_b is the viscosity of the bitumen, ${D_{bs}}^{\infty}$ is the infinite dilution diffusivity of bitumen in solvent in m^2/s, and ${D_{sb}}^{\infty}$ is the infinite dilution diffusivity of solvent in bitumen. The former is given by the Hayduk-Minhas equation:

$$ {D_{bs}}^{\infty} = \frac{13.3 * 10^{-12} T^{1.47} {\mu_s}^{\left(10.2/V_b - 0.791\right)}}{V_b^{0.71}} \qquad (2.25) $$

where V_b is the liquid molar volume of bitumen at its normal boiling point in cm^3/mol. The latter is given by:

$$ {D_{sb}}^{\infty} = \frac{5.18 * 10^{-10} T}{{V_s}^{0.946} {\mu_b}^{0.403}} \qquad (6.26) $$

where V_s is the liquid molar volume of solvent at its normal boiling point in cm^3/mol.

The values of *n* predicted using this correlation are fairly constant for each solvent: 0.224 to 0.240 for methane, 0.306 to 0.321 for ethane, and 0.323 to 0.327 for propane. Das and Butler (1996) fit propane diffusion data to the Hayduk Cheng Equation with a power of 0.46, although their model did not include a temperature term, which could account for the difference. As shown in Section 6.4, the best fit exponents to the Hayduk-Cheng equation (Table 12) were higher than those for the modified equation which included the temperature (Table 14).

The form of the concentration dependence of diffusivity is illustrated in Figure 6.32 at two conditions. At low concentrations of either the solvent or the bitumen, the concentration dependence of the diffusivity is linear, consistent with the findings from James *et al*. (2012) who found the best fit to their mass diffusion data was achieved with a diffusivity linearly dependent on concentration.

To illustrate the performance of the correlation, the predicted mass transfer for two experiments (a good match and a poor match) are compared with the measured data in Figure 6.33. In the former case, the error in the infinite dilution of solvent diffusivity prediction error was 5.4% and

in the latter case, the error was 37%. Despite the error in the prediction of the infinite dilution diffusivity, the prediction from the correlation matches the mass diffused within 0.1 g corresponding to less than 20% error in the total mass diffused at any time.

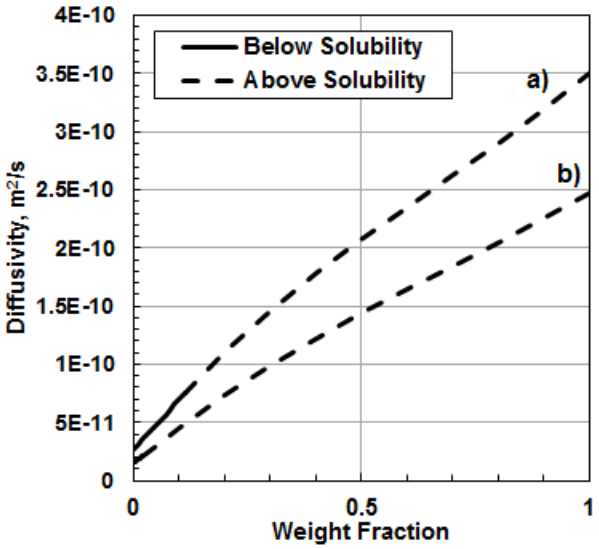

Figure 6.32. Correlated diffusivity as a function of concentration for a) 86°C and 2300kPa (A=4.36*10^{-13}, n=0.329) and b) 74°C and 520kPa (A=3.24*10^{-13}, n=0.331).

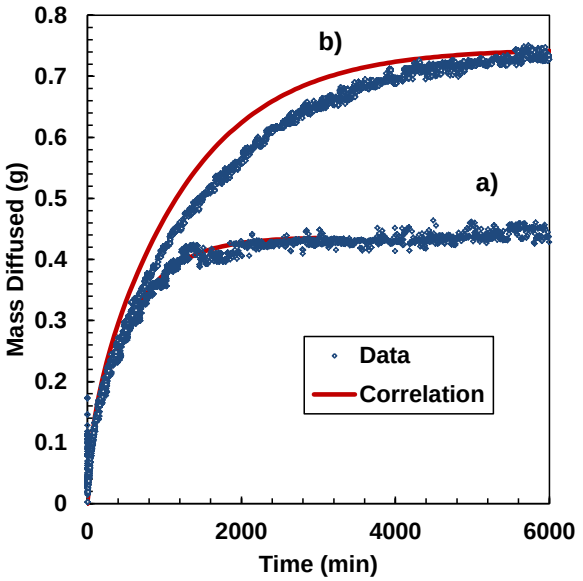

Figure 6.33. Comparison of total mass diffused from the correlation with experimental data at these conditions. For a) 81°C and 720 kPa with a D_{sb}^{∞} error of 5.4% and b) 60°C and 600kPa, with a D_{sb}^{∞} error of 37%.

6.6 Testing the Proposed Diffusivity Correlations

The correlation was tested against the results from additional pressure decay experiments of three mixtures not included in the correlation: 1) butane in the whole bitumen, 2) methane in the bitumen degassed at 176^{o}C and 3) methane in bitumen maltenes. The constant diffusivity correlation was also tested against diffusivity measurements from the literature. The concentration dependent correlation could not be tested against literature data because the required pressure decay data were not available.

6.6.1 Preliminary Evaluation of Butane Diffusivity in Bitumen

Constant Diffusivity Correlation

Figure 6.34 shows the cross plot of the modeled versus measured diffusivity of solvent in bitumen, including butane. The butane diffusivity was not included in the fitting of the correlation and was predicted to within 38%. The high average error in the butane may arise from the relatively high solubility of butane which violates the assumption of constant diffusivity more severely than the other solvents and therefore is harder to correct for.

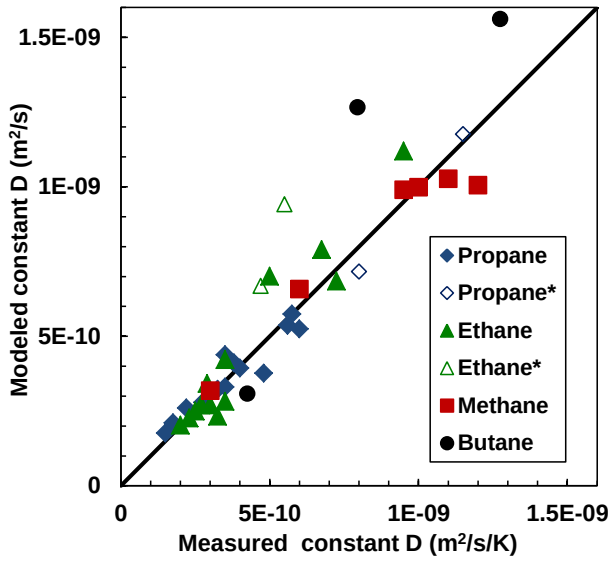

Figure 6.34. Dispersion of diffusivities correlated with the pressure corrected Hayduk-Cheng correlation (* denotes experiments with solvent initially dissolved in the oil).

Concentration Dependent Diffusivity Correlation

Figure 6.35 shows the measured and modeled infinite dilution diffusivities from the concentration dependent diffusivity model, including predictions for butane. The predicted infinite dilution diffusivities for butane are low compared to the experimental data. However, there are few butane experiments with which to compare the results, and two of the three results are within the observed scatter of the data form propane and ethane diffusivity. The error in the butane experiments is expected to be the highest of gases studied because it is the most likely to condense in the lines during the pressure decay experiments. Another factor is that the correlation (Eq. 6.24) relates the diffusivity to the size of the diffusing molecule; the greater the size of the diffusing molecule, the less the diffusivity. However, size may not be the only factor differentiating the solvents. Butane is more soluble in bitumen than the lower carbon number *n*-alkanes and may therefore have a greater diffusivity. An activity coefficient based diffusivity would be required to account for the interaction between the solvent and the oil. Since the correlation does not perform well at predicting the diffusivities outside of the mixtures used to fit it, it is not recommended to use correlation for other solvents without collecting more data.

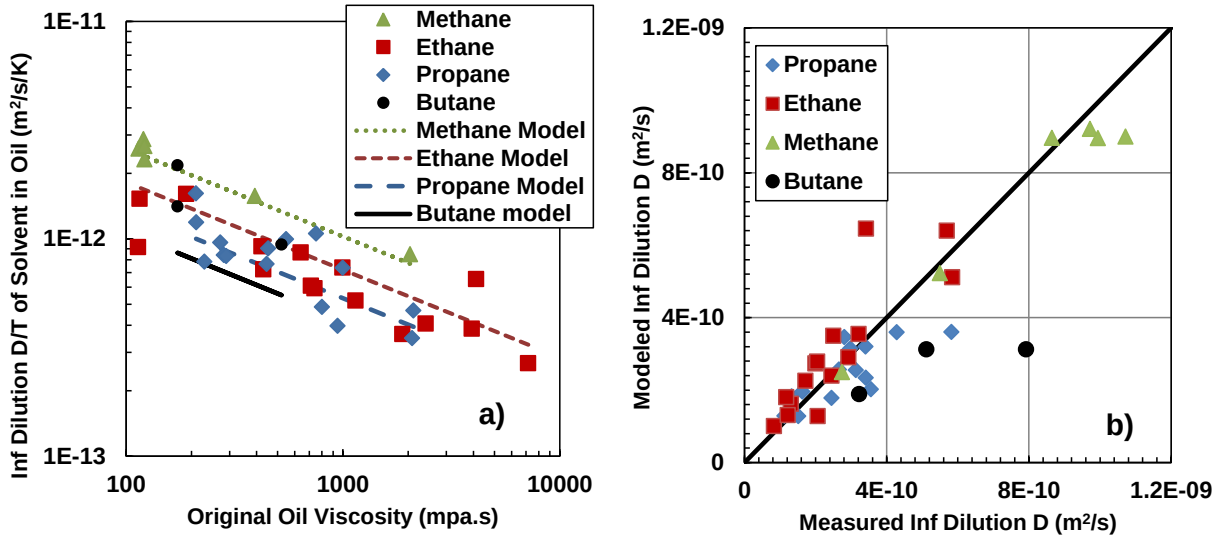

Figure 6.35. Infinite dilution of solvent diffusivity fit with the correlated infinite dilution diffusivity model: a) ratio of diffusivity to temperature versus viscosity; b) dispersion of error of predicted versus measured diffusivity.

6.6.2 Effect of Oil Composition

To assess the effects of oil composition on the diffusivity beyond simply the viscosity, pressure decay experiments were performed with methane in maltenes and the bitumen degassed at 176^{o}C.

Constant Diffusivity Correlation

The constant diffusivities fit to the pressure decay data for methane in the original bitumen, degassed bitumen and maltenes are plotted against viscosity in Figure 6.36. In all cases, the correlation qualitatively captures the trend in diffusivity versus initial oil viscosity. The average and maximum deviations of the constant diffusivity correlation are listed in Table 6.39.

The maltene data are scattered around the expected trend and it is possible that the deviations relate to the data rather than the correlation. First, the viscosities were measured for maltenes from a different oil sample from the same source reservoir and may not be identical to the viscosity for the sample used in the diffusivity measurements. Second, two batches of maltenes were recovered for the diffusivity measurements and the batches could have different residual solvent contents. However, as will be shown later, the concentration dependent diffusivity correlation results in far less scatter. Therefore, the deviations likely reflect the limitations of this simple correlation.

The correlation under-predicts the diffusivity of the degassed oil. The viscosity of the degassed oil was unknown, but the expected viscosity would be higher than that of the original oil. Therefore, the deviation would be even greater if the correct viscosity were used. The poor match indicates that the constant diffusivity correlation based on oil viscosity and pressure is not sufficient to capture the effects of different oil composition.

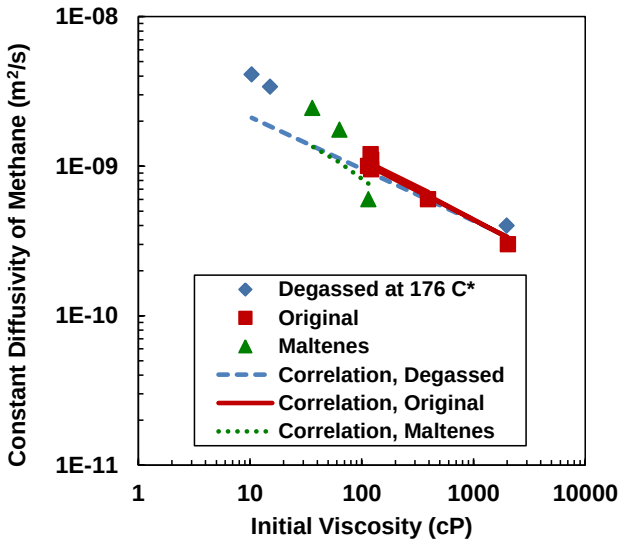

Figure 6.36. Methane diffusivity in the original bitumen, maltenes, and the bitumen degassed at 176°C* versus initial oil viscosity. The degassed viscosity was unknown and its diffusivities are plotted versus the original viscosity.

Table 6.39. Average and maximum deviation of the constant diffusivity correlation when predicting the diffusivity of methane in maltenes and bitumen degassed at 176°C

Oil	Solvent	AARD, %	MARD %
Degassed bitumen	Methane	70	100
Bitumen maltenes	Methane	56	81

Concentration Dependent Diffusivity Correlation

The infinite dilution diffusivity from the concentration dependent diffusivity model are plotted against viscosity in Figure 6.37 and are compared to the values predicted from the infinite dilution correlation. The deviations from the constant diffusivity correlation are listed in table 6.40. The infinite dilution correlation systematically over-predicted the methane diffusivity in maltenes but was within 35% of the experimental values. The correlation systematically under-predicted the infinite dilution diffusivity of methane in degassed bitumen but was within 45% of the data. The systematic deviations suggest that a simple correction could be introduced to account for oil fractions or different oils. More data on a variety of oils and fractions are required before such a correction can be developed.

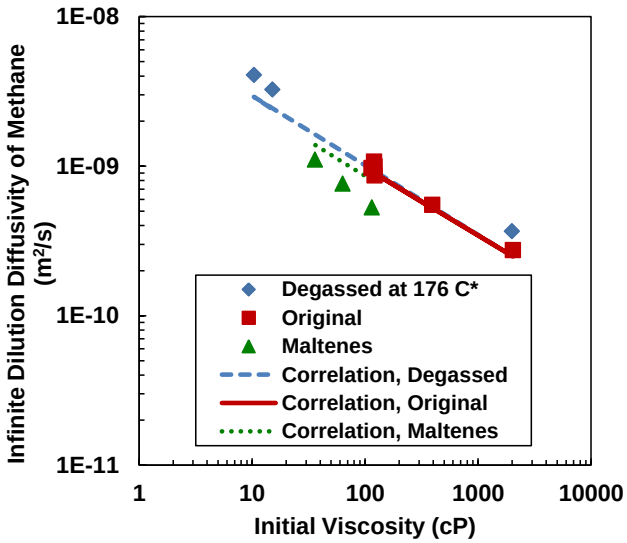

Figure 6.37. Methane diffusivity in the original bitumen, maltenes and the bitumen degassed a 176°C. * is plotted against the initial oil viscosity, as the degassed viscosity was unknown.

Table 6.40. Average and maximum deviation of the constant diffusivity correlation when predicting the diffusivity of methane in maltenes and bitumen degassed at 176°C.

Solvent	AARD, %	MARD %
Degassed Bitumen	40	45
Maltenes	28	34

6.6.3 Constant Diffusivity Correlation Tested on Literature Data

The constant diffusivity correlation was also tested against the screened literature data presented in Section 6.3. The ethane and methane diffusivity data collected by Upreti and Mehrotra (2002) and by Tharanivasan *et al.* (2006) are compared with the correlation in Figure 6.38 and the average and maximum deviations are listen in Table 6.41. The correlation predicts the correct qualitative trend of diffusivity versus initial oil viscosity and pressure but over-predicts the pressure effect for both solvents.

The largest deviation of 227% is in the dataset from Upreti and Mehrotra (2002) and is attributed to an outlier data point which is off-trend from all of the other data. If this data point is excluded the maximum deviation is 68% (for high pressure methane). Possible explanations for the deviation are: 1) the correlation does not apply well to viscosities 100 times higher than those

used in its development, possibly because the solubilities differ from the solubility effect indirectly accounted for within the correlation; 2) experimental issues such as ethane condensation in the system. The experiment was performed at 25°C and 4MPa near the critical point of ethane of 32°C and 4.9 MPa (Green and Perry, 2008).

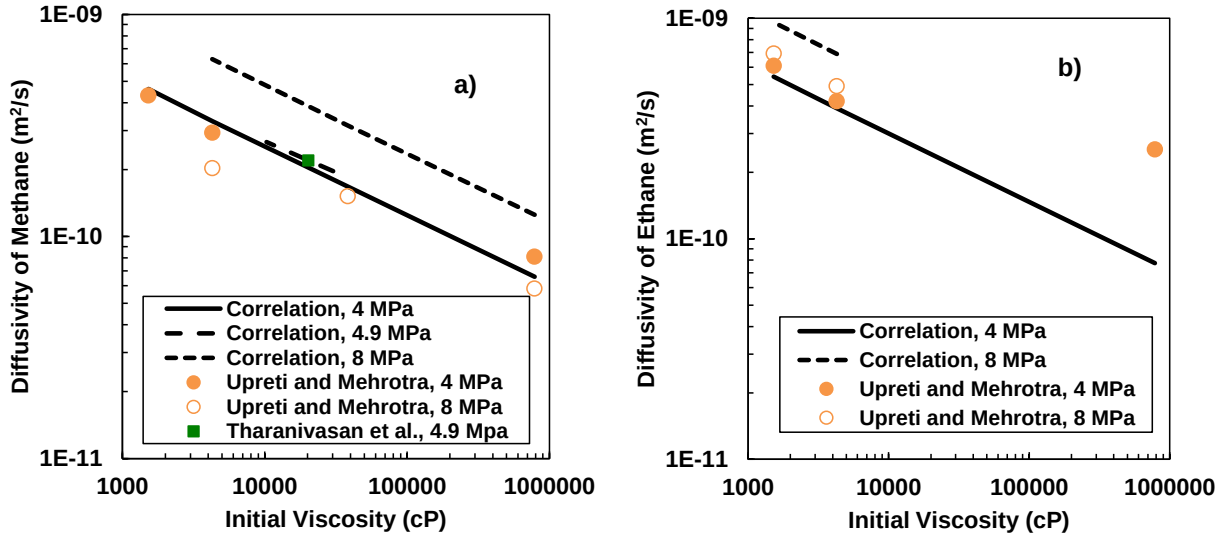

Figure 6.38. Constant diffusivity of a) methane and b) ethane in Athabasca bitumen

Table 6.41. Average and maximum deviation of the constant diffusivity correlation when predicting the diffusivity of methane in maltenes and Athabasca bitumen (data from Upreti and Mehrotra, 2002).

Oil	Solvent	AARD, %	MARD %
Upreti and Mehrotra (2002), 4 MPa	Methane	14	23
Upreti and Mehrotra (2002), 8 MPa	Methane	58	68
Upreti and Mehrotra (2002), 4 MPa	Ethane	82	227
Upreti and Mehrotra (2002), 8 MPa	Ethane	28	29
Tharanivasan *et al.* (2004), 4.9MPa	Methane	-	4.4

The correlation was next tested on Jalialahmadi *et al.'s* (2006) diffusivities of methane in a light oil (0.26 mPa.s at 25°C), as shown in Figure 6.39. Although this oil has a viscosity three orders of magnitude lower than the data used to develop the correlation, the correlation predicts the diffusivity to within 18% at pressures below 15 MPa but the error increases to over 115% at

pressures of 28 MPa. A possibly explanation for the deviation is that the correlation does not correctly account for solubility effects at higher pressures.

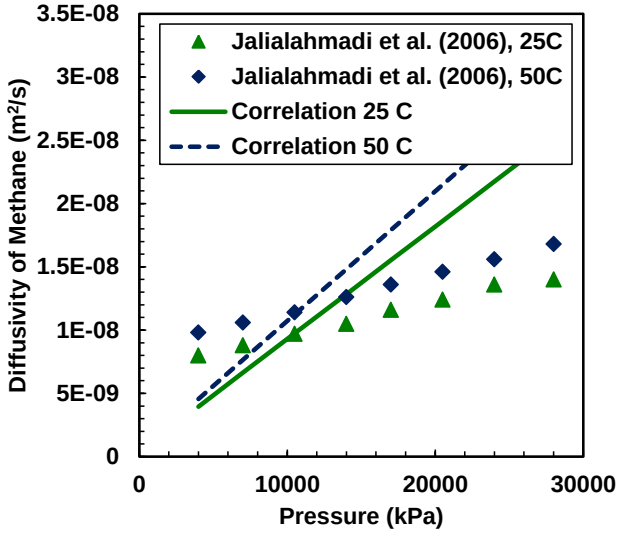

Figure 6.39. Constant diffusivity of propane in an Iranian Crude oil (0.35 mPa.s at 25°C). Data from Jalialahmadi *et al.* (2006).

The effect of pressure on the constant diffusivities of methane, ethane and propane in Lloydminster heavy oil was investigated by Yang (2005) and Yang and Gu (2006, 2007) at 23.9°C. Similar data were obtained by Etminan *et al.* (2014b) for propane diffusivity in heavy oil at 23.9°C. Note, the solubility in Etminan's higher pressure experiment may have caused asphaltene precipitation, as discussed in Section 6.3.3. Figure 6.40 compares the predicted and measured diffusivities versus pressure. The correlation over-predicted the methane diffusivity at all conditions and the deviations increased slightly with pressure (maximum error of 67%). In contrast, the correlation under-predicted the diffusivities of ethane and propane at all conditions and the deviations increased significantly with pressure (10% error at low pressure increasing to over 500% at high pressure). Here, low pressure indicates a pressure that is low relative to the solvent vapor pressure).

As noted in Section 6.3, the magnitude of the change in diffusivity with pressure reported by Yang and Gu (2006, 2007) for ethane and propane is much higher than that observed in this thesis and by Upreti and Mehrotra (2002). Ethane diffusivity measured by Upreti and Mehrotra

(2002) is plotted in Figure 6.40b) to illustrate the pressure effect on their reported diffusivities. Note, the magnitude of the diffusivities from each oil differ because the oil viscosities are different. It is not obvious why the pressure trends differ. The Yang and Gu and Etminan data were collected at 24°C, 13^{o}C lower than any of the data from this thesis or Upreti and Mehrotra. It is possible that at low temperature, particularly at higher pressures, the solubility of the solvent increases more significantly that is indirectly accounted for in the proposed correlation. If the correlation under-"predicted" the solubility, it would predict too low a diffusivity.

Marufuzzaman and Henni (2014) also reported propane diffusivities at temperatures of 15 and 26°C. The correlation is compared with their data in Figure 6.41. Note, the experiments at 500 and 600 kPa had an initial solvent concentration equal to the solubility at the previous pressure. The viscosities at these conditions were estimated using a double log mixing rule and the effective viscosity of propane. The change in viscosity with solubility (pressure) was greater at 15°C than at 26°C and, as a result, the predicted diffusivity curves crossed at 500 kPa.

The correlation predicted the diffusivities at 15°C with a maximum error of 50% but under-predicted the diffusivity at 26^{o}C with a maximum error of 140%. As noted in Section 6.3.3 the diffusivity increase between 15 and 26^{o}C is much more than would be expected by the viscous changes alone. The reason for this discrepancy is not clear because the experimental procedure was not fully described. Interestingly, the correlation was able to predict the magnitude of the change in the diffusivity with pressure. It is possible that the correlation is least accurate when both the temperature is low and the pressure is high; that is, when solvent solubilities in the oil are highest.

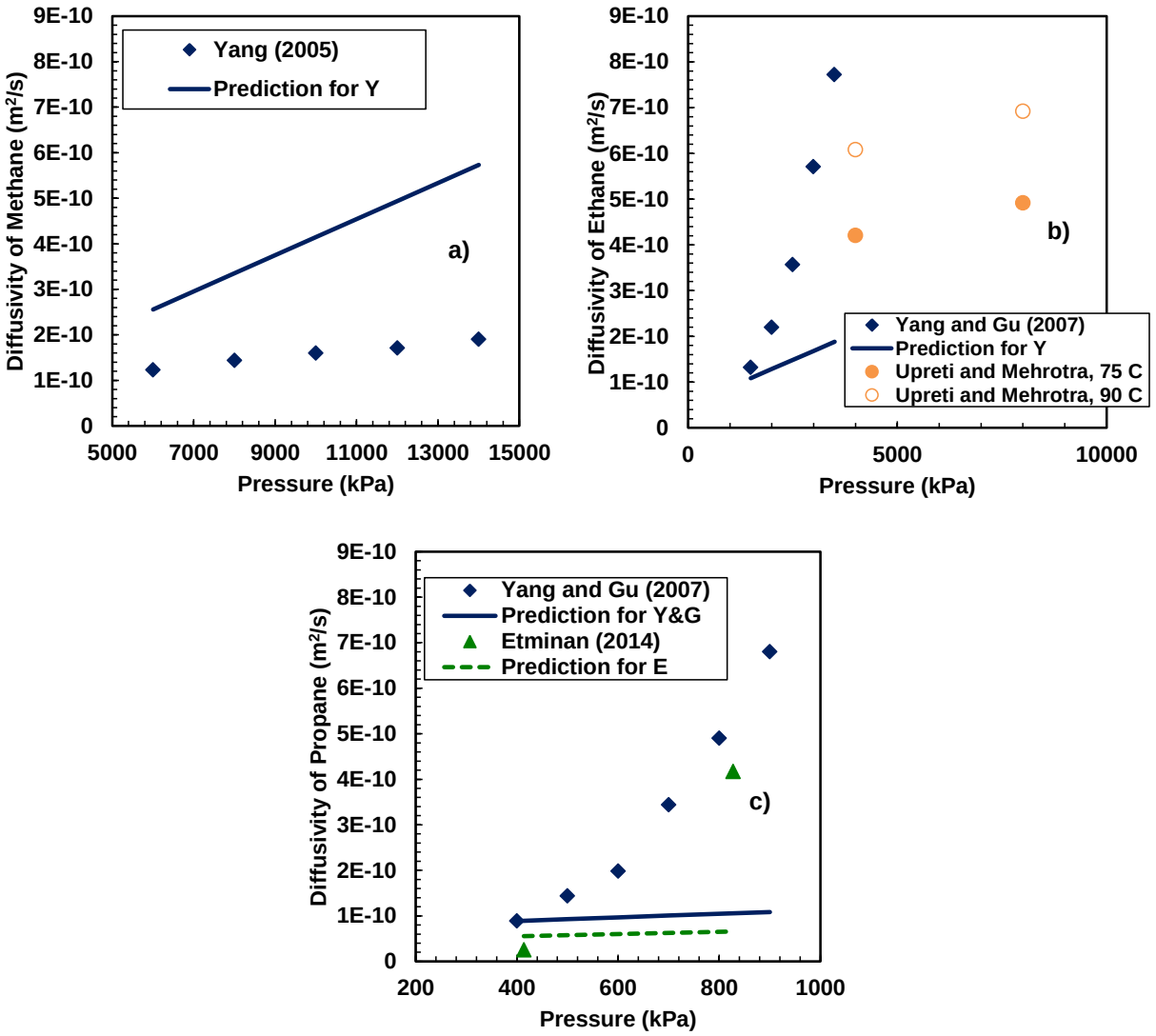

Figure 6.40. Constant diffusivity of a) methane, b) ethane, c) propane in heavy oil compared to the predictions from the constant diffusivity correlation. Data measured by Yang and Gu (2006), Yang and Gu (2007), Etminan *et al.* (2014b), and Upreti and Mehrotra (2002)

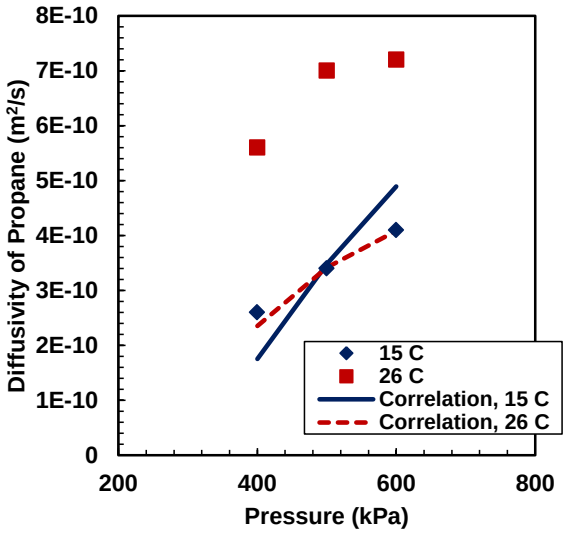

Figure 6.41. Constant diffusivity of propane in Cactus Lake oil (742 mPa.s at 26°C). Data from Marufuzzaman and Henni (2014).

6.6.4 Towards an Improved Correlation

Overall, the constant diffusivity correlation developed in this thesis over-predicts methane diffusivity in heavy oils at higher pressures. The correlation uses pressure as a proxy for the solubility of the solvent in the oil. The pressure effect was assumed to be the same for each solvent and is an average of all the data collected. Since more data were collected for ethane and propane, the average trend is less accurate for methane.

For ethane and propane, the correlation matched trends with pressure for some datasets (Upreti and Mehrotra, 2002; Tharanivasan *et al.*, 2006; Marufuzzaman and Henni, 2014) but not others (Yang and Gu, 2006, 2007; Etminan *et al.*, 2014b). It is not clear if the deviations are data issues or a flaw with the correlation. The deviations were highest when both temperature was low (<30°C) and pressure was high relative to the solvent vapor pressure. This trend suggests that the linear pressure proxy is not adequate to account for the changes in solubility.

An alternative to correlating the constant diffusivity to pressure is to correlate to a normalized pressure given by the ratio of the pressure to the solvent vapor pressure. The vapor pressures were determined from the vapor pressure correlation developed in Section 5 (extrapolated when above the critical temperature). The revised correlation has the following form:

$$D_{sb} = \frac{Tf(P_N)}{{\mu_0}^n} \tag{6.27}$$

where $f(P_N)$ is a function of the normalized pressure, P_N, T in the temperature in K, n is a fitting parameter, and μ_0 is the viscosity of the initial fluid in mPa.s.

To determine the form of $f(P_N)$, Eq. 2.24 was rearranged to calculate experimental values of the function as follows and as a preliminary estimate the value of n was assumed to be 0.28 (the value of the constant diffusivity correlation):

$$f(P_N) = \frac{D_{sb,exp}}{T}{\mu_0}^{0.28} \tag{6.28}$$

where $D_{sb,exp}$ is the experimental diffusivity in m^2/s. The experimental $f(P_N)$ are plotted versus the normalized pressures in Figures 6.42a, 6.42b, and 6.42c for methane, ethane, and propane, and for all three *n*-alkanes respectively. Most of the data follow a similar trend except for the methane diffusivities of the low viscosity Iranian oil (Jalialahmadi *et al.*, 2006)). These data were excluded from any further fit to the data. For each solvent, the function tends to a constant (infinite dilution) diffusivity far from the vapor pressure (P_N goes to zero). The infinite dilution value is slightly different for each solvent. The function appears to increase exponentially as P_N goes to unity, although the data are highly scattered at P_N above approximately 0.65. Note, most of the data in this thesis were collected at P_N below 0.65 and therefore the trend at high normalized pressure was not detected and supports why a linear pressure dependence was sufficient to fit the thesis data.

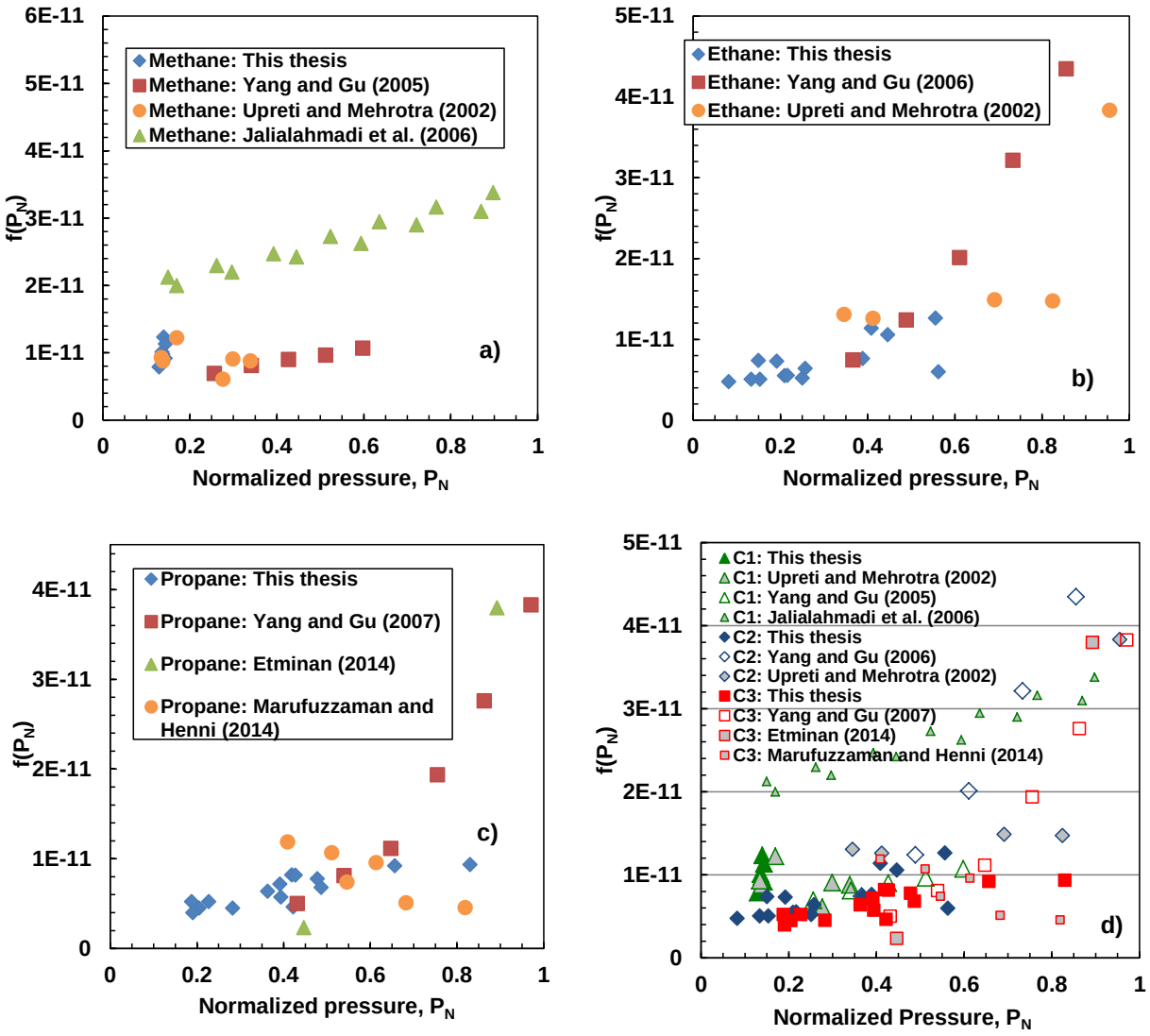

Figure 6.42. Normalized experimental diffusivity from this thesis and literature plotted against normalized pressure for a) methane, b) ethane, c) propane, and d) all components.

The following preliminary correlation is proposed that accounts for the different diffusivity for each solvent as P_N goes to zero and the apparent sharp increase in diffusivity as P_N goes to unity:

$$D_{sb} = A_N \frac{T(1 + 9.79P_N^{3.69})}{\mu_0{}^{0.312}} \tag{6.29}$$

where

$$A_N = (14.5316 - 0.2023M_s) \cdot 10^{-12} \tag{6.30}$$

and M_s is the molecular weight of the solvent. The form of the function is best observed in a plot of $f(P_N)/A_N$ as shown in Figure 6.42. The parameters of Equations 6.29 and 6.30 were regressed using the all data sets listed in Figure 6.43.

Fitting the proposed correlation exclusively to the data obtained in this thesis does not predict the sharp increase in diffusivity at higher normalized pressures. The proposed correlation fits all of the data sets with an average error of 23% (90% maximum) and fits the data from this thesis with an average error of 17% (67% maximum). The correlation was fit with external data at a large range of normalized pressures and was not expected to perform as well at as the linear corrected correlation when matching data from this thesis (average error of 12%). The main issue with the proposed correlation is the scatter in the data above P_N of 0.65 and the consequent uncertainty in the diffusivity trend with P_N. More data are required to test the correlation at these conditions.

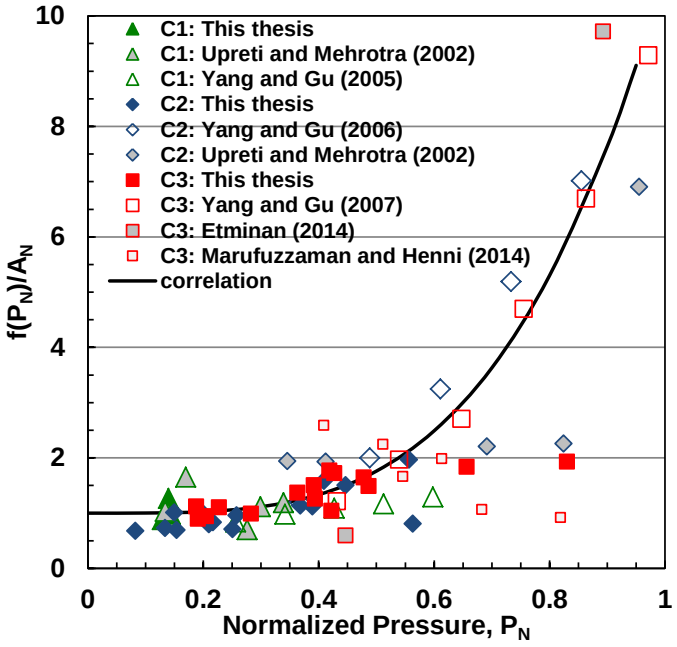

Figure 6.43. Diffusivity pressure function versus normalized pressure normalized by solvent constant A_N and including preliminary correlation.

6.7 Summary of Correlations

In this thesis, correlations were developed for both the constant diffusivity and the concentration dependent diffusivity of solvents in heavy oil. These correlations are summarized below.

6.7.1. Correlations for Constant Diffusivity

The constant diffusivity data collected in this thesis was fit to the following power law function of the initial viscosity of the oil phase:

$$D_{sb} = \frac{(1.104 * 10^{-13} M_S - 7.869 * 10^{-13} + 2.224 * 10^{-15} P)T}{\mu_o^{0.280}} \quad (6.10)$$

where M_S is the molecular weight of the solvent, P is the pressure in kPa, T is the temperature in K, μ_o is the initial viscosity of the oil phase in mPa.s and D_{sb} is the constant diffusivity of solvent in bitumen in m^2/s. Although it fit the data from this thesis with an average error of 12%, it was unable to predict much of the literature data at low temperature and high pressure, outside the ranges studied in this thesis. The following modified correlation was fit to the data collected for this thesis as well as the literature data discussed in Section 6.6.

$$D_{sb} = A_N \frac{T(1 + 9.79 P_N^{3.69})}{{\mu_0}^{0.312}} \quad (6.29)$$

where

$$A_N = (14.5316 - 0.2023 M_s) \cdot 10^{-12} \quad (6.30)$$

and M_s is the molecular weight of the solvent, P_N is ratio of the system pressure to the vapour pressure of the gas at the system temperature, T is the temperature in K, μ_o is the initial viscosity of the oil phase in cP and D_{sb} is the constant diffusivity of solvent in bitumen in m^2/s.

6.7.2. Correlations for Concentration Dependent Diffusivity

The concentration dependent diffusivity data collected in this thesis was fit to a power law function of the viscosity of the solvent-oil mixture as follows:

$$D_{sb} = \frac{AT}{{\mu_{mix}}^n} \tag{6.22}$$

where D_{sb} is the diffusivity of solvent in bitumen in m^2/s, T is the temperature in K, μ_{mix} is the viscosity of the solvent and bitumen mixture in mPa.s, and the parameters A and n are given by:

$$n = \frac{\log \frac{{D_{bs}}^{\infty}}{{D_{sb}}^{\infty}}}{\log \frac{\mu_s}{\mu_b}} \tag{6.23}$$

$$A = \frac{{D_{sb}}^{\infty}}{T} {\mu_{bit}}^n \tag{6.24}$$

where μ_s is the predicted viscosity of the liquid solvent in mPa.s, μ_b is the viscosity of the bitumen, ${D_{bs}}^{\infty}$ is the infinite dilution diffusivity of bitumen in solvent in m^2/s, and ${D_{sb}}^{\infty}$ is the infinite dilution diffusivity of solvent in bitumen. The former is given by the Hayduk-Minhas equation:

$${D_{bs}}^{\infty} = \frac{13.3 * 10^{-12} T^{1.47} {\mu_s}^{\left({}^{10.2}/_{V_b} - 0.791\right)}}{V_b^{0.71}} \tag{2.25}$$

where V_b is the liquid molar volume of bitumen at its normal boiling point in cm^3/mol. The latter is given by:

$${D_{sb}}^{\infty} = \frac{5.18 * 10^{-10} T}{{V_s}^{0.946} {\mu_b}^{0.403}} \tag{6.26}$$

where V_s is the liquid molar volume of solvent at its normal boiling point in cm^3/mol.

CHAPTER SEVEN: CONCLUSIONS AND RECOMENDATIONS

The purpose of this thesis was to experimentally determine the diffusivity of light hydrocarbon gases in bitumen from pressure decay experiments and to develop a model for this mass transfer process. This model was to include swelling, a predictive correlation for the diffusivity, and methods to predict the physical properties required to fully define the model, such as the gas solubility in the oil and the viscosity of the mixture. This chapter lists the major contributions of this thesis in achieving this end and recommendations for future work to improve the quality and reliability of diffusion models.

7.1 Contributions and Conclusions

The major contributions from this thesis are:

1. the measurement of constant and concentration dependent diffusivity for methane, ethane, and propane gases (using several diffusivity models) over a range of temperatures and pressures,
2. the measurement of gas solubilities in bitumen and their correlation using easily applied models,
3. the development of a correlation for the constant diffusivity as a function of the initial liquid viscosity and the pressure of the system,
4. the development of a procedure to calculate the concentration dependence of diffusivity from pressure decay experiments,
5. the development of a correlation to predict the concentration dependent diffusivity.

Each contribution and the major conclusions related to that contribution are discussed below.

7.1.1. Diffusivity Measurements

The available literature data for the diffusivity of hydrocarbon gases in heavy oil has largely been measured at or near room temperature. At these conditions, the diffusivity of methane, ethane, and propane have all been investigated, but with the exception of Upreti and Mehrotra (2002), no two solvents have been investigated with the same method over a wide range of conditions. This thesis contributes to the data available in literature by measuring the diffusivity

of methane, ethane, and propane in heavy oil at temperatures from 40 to 90^{o}C and pressures from 300 to 2100 kPa using a consistent method and model.

7.1.2. Solubility Measurements

The solubilities and saturation pressures of methane, ethane, and propane in heavy oil were measured from the pressure decay experiments and in blind PVT cells using a constant composition expansion method. The data were shown to be consistent with solubility data available in literature for similar oils. Two models were fit to the experimental solubilities: 1) Henry's law, which was modified with a pressure dependent Henry's constant, and; 2) the Margules activity coefficient model, which required an extrapolation of the vapour pressure curve of the solvents to accommodate mixtures above the critical temperature of the solvent. Henry's law fit the solubility data within and average error of 8 % and the Margules equation fit the data with an average error of 9 %. Within the measured pressures, the Henry's law is the superior of the two models because it successfully predicts the increasing saturation pressure at higher solvent solubilities. However, at pressures above the range of available data, the Henry's law model predicts a non-physical reversal in solubilities, caused by the added pressure dependence. Therefore, the equation should not be extrapolated to temperatures and pressures outside the range studied in this thesis.

7.1.3. Constant Diffusivity Correlation

The constant diffusivities measured in this thesis are, in essence, an average diffusivity over the concentration ranges studied. However, diffusivity correlates strongly to the viscosity of the mixture and therefore changes dramatically over the course of a pressure decay experiment. For example, the constant diffusivity did not correlate strongly to the initial viscosity of the oil as would be expected from the Hayduk and Cheng (1971) equation. More compellingly, the diffusivity with a non-zero initial solvent content in the bitumen was significantly higher than the diffusivity with zero initial solvent content.

To account for this change in viscosity with increasing concentration, several corrections to the initial correlation were investigated. It was found that a linear pressure correction could decrease the average error of the correlated diffusivity from 22% to 12% from the original fit with

Hayduk-Cheng equation. The pressure corrected correlation was tested on the available data from literature and was shown to adequately predict many of the diffusivities measured at similar conditions to those studied in this thesis. The correlation was shown to under-predict the documented pressure effect on diffusivity at low temperature and over-predict the pressure effects at high pressure. After considering data from the literature, a preliminary modification to the correlation was developed that accounts for the pressure effect on the diffusivity through the ratio of the system pressure to the vapour pressure of the diffusing gas. This new correlation was fit to all of the tested literature data as well as the data from this thesis with an average error of 23% (17% error for the data from this thesis).

7.1.4. Concentration Dependent Diffusivity Determination

It was shown in this thesis and previously by James *et al*. (2012) that it is impossible to determine the form of the concentration dependence of diffusivity from pressure decay data alone (or other methods that measure the total mass of solvent diffused). Furthermore, indistinguishable fits to the experimental data can be achieved with multiple sets of parameters for the same diffusivity model. To determine a unique set of parameters when matching the experimental data, the concentration dependent diffusivity models were constrained to pass through a hypothetical infinite dilution diffusivity of oil in solvent. In this thesis, the Hayduk and Minhas (1982) equation was chosen to predict the infinite dilution diffusivity of oil in solvent.

The pressure decay experiments were analysed using three concentration dependent diffusivity models: 1) the Vignes (1966) equation; 2) a modified Bearman (1961) equation, and; 3) a modified Hayduk and Cheng (1971) equation. For the Vignes (1966) equation, the above constraint directly provides one of the model parameters and in the case of the modified Bearman (1961) or the modified Hayduk and Cheng (1971), it gives an equation relating the two parameters. In all cases this constraint reduced the number of independent fitting parameters to one and the model could be uniquely fit to the pressure decay experiments. The single parameter for each model is sufficient to calculate the diffusivity at any concentration at the given experimental condition.

7.1.5. Concentration Dependent Diffusivity Correlation

The concentration dependent correlation was formulated so that the diffusivity at any concentration could be determined from the end points; that is, the infinite dilution diffusivity of bitumen in solvent and the infinite dilution diffusivity of solvent in bitumen. As noted above, the infinite dilution diffusivity of bitumen in solvent was determined with the Hayduk and Minhas (1982) equation. The experimental derived infinite dilution diffusivity of solvent in bitumen for each model was correlated to the viscosity of the original oil. The best results were obtained with the modified Hayduk and Cheng (1971) equation with an average error of 23%. The correlation followed the expected trend with viscosity and molecular weight of the solvent and is a simpler model than the other equations tested. Therefore, it was selected as the model for the infinite dilution diffusivity of solvent in heavy oil. With the infinite dilution diffusivity end points of the correlation established; at a given temperature and pressure there is sufficient information to calculate the parameters of the modified Hayduk and Cheng equation. The proposed correlation is valid for all solvent contents and could therefore be expanded to predict the diffusivities in liquid-liquid systems.

7.2 Recommendations

Recommendations for future studies are as follows:

1) Develop a two or three dimensional diffusion model to more accurately represent the horizontal cylindrical geometry of the Computer Tomography experiments. Solving the continuity equation in higher dimensions can be computationally expensive and more sophisticated algorithms than those presented in this thesis may be required to shorten the run rime.
2) Update the material balance equation to be in terms of weight fraction instead of concentration in g/mL. This updated model will be more applicable to systems of higher solubility such as in liquid-liquid mixtures.
3) Investigate the effect of the medium properties (other than viscosity) on the concentration dependence of the diffusivity by measuring the diffusivity of solvents in different oil fractions and in more oils.

4) Further investigate the effects of pressure on constant diffusivity of gaseous solvents in oil. In particular, measure the diffusivity at high P/P_v ratios at different temperatures to confirm the strong pressure dependence seen in literature.
5) Expand the existing correlations to include the diffusivity of liquid solvents in bitumen. This expansion would require measuring the diffusivity of liquid solvents in bitumen to supplement the small amount of data available in literature. In the preliminary constant diffusivity correlation, the normalized pressure dependence based on vapour pressure would have to be reassessed.
6) Re-analyse the pressure decay data with the Vignes (1966) equation using different models for the thermodynamic correction factor (from an equation of state or a more comprehensive activity coefficient model). There is sufficient data collected for propane-bitumen mixtures to fit such a model, Mancilla-Polanco (2017); however, supplementary PVT data would need to be collected for ethane/bitumen and methane/bitumen.

REFERENCES

Afashi, B. and Kantzas, A. **2007.** Advances in Diffusivity Measurement of Solvents in Oil Sands. *Journal of Canadian Petroleum Technology,* 46(11), 56-61.

Agrawal P. **2012.** *Measuremetn and Modeling of the Phase Behaviour of Solvent Diluted Bitumen*. master's thesis, M.Sc. Dissertation.

Agrawal. P., Schoeggl, F.F., Satyro, M.A., Taylor, S.D. and Yarranton, H.W. **2012.** Measurement and Modeling of the phase behaviour of solvent diluted bitumens. *Fluid Phase Equilibrium*, 334, 51-64.

Alazard, N. and L. Montadert, L. **1993.** Oil resources for the 21st century: Constraints and outlook. *Revue de l'Institute Francais du Petrol,* 48, 69-82.

Alboudwarej, H. **2003.** *Asphaltene Deposition in Flowing Systems.* Ph.D. Dissertation, University of Calgary.

Arnold. J. H. **1930.** Studies in Diffusion II: A Kinetic Theory of Diffusion in Liquid Systems. *Journal of the American Chemical Society*, 52. 3937-3955.

Badamchi-Zadeh, A., Yarranton, H.W., Svrcek, W.Y. and Maini, B. B. **2009.** Phase Behaviour and Physical Property Measuremetns for Vapex Solvents: Part I. Propane and Athabasca Bitumen. *JCPT*, 48, pp. 54-61.

Bearman, R.J. **1960**. Statistical Mechanical Theory of the Diffusion Coefficients in Liquid Solutions. *Journal of Chemical Physics*, 32(5), 1308-1313.

Bearman, R.J. **1961.** On the Molecular Basis of some Current Theories of Diffusion. *Journal of Chemical Physics*, 28, 1961-1968.

Bird, B.B, Stewart, W. E. and Lightfoot, E. N. **2007.** *Transport Phenomenon*, 2nd Ed., John Wiley & Sons: New York.

Black, C. and Twu, C.H. **1983.** Correlations and Prediction of Thermodynamic Properties for Heavy Petroleum Shale Oils, Tar Sands, and Coal Liquid. *AIChE Spring National Meeting, Houston, USA.*

Boustani, A and Maini, B.B. **2001**. The Role of Diffusion and Convective Dispersion in Vapour Extractions Process. *JCPT*, 40(4), 68-77.

Butler, R.M. **1997.** *GravDrain's Blackbook: Thermal recovery of oil and bitumen,* GravDrain Inc: Calgary, Alberta.

Butler, R.M. and Mokrys, I.J. **1991.** A New Process (VAPEX) for Recovering Heavy Oils Using Hot Water Hydrocarbon Vapour. *Journal of Canadian Peyroleum Technology*, 30, 97-106.

Carman, P.C. and Stein, L.H. **1956.** Self Diffusion in Mixtures. Part 1: Theory and its Application to a Nearly Ideal Binary Liquid Mixture. *Transactions of the Faraday Society*, 52, 619-627.

Chapman, S. and Cowling, T.G. **1970.** *The Mathematical Theory of Non-uniform Gases*, Cambridge University Press: London.

Chapman, W.G., Gubbins, K.E., Jackson, G. and Radosz, M. **1989.** SAFT: Equation-of-State Solution Model for Associating Fluids. *Fluid Phase Equilibrium*, 52, 31-38.

Chung, T.H., Ajlan, M., Lee, L.L. and Starling, K.E. **1988.** Generalized multiparameter correlation for nonpolar and polar fluid transport properties. *Ind. Eng. Chem. Res.*, 27, 671-679.

Civan, F. and Rasmussen, M. L. **2009.** Rapid simultaneous evaluation of four parameters of single-component gases in nonvolatile liquids from a single data set. *Chemical Engineering Science*, 64, 5084-5092.

Darken, L.S. **1948.** Diffusion, Mobility and Their Interrelation Through Free Energy in Binary Metalic Systems. *Transactions of the American Institute of Mining and Metallurgical Engineers*, 175, 184-201.

Das, S.K. and Butler, R.M. **1994.** Effect og Asphaltene Deposition on the Vapex Process: a Preliminary Investigation Using a Hele-Shaw Cell. *The Journal of Canadian Petroleum Technology,* 33, 39-45.

Das, S.K. and Butler, R.M. **1996.** Diffusion Coefficients of Propane and Butane in Peace River Bitumen. *The Canadian Journal of Chemical Engineering,* 74, 985-992.

Diedro, F., Bryant, J and Kantzas, A. **2014.** Personal Communication.

Diedro, F., Bryant, J., Kryuchkov, S. and Kantzas, A. **2015**. Evaluation of diffusion of light hydrocarbon solvents in bitumen. Paper SPE-174424 presented at the SPE Canada Heavy Oil Technical Conference, 9-11 June 2015, Calgary, Canada.

Do, H.D. and Pinczewski, W.V. **1991.** Diffusion-controlled swelling of reservoir oil by indirect contact with injection gas. *Chemical Engineering Science,* 46, 1259-1270.

Dullien, F.A.L. **1963.** New Relationship Between Viscosity and the Diffusion Coefficients Based on Lamms Theory. *Transactions of the Faraday Society,* 59, 856-868.

Dullien, F.A.L. **1971.** Statistical Test of Vignes Correlation of Liquid-Phase Diffusion Coefficietns. *Ind Eng Chem Fundam,* 10(1),41-49.

Dusseault, M. B. **2001.** Comparing Venezuelan and Canadian Heavy Oil and Tar Sands Presented at the Petroleum Society of Canada, Canadian International Petroleum Conference, Calgary, Alberta, 12-14 June 2001.

Einstein, A. **1956.** *Investigation on the Theory of Brownian Mouvement,* 1st English Edition Dover: New York.

ERCB (Energy Resources Conservation Board). **2015.** Alberta Energy Reserves 2014 and Supply/Demand Outlook for 2015-2024, ST98-2015, Calgary.

Elliott, J. and Lira, C. **1999.** *Introductory Chemical Engineering Thermodynamics,*1st Ed.,. Prentice Hall: Upper Saddle River, New Jersey.

Etminan, S.R. **2014.** *Improved Experimental and Mathemacial Techniques for Measurement of Solvent Gas Diffusivity in Heavy Oils.* Ph.D.Dissertation, University Of Calgary.

Etminan, S.R.,. Maini, B.B, Chen, Z. and Hassanzadeh, H. **2010.** Constant-Pressure Technique for Gas Diffusivity and Solubility Measurements in Heavy Oil and Bitumen. *Energy & Fuels*, 24, 533-549

Etminan, S.R, Maini, B.B and Chen, Z. **2014a**. Determination of Mass Transfer Parameters in Solvent-Based Oil Recovery Techniques using a Non-Equilibrium Boundary Condition at the Interface. *Fuel*, 120, 218-323.

Etminan, S.R., Maini, B.B. and Chen, Z. **2014b**. Modeling the Diffusion Controlled Swelling and Determination of Molecular Diffusion Coefficient in Propane-Bitumen System Using a Front Tracking Moving Boundary Technique. Paper SPE-170182 presented at the SPE heavy oil conference Alberta, Canada, 10-12 June 2014. doi:10.2118/170182-MS.

Etminan, S.R, Pooladi-Darvish, M., Maini, B.B and Chen, Z. **2013.** Modeling the Interface Resistance in Low Soluble Gaseous Solvents-Heavy Oil Systems. *Fuel*, 105, 672-687.

Fisher, D.B., Singhal, A.K., Das, S.K., Goldman, J. and Jackson, C. **2000.** Use of Magnetic Resonance Imaging and Advanced Image Analysis as a Tool to Extract Mass Transfer Information from a 2D Physical Model of the Vapex Process. Paper SPE- 59330 presetned at the SPE/DOE Improved Oil Recovery Symposium, Tulsa, 3-5 April 2000. doi:10.2118/59330-MS.

Fletcher, C.A.J. **1991.** *Computational Techniques in Fluid Dynamics: Volume 1*, 2nd Ed., Springer-Verlag: Berlin, Germany.

Fotland, P., Anifsen, H., Foerdal, H. and Hjermstad, H. P. **1997.** The phase diagrams of asphaltenes: Experimental technique, results and modelling on some North Sea crude oils. Presented at the *Proceedings of the Symposium on the Chemistry of the Asphaltene and Related Substances*, Cancun, Mexico, 11−15 November 1997.

Fu, C., Putaganna, V.R. and Vilcsak, G. **1984.** VLE Properties for CO_2-Athabasca bitumen and N2-Athabasca Bitumen. presented at *Pac Chem*, 1984, Hawaii, USA.

Fu, C. and Putaganna, V. R. **1985.** Binary Interaction Coefficients of the Modified Redlich-Kwonq-Soave Equation of State for Bitumen-Containing Systems at In-Situ Conditions. Presented at the 6th Annual Technical Meeting of the Petroleum Society of the Canadian Institute of Mining, Edmonton, Alberta, Canada, 1985.

Fu, C., Puttagunta, R., Baumber, L. and Hso, C. **1986.** Pseudo-Critical Properties of Heavy Oils and Bitumens. *Fluid Phase Equilibrium,* 30, 281-295.

Ghaderi, S.M., Tabatabaie, S.H., Hassanzadeh, H. and Pooladi-Darvish, M. **2011.** Estimation of concentration-dependant diffusion coefficient in pressure decay experimentsof heavy oils and bitumens. *Fluid Phase Equilibria,* 305, 132-144.

Ghai, R.K., Erlt, H. and Dullien, F.A.L. **1973**. Liquid Diffusion in Nonelectrolytes. *AIChE Journal*, 5, 881-900.

Green, D.W. and Perry, R.H. **2008.** *Perry's Chemical Engineer's Handbook*, 8th ed. McGraw-Hill: New York.

Greiner-Schmid, A., Wappmann, S., Has, M. and Lüdemann, H.D. **1991.** Self-diffusion in the compressed fluid lower alkanes: Methane, ethane, and propane. *Journal of Chemical Physics*, 94, 5643-5649.

Grey, M.R. **2015**. *Upgrading Oilsands Bitumen and Heavy Oil*, 1st Ed., University of Alberta Press: Edmonton.

Guerrero-Aconcha, U. and Kantzas, A. **2009**. Diffusion of Hydrocarbon Gases in Heavy Oil and Bitumen. Paper SPE- 122783 Presented at the SPE Latin American and Caribean Petroleum Engineering Conference Cartagena, Colombia, 31 May -3 June 2009. doi:10.2118/122783-MS

Guerrero-Aconcha, U., Salama, D. and Kantzas, A. **2008.** Diffusion Coefficient of n-Alkanes in Heavy Oil. Paper SPE-115346 presented at the SPE Annual Technical Conference and Exhibition, Denver, 21-24 September 2008. doi:10.2118/115346-MS

Gupta, S., Gittins, S. and Picherack, P. **2002.** Field Implementation of Solvent Aided Process. Paper 2002-299 presented at the 53rd Canadian International Petroleum Conference, Calgary, Alberta, 11-13 June 2002.

Gupta, S., Gittins, S. and Picherack, P. **2003.** Insights into some key issues with Solvent Aided Process. *J Can Pet Tech*, 42, 54-61.

Hartley, G.S. and Crank,J. **1949.** Some Fundamental Definitions and Concepts in Diffusion Processes. *Transactions of the Faraday Society*, 45, 801.

Hayduk, W. and Cheng, S.C. **1971.** Review of Relation Between Diffusion and Solvent Viscosity in Dilute Liquid solutions. *Chemical Engineering Science*, 26, 635.

Hayduk, W. and Minhas, B.S. **1982** Correlation for Prediction of Molecular Diffusivities in Liquids. *Canadian Journal of Chemical Engineering*, 60, 295-299.

James, L.A. **2009**. *Mass Transfer Mechanisms during the Solvent Recovery of Heavy Oil.* Ph.D. Dissertation, Univerisity of Waterloo.

James, L.A., Ioannidis, M.A. and Chatzis, I. **2012.** Experimentally Validated Model for the Determination of Concentration-Dependant Diffusion of a Light Hydrocrabon in Bitumen. *Energy and Fuel*, 26, 6200-6209.

Jamialahmadi, M., Emandi, M. and Muller-Steinhagen, H. **2006.** Diffusion Coefficients of Methane in Liquid Hydrocarbons at High Pressure and Temperature. *Journal of Petroleum Science and Engineering*, 53, 47-60.

Jamaluddin, A.K.M., Joshi, N., Iwere, F. and Gurpinar, O. **2002.** An investigation of asphaltene instability under nitrogen injection. Paper SPE-74393 presented at the Proceedings of the Society of Petroleum Engineers (SPE) International Petroleum Conference and Exhibition in Mexico, Villahermosa, Mexico, 10−12 February 2002.

Johnston, K. **2016.** Personal Communication.

Kesler, M.G. and. Lee, I.K. **1976.** Improve Prediction of Enthalpy of Fractions. *Hydrocarbon Processing*, 55, 153-158.

Kokal, S. and Sayegh, S.G. **1993.** Phase behavior and Physical Properties of CO_2-Saturated Heavy Oil and its Constitutive Fractions: Experimental Data and Correlation. *Journal of Petroleum Science and Engineering*, 9, 289-302.

Kontogeorgis, G.M., Voustas, E.C., Yakoumis, I.V. and Tassios, D. P. **1996.** An Equation of State for Associating Fluids. *Industrial & Engineering Chemistry Research*, 35, 4310-4318.

Kooijman,H. and Taylor, R. **1991.** Estimation of Diffusion Coefficients in Multicomponent Liquids. *Industrial & Engineering Chemistry Research*, 30, 1217-1222.

Lamm, O. **1943.** Die Theorie der Diffusion biniirer Mischungen und die Interpretierung von Diffusionsmessungen. *Arkiv Kemi, Min. Geol.*, 17(A).

Lamm, O. **1944.** Theorie der Diffusion ternarer Losunger. *ibid.*, 18(A).

Li, J.C.M. and Chang, P. **1955.** Self-Diffusion Coefficient and Voscosity in Liquids. *Journal of Chemical Physics*, 23, 518-520.

Leaute, R. P. **2002.** Liquid addition to steam for enhancing oil recovery of bitumen with CSS: evolution of technology from research concept to a field pilot at cold lake. Paper SPE- 79011 presented at the SPE International Thermal Operations and Heavy Oil Symposium and International Horizontal Well Technology Conference, Calgary, Alberta, 4-7 November 2002. doi:10.2118/79011-MS

Lundberg, J. L., Wilk, M.B., and Huyett, M.J. 1963. Sorption Studies Using Automation and Computation. *Industrial and Engineering Chemistry Fundamentals*, 2 (1), 37-43.

Luo H. and Kantzas, A. **2011.** Study of Diffusivity of Hydrocarbon Solvent in Heavy Oil Saturated Sands Using X-Ray Compuer Assiusted Tomography. *Journal of Canadian Petroleum Technology*, 50, 24-34.

Luo, H., Salama, D., Kryuchov, S. and Kantzas, A. **2007.** The Effect of Volume Changes Due to Mixing on Diffusion Coefficient Determination in Heavy Oil and Hydrocarbon Solvent Systems. Paper SPE- 110522 Presented at the SPE Annual Technical Conference and Exhibition, Anaheim, 11-14 November 2007. doi:10.2118/110522-MS

Ma, M., Chen, S. and Abedi, J. **2016.** Modeling the density, solubility and viscosity of bitumen/solvent systems using PC-SAFT. *Journal of Petroleum Science and Engineering*, 139, 1-12.

Mancilla-Polanco, A., Schoeggl, F.F., Johnston, K., Richardson, W.D., Yarranton, H.W. and Taylor, S.D. 2017. The Phase Behavior of Heavy Oil and Propane Mixtures. Paper SPE- presented at the SPE Canada Heavy Oil Technical Conference held in Calgary, Alberta, Canada, 15—16 February 2017.

Margules, M. **1895.** Über die Zusammensetzung der gesättigten Dämpfe von Misschungen. S*itzungsberichte der Kaiserliche Akadamie der Wissenschaften Wien Mathematisch-Naturwissenschaftliche Klasse*, 2, 1243-1278.

Marufuzzaman M. and Henni, A. **2015.** Solubility of CO2 and C2H6 in Heavy Oil and it's SARA Fractions. *Canadian Journal of Chemical Engineering*, 93, 553-564.

Marufuzzaman M. and Henni, A. **2014.** Solubility and Diffusivity of Propane in Heavy Oil and it's SARA Fractions. *Canadian Journal of Chemical Engineering*, 92, 1421-1431.

Mehrotra, A.K. and Svrcek, W.Y. **1982.** Correlations for Properties of Bitumen saturated with CO2, CH4 and N2, and experiments with Combustion Gas Mixtures. *Journal of Canadian Petroleum Technology*, 21, 95-104.

Mehrotra, A.K. and Svrcek, W.Y. **1984.** Correlation and Measurement of Viscosity, Density and Gas Solubility of Marguerite Lake Bitumen saturated with Carbon Dioxide. *AOSTRA Journal of Research*, 1, 51-62.

Mehrotra, A.K. and Svrcek, W.Y. **1985a.** Viscosity, Density and Gas Solubility Data for Oil Sand Bitumens. Part I: Athabasca Bitumen Saturated with CO and C2H6. *AOSTRA Journal of Research*, 1, 263-268.

Mehrotra, A.K. and Svrcek, W.Y. **1985b.** Viscosity, Density and Gas Solubility Data for Oil Sand Bitumens. Part II: Peace River Bitumen Saturated with N_2, CO, CH_4, CO_2, C_2H_6. *AOSTRA Journal of Research*, 1, 269-279.

Mehrotra, A.K. and Svrcek, W.Y. **1985c.** Viscosity, Density and Gas Solubility Data for Oil Sand Bitumens. Part III: Wabasca Bitumen Saturated with N_2, CO, CH_4, CO_2, C_2H_6. *AOSTRA Journal of Research*, 1, 269-279.

Mehrotra, A.K. and Svrcek, W.Y. **1988a.** Properties of Cold Lake Bitumen Saturated with Pure Gases and Gas Mixtures. *Canadian Journal of Chemical Engineering*, 66, 656-665.

Mehrotra, A.K. and Svrcek, W.Y. **1988b.** Correlation and Prediction of Gas Solubility in Cold Lake Bitumen. *Canadian Journal of Chemical Engineering*, 66, 666-670.

Mehrotra, A.K. and Svrcek, W.Y. **1988c.** Characterization of Athabasca Bitumen For Gas Solubility Calculations. *Canadian Journal of Chemical Engineering*, 27, 107-110.

Motahhari, H. **2013.** *Development of Viscosity Model for Petroleum Industry Applications.* Ph.D.Dissertation, University Of Calgary.

Motahari, H., Satyro, M.A., Taylor, S.D. and Yarranton, H.W. **2013a**. Extension of the Expanded Fluid Viscosity Model to Characterized Oils. *Energy & Fuels*,27, , 1881-1898.

Motahhari, H., Schoeggl, F.F., Satyro, M.A. and Yarranton, H.W. **2013b.** The Effect of Solvents on the Viscosity of an Alberta Bitumen at In Situ Thermal Process Conditions," Paper SPE-165548 prestented at the SPE Heavy Oil Conference Canada, Calgary, Alberta, Canada, 11-13 June 2013. doi:10.2118/165548-MS

Motahhari, H., Schoeggl, F.F., Satyro, M.A. and Yarranton, H.W. **2013c**. Viscosity Prediction for Solvent-DilutedLive Bitumen and Heavy Oil at Temperatures up to 175^{o}C. *Journal of Canadian Petroleum Technology*, 52, 376-390.

Nasr, T. N. and Ayodele, O.R. **2006.** New Hybrid Steam-Solvent Processes for the Recovery of Heavy oil and Bitumen. Paper SPE-101717 presented at the 12th Abu Dhabi International

Petroleum Exhibition and Conference, ADIPEC, Abu Dhabi, UAE, 5-8, November 2006. doi:10.2118/101717-MS.

Nenninger, J. and N-Solv Corporation. **2012**. Method and apparatus for stimulating heavy oil production. Canadian Patent 2633061, 25 Sept 2012.

NIST. **2016.** NIST Standard Reference Database 69: *NIST Chemistry WebBook*. Online: http://webbook.nist.gov/chemistry/fluid/

Oballa, V. and Butler, R.M. **1989.** An Experimental Study of Diffusion in the Bitumen-Toluene System. *The Journal Of Canadian Petroleum Technology,* 28(2), 63-69.

Peng, D.Y. and Robinson, D.B. **1976.** A New Two-Constant Equation of State. *Industrial and Engineering Chemistry*, 15, 59-64.

Quail, B., Hill.G.A. and Jha, K.N. **1988.** Correlations of Viscosity, Gas Solubility, and Density for Saskatchewan Heavy Oils. *Industrial Engineering Chemistry Research*, 27, 519–523.

Reamer, H., Opfell, J. and Sage, B. **1956.** Diffusion Coefficients in Hydrocarbon Systems: Methane-Decane-Methane in Liquid Phase. *Industrial and Engineering Chemistry*, 48, pp. 275-282.

Reid, R.C., Prausnitz, J. M. and Poling, B.E. **1987**. *The Properties of Gases and Liquids*, 4th Ed., McGraw Hill: New York.

Riazi, M.R. **1996.** A New Method for experimetnal Measurment of Diffusivity Coefficients in Reservoir Fluids. *Journal of Petroleum Science and Engineering,* 14, 235-250.

Riazi, M.R. **2005.** *Characterization and Properties of Petroleum Fractions*, 1st Ed., ASTM International:Conshohocken, USA:

Riazi, M.R. and Al-Sahhaf, T.A. **1996.** Physical properties of heavy petroleum fractions and crude oils. *Fluid Phase Equilibria*, 117, 217-224.

Riazi, M.R. and Daubert, T.E. **1980.** Simplify Property Predictions. *Hydrocarbon Processing*, 59, 115-116.

Robinson, D.B. and Sim, S.K. **1980.** Behaviour of Bitumen-Water-Gas System. Report, *D. B. Robinson & Associates*, Edmonton, Alberta, Canada.

Salama, D. and Kantzas, A. **2005.** Monitoring of Diffusion of Heav Oil with Hydrocarbonb Solvents in the presence of sand. Paper SPE-97855 presented at the *SPE internationsl Thermal Operatins and Heavy Oil Symposium*, Calgary Canada, 1-3 November 2005. doi:10.2118/97855-MS.

Sanchez-Lemus, M.C. **2015.** *Extended Distillation Property Correlations for Heavy Oil*. Ph.D. dissertation, University of Calgary.

Sarafianos, N.J. **1986.** An analytical method of calculating variable diffusion coefficients. *Journal of Materials Science*, 21(7), 2283-2288.

Saryazdi, F., Motahhari, H., Schoeggl, F.F., Taylor, S.D. and Yarranton, H.W. **2013.** Density of Hydrocarbon Mixtures and Bitumen Diluted With Solvents and Dissolved Gasses. *Energy & Fuel*. 27. 3666-3678.

Schmidt, T., Jossy, E. and Puttagunta, T.R. **1986.** Mass Transfer Studies, *Final Report of Project 188, Alberta Research Council,* Edmonton, AB, 1986

Schmidt, T., Leshchyshyn, T.H. and Puttagunta, V.R.**1982**, June. Diffusivity of CO2 into reservoir fluids. Presented at the 33rd Annual technical meeting of the petroleum society of CIM, Calgary, Canada, 6-9.

Sheikha, H., Mehrotra, A.K. and Pooladi-Darvish, M. **2006**. An inverse solution methodology for estimating the difusion coefficients of gases in Athabasca bitumen from pressure decay data. *Journal of Petroleum Science & Engineering*, 53, 189-201.

Sheikha, H., Pooladi-Darvish, M. and Mehrotra, A.K. **2005.** Development of graphical methods for estimating the diffusivity coefficients of gases in bitumen from pressure-decay data. *Energy & Fuels*, 19, 2041-2049.

Signhal, K., Das, S.K., Leggitt, S.M., Kasraie, M. and Ito, Y. Screening of reservoirs for exploitation by application of Steam Assisted Gravity Drainage/Vapex processes. Paper SPE-37144 presented at the 2nd International Conference on Horizontal Well Technology, 18 November.

Song, L., Kantzas, A. and Bryan, J. **2010a.** Experimetnal Measurement of diffusion Coefficient of CO2 in Heavy Oil using X-Ray Computer Tmography Under Reservoir Conditions. Paper SPE- 137545 Presented at the Canadian Unconventional Resources and Internaltional Petroleum Conference, Calgary, Alberta, 19-21 October 2010. doi:10.2118/137545-MS

Song, L., Kantzas, A. and Bryan, J. **2010b.** Investigation of Co2 Diffusivity in Heavy Oil Using X-Ray Computer-Assisted Tomography Under Reservoir Conditions. Paper SPE- 138205 Presented at SPE International Conference on CO2 Capture, Storage, and Utilization, New Orleans, 10-12 November 2010. doi:10.2118/138205-MS

Srivastan, S., Darwish, N., Gasem, K. and Robinson, R. **1992.** Solubility of Methane in Hexane, Decane and Dodecane at Temperatures from 311 to 423 K and Pressures to 10.4 MPa. *Journal of Chemical and Engineering Data,* 37, 516-520.

Svrcek, W.Y. and Mehrotra, A.K. **1982.** Gas Solubility, Viscosity and Density Measurements for Athabasca Bitumen. *Journal of Canadian Petroleum Technology,* 21, 31-38

Tan, K.K. and Thorpe, R.B. **1992.** Gas diffusion into viscous and non-Newtonian liquids. *Chemical Engineering Sciecne,* 47(13-14), 3565-3572

Tan, K.K. and Thorpe, R.B. **1999**. The onset of convection induced by buoyancy during gas diffusion in deep fluids. *Chemical Engineering Sciecne,* 54(19), 4179-3572

Tharanivasan, A.K., Yang, C. and Gu, Y. **2004**. Comparison of Three different Mass Transfer Models Used in the Experimental Measurement of Solvent Diffusivity in Heavy Oil. *Journal of Petroleum Science and Engineering,* 44, 269-282.

Tharanivasan, A.K., Yang, C. and Gu, Y. **2006**. Measurements of Molecular Diffusion Coefficients of Carbon Dioxide, Methane, and Propane under Reservoir Conditions. *Energy & Fuels*, 20, 2509-2517.

Upreti, S.R., Lohi, A., Kapadia, R.A. and El-Haj, R. **2007.** Vapor extraction of heavy oil and bitumen: A review. *Energy & Fuels,* 21, 1562-1574.

Upreti, S.R. and Mehrotra, A.K. **2002.** Diffusivity of CO2, CH4, C2H6 and N2 in Athabasca Bitumen. *The Canadian Journal of Petroleum Engineering,* 80, 116-125.

Varet, G., Montel, F, Marsi, D. and Daridon, J. **2013.** Gas Solubility Measurement in Heavy Oil and Extra Heavy Oil at Vapour Extraction (VAPEX) Conditions. *Energy & Fuels,* 27, pp. 2528-2535.

Vignes, A. **1966.** Diffusion in Binary Solutions: Variation of Diffusion Coefficient with Composition. *Industrial and Engineering Chemistry Fundamentals,* 5(2), 189-199.

Virtual Materials Group, Inc. **2010.** *VMG Sim 6.0 User's Manual*, Calgary, Alberta, Canada.

von Solms, N., Michelsen, M.L. and Kontogeorgis, G.M. **2003.** Computational and Physical Performance of a Modified PC-SAFT Equation of State for Highly Asymmetric and Associating Mixtures. *Industrial and Engineering Chemistry Research,* 42, 1098–1105.

Wen, Y.W. and Kantzas, A. **2005a.** Monitoring Bitumen-Solvent Interactions with Low-Field Nuclear Magnetic Resonance and X-ray Computer-Assisted Tomography. *Energy & Fuels,* 19, 1319-1326.

Wen, Y.W., Bryan, J. and Kantzas, A. **2005b**. Estimation of Diffusion Coefficients in Bitumen Solvent Mixtures as Derived from Low Field NMR Spectra. *The Journal of Canadian Petroleum Technology,* 44(4), 29-34.

Whitson, C.H. and Brule, M.R. **2000** *Phase Behaviour: SPE Monographs Volume 20,* Society of Pertoleum Engineers.

Wilke, C.R. **1950.** A Viscosity Equation for Gas Mixtures. *Journal of Chemical Physics,* 18, 517-519.

Wilke, C.R. and Chang, P. **1955.** Correlation of Diffusion Coefficients in Dilute Solutions," *Chemical Engineering Progress*. 48, 2645-270.

Yang, C. **2005.** *A New Method For Measuring Solvent Diffusion Coefficietns and Oil Swelling Factors of Heavy Oil-Solvent System.* Ph.D. Dissertation, University of Regina.

Yang, C. and Gu, Y. **2005.** A New Method for Measuring Solvent Diffusivity in Heavy Oil by Dynamic Pendant Drop Shape Analysis. *SPE Journal*, 11, 48-57.

Yang, C. and Gu, Y. **2006.** Diffusion Coefficients and oil swelling factors of carbon dioxide, methane, ethane, propane, and their mixtures in heavy oil. *Fluid Phase Equilibria*,. 243, 64-73.

Yang, C. and Gu, Y. **2007.** A Novel Experimental Technique for studying Solvent Mass Transfer and Oil-Swelling Effect in the Vapour Extration (VAPEX) Process. *The Journal or Canadian Petroleum Technology*, 46, 44-48.

Yarranton, H.W and Satyro M.A. **2011.** Expanded Fluid-Based Viscosity Correlation for Hydrocarbons. *Industrial and Engineering Chemistry Research*, 48, 3640-3648.

Yaws, C.L. **1999.** *Yaws' Handbook of Thermodynamic and Physical Properties of Chemical Compounds*, McGraw-Hill: New York.

Yazdani, A. and Maini, B.B. **2010.** Measurements and modelling of phase behaviour and viscosity of a heavy oil/butane system. *Journal of Canadian Petroleum Technology*, 49, 9-14.

Yokozeki. A. **2002.** Time-dependent behavior of gas absorption in lubricant oil. *International Journal of Refrigeration*, 25(6), 695-704

Yonebayashi, H., Masuzawa, T., Dabbouk, C. and Urasaki, D. **2009.** Ready for gas injection: Asphaltene risk evaluation by mathematical modeling of asphaltene precipitation envelope (APE) with integration of all laboratory deliverables. Paper SPE-125643 presented at the *Proceedings of the Society of Petroleum Engineers (SPE)/European Association of Geoscientists and Engineers (EAGE) Reservoir Characterization and Simulation Conference*; Abu Dhabi, United Arab Emirates, 19−21, October 2009.

Zainal, S., Yee, H.V. and Saaid, I.M. **2011.** Gas Diffusivity Measuremetn In Reservoir Fluid at Elevated Pressures Systems for Transient Shut-in Modeling. Paper SPE-139004 presented at the

SPE Offshore Europe Oil and Gas Conference and Exhibition, Aberdeen, UK, 6-8 September 2011. doi:10.2118/139004-MS

Zhang, Y.P., Hyndman, C.L. and Maini, B.B. **2000**. Measurement of Gas Diffusivity in Heavy Oils. *Journal of Petroleum Science and Engineering*, 25, 37-47.

Zhang, X., Pedrosa, N. and Moorwood, T. **2012.** Modelling Asphaltene Phase behavior: Comparison of methods for flow assurance studies. *Energy & Fuels*, 26, 2611-2620.

Zhang, X. and Shaw, J.M. **2007.** Liquid Phase mutual Diffusion Coefficients for heavy oil +Light Hydrocarbon Mixtures. *Petroleum Science and Technology*, 25(6), 2007.

Zhao, L. L. **2004.** Steam Alternating Solvent Process. Paper SPE-86957 presented at the SPE International Thermal Operations and Heavy Oil Symposium and Western Regional Meeting, Bakersfield California, USA, 16-18 March 2004

APPENDIX A

The following six tables list the values of the solvent viscosity and the corresponding infinite dilution diffusivity or self-diffusivity of bitumen in solvent. These values are used as constraints for the concentration dependent diffusivity models.

Table A.1. The infinite dilution diffusivity of bitumen in liquid methane, *predicted with the Hayduk-Minhas Equation

Temperature ^{o}C	Pressure kPa	Effective Methane Viscosity mPa.s	Infinite Dilution Diffusivity* $10^{-9}m^2/s$
50	3451	0.163	2.40
76	4161	0.122	3.39
100	4226	0.097	4.46
100	4169	0.097	4.47
100	4340	0.097	4.45
101	4119	0.096	4.51

Table A.2. The infinite dilution diffusivity of bitumen in liquid ethane, *predicted with the Hayduk-Minhas Equation

Temperature ^{o}C	Pressure kPa	Effective Ethane Viscosity mPa.s	Infinite Dilution Diffusivity* $10^{-9}m^2/s$
37	2964	0.081	3.90
42	2168	0.078	4.10
47	1394	0.076	4.29
50	1741	0.075	4.39
58	2962	0.073	4.65
59	1495	0.072	4.74
64	1751	0.070	4.92
64	1120	0.070	4.95
73	774	0.067	5.30
75	4324	0.068	5.31
90	4741	0.063	5.96
100	1916	0.060	6.47
100	1970	0.060	6.49

Table A.3. The infinite dilution diffusivity of bitumen in liquid ethane, *predicted with the Hayduk-Minhas Equation. Data in this table was used in the analysis of diffusion experiments with an initial ethane concentration in the bitumen.

Temperature ^{o}C	Pressure kPa	Effective Propane Viscosity mPa.s	Infinite Dilution Diffusivity* $10^{-9}m^2/s$
42	3316	0.079	4.08
64	2104	0.070	4.93

Table A.4. Self-diffusivity of propane and the infinite dilution diffusivity of bitumen in liquid propane, *predicted with the Hayduk-Minhas Equation

Temperatue ^{o}C	Pressure kPa	Effective Propane Viscosity mPa.s	Self-Diffusivity of Propane $10^{-9}m^2/s$	Infinite Dilution Diffusivity* $10^{-9}m^2/s$
50	327	0.114	13.0	3.18
50	724	0.114	13.0	3.18
59	824	0.108	14.1	3.46
60	602	0.107	14.2	3.49
62	1080	0.106	14.4	3.54
70	1077	0.102	15.4	3.78
74	523	0.099	15.9	3.92
74	1006	0.100	15.9	3.91
80	607	0.096	16.8	4.15
80	1507	0.096	16.7	4.14
81	720	0.096	16.8	4.16
81	1367	0.096	16.8	4.17
85	702	0.093	17.4	4.31
86	1374	0.093	17.5	4.34

Table A.5. Self-diffusivity of propane and the infinite dilution diffusivity of bitumen in liquid propane, *predicted with the Hayduk-Minhas Equation. Data in this table used in the analysis of diffusion experiments with an initial propane concentration in the bitumen.

Temperatue ^{o}C	Pressure kPa	Effective Propane Viscosity mPa.s	Self-Diffusivity of Propane $10^{-9}m^2/s$	Infinite Dilution Diffusivity* $10^{-9}m^2/s$
64	1890	0.106	14.5	3.6
86	2303	0.094	17.4	4.3

Table A.6. The infinite dilution diffusivity of bitumen in liquid butane, *predicted with the Hayduk-Minhas Equation

Temperature ^{o}C	**Pressure kPa**	**Effective Butane Viscosity mPa.s**	**Infinite Dilution Diffusivity* $10^{-9}m^2/s$**
69	284.3	0.163	2.40
90	738.2	0.097	4.45
90	874.3	0.096	4.51